Improving the performance of internal combustion engines through lubricant engineering

Oliver Taylor, New College, Oxford

Department of Engineering Science

Trinity Term 2016

Supervisors: Professor Richard Stone, University of Oxford

and

Dr Richard Pearson, BP

Improving the performance of internal combustion engines through lubricant engineering

Oliver Taylor, New College, Oxford

Department of Engineering Science

Trinity Term 2016

Abstract

Low friction lubricant development provides a worthwhile contribution to vehicle CO_2 emission reduction. Conventional low friction lubricant development focuses on empirical processes using out-dated engine technology and old test methods. This strategy is inefficient and restricts the lubricant's potential. A new method proposed in the present research combines tribological simulations with rig, engine and vehicle tests. This approach provides insights undocumented until now. The contribution to CO_2 emission reduction from individual engine components on vehicle drive cycles that include warm-up is predicted using lubricants down to the new SAE 8 viscosity grade.

A bearing model is used to design the lubricant's non-Newtonian characteristics to achieve friction reduction. An isoviscous lubricant with a viscosity of 4.6 cSt is shown to achieve the minimum friction in the bearing. The research shows that by starting with lubricants having kinematic viscosities higher than this value, it is possible to improve lubricant performance by lowering viscosity index (VI), introducing shear-thinning, or reducing the density and pressure viscosity coefficient. Conversely, for lubricants with lower starting viscosities it is shown that higher VI values, more shear-stable lubricants and higher densities and pressure viscosity coefficients are required. The model predicts that high oil film pressures occur in the bearing and cause significant local lubricant viscosity increase (300%), indicating that the lubricant's pressure viscosity behaviour is important here, despite the contact being conformal.

Simulation and motored engine testing establishes lubricant behaviour in the piston-to-bore conjunction. This analysis identifies a poor correlation between measured and predicted values at low engine speeds. A rig-on-liner tribometer shows that this

error is attributable to a deficiency in the simulation's characterisation of boundary regime friction.

An oil pump test determines how a modern variable displacement oil pump (and its control system) responds to lowering viscosity. The hypothesis that low viscosity lubricants cause the parasitic load from this component to increase is disproven using this component-level rig test.

Chassis dynamometer testing compares the CO_2 reduction performance of lubricant thermal management systems to the values achieved by reducing the viscosity grade. CO_2 reductions of between 0.4% and 1.0% are identified using a cold-start new European drive cycle (NEDC) with a 5W-30 preheated to 60˚C and 90˚C respectively. Reductions in CO_2 emissions between 0.4% and 1.2% are found on the NEDC by lowering the oil fill volume from 5.1 L to 2.1 L. For the unmodified case, a 3.7% reduction in CO_2 emissions is reported by reducing the viscosity grade from a 5W-30 to an SAE 8 in the NEDC.

The performance of a novel external oil reservoir is simulated to understand its ability to retain oil temperature during the vehicle cool-down procedure. An oil temperature of 65˚C at the end of the soak period (following a prior test where the oil was assumed to reach 90˚C) is predicted by installing insulation to the reservoir and indicates that a viable method to achieve the CO_2 benefits identified through lubricant preheating tests exists.

A full vehicle model combines the outputs from each of these sub-models to predict lubricant performance on the NEDC the new World-wide harmonized light duty test cycle (WLTC). This new approach provides a tool that enables next generation low friction lubricants to be developed. The model predicts that an SAE 8 lubricant can reduce CO_2 emissions by 2.8% on the NEDC and 1.9% on the WLTC compared to a 5W-30. A theoretical experiment, where all lubricant related friction was deleted from the simulation, predicts that lubricant-related CO_2 emissions are 8.7% on the NEDC and reduce to 6.3% on the WLTC. These results indicate that the planned adoption of the WLTC in September 2017 reduces the potential contribution to CO_2 emission reduction from lubricants by 28%.

Table of Contents

1. Introduction 1

1.1. Lubricant composition and evaluation 5

1.2. Low friction lubricant development 7

1.3. A modelling approach to friction reduction 10

1.4. A new approach combining simulations with rig and engine tests 13

2. Viscometric characterisation of lubricants 14

2.2. Viscosity variation with temperature 16

2.3. Viscosity variation with shear rate 17

2.4. Viscosity variation with pressure 18

2.5. Viscosity index (VI) and its limitations for lubricant characterisation 19

3. Lubricant behaviour in journal bearings 24

3.1. Simulation of lubricant performance in a big-end bearing 27

3.2. Validation of the big-end bearing model 47

3.3. Isoviscous lubricants 50

3.4. The effect of VI in the big-end bearing 53

3.5. The effect of shear thinning in the big-end bearing 58

3.6. The effect of lubricant density in the big-end bearing 62

3.7. The effect of piezo-viscosity in the big-end bearing 63

3.8. Chapter 3 conclusions and recommendations 65

4. Piston Friction 69

4.1. Development of a validated piston friction simulation during warm-up 70

4.2. Motored rig testing 70

4.3. Simulation tools and component characterisations 74

4.4. Simulation results and comparison to measured values 82

4.5. Tribometer measurement of the boundary regime friction coefficient..... 86

4.6. Chapter 4 conclusions and recommendations 95

5. Variable displacement oil pumps (VDOPs) using low viscosity lubricants..... 98

5.1. Oil pump design specification 101

5.2. VDOP technology 103

5.3. VDOP performance with low viscosity lubricants 107

5.4. Summary and selection of approach for VDOP characterisation..... 110

5.5. VDOP rig testing 117

5.6. Results 119

5.7. Summary of VDOP performance 129

5.8. VDOP performance in an engine 130

5.9. Chapter 5 conclusions and recommendations 141

6. Lubricant thermal management 146

6.1. Thermal management approaches 149

6.2. Summary and plan for further work 158

6.3. Vehicle testing using two vehicles mounted to chassis dynamometers 159

6.4. Vehicle CO_2 emission changes from lubricant thermal management 160

6.5. Chassis dynamometer test results 163

6.6. Summary of test results 182

6.7. Lubricant thermal management of an external oil reservoir 185

6.8. Chapter 6 conclusions and recommendations 193

7. Vehicle level simulation 198

7.1. Friction calculation approach 200

7.2. Drive cycles 208

7.3. Validation of the vehicle level simulation 209

7.4. Results 210

7.5. Chapter 7 conclusions and recommendations 225

8. Conclusions 230

9. Recommendations for further work 237

10. References 240

1. Introduction

The science of lubricant engineering is compelling and diverse. Almost all moving engine components need lubrication to minimise friction and wear. Hence, lubricant performance is relevant to nearly every powertrain designer. The engineer responsible for developing low friction lubricants requires knowledge of the engine as a whole, its subsystems and constituent components. Drive cycles that include engine warm-up, speed variation and changing loads further complicate the issue and demand an understanding of components' friction in transient conditions. The challenge is both complex and motivating. It requires breadth and depth from the researcher and provides an opportunity to pioneer and innovate, even on cutting-edge engines.

As the study of interacting surfaces in relative motion is crucial in many diverse applications, many researchers have dedicated time to understanding tribology and lubricated contacts. Analysing surface contact is critical to the reduction of friction and wear. Some tribologists extend their research to the performance of a component or subassembly. However, few evaluate the efficiency of all the components in a complete system like an engine. Such insight is crucial, especially in developing low friction lubricants, as the fluid's ability to reduce friction is the summation of its behaviour at the surfaces of each component, and different components operate in different regimes.

Reducing engine friction is important, because this helps to lower engine CO_2 emission and fuel consumption [1], [2], [3], [4]. Most major automotive markets have strict legislative targets enforced by fiscal penalties for vehicle-derived greenhouse gas emissions or fuel economy [5]. Thus, these parameters have focused powertrain and lubricant engineers' research. Large improvements in vehicle efficiency on mandated test cycles have been made through the widespread adoption of technologies such as downsizing or dieselisation. However, there is now increased focus on approaches that

offer smaller, but significant, incremental efficiency benefits such as reducing parasitic losses by addressing engine friction. Low friction lubricants rank highly compared to other technologies on a cost-per-percentage improvement scale [6], [7], therefore, they appeal to engine and vehicle manufacturers [8].

For engines with components operating predominantly in the hydrodynamic lubrication regime, the most significant lubricant parameter that can be changed to reduce friction is its viscosity [9], [10]. In these conditions, a lubricant film separates the surfaces and imposes viscous shear stress on the moving components [11]. Lowering the viscosity reduces this viscous friction. Thus, it is well documented that decreasing viscosity can lower vehicle CO_2 emissions [1], [2], [3], [4].

As film thicknesses become thinner with low viscosity lubricants, the manufacturer and oil provider must cooperate to ensure satisfactory engine lubrication persists. Co-engineering of the engine and lubricant together has been used successfully by some researchers [12], [13] and since vehicle manufacturers and oil classification bodies continue to accept viscosity grades far below those currently in market [14] [15], this research is likely to endure.

Cost-benefit analysis can usefully inform discussions comparing various technologies with lubricant-related CO_2 reductions, but the magnitude of the reduction achievable varies widely. Engine design, vehicle loss factors and the drive cycle dictate the magnitude of friction and its proportion compared to useful work output. Engines with high friction losses, operated at low load, present the biggest opportunity for lubricants to reduce CO_2 emissions, since much of the fuel is combusted to overcome friction. Conversely, engines with low friction losses, operated at high loads, provide the smallest opportunity for lubricants to reduce CO_2 emissions. Additionally, variations in the engines' oil supply pressure and temperature, metallurgies, surface finishes and

speeds, clearances and loads change the tribological contact conditions and the lubricant's behaviour. Thus, a lubricant's capability to reduce CO_2 is application-specific, and one must consider both the engine and drive cycle to understand a lubricant's performance.

Stribeck's work [16] is often used to interpret friction coefficient changes in lubricated conjunctions. His testing revealed that friction depends on viscosity, surface speed and load. For a given viscosity, increasing surface speed allowed the oil film to resist greater loads before it broke down. Similar behaviour was recorded with fixed speed but higher lubricant viscosity. Experiments increasing the force normal to the surface caused oil film breakdown sooner, indicating an inverse relationship with load. Stribeck discovered that the relationship between these factors and friction coefficient took the form:

$$f \propto \frac{\mu V}{L} \tag{1}$$

where f is the friction coefficient, μ is the viscosity, V is the relative surface speed and L is the load.

His discoveries had long-lasting relevance and remain applicable today. Figure 1 shows a stylised Stribeck curve. On the right of the curve, a thick lubricant film separates the surfaces and the losses are attributable to viscous shear effects. This regime is termed hydrodynamic. Under conditions of high oil film pressure (e.g. >100 bar) an elastohydrodynamic condition prevails in this area and the load is supported by lubricant piezo-viscosity increase and local elastic deformation of the surfaces. On the left of the curve, the contact force is supported by direct interaction between the two surfaces. Microscopic asperity-to-asperity contacts transfer the load. This regime is termed boundary contact. Between these two regimes a friction minima

exists and contributions from asperity-to-asperity contact and hydrodynamic pressures support the load. This regime is termed mixed.

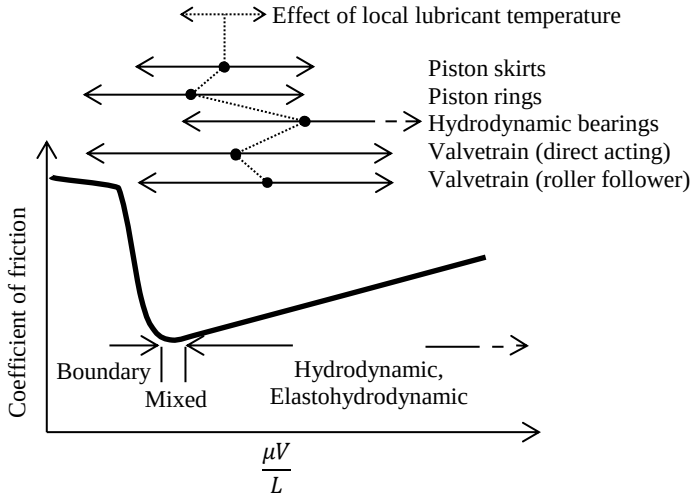

Figure 1. Stribeck curve. μ is the viscosity, V is the relative surface speed and L is the load.

Figure 1 approximates the operating location of various engine components on the Stribeck curve. Each component's differing surface speeds, loads and local lubricant viscosities underpin their locations. These variations mean each component needs different characteristics from a lubricant to achieve low friction levels. Moreover, even at steady engine conditions, a single component's working position on the Stribeck curve can vary within each firing cycle due to temporal and cyclical load variations.

Theoretically, the mean position for all engine components can be plotted as a single point on the Stribeck curve. Reducing the lubricant viscosity causes this point to shift from right to left. This change could result in a total friction reduction if the system's operation were on average hydrodynamic. However, with this same change, some components transition into the mixed and even boundary lubrication regimes. If a significant number of subsystems fall in the boundary contact regime, an overall friction increase for the engine can occur [3]. Advanced lubricant formulations and engine design changes can control this behaviour. Lubricant engineering is the study of these

effects in order to increase the robustness of the formulation process and so enable low viscosity lubricants to keep assisting in the reduction of vehicle CO_2 emissions.

A lubricant's primary purpose is to reduce friction, but its functional specification includes:

1. minimising wear of components
2. transferring hydraulic power to actuate components such as variable valve timing systems, tappet lash adjusters and timing chain tensioning systems
3. cooling through direct heat transfer with engine surfaces
4. cleaning through the control of carbonaceous deposits, removal of wear debris and dispersion of soot
5. chemical control of their own oxidative degradation
6. sealing (e.g. in the piston ring-to-liner contact and in the control of engine seal thermal and chemical degradation)
7. reduction in engine noise by hydraulic damping in tribological contacts

1.1. Lubricant composition and evaluation

An engine lubricant contains a variety of different chemicals to achieve its performance level. Figure 2 shows a typical passenger car lubricant's composition. The formulation comprises of around ten components. Base oil, a refined crude oil, dominates the oil's mass composition. Numerous (e.g. over 300) base oil variants are available to the formulator, each with different characteristics. However, cost-saving targets and regional availability may restrict the formulator to around five options.

Usually, viscosity modifiers form the second largest constituent after the lubricant mass. The proportion of viscosity modifiers depends on the desired lubricant viscosity. Different modifiers exist but each of these causes the lubricant viscosity to vary with shear rate. Under normal conditions, this process is reversible and the viscosity

reduction occurs only while the shear stress is present. However, permanent viscosity reduction is also possible if the viscosity modifier molecular structure is broken, e.g. under extreme contact conditions [17].

The other additives give the lubricant the chemical capability it needs. A similarly numerous variety of additives is available in each category. Alongside their primary chemical functions, these components affect the lubricant's viscosity and the friction coefficient in the boundary regime.

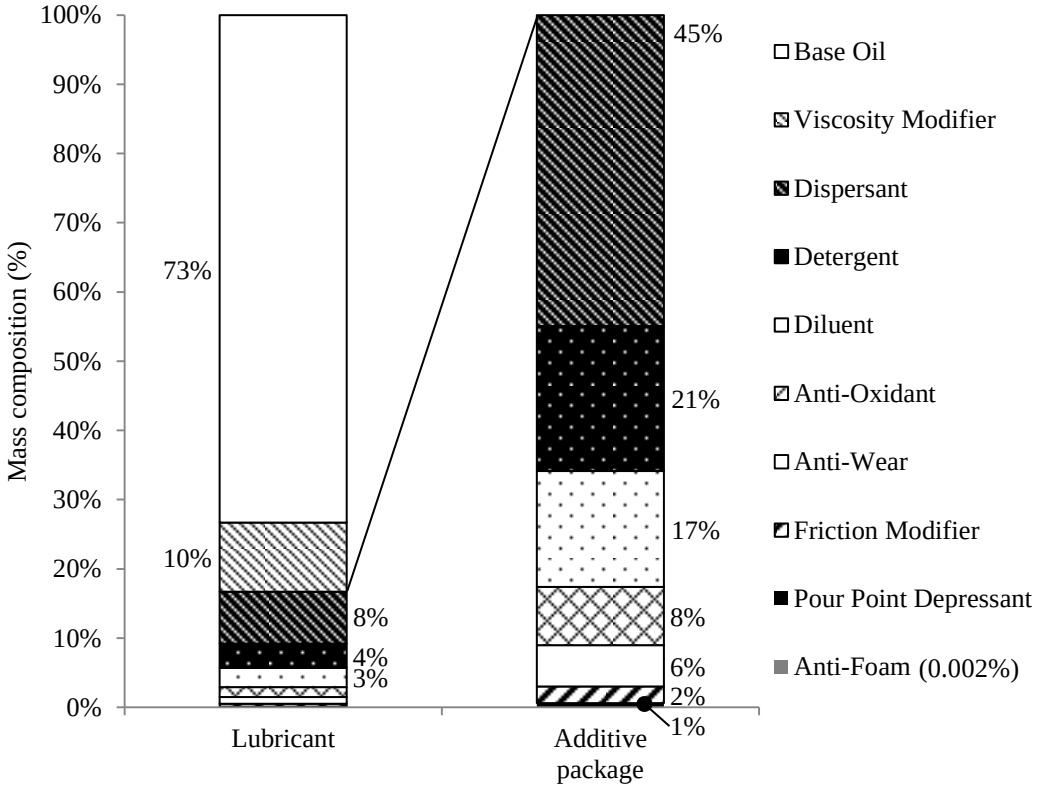

Figure 2. Chart showing the composition, by percentage mass, for a passenger car lubricant.

Lubricant composition varies widely due to the large choice of base oils and chemical additives described. Consequently, a performance specification is achievable in a number of ways. The global availability of the raw materials, local patent protections and strategic supply arrangements add variables that influence a lubricant's chemistry. These factors, alongside cost targets, trade secrets, tacit knowledge and marketing demands lead to performance variations from different lubricant brands.

The present research focuses on improvements in lubricant frictional performance. However, it is understood that compromise may be required in developing a lubricant to provide optimal friction reduction while achieving its other functional requirements and cost targets. The detailed nature of the compromise is left for future research.

1.2. Low friction lubricant development

To evaluate the performance of different lubricant compositions, consortia of manufacturers, lubricant developers and governing bodies have defined specifications comprising chemical, subsystem and engine tests. Both the test type and performance level defines the lubricant's acceptability [18], [19]. This work relies on empiricism.

Chemical tests on lubricants include investigating its ability to neutralise acid, chemical concentration levels of sulfur and phosphorous (for compatibility with exhaust catalysts), volatility and quantification of its remaining ash mass after combustion. Subsystem tests include investigating any antagonistic effects with engine seals and compatibility with biofuels. Mechanical tests include the use of fully-fired engines to evaluate deposit formation, sludge, wear, soot dispersion, viscosity change and fuel economy.

A full list of requirements can be found in [18] and [19]. Whether a lubricant achieves these specifications (or exceeds them) is decided by the lubricant manufacturer, who is also free to market lubricants not explicitly covered by any specifications [20].

To develop low friction lubricants, fuel economy tests from both the American Petroleum Institute[1] (API) and the Association des Constructeurs Européens

[1] Individual tests within these specifications are developed by the American Society for Testing Materials (ASTM)

d'Automobiles[2] (ACEA) are often used. API use the ASTM Sequence VID (ASTM D7589) [21] in their latest GF-5 specification test to determine a lubricant's fuel economy versus a 20W-30 reference oil. The test uses a 3.6 L V6 General Motors LY7 engine. Roller followers actuate the valves. The engine's earliest production date was circa 2004. ACEA uses the CEC L-054-96 engine test [22] to determine a lubricant's fuel economy improvement versus a 15W-40 reference oil. The test uses the 2.0 L 4-cylinder gasoline Mercedes-Benz M111 E20 engine. Direct-acting tappets activate the valves, increasing the magnitude of boundary friction in the engine [23]. The engine's earliest production dates back to the 1990s. The widespread use of API and ACEA specifications means these tests often determine the performance of new formulations or chemical components. However, this empirical process is expensive and time-consuming, and the engine technologies are outdated.

Focused on improving this situation, research projects [10], [24], [25], [26] performed correlation exercises comparing the lubricant's performance in engines to that in smaller, cheaper, and faster-to-run rig tests. However, this approach is often still inefficient and subject to error [10]. It favours correlation over causality, generally relying on statistical comparisons between the rig and engine to inform the performance evaluation. Moreover, this methodology does not address the issue that industry-defined test engines and procedures lag behind the rate of new engine technology development. Thus, if good performance in the industry-standard tests is prioritised, the formulation of 'low friction lubricants' may then be most suitable for a substantially different engine technology to that on which it is used in the real world.

In some cases, a co-engineering approach has recently been adopted in which lubricant manufacturers have been working with the engine manufacturer to develop

[2] Individual tests within these sequences are developed by the coordinating European council (CEC) for the development of performance tests for lubricants and engine fuels.

lubricants tailored to the latest engine designs [12], [13]. This modern methodology provides the engineer with a new paradigm. It becomes possible to understand a single engine's appetite for the lubricant's properties and to engineer the lubricant to meet these requirements. Ford and BP achieved a 1.3% CO_2 reduction (in comparison to a lubricant of the same viscosity grade) in the new 1.0 L EcoBoost engine using this technique [12]. However, the variety and complexity of the tribological interactions in an engine mean this performance improvement is still achieved using a time-consuming and expensive testing process, e.g. fitting the engine to a dynamometer and running hundreds of tests. Typically, co-engineering a lubricant can take from six months to several years depending on the project's scope and the number of drive cycles studied.

This empirical method precludes detailed understanding of how the lubricant achieves its low friction level, thus preventing the scientist from understanding:

1. why any given physical or chemical parameter of the lubricant may correlate with reducing CO_2
2. how a lubricant's performance may shift between engine types or drive cycles
3. how to predict the effect of emerging engine hardware technologies (e.g. start-stop systems, thermal management technologies, variable displacement oil pumps, roller-follower valvetrains, cylinder axis offset, surface texturing, downsizing or down speeding) on the ability of low friction lubricants to reduce CO_2 emissions

Developing lubricants in this way is also expensive, requiring specialist equipment and facilities. The continuing importance of addressing friction-related CO_2 emissions and the adoption of co-engineering philosophy creates an opportunity for the use of alternative methods that can provide greater insight in to the formulation process and reduce the time required to get products to market.

1.3. A modelling approach to friction reduction

Theoretically, the shortcomings of empirically-focused lubricant development can be overcome with modern engine friction-modelling computer programs. Using such component-level simulations should allow friction changes to be understood as the viscosity is lowered. Components transitioning from hydrodynamic to boundary contact regimes can be identified and the effect of changing lubricants' properties investigated (e.g. pressure viscosity coefficient, shear viscosity behaviour, density, viscosity index and boundary friction coefficient). Incorporating these friction models into vehicle-level simulation would allow novel research into the changing contributions to friction reduction on modern legislative drive cycles. The insights from such work would be valuable to lubricant development and lowering friction in engine design. This approach requires high fidelity, component-level models to be developed to characterise lubricant behaviour, and that these are close-coupled to form a holistic engine model.

Many authors [27], [28], [29], [30] predicting engine friction cite Patton et al's work [31] or later improvements by Sandoval and Heywood [32]. This approach characterises measured friction using an equation defined for key sub-assemblies in the engine. However, the equations do not attempt to model surface interactions, or lubricants' non-Newtonian behaviour. Thus, they cannot resolve friction changes between hydrodynamic, mixed and boundary regimes, limiting their use in developing low friction lubricants.

Thring [33] applies a friction model to analyse engine behaviour. For most components, he predicts friction using a Stribeck characterisation:

$$f_c = \left(\frac{\eta V_c}{W_c}\right) \tag{2}$$

where f_c is the friction coefficient for component c, η is the oil viscosity, V_c is the component's surface speed (e.g. the piston speed), W_c is the component's load.

This approach faces similar shortcomings to those of Patton et al. [31] and Sandoval and Heywood's [32]. Thring [33] uses a more detailed camshaft to follower friction model in his work. Crane and Meyer [34] developed this sub-model using the oil film thickness equations defined by Dowson and Higginson [35]. This model uses an approximate form of the Reynolds equation in a Hertzian contact. Boundary friction is not included nor is assessment of component deflection under load. The approach differs from the work of Patton et al. [31], but still lacks the fundamental tribology model required to assess lubricant behaviour.

Goenka et al. [30] describe their development of General Motors' Friction and Lubrication Analysis of Reciprocating Engines (FLARE) software. The software focuses on engine design rather than lubricant development. Thus, they make various simplifications, which limit its use for assessing lubricant performance. Goenka and Meernik [36] describe FLARE's piston skirt model. Surface roughness is not accounted for in the piston skirt and liner characterisation, making robust assessment of boundary friction impossible. FLARE predicts friction in the bearings, skirt, rings and valvetrain. Other subsystems, such as the oil pump, seals and auxiliary drives are not characterised.

Taylor and Coy [37] and Taylor [38], [23] discuss a more fundamental approach to friction simulation. They use tribological models incorporating non-Newtonian viscosity characterisation to predict friction. Taylor and Coy [37] model the Ford 4.6 L V8 engine being operated in the sequence VI A[3] fuel economy test defined by the API [19]. They conclude that simulating engine friction in this way is a viable method to understand lubricant performance in fuel economy tests. Their predicted ordering of friction for two oils correlates to the ranking from fuel economy tests, although they do not say if their model can predict fuel economy directly. Taylor [38] simulates a generic

[3] This engine test was used in the GF-2 specification, which became obsolete in March 31, 2002.

high-speed motorsport engine and passenger car engine. The investigation describes friction reduction occurring when the viscosity grade is reduced from 20W-50 to 0W-20. The friction contributions from the valvetrain, pistons and bearings are reported under steady state conditions. The viscosity variation of the lubricants with temperature, shear and pressure is characterised. However, Taylor [38] does not report work which interprets friction changes occurring when these parameters are varied. Taylor [23] also analyses the Mercedes-Benz M111 2.0 gasoline engine used in ACEA's M111 fuel economy test [18]. He predicts the contribution to friction from the lubricant at the valvetrain, pistons and bearings for cold start and fully warm conditions. His focus is on understanding the engine's proportion of hydrodynamic and boundary friction in this cycle to inform whether either reducing viscosity or increasing friction modifier levels were likely to improve fuel economy.

Ma et al. [39] develop Taylor et al's work [37], [38], [23] to predict fuel economy using low friction 5W-30 and 0W-20 lubricants. They use the M111 FE (CEC L-054-96) and Sequence VID (ASTM D 7589) in their model validation and predict fuel economy for three passenger cars over drive cycles. Their simulation predicts fuel economy reduction of 10.6% to 17.3% in the idealised case where all lubricant-related friction is deleted. They propose that in practice 30% of this reduction is achievable, suggesting lubricants could reduce fuel consumption by 3.2% to 5.2%.

A review of recent literature indicates that Taylor and Coy [37], Taylor [38], [23] and Ma et al's work [39] comes closest to satisfying the aims of the present research. However, more work is needed to: interpret how CO_2 emission reductions are achieved on modern drive cycles (e.g. the World-wide harmonized Light duty Test Cycle or WLTC); bring the research up-to-date using modern downsized engines; use the models to inform what lubricant properties are desirable (i.e. to engineer the lubricant); and investigate behaviour with new very low viscosity lubricants. Furthermore, whilst

lubricants can provide component-level friction reduction, the associated changes in whole engine performance (e.g. due to variation in hydraulic power demands to pump lubricant through the oil circuit and lubricant derived variations in engine thermal balance) can have a significant impact on the measured fuel economy performance, although these changes are, as yet, undocumented.

1.4. A new approach combining simulations with rig and engine tests

The present research develops a new approach in order to provide detailed understanding into methods of lubricant-related friction reduction in modern engines. Tribological simulations are used to predict friction based on the non-Newtonian physical parameters of lubricants using realistic surface and geometric models. To improve the model's output, component-level rig, engine and chassis dynamometer tests offer results that supplement the simulation results to define the lubricant behaviour. A new vehicle-level model, built using these results, predicts the performance of lubricants over drive cycles. The lubricant engineering approach pioneered in this research allows the engineer to interpret how low friction lubricants achieve CO_2 emission reductions on drive cycles, alongside enabling the design of new lubricants (and engine components) to improve the performance of modern internal combustion engines. The approach is also valid for other powertrain systems, provided they are lubricated.

2. Viscometric characterisation of lubricants

The SAE J300 oil viscosity classification [15] specifies limits that categorise engine lubricants into grades based on their rheological performance. J300 uses dynamic and kinematic viscosity (KV)[4] results from four viscometers. Each instrument measures viscosity at various temperatures and shear rates. Table 1 lists the specifications for each grade. Cold viscosity tests (e.g. -35˚C for the 0W grade) at shear rates replicating cold cranking (specified as between 10^4 s^{-1} and 10^5 s^{-1}) [40] and under pumping conditions (e.g. -40˚C for the 0W grade) define lubricants' low temperature performance (historically its winter behaviour). High temperature performance (historically its summer behaviour) is addressed by measuring KV100 in low shear conditions, e.g. with a Houllion viscometer's capillary tube [41]. High-temperature-high-shear (HTHS) behaviour is tested at 150˚C and 10^6 s^{-1} for all grades [42].

Table 1. Summary of viscosity grade criteria listed in SAE J300.

SAE viscosity grade	Low-temperature cranking viscosity (mPa.s). Max.	Low-temperature pumping viscosity (mPa.s). Max with no yield stress.	Low-shear-rate kinematic viscosity (mm^2/s) at 100°C. Min.	Low-shear-rate kinematic viscosity (mm^2/s) at 100°C. Max.	High-shear-rate viscosity (mPa.s) at 150°C. Min.
0W	6200 at -35°C	60 000 at -40°C	3.8	—	—
5W	6600 at -30°C	60 000 at -35°C	3.8	—	—
10W	7000 at -25°C	60 000 at -30°C	4.1	—	—
15W	7000 at -20°C	60 000 at -25°C	5.6	—	—
20W	9500 at -15°C	60 000 at -20°C	5.6	—	—
25W	13 000 at -10°C	60 000 at -15°C	9.3	—	
8	—	—	4	<6.1	1.7
12	—	—	5	<7.1	2
16	—	—	6.1	<8.2	2.3
20	—	—	6.9	<9.3	2.6
30	—	—	9.3	<12.5	2.9
40	—	—	12.5	<16.3	3.5 (0W-40, 5W-40, and 10W-40 grades)
40	—	—	12.5	<16.3	3.7 (15W-40, 20W-40, 25W-40, 40 grades)
50	—	—	16.3	<21.9	3.7
60	—	—	21.9	<26.1	3.7

[4] When a kinematic viscosity is referenced it is denoted as KV followed by a number representing the temperature in degrees Celsius, e.g. the kinematic viscosity at 100˚C becomes KV100.

The J300 specification was recently revised [14] [43]. Classification of a new SAE 16 viscosity grade in April 2013 and SAE 12 and 8 grades in January 2015 were milestones for low friction lubricants. These new grades facilitate engine designers and lubricant manufacturers specification and development of modern low viscosity, low friction oils suitable for the latest generation of engines.

2.1.1. Lubricants used in the present research

The present research focuses on three viscosity grades: 5W-30, 0W-20 and the new SAE 8. Table 2 shows the key attributes of these lubricants. *T* is lubricant temperature.

Table 2. Summary of test lubricants.

	5W-30(R)[5]	5W-30	0W-20	SAE 8
BP Code	A0364P/265C	A09040P/069A	A1293P/176A	E0966A/005A
KV120 (cSt)ˆ	6.64	8.0	6.11	3.84
KV100 (cSt)	9.7	11.7	8.5	5.4
KV90 (cSt)ˆ	12.06	14.6	10.26	6.57
KV40 (cSt)	55.0	68.0	36.7	26.0
KV20 (cSt)ˆ	137.25	170.0	77.17	60.39
Viscosity index	163	169	220	149
HTHS (cP)	3.0	3.5	2.6	1.9
Density (kg/m^3) at temperature, *T*	862.2 -0.623 * *T*	860.6 -0.623 * *T*	851.4 -0.648 * *T*	844.2 -0.633 * *T*
Specific heat capacity at 20˚C ($J\ kg^{-1}\ K^{-1}$)	2232	2049	-	2022
Specific heat capacity at 90˚C ($J\ kg^{-1}\ K^{-1}$)	2502	2323	-	2253
Base oil grade	Group 3	Group 3	Group 3 Plus	Group 4
Specification	ACEA A5/B5-12, API SN and GF-4	ACEA C3-12	Equivalent to GF-5	Not classified

The lubricants' physical measurements were made using BP's analytical internal testing facility and a third party supplier.

[5] 5W-30(R) is a 5W-30 used in Chapter 6 as a reference lubricant during chassis dynamometer testing
ˆ Calculated values

2.2. Viscosity variation with temperature

The Walther (3) and Vogel equations (4) calculate viscosity variation with temperature. The present research uses them interchangeably. The Walther equation takes the form:

$$\log(\log(\mu + k)) = A + B \log T \tag{3}$$

where μ is the lubricant kinematic viscosity, k is a constant equal to 0.6, A and B are empirically derived constants and T is the absolute temperature of the lubricant. A and B can be calculated by substituting empirically measured viscosities for the lubricant at two temperatures, frequently 40˚C and 100°C [44].

The Vogel equation takes the form:

$$\log\left(\frac{\mu}{a}\right) = \frac{b}{T + c} \tag{4}$$

where μ is the kinematic viscosity of the lubricant, a, b and c are empirically derived constants and T is the absolute temperature of the lubricant. Three viscosity measurements are required to define the constants.

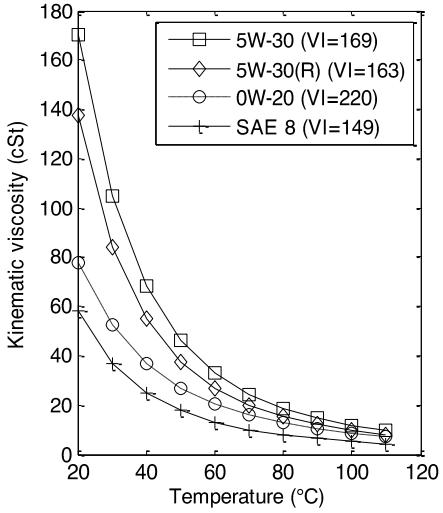

Figure 3. Variation of kinematic viscosity with temperature for the lubricants defined in Table 1.

Viscosity follows a logarithmic increase with reducing temperature. Thus, its magnitude becomes large under cold conditions. This behaviour increases engine

friction [45], [46]. Figure 3 shows the KV variation with temperature for the lubricants in this research. Lowering the viscosity grade reduces the viscosities of the lubricants at low temperature, which helps CO_2 emission reductions in drive cycles including warm-up. However, lubricant composition changes can also allow viscosity reduction within a grade. Figure 3 demonstrates that lubricants of the same grade (cf. 5W-30(R) and 5W-30) can have different low temperature viscosities. This variation highlights a requirement to understand more detail than solely the viscosity grade when assessing lubricant performance.

2.3. Viscosity variation with shear rate

The present research uses the Cross equation [47] to define lubricant viscosity variation with shear rate:

$$\mu = \mu_\infty + \frac{\mu_0 - \mu_\infty}{1 + \left(\frac{\gamma}{\gamma_c}\right)^m} \quad (5)$$

where $\mu(\gamma)$ is the lubricant viscosity at shear rate, γ, μ_∞ is the fully shear-thinned lubricant viscosity (also known as the viscosity in the second Newtonian regime), μ_0 is the zero-shear lubricant viscosity (equal to the 'low shear' dynamic viscosity measured for calculation of lubricant viscosity variation with temperature), γ_c is the shear rate at which the lubricant viscosity is equal to the mean of μ_0 and μ_∞ and m is a dimensionless parameter which can be derived empirically.

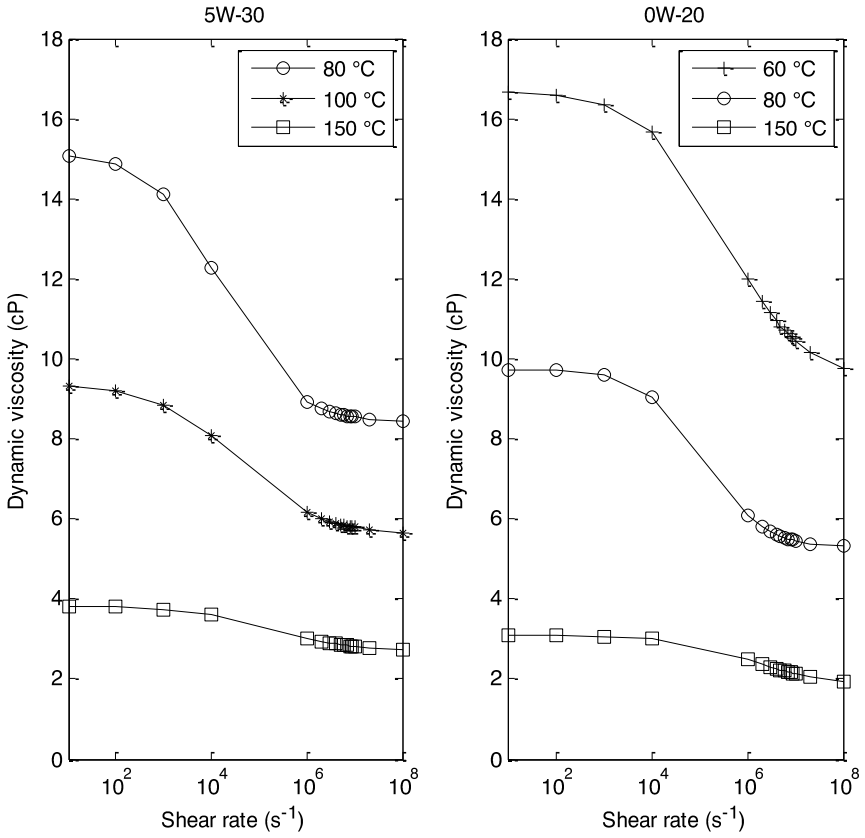

Figure 4. Variation of viscosity with shear rate for 5W-30 and 0W-20.

Figure 4 shows measured viscosity for the 5W-30 and 0W-20 under shear rates to 10^8 s^{-1}, taken using a PCS Instruments Ultra Shear Viscometer. The viscosity of the SAE 8 did not reduce under shear, as it is a monograde.

2.4. Viscosity variation with pressure

The Barus equation defined the lubricants' viscosity change with pressure using:

$$\mu = \mu_0 e^{\alpha P} \tag{6}$$

where μ_0 is the lubricant viscosity at atmospheric pressure, α, is the piezo-viscosity coefficient, which can be derived empirically, and P is the local oil film pressure.

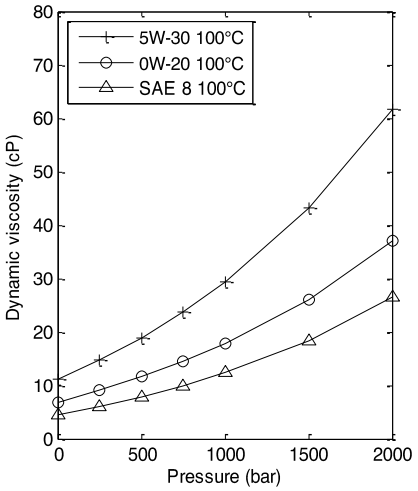

Figure 5. Variation of viscosity with pressure for 5W-30, 0W-20 and SAE 8.

A high-pressure rheometer measured the viscosity variation with pressure for each lubricant. Figure 5 shows the test results.

2.5. Viscosity index (VI) and its limitations for lubricant characterisation

Comparing the viscosity-temperature performance of different lubricants has been attractive to lubricant formulators for many years. The prevailing system today is the viscosity index (VI) deriving from Dean and Davis' work [44], [48]. API 1509 [19] uses the VI method as a performance criterion for base oils. Lubricant engineers influence performance at low temperatures by choosing base oils and adding polymeric additives. A plurality of these additives, known as VI improvers or modifiers, is available.

A lubricant's VI is determined by comparing it to historic reference lubricants, refined from Pennsylvania and Gulf Coast crude oils [44], [48]. Base oils and fully formulated lubricants' VI's can be evaluated this way. The two reference oils were refined into a range of base oil viscosities (a family or slate) that had KV100s of between 2 cSt and 70 cSt. The Pennsylvania oil showed a low viscosity change with temperature and was designated a VI of 100. The Gulf Coast oil had a large viscosity change with temperature and was designated a VI of 0. Lubricants whose viscosity change lay between these values were given VIs from 0 to 100. ASTM D2270-10 [49]

tabulates the KV40s for the two reference lubricants (H and L for Pennsylvania and Gulf Coast respectively), alongside describing the VI calculation method.

The VI calculation method is discontinuous and separated into three conditions encompassing lubricants whose VI is: 1) lower than 100; 2) equal to 100; and 3) greater than 100. The VI of contemporary fully formulated lubricants often exceeds 100, so calculations falling within option 3 are normal, and the VI is calculated using:

$$VI = \frac{(10^N - 1)}{0.00715} + 100 \tag{7}$$

where:

$$N = \frac{\log H - \log U}{\log Y} \tag{8}$$

where H is the KV40 for the 100 VI reference having the same KV100 as the new oil, U is the new oil's KV40 and Y is its KV100.

Equation (7) causes VI calculations to respond counterintuitively for new low viscosity lubricants (e.g. low Y values), and for high VI fluids, where Y and U are similar sizes. This behaviour is explicable by considering lubricants with a high VI. For these oils U tends to Y, so N can be defined with:

$$N \rightarrow \frac{\log H - \log Y}{\log Y} \tag{9}$$

which can be simplified to:

$$\boldsymbol{N \rightarrow \frac{\log H}{\log Y} - 1} \tag{10}$$

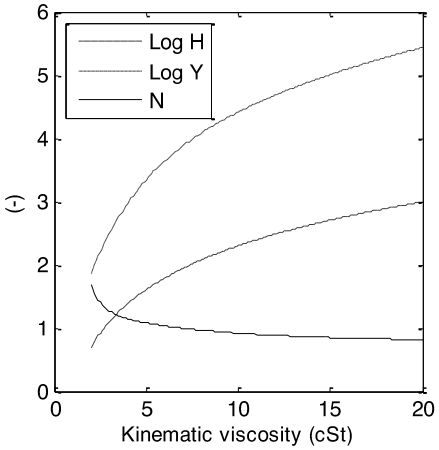

Figure 6. Variation of N with KV100 where *U* tends to *Y*.

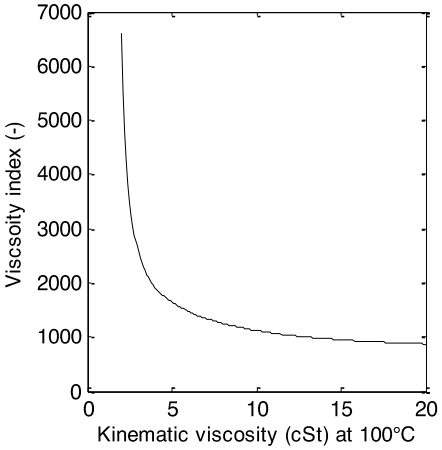

Figure 7. Variation of viscosity index with KV100 for a range of isoviscous fluids.

Figure 6 plots this equation for different KV100 values. *N* becomes increasingly non-linear at low viscosity values (<5cSt KV100), which is critical in VI calculations for lubricants below SAE 16. Figure 7 shows the effect of varying this parameter on VI. It plots the calculated VIs for an extreme case of idealised isoviscous fluids. The graph is non-linear at low viscosity values, causing the achievable VI to vary with the KV100. This behaviour can undermine the use of VI to assess viscosity change when comparing lubricants of different KV100s. Practically, this issue commonly occurs as formulators compare the performance of lubricants from different viscosity grades [7]. However, few realise the method's limitations [48]. Zakarian [48] completed work to understand the limitations of the VI method, concentrating on the performance of base oils. He also discovered that a limitation exists in this method, although he arrived at this conclusion through empiricism.

2.5.1. ASTM D2270-10's shortcomings for new lubricants

The lubricant viscosity ratio, x, is defined as:

$$x = \frac{KV40}{KV100} \tag{11}$$

This ratio allows comparison of a range of lubricant viscosities. Figure 8 shows the VIs for x from 1 (idealised isoviscous fluid) to 3. As the KV100 is lowered, the VI becomes non-linear and varies with different x values. Where $x < 2$, the VI increases as the KV100 is reduced. However, where $x > 2$, the VI decreases with the KV100.

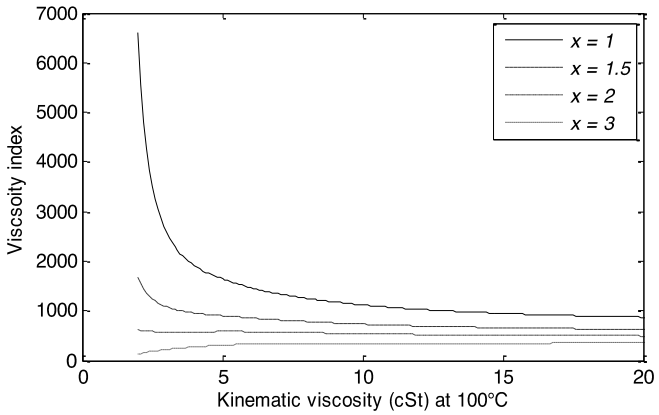

Figure 8. Calculated VI for a range of *x* values.

Table 3 compares the calculated VIs for two lubricants with different KV100s. The higher viscosity lubricant has a smaller range of achievable VI values, with a maximum value of 1119, compared to 1646 for the lower viscosity case. Thus, the VI calculation is less sensitive to changes in low temperature viscosity as the KV100 is increased. This behaviour causes the calculated VI to be higher despite an equivalent x value (cf. 192 for the 5W-30; 129 for the SAE 8 at $x = 5$), and further confuses engineers attempting to compare the lubricants.

Table 3. Comparison of VIs for 5W-30 and SAE 8 lubricants.

Viscosity grade	KV100 (cSt)	KV40 (cSt)	*x (*KV40/KV100)	VI (ASTM method)
5W-30	10	50	5	192
	10	40	4	250
	10	30	3	347
	10	20	2	541
	10	10	1	1119
SAE 8	5.0	25	5	129
	5.0	20	4	192
	5.0	15	3	310
	5.0	10	2	586
	5	5	1	1646

2.5.1. A resolution to ASTM D2270-10's shortcomings for new lubricants

This analysis shows that using VI can be misleading, particularly in developing low friction lubricants. A remedy is to use KV measurements at the engine starting temperature and at its peak temperature in the test cycle. This approach avoids the complexity of the VI, while allowing a direct comparison of the KVs to inform lubricant choices. The recent introduction of the SAE 16, 12 and 8 grades into SAE J300 and the widespread use of VI to judge lubricants performance make communication of the method's limitations and this proposed solution important.

3. Lubricant behaviour in journal bearings

Engine designers frequently use journal bearings to support automotive engines' rotating components [50]. These bearings are usually called hydrodynamic since in their intended operation lubrication is primarily in the hydrodynamic regime. Typically, both the crankshaft and connecting rod assemblies, as well as components such as the camshaft and oil pump use this bearing type. The key components in a journal bearing system are the journal, bearing and lubricant. The journal and bearing are notionally circular, but the journal is slightly smaller than the bearing to provide clearance for an oil film. The clearance size is significant to the bearing's performance [51].

In normal operation, the bearing receives a steady lubricant supply, so an oil film separates the running surfaces. Thus, the journal load is supported by the lubricant then passed into the bearing. If the load's direction reverses so does the load path, i.e. load is transferred from the bearing into the lubricant then into the journal. Hence, the lubricant is critical to the bearing's load carrying, wear protection and frictional performance. When the bearing or journal is loaded, the journal moves to a position eccentric from the bearing's geometric centre. This movement occurs because the lubricant's entrainment into the converging gap between the journal and bearing (caused by journal rotation) generates a hydrodynamic pressure that supports the load.

Figure 9 depicts a loaded journal, showing that oil film thickness varies with the bearing angle, *Ø*, due to its eccentricity. If the oil film breaks down, or its thickness is insufficient to separate the surfaces, the bearing and journal may touch. The resultant interaction leads to significant, and undesirable, bearing wear [51], [52].

The combustion chamber pressures, alongside the component inertial forces from rotating and reciprocating motion, generate the loads imposed on the crankshaft and connecting rod big-end bearings. Thus, the loading profile for a typical automotive

engine crankshaft and connecting rod big-end bearings is temporal and cyclical in nature. Speed and load variations occur due to driver-imposed changes and, even at a nominally steady condition, intra-cyclic rotational speed variations occur due to the unsteady forces acting on the system, the changes in system effective inertia over a cycle and the crankshaft's torsional flexibility.

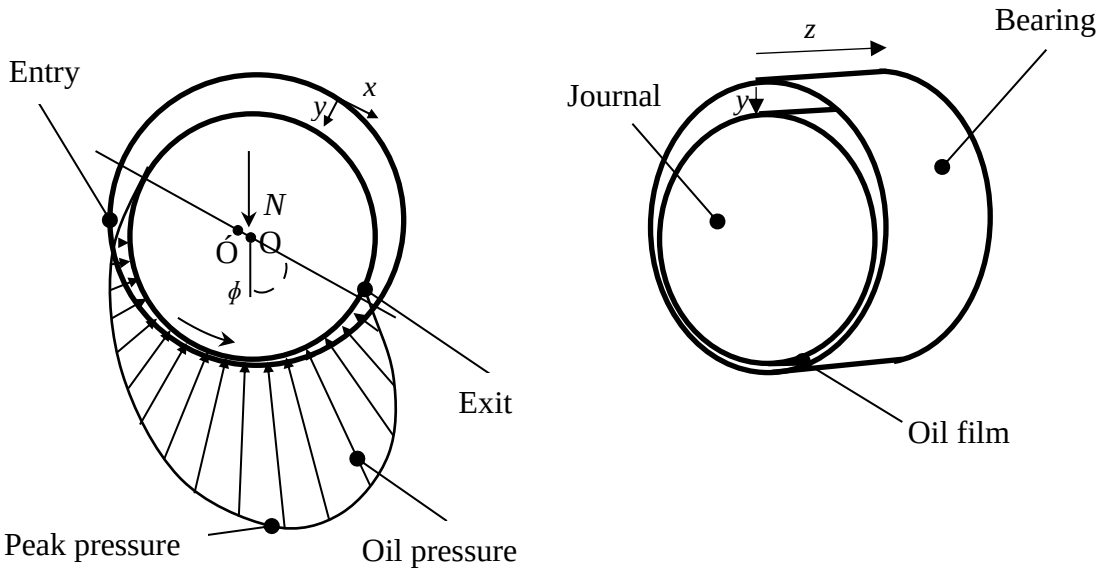

	Entry	Peak pressure	Exit
Pressure (MPa)	0.4	117	0.1
Temperature (˚C)	120	125	130
Shear rate (s^{-1})	0	$2x10^{7}$	0

Figure 9. Schematic and cross section of plain journal bearing showing location of coordinate axis and typical variation in lubricant temperature, pressure and shear rate. Figure adapted from [51].

N is the load on the journal, Ó is the geometric centre of the bearing shell, O is the rotational centre of the journal, *y* is the characteristic dimension through the oil film, *x* is the characteristic dimension along the bearing length, *z* is the characteristic dimension along the bearing width, Ø is the angle from the vertical and the length of the arrows indicates the relative size of the hydrodynamic pressure in the oil film.

As the lubricant travels through the bearing, its viscosity changes due to the oil film's variation in pressure, temperature and shear rate. Figure 9 shows lubricant pressure, temperature and shear rate values for the big-end bearing system of a 1.6 L

4-cylinder turbocharged passenger car engine, at 2000 rev/min and full load. The simulation model described later in this chapter generated the data in the figure.

The data in Figure 9 shows that the local values for bearing oil pressure, shear rate and temperature vary spatially. The oil film pressure is predicted to vary from the supply pressure, about 0.4 MPa absolute, to 117 MPa at the point of peak hydrodynamic pressure, and then to a low pressure condition at the bearing exit. The final low pressure is typically the crankcase pressure. The shear rate is predicted to vary from a nominal level to $2x10^7\ s^{-1}$ at minimum film thickness, then to reduce to zero at the bearing exit. The oil film temperature is predicted to increase by 10 K due to friction losses being dissipated as heat and the combined effects of conduction, convection and advection.

The lubricant's non-Newtonian behaviour causes viscosity to change in response to the local variations in pressure, shear rate and temperature. The resultant net viscosity is a function of the lubricant's piezo-, shear and thermal viscosity behaviour[6]. The tribological contact conditions are interdependent with the lubricant viscosity so detailed analysis of the lubrication regime normally requires the use of a simulation.

Typical friction loss across all big-end bearings for a 4-cylinder gasoline passenger car engine at 2000 rev/min and 90˚C lubricant temperature is 5% of the total engine friction in motored conditions. The frictional loss from the main bearings in similar conditions is 6% to 15% [53]. Thus, the bearing system's contribution to total engine friction is significant and attempts to reduce these losses warrant investigation.

Being able to change the lubricant's viscometric response, by changing the lubricant chemical formulation, makes it is possible to change the bearing's friction. A simulation model is built in this study to predict the friction in a bearing system when

[6] The equations that describe the variation of viscosity with temperature, pressure and shear rate are given in section 2.2 through to 2.4.

lubricant viscosity parameters are varied. The correlations between predicted friction and lubricant viscosity index, temporary shear, density and piezo-viscosity are studied. The importance of each input variable was evaluated using a simulation run matrix where the input values were systematically perturbed to see their impact on the outcome. The results generated for the lubricant form the basis for the discussion below.

3.1. Simulation of lubricant performance in a big-end bearing

A mathematical simulation model of a big-end bearing from a 1.6 L 4-cylinder turbocharged passenger car engine was built for this study. Table 4 details the engine from which the bearing system was analysed. The engine uses hydrodynamic shell-type bearings. Table 5 gives the bearing's composition and characteristic dimensions which were measured on section cut through a bearing shell using a scanning electron microscope.

Table 4. Description of test engine on which the bearing simulation was based.

Engine Type	EP6 CDTX
Manufacturer	PSA group
Power (kW)	147
Torque (Nm)	270
Capacity (cc)	1598
Stroke (mm)	85.8
Bore (mm)	77
Cylinders	4
Fuel type	Gasoline
Injection	Direct
Valvetrain	Double VANOS[7] & variable lift
Connecting rod length (mm)	138.5
Connecting rod mass (g)	497.1
Piston assembly mass (g)	350.9
Cylinder centre distance (mm)	84.0
Oil feed hole diameter (mm)	7.8

This engine was chosen as representative of downsized, boosted gasoline engines that are typical in the European marketplace. The engines were taken from a selection of both new and used stock so that tests and measurements could be completed. In service, these engines were fitted to 2011/2012 Peugeot RCZ and 207 GTi road cars.

[7] Variable Nockenwellensteuerung (VANOS) is a variable valve timing system produced by Bayerische Motoren Werke AG (BMW group)

Table 5. Specification of the big-end bearings used in the EP6 CDTX test engine.

Bearing Type	Plain Bearing
Metallic composition of bearing surface	86% Aluminium 13% Tin 1% Copper
Bearing journal nominal diameter (mm)	45.3
Bearing effective length (mm)	16.3
Notional diametric bearing clearance (mm)	0.076
Bearing temperature (˚C)	120

Research precedent allows accurate modelling of bearing and lubricant behaviour. Table 6, points 1 to 4, list Zhang and Gui's requirements [52] to create a high fidelity journal bearing simulation model. Zhang and Gui's parameters are useful, but a review of more modern literature, dedicated to the simulation of bearing systems, suggests that these requirements are insufficient. Table 6, points 5 to 9, list the additional steps in the present research.

Table 6. Bearing modelling requirements.

Zhang and Gui [52] requirements	1	Calculation of the bearing journal orbit centres
	2	Characterisation of the surface roughness
	3	Calculation of the thermal effects
	4	Consideration of the oil feed features
Additional requirements	5	Dynamic bearing profile calculation
	6	Elastohydrodynamic behaviour
	7	Measurement of the worn-in bearing profile
	8	Inclusion of non-Newtonian lubricant behaviour
	9	Simulation of the lubricant cavitation effects
	10	Interaction with different bearing materials

3.1.1. Calculation of the bearing journal orbit centres

Zhang and Gui [52] consider calculation of the journal centre orbits. The starting point for the calculation of the bearing orbit locations is the Reynolds equation:

$$\frac{\partial}{\partial x}\left(\frac{h^3}{\mu}\frac{\partial P}{\partial x}\right)+\frac{\partial}{\partial z}\left(\frac{h^3}{\mu}\frac{\partial P}{\partial z}\right)=6(U_1-U_2)\frac{\partial h}{\partial x}+12(V_2-V_1) \quad (12)$$

where *x* and *z (*and *y)* are co-ordinates as defined in Figure 9, h is the radial bearing to journal clearance (and the film thickness in fully flooded conditions), P is the local oil film pressure, μ is the dynamic viscosity of the lubricant, U_1 is the circumferential velocity of the journal, U_2 is the circumferential velocity of the bearing, V_1 is the

velocity of the bearing along co-ordinate *z* (i.e. the velocity in the film squeeze axis) and V_2 is the velocity of the journal along the z co-ordinate [54].

The Reynolds equation allows the clearance around the bearing to be resolved by calculating the pressure distribution and oil film thickness in the bearing. Eleven key assumptions underpin this equation [54]:

1. Laminar flow of lubricant within the bearing
2. A continuous oil film for which the fluid is Newtonian and incompressible
3. A no-slip condition at the boundary between the lubricant and bearing/journal surface
4. The velocity component across the film is negligible in comparison to the velocity profile along the bearing circumference or across the bearing width
5. The velocity gradients along the fluid film are small and negligible compared to the velocity gradients across the film, because the film is thin (leading to the omission of the term $\frac{\partial}{\partial y}\left(\frac{h^3}{\mu}\frac{\partial p}{\partial y}\right)$ from equation (12) characterising the oil film pressure variation in co-ordinate *y*)
6. Consistent film pressure concomitant with the lack of velocity gradient
7. The effect of the journal (and bearing) curvature can be ignored
8. The force attributable to gravity is negligible compared to the viscous forces
9. The effect due to fluid inertia is negligible compared to the viscous forces (i.e. low Reynolds number, laminar flow)
10. The fluid is incompressible
11. The flow is quasi-steady

The Reynolds equation has several partial differential variables. Inputting the known values for the bearing geometry, loads, lubricant viscosities and speeds defines

the geometrical boundary conditions. However, defining these variables' values is insufficient to solve the equation fully, so fluid boundary conditions are also applied.

Selection of boundary conditions varies in the literature. Researchers select their conditions based on their ability to accept different levels of computational intensity and solution accuracy. The mobility method proposed by Booker [55] provides a simple way to predict bearing orbit centres. It does not solve the Reynolds equation directly, but uses predefined mobility maps, expressed in graphical or tabulated form, to allow calculation of oil film thickness. The method provides a fast simulation run time, but the simplifications made do not allow: bearings with non-circular geometry or compliance to be simulated; the effects of journal misalignment to be studied; the inclusion of oil feed hole effects [55], [56] or non-Newtonian fluids to be evaluated. Thus, Booker's method is not useful for the present research.

Finite difference and finite volume techniques can be used to provide a more rigorous solution to the Reynolds equation [56]. In these approaches, the space defined by the bearing clearance and circumference is discretised to generate a series of algebraic equations solved in a matrix format. These solution techniques allow non-circular bearing geometries to be studied and can accommodate non-Newtonian lubricant characterisations. Some authors using these techniques do not respect mass conservation requirements [56]. However, the principal limitation of ignoring mass conservation appears to be that the effects of film rupture (e.g. cavitation) are not captured. Gulwadi and Shrimpling [56] recommend that the finite volume solution and conservation of mass equations are included in the discretisation step. Their approach tracks cavitation regions (oil film rupture) and can model non-circular bearing geometry. The finite volume approach was chosen for the simulation model built in the present research, using the Ricardo Software program ENGDYN. Ricardo ENGDYN is an engine design and analysis program. It can resolve loads on engine components and

calculate the component stiffness in order to predict dynamic distortion under running engine conditions.

3.1.2. Clearance

The bearing diametric clearance is important when calculating the journal orbit position. It is also key in determining the bearing's performance [51] since:

1. The bearing's load carrying capacity is inversely proportional to the clearance and can be calculated from:

$$W \propto \left(\frac{R}{C^2}\right) \tag{13}$$

   where W is the load carrying capacity of the bearing, R is the bearing radius and C is the bearing clearance
2. Oil flow rate through the bearing becomes larger with increasing clearance (which affects the running temperature and windage)
3. Oil film thickness (at all points on the bearing circumference) depends on the clearance
4. Power loss in the hydrodynamic regime depends on the clearance [38] and can be expressed as:

$$\dot{W}_{\mathrm{F}} \approx \frac{2\pi\mu^{0.75}\omega^{1.75}L^{0.25}R^{2.75}N^{0.25}}{C^{0.5}} \tag{14}$$

   where $\dot{W}_{\mathrm{F}}$ is the power loss to friction (W), μ is the lubricant dynamic viscosity, ω is the shaft speed, L is the bearing length, R is the bearing radius, N is the load and C is the clearance [57]. This equation is valid when $h_{\mathrm{min}} << C$, where h_{min} is the minimum film thickness in the bearing.

Theoretically, maximising the bearing clearance is desirable in order to minimise the power loss in the hydrodynamic regime. However, a compromise is needed since the bearing's load carrying capacity is inversely proportional to the clearance and large

values may cause the contact regime to transition into boundary lubrication. In selecting an acceptable bearing clearance, consideration must be given to: controlling the bearing and journal orbits; controlling the oil flow rate; mitigation of lubricant contamination effects; and minimising noise, vibration and impact loading. The choice of clearance can also be dependent on the achievable manufacturing tolerance [51].

Typically, the bearing and lubrication systems are designed so that the oil film is 10-100 times thicker than the composite surface roughness to prevent asperity contact during operation [51]. A typical design guideline for clearance is 0.9 μm per millimetre of bearing diameter ± 20 μm for a big-end bearing [58].

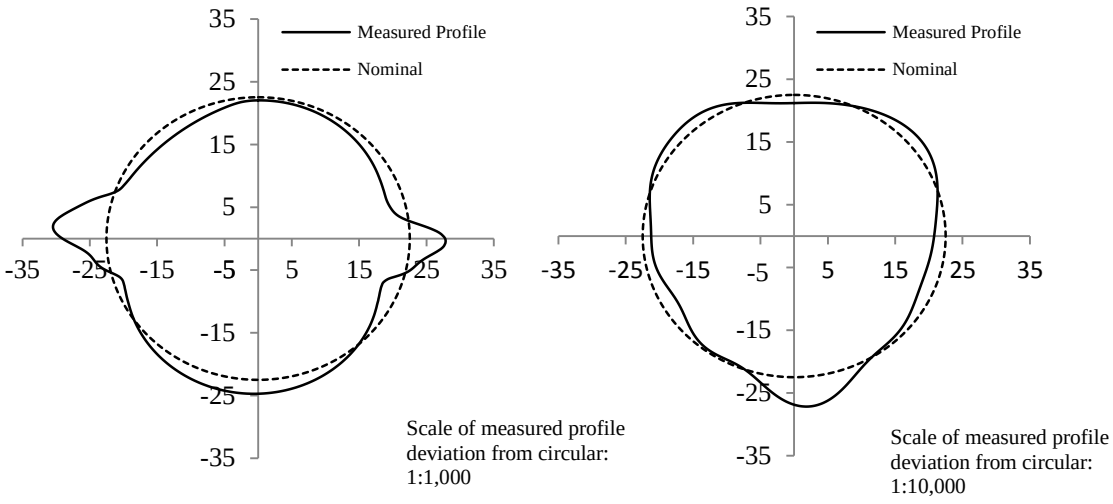

Figure 10. Big-end bearing (left) and crank pin (right) profile measurement.

To build the model used in this investigation, clearance was calculated by measuring the size of the crank pin and bearing. After disassembling an engine, a coordinate-based surface tool was used to measure the bearing and journal profiles. The profiles were measured from run-in components, thermally soaked for 24-hours at room temperature (294 K) prior to measurement. The bearing was assembled by following the procedure defined by PSA group which was to tighten each bolt to 5 Nm, then to 10 Nm and then to rotate each bolt by 130˚. Figure 10 shows the measured bearing and journal profiles used in the simulation.

The bearing profile measurement showed that this deviated significantly from being circular. This non-circularity was especially pronounced at the split line (the location of the x-axis in Figure 10). The profile represented a ‘lemon bore’ shape and at the ends of this profile the clearance was increased by a maximum of 15 microns from the notional circular profile. The lemon bore feature is designed to help reduce the effect of bearing whirl and the local distortion due to the bolt clamp loading. The profile is key to the bearing tribology since this affects the entrainment of lubricant into the loaded contact [51], [59] and increases the oil flow rate through the bearing [60].

Figure 10 also shows the profile of the journal. The maximum deviation from circular for this profile was 1 micron. It is likely that the variation from circular is attributable to manufacturing variability, since this is within the tolerance achievable using cylindrical grinding processes. The simulation used the measured profiles.

3.1.3. Characterisation of the surface roughness

Zhang and Gui specify that surface roughness must be characterised in the bearing model. The inclusion of this parameter is important since the bearing’s surface roughness is of a similar magnitude to the minimum film thickness [52]. Mishra and Rhanejat [59] also consider the effect of surface roughness to be important, since in heavily loaded, or in fluctuating load conditions, severe asperity interactions can occur. The orientation of the roughness (if the surface is anisotropic) is also important, because this affects the flow of lubricant in the bearing. Circumferential (or transverse) roughness causes small oil film wedges to develop which can severely limit the flow rate of lubricant into the bearing. Axial surface roughness primarily affects the flow rate of lubricant through the bearing width. High roughness values increase the flow rate, which can aid convective cooling, but also degrade the load carrying capability of the bearing [59]. Uehara and Peixoto’s engine tests [61] showed that bearing temperatures

reduced when high axial surface roughness (micro-profiled) bearings were used [61]. This observation concurs with Mishra and Rhanejat's work [59]. Characterising the surface roughness is particularly important when the tribological contact moves from full film lubrication into a mixed regime, which can occur in the highly loaded bearings of modern engines [56], [62], [63], [64], [65]. A typical surface roughness value for a crank journal is between 0.2 μm Ra (where Ra is the average height of the asperity peaks above the mean plane) and 0.3 μm Ra although some vehicle manufacturers have reduced it (e.g. Renault-Nissan and BMW group) to 0.02 μm Ra [58]. Typically, the bearing is manufactured to be rougher than the journal.

A profilometer measured the bearing and journal surface finish [66]. Bearing roughness was only evaluated in the components' direction of motion, since the simulation tool could not model anisotropic surface roughness. This simulation limitation is recognised and further refinement of the model is recommended. ENGDYN used a boundary lubrication model based on Greenwood and Tripp's work [67]. The calculated oil film thickness was divided by the composite surface roughness for each spatial and temporal node. If the result was less than 4 then the Greenwood-Tripp algorithm was used to calculate the asperity contact load.

3.1.4. Calculation of the thermal effects

Zhang and Gui [52] cite bearing temperature analysis as being essential. Unless the lubricant is preheated (see Chapter 6), the oil temperature is predicted to increase as the lubricant flows through the bearing, due to friction losses being dissipated as heat and heat transfer from the hotter engine components. Allmaier et al's work [68] shows that the model results depend significantly on the assumed thermal boundary conditions. The flow rate and distribution of the lubricant in the bearing determine the rates of convective and conductive heat transfer. The resultant temperature of the bearing,

journal and the lubricant determine the bearing clearance and contribute to the local lubricant viscosity. These parameters are interdependent.

Conway-Jones et al. [63] completed engine tests to measure the temperature distribution around an engine's connecting rod bearing. The maximum oil film temperature variation measured was 4 K, although the reported test details are insufficient to understand the operating conditions fully. The variation in oil temperature was found to be mainly due to heat flow from the crankshaft, not frictional heating in the bearing. However, this conclusion is only valid under hydrodynamic contact conditions. The crankpin's temperature is determined by: the heat flux from the bearing due to lubricant cooling; heat transfer from the journal to the (ordinarily cooler) main bearings; windage effects; and heat flow from the piston through the connecting rod assembly. Thus, simulating crankshaft temperature is complex.

Calculating the bearing's hydrodynamic frictional power loss (and assuming this is dissipated into the lubricant) allows approximation of the heat input due to viscous shear. Figure 11 depicts a simplified bearing. The upper surface is the journal and the lower surface is the bearing. This analysis assumes the bearing is stationary.

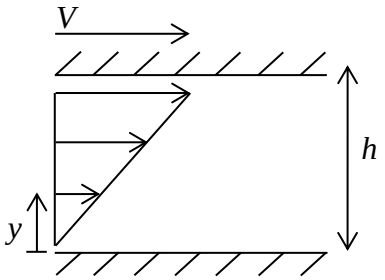

Figure 11. Schematic representation of two sliding surfaces separated by a clearance.

Newton's law of viscosity calculates the shear stress acting on the lubricant as

$$\tau_{\mathrm{y}} = \mu\left(\frac{\delta V}{\delta y}\right) \tag{15}$$

where τ_y is the shear stress acting on the lubricant in the *y* direction, μ is the lubricant dynamic viscosity, *V* is the velocity of the journal and *y* is the characteristic dimension perpendicular to the bearing.

The total friction power per unit area can be calculated as:

$$\dot{W}_{\mathrm{F}} = \tau_y v = \frac{\mu V^2}{h} \tag{16}$$

where P_{F} is the friction power and *h* is the bearing clearance.

By assuming that all of the bearing friction is dissipated as temperature rise in the oil film, that the lubricant entering the bearing, journal and bearing surfaces are isothermal, and that no heat transfer occurs to the bearing or journal, the temperature increase attributable to shear heating can be calculated following Fourier's law of thermal conduction in the form:

$$\Delta T = \frac{\dot{W}_{\mathrm{F}} h}{k} \tag{17}$$

where ΔT is the lubricant temperature rise through the oil film thickness and *k* is the lubricant thermal conductivity. Figure 12 shows a schematic representation of this problem.

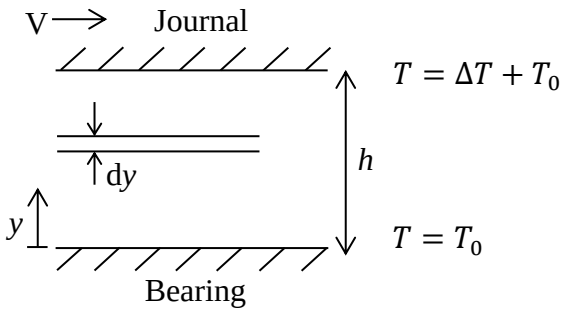

$$\frac{\mathrm{d}T}{\mathrm{d}y} k = \frac{\dot{W}_{\mathrm{F}}}{h} y$$

$$\Delta T = \int_0^h \frac{\dot{W}_{\mathrm{F}}}{kh} y \mathrm{d}y$$

$$\Delta T = \frac{\dot{W}_{\mathrm{F}}}{k} \frac{h}{2}$$

Figure 12 Simplified representation of power flow during shear heating.

Assuming an oil film thickness of 10 μm, dynamic viscosity of 4.4 cP (0.0044 Ns/m^2), engine speed of 3000 rev/min and bearing journal diameter of 45.3 mm, the frictional power rise per unit area is 2.23 W/cm^2. Thus, for an oil with a thermal conductivity equal to 0.182 W/mK the mean temperature rise is equal to 0.6 K. Clearly, this calculation is an over simplification, but it is useful to understand the theoretical maximum temperature rise in the oil film due to shear heating.

Re-arranging (16) and (17), it can be shown that:

$$\Delta T = \frac{\dot{W}_F h}{K} = \frac{\mu V^2}{h}\frac{h}{K} = \frac{\mu V^2}{K} \tag{18}$$

and, therefore, that the theoretical temperature rise due to shear heating depends on the bearing velocity alongside the lubricant's viscosity and thermal conductivity, but is independent of the clearance. Conway-Jones et al [63] also reach this conclusion.

The flow rate of oil entering the bearing is also important to determine heat transfer. Due to the transient nature of the loading, oil flow in a big-end bearing exhibits time-dependent behaviour. The bearing orbit motion (e.g. due to whirl) also causes unsteady oil flow conditions to prevail. Averaged over a cycle, the mass flow rate of lubricant into and from the bearing must be equal to respect mass conservation, yet because of the cyclical and temporal nature of the speed and load, the instantaneous oil flow varies considerably. According to Beodo [69], prediction of oil flow rate requires temporal and spatial tracking of lubricant density in the bearing. Lubricant cavitation effects must also be included to calculate the oil film's heat transfer properties.

Lubricant temperature also rises due film 'squeeze' motion [69], so this must be characterised. The increased pressure from this behaviour also raises the lubricant's viscosity. The squeeze velocity vector (second term on the right of equation (12)) is found by considering the direction, rate and magnitude of the relative journal orbit centre movement.

The simulation model in the present research included a thermal balance, calculated oil flow rate and characterised squeeze behaviour. However, the resolution was limited, as the oil film temperature was only permitted to vary through the bearing's width (i.e. local, circumferential, oil temperature changes could not be accounted for).

3.1.5. Consideration of oil feed features

A robust simulation must include analysis of the oil feed features, since for a big-end bearing it is common for the oil feed to be machined into the journal, reducing the effective bearing area. The lubricant pressure in the oil gallery is typically lower than the pressure in the bearing, so, as the oil supply hole passes through the bearing contact region, a pressure reduction in the contact is measured. It is also normal for the oil gallery temperature to be lower than the bearing temperature. The effect of the low temperature oil flowing into the oil film should be included in the model.

Conway-Jones et al. [63] consider the simulation of the oil feed behaviour as a significant parameter in evaluating the bearing temperature. The oil flow is dependent on the oil hole size in the crankpin and the detail of how this breaks out into the bearing (e.g. through a chamfer) as well as the bearing clearance, width and roughness [59].

In this simulation, the oil feed hole geometry was measured from used engine components. The breakout chamfer was included in the definition of this feature.

3.1.6. Calculation of the dynamic bearing profile

Allmaier et al. [68] include the dynamic bearing geometry in their simulations. They achieve this by coupling a finite element model to a bearing simulation so that the effect of the component flexibility on the true bearing profile can be characterised. This effect is important since the elastic deformation can be significant compared to the oil film thickness. Bischoff [65], like Gulwadi and Shrimpling [56], considers calculation

of the bearing profile including elastic deformation and elastohydrodynamic lubrication, but not all authors do. Mishra and Rahnejat [59] simplify their analysis by disregarding this effect. Zhang and Gui [52] ignore this effect because their models could not process the large number of interdependent non-linear equations.

Choi et al. [62] compared the accuracy of a simulation model including flexibility with one that assumed the components were rigid. A simple rig test investigated the accuracy of each approach. The oil film pressure was measured at several points around the bearing and this parameter was used in the comparison. The simulation that included flexibility achieved a higher fidelity.

Sato et al. [70] measured the oil film pressure in a connecting rod bearing using a thin film sensor and compared these results to a simulation output. Their test work used a simple rig. The results showed that the oil film pressure was sensitive to changes in the connecting rod stiffness. This conclusion indicated that the bearing system geometry varied under the applied load. Reducing the connecting rod stiffness to values more representative of real engine components, lowered the peak bearing pressure as the load spread over a larger area. When the flexible connecting rod was tested, two pressure peaks occurred, due to the stiffness profile of their connecting rod. Good agreement was achieved between the measured and simulated bearing conditions when the calculations included elastohydrodynamic effects.

The ENGDYN simulation in the present research accounted for the effect of bearing profile distortion due to the connecting rod's compliance. A Computer-Aided Design (CAD) model of the connecting rod was built from physical measurements. Its accuracy was confirmed by comparing the connecting rod's mass to the value predicted by the CAD program.

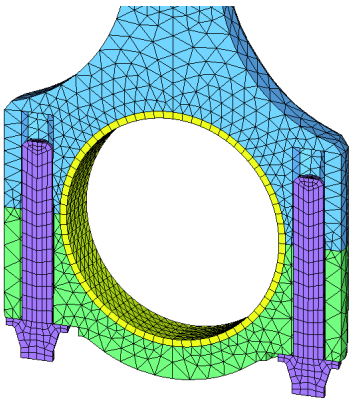

Figure 13. Big-end bearing cross section showing the mesh used in the finite element analysis.[Y]

The CAD model was used in a Finite Element Analysis (FEA) program to resolve the distortion from the applied combustion and inertial loadings. Figure 13 shows the finite element mesh overlaid on a cross section through the bearing. Co-incident meshes were specified between the connecting rod and cap and at the interface between these two components and the bearing shell. The bolt-to-connecting rod thread contact was specified as a kinematic connection, so these could move relative to each other. A kinematic connection was also specified between the bolt head and its land on the cap. It was assumed that the system's dynamic geometry variation would occur in the bearing because the journal had a significantly greater stiffness.

3.1.7. Elastohydrodynamic behaviour

A review of modern literature revealed that a bearing's oil film pressure can be high enough to cause viscosity increase, due to piezo-viscosity behaviour [68]. However, not all authors characterise this behaviour. Mohammadpour et al. [71] and Mishra and Rahnejat [59] ignore this possibility by assuming that the deformation of the soft bearing overlay (e.g. tin-based alloys like Babbitt) avoids significant pressures being generated. However, later in their analysis, they indicate this assumption was not valid, especially for highly loaded bearings. Boedo [69] also did not characterise piezo-viscosity behaviour, although the significance of this assumption was understood. Allmaier et al. [68] analyse the importance of the lubricant piezo-viscosity effects in

detail using a simulation that is validated with a subsystem test. Their analysis shows that the lubricant's piezo-viscosity response becomes important when the contact conditions transition to a mixed regime. Allmaier et al.'s investigation [68] demonstrated that piezo-viscosity effects are significant in highly loaded systems and in bearings using low viscosity lubricants. Therefore, incorporating a piezo-viscosity model is likely to be important for modern, highly rated engines, which now use low viscosity lubricants.

Kataoka et al. [70] installed thin film pressure sensors onto main bearing surfaces to measure the oil film pressure. They compared the output from these measurements to their simulation results. The details of their model are not shared. However, the numbers output by the model are high (e.g. a maximum oil film pressure of 260 MPa was predicted cf. 120 MPa in the simulation work by Allmaier et al.), although it is not clear if this is attributable to the assumptions made in the simulation or to the specified boundary conditions. The maximum oil film pressure measured in the work of Kataoka et al [70] was ~150 MPa and occurred at the bearing edge because the bearing housing and crankshaft deformed elastically. These pressures are high enough to trigger a significant (2 to 3 times) increase in viscosity (see Section 2.4, Figure 5). Thus, lubricant viscosity variation with pressure was characterised in the present research using the Barus equation (see Section 2.4).

3.1.8. Measurement of the worn-in bearing profile

When a new engine first runs, the mating tribological surfaces conform during a process called 'running-in'. The bearing profile changes during this period. Allmaier et al. [68] and Uehara and Peixoto [61] investigated the effect of the running-in. Their results also showed that asperity contact pressures, and thus friction, were much lower when worn bearing profiles were used (Figure 14).

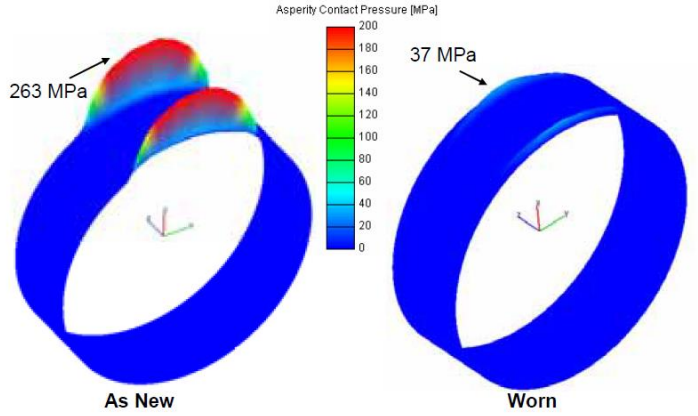

Figure 14. Predicted asperity contact pressure for new and worn bearing profiles (Reprinted with Permission from SAE International [61]).

The bearing surface roughness also varies during running-in. Measurements during the present research showed a variation from 0.4 µm Ra to 0.2 µm Ra between unworn and worn parts of a big-end bearing shell respectively [53]. In the present research measurements were taken from worn bearings to define the bearing's run-in profile.

3.1.9. Non-Newtonian lubricant behaviour

Most authors characterise lubricant viscosity variation with temperature. Thus, this behaviour was characterised in the present research using the Vogel equation (equation (4).)

Predicted shear rates in bearings can be high. Consequently, Taylor [72] applies the Cross equation (equation (5)) to an isothermal short bearing model. He concludes that including characterisation of this behaviour is important in predicting the performance of a connecting rod's lubrication. His calculations predict shear rates of between $0.2x10^6$ s^{-1} and $3.9x10^6$ s^{-1} at 150˚C lubricant temperature for a highly loaded passenger car big-end bearing. These shear rates were between the lubricant's first and second Newtonian regimes, increasing the model's sensitivity to the assumed shear-viscosity curve in this area. Thus, the present research characterised lubricant viscosity variation with shear rate using the Cross equation (equation (5).)

3.1.10. Lubricant Cavitation

The Reynolds equation assumes the bearing clearance region is fully flooded (see Section 3.1.1). However, entrainment of oil into the bearing clearance results in a local lubricant pressure increase (to support the load) and then reduction. In the pressure-reducing section, the possibility exists for the pressure to fall below the lubricant's gas-saturation pressure, and for cavitation to occur. This process can cause discontinuity in the oil film, meaning the Reynolds equation is no longer valid to model it. Zhang and Gui [52] do not robustly deal with the effects on the lubricant film pressure due to cavitation. However, Gulwadi and Shrimpling [56] simulate the cavitation effect. In their simulation, a user-defined, constant cavitation pressure is assumed when the oil film pressure reduces below the saturation pressure. Other authors, such as Booker [55], conclude simulation of oil film rupture (a feature of his method) is important. Cavitation was simulated in the present research using Gulwadi and Shrimpling's [56] approach.

The cavitation pressure for the lubricants was taken from measurements using an engine mounted to a steady state dynamometer and fitted to a lubricant "aeration" meter, the Air-X. An engine of the type listed in Table 4 was used in this study. Deconninck et al. [73] describe the working principles of the Air-X. Although aeration is a general term, encompassing foam, entrained gas bubbles and dissolved gas, the meter only measures the percentage volume of entrained gas in the lubricant. Since no free surface exists in the bearing, the foaming properties of the lubricant were irrelevant, and the simulation was unaffected by the unit's inability to measure foam. The lubricant was assumed to be fully saturated with dissolved air at atmospheric pressure, so the entrained gas measurements from the Air-X defined the lubricant's values. Cavitation pressures were calculated using the equation defining the Bunsen coefficient from Dalton's law of partial pressures as:

$$V_{\mathrm{G}} = \lambda\, V_{\mathrm{o}} \frac{P}{P_{\mathrm{o}}} \tag{19}$$

where V_{G} is the volume of gas which is soluble, V_{o} is the oil volume at P_{o}, P_{o} is the normal absolute pressure (e.g. atmospheric), P is the absolute instantaneous oil pressure and λ is the Bunsen constant.

The Air-X sampled lubricant from the sump in a continuous manner, its feed was proximal to the oil-pump pick up to ensure representative values. The test conditions replicated those in the simulation. The engine was run for 3 hours to ensure steady-state conditions prevailed. The magnitude of entrained air was calculated using the mean of the data recorded over the final hour. A value of 6.3% entrained air by volume at atmospheric pressure was determined using this test with a 0W-20 lubricant.

The cavitation pressure was calculated by assuming a Bunsen coefficient equal to 0.09 (taken from [74]) and was calculated by solving equation (19) for P. A value of 0.7 bar gauge was used in the simulation. The simulations (described below) used theoretical fluids which could not be blended. Consequently, it was not possible to measure entrained air levels for each lubricant. The cavitation pressure value was kept constant at the calculated value for every simulation.

3.1.11. Consideration of bearing material composition

Zhang and Gui [52] do not consider the relationship between the coefficient of friction in the boundary regime and the bearing's material composition. However, the present research includes characterisation of the interdependence.

Typically, journal bearings in the crankshaft system use steel backing with aluminium-tin alloy overlay [53]. Recently, polymer overlays have also been specified because of their superior friction and wear performance in stop-start duty cycles [75] [76], [58]. This change is important since when oil film thickness is low, the lubricant's

surface-active additive components interact with the bearing's surface to reduce the friction coefficient [58].

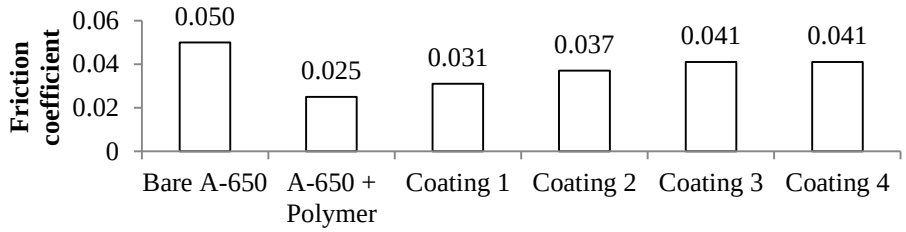

Figure 15. Coefficients of friction measured using HFRR test rig with different bearing surfaces (data reproduced from Achim [76]).

Achim et al. [76] used a High Frequency Reciprocating Rig (HFRR) to measure boundary regime friction using a range of bearing overlays. Their test shows that varying the bearing overlay's composition changed the boundary regime friction coefficient. A "bare aluminium" overlay had a friction coefficient of 0.05, but this reduced to 0.025 when a polymeric coating was applied. Figure 15 summarises the data from Achim et al [76].

The bearing composition for the present research was confirmed by taking a section through one bearing and completing an elemental analysis with a scanning electron microscope [77]. This analysis showed the bearing surface overlay was ~300 μm thick and the aluminium material formed the substrate for the running surface. Tin was spatially distributed in the aluminium. The spatial distribution of copper in the bearing overlay was unconfirmed, as its concentration was too low. Bearing material and lubricant property changes were investigated by varying the boundary regime coefficient of friction.

Achim [76] notes that the use of polymer materials in the bearing can also change the bearing's thermal behaviour, because the polymeric (polyamide-imide) coatings provide high thermal insulation values. The effects of this behaviour are beyond the scope of the present investigation, but warrant further study. Theoretically, this

behaviour could be exploited to control viscosity loss in the bearing and therefore reduce their optimum viscosity requirements.

3.1.12. Big-end bearing load input data

The bearing load used as an input condition to the simulation was calculated by completing a force balance on the piston and connecting rod assembly. The loads due to the component accelerations were defined from the kinematics of the crank-slider mechanism. Masses and inertiae for the piston and connecting rod assemblies were measured from used components (Table 5 shows the mass values).

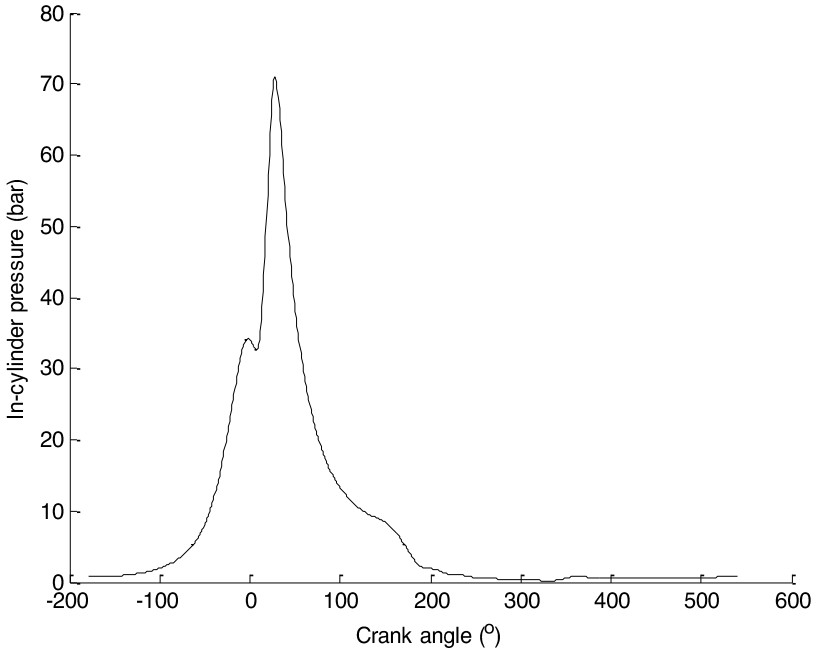

Figure 16. Measured cylinder pressure trace from EP6 CDTX test engine at 2000 rev/min engine speed and 22 Bar BMEP engine load.

The pressure profile on the piston crown with respect to crank angle was measured by mounting an engine (specification in Table 4) to a dynamometer. Figure 16 shows the pressure trace used in the simulation. These results were measured using a spark plug type pressure transducer supplied by Kistler Instrumente AG. This probe was connected to a Kistler 5018A amplifier and a National Instruments data acquisition system. The engine was preconditioned to 90˚C coolant and lubricant (gallery)

temperature prior to the measurements being taken. The pressure trace was taken from the mean of 100 combustion cycles with the engine operating at 22 bar brake mean effective pressure (BMEP) which is the full load condition at this engine speed.

The engine tests and simulations were completed at full load (22 bar BMEP) and low engine speed (2000 rev/min) because this condition is severe and encouraged a high bearing wear rate. This specification was desirable, as the ability to mitigate bearing wear using lubricants was researched separately. The instantaneous bearing wear was measured using a radio-isotope technique and a range of lubricants. The results are beyond the scope of this research, but are reported by Taylor [78], [79].

3.2. Validation of the big-end bearing model

Comparing the bearing's predicted and observed wear profiles validated the simulation model. An engine having completed 60,000 km was taken from a used vehicle to allow a comparison between the real and simulated wear profiles. This engine was stripped and the bearings examined. Its utilisation is not exactly known. However, the wear appeared normal. It has been assumed that the wear of these bearings is typical for an engine that was run-in and had been used across various speeds and loads.

Figure 17 compares the wear pattern predicted by the model with the wear seen in one of the connecting rod bearings from this engine. In this image, the bearing's circular geometry has been unwrapped and is presented as if this were flat.

Zone A sits between 0˚ and 45˚ bearing angles and is where the maximum loading on the bearing from combustion-gas generated pressure is reacted into the journal.

Zone B has the same circumferential position as Zone A, but the boxes are located at the bearing edge. The oil film thickness is predicted to reduce in this region, due to temperature rise across the bearing width reducing the lubricant viscosity. The reduction

in film thickness increased the wear rate. Crank pin deflection in the engine was not characterised by the simulation, but is likely to have contributed to the real wear pattern.

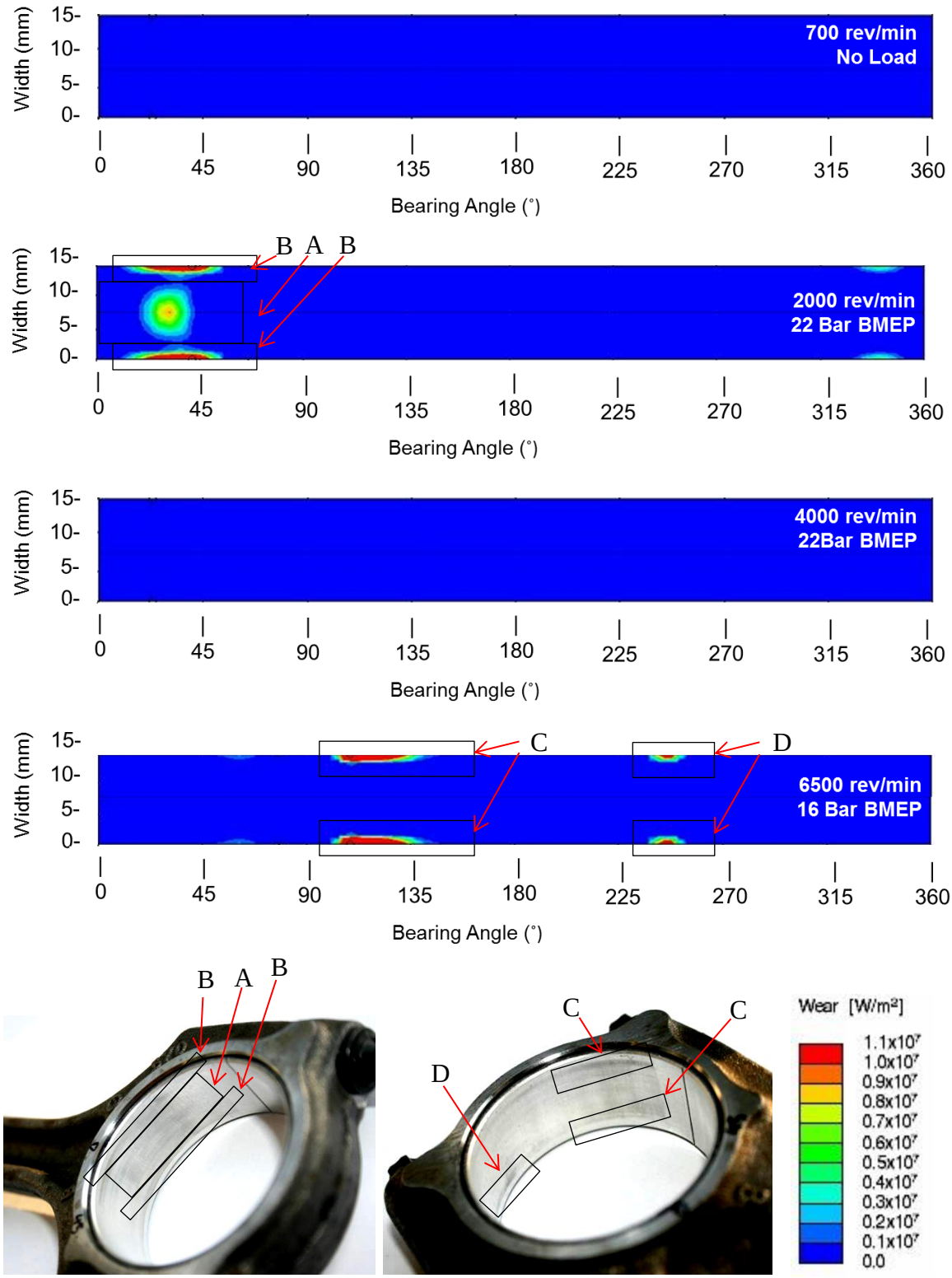

Figure 17. Comparison of wear between predicted locations and those seen in a used engine.[y]

Zones C and D are on the bearing cap. This part of the bearing is predominantly loaded by inertial forces, which decelerate and accelerate the piston assembly and

connecting rod's reciprocating motion. Some loading is also present on the intake stroke and in over-run conditions if the cylinder pressure is subatmospheric.

The wear profile predicted by the simulation correlated well with the observed behaviour. A review of other research provided further confidence in the simulation results. Gulwadi and Shrimpling validated the ENGDYN program's underlying physics [56]. They refer to the Ricardo ORBIT program not ENGDYN, but the two programs use the same simulation techniques (the ORBIT program was incorporated into ENGDYN) [80]. In the same study, the outputs from the simulation model are compared against other simulation tools. The Ricardo ORBIT model predicted similar values to commercially available simulation tools. The oil flow rate and temperature rise on the first main bearing from the Ricardo Hydra single-cylinder engine and those predicted by ORBIT were also compared. A good agreement was found.

Empirical work reported by Allmaier et al. [68] and Kataoka [81] predicts a similar peak lubricant pressure in the bearing to that in the present work. Allmaier et al. [68] uses the same Barus piezo-viscosity characterisation as used in the present research, although Anstalt für Verbrennungskraftmaschinen List's (AVL's) EXCITE simulation software is used. The simulation model built by Allmaier et al. [68] was validated using a subsystem test.

The correlation between predicted and measured wear profiles alongside the comprehensive validation work completed by Gulwadi and Shrimping [56] has been used to validate the simulation in the present research. A more robust validation, specific to this test work, is desirable. However, this confirmation would require the design, build and commissioning of a specific rig, which was beyond this investigation's scope.

3.2.1. Lubricant characteristics used in the simulations

The simulation's response to viscosity changes from VI, shear, pressure and density variations were investigated in the present work. Table 7 lists the lubricants used in the simulation. The lubricant matrix has five key sections. Test runs 1 to 5 allow investigation into the correlation between predicted friction and VI obtained by targeting 6.4 cSt[8] KV100, whereas 6 to 9 and 10 to 13 allow a similar investigation, but using 4.6 cSt and 3.0 cSt KV100 values respectively. Runs 14 to 17 allow investigation into temporary shear thinning behaviour. Finally, Runs 18 and 19 allow the effect of density and piezo-viscosity to be concluded.

Table 7. Description of the model lubricants used in the simulation work.

Run number	Description	KV40 (cSt)	KV100 (cSt)	Viscosity ratio, x. (Equation (11))	VI
1	KV100 = 6.4 cSt, non-shear-thinning	6.4	6.4	1.0	1409
2		9.98	6.4	1.6	800
3		12.3	6.4	1.9	600
4		20.6	6.4	3.2	300
5		27.3	6.4	4.3	200
6	KV100 = 4.6 cSt, non-shear-thinning	4.6	4.6	1.0	1728
7		5.8	4.6	1.3	1200
8		8.2	4.6	1.8	700
9		17.3	4.6	3.8	200
10	KV100 = 3 cSt, non-shear-thinning	3.0	3.0	1.0	2584
11		4.0	3.0	1.3	1400
12		5.5	3.0	1.8	700
13		9.4	3.0	3.1	200
14	Shear-thinning, base oil viscosity = 5 cSt	6.4	6.4	1.0	1409
15	Shear-thinning, base oil viscosity = 4 cSt	6.4	6.4	1.0	1409
16	Shear-thinning, base oil viscosity = 3 cSt	6.4	6.4	1.0	1409
17	Shear-thinning, base oil viscosity = 2 cSt	6.4	6.4	1.0	1409
18	Density sensitivity	4.6	4.6	1.0	1728
19	Pressure-viscosity sensitivity	9.4	3.0	3.1	200

3.3. Isoviscous lubricants

Prior to investigating the simulation response to the test variables, the results from Runs 1, 6 and 10 were compared to understand the relationship between friction and lubricant kinematic viscosity. The fluids used in this part of the matrix were theoretical

[8] This value was equal to the KV100 of test lubricants used in the bearing wear testing programme reported by Taylor [78], [79].

and displayed Newtonian behaviour, since they did not exhibit any viscosity variation with temperature, shear-rate or pressure changes. Therefore, this part of the matrix allowed the effect of varying the kinematic viscosity to be understood in isolation from other effects. Ordinarily, testing completed to investigate this relationship would require different lubricant chemistries, which could confound the results. The results from these runs yield insights that cannot be obtained experimentally. Figure 18 shows the simulation outputs. The graph shows the predicted contributions of hydrodynamic and boundary friction, along with the calculated friction total.

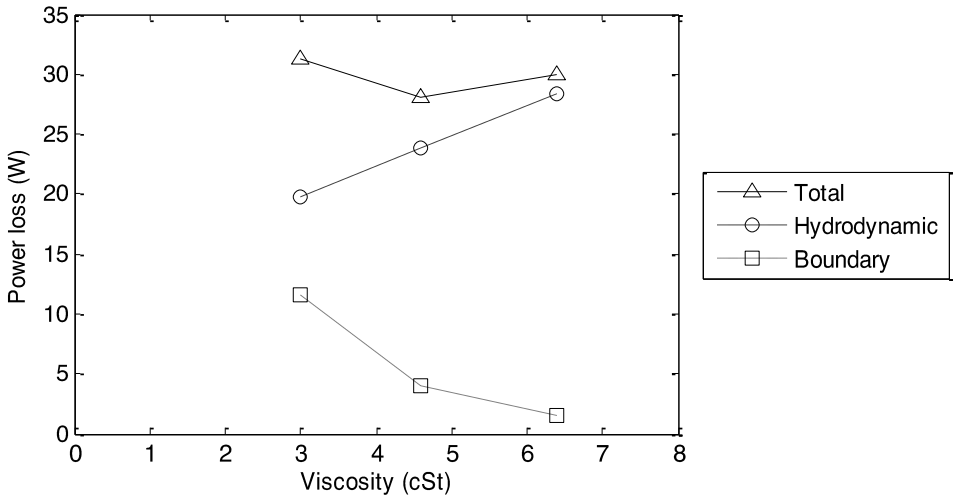

Figure 18. Simulation results for three isoviscous lubricants showing the relative contributions of hydrodynamic and boundary frictional power loss at 22 Bar BMEP engine load and 2000 rev/min.

The simulation results show that as the lubricant's KV was lowered, the hydrodynamic friction in the bearing reduced. Initially, this resulted in the total bearing friction power loss becoming smaller. Concurrently, the magnitude of boundary friction present increased due to a reduction in oil film thickness and consequent increase in asperity-asperity interaction. The hydrodynamic regime friction reduction followed a linear behaviour and the increase in boundary regime friction followed a square-law behaviour. The optimum lubricant viscosity at which the frictional loss was minimised occurred when the sum of the contributions from boundary and hydrodynamic regime losses reached a minimum. This behaviour explains why frictional power loss does not

decrease monotonically as lubricant viscosity is reduced. The findings align with Stribeck's [16] work, discussed in Section 1. For the boundary conditions imposed on this model, and considering the simplifications made, an optimum KV for minimum friction in this component appears to be present at approximately 4.6 cSt.

3.3.1. Frictional power loss due to boundary friction

The power loss attributable to boundary regime friction was calculated by multiplying asperity contact load with a user-defined friction coefficient using:

$$\dot{W}_{\mathrm{F}} = \mu R V \tag{20}$$

where $\dot{W}_{\mathrm{F}}$ is the frictional power expended to overcome boundary regime friction, μ is the coefficient of friction for the boundary regime contact, R is the load carried by asperity–asperity interaction and V is the composite sliding speed of the surfaces.

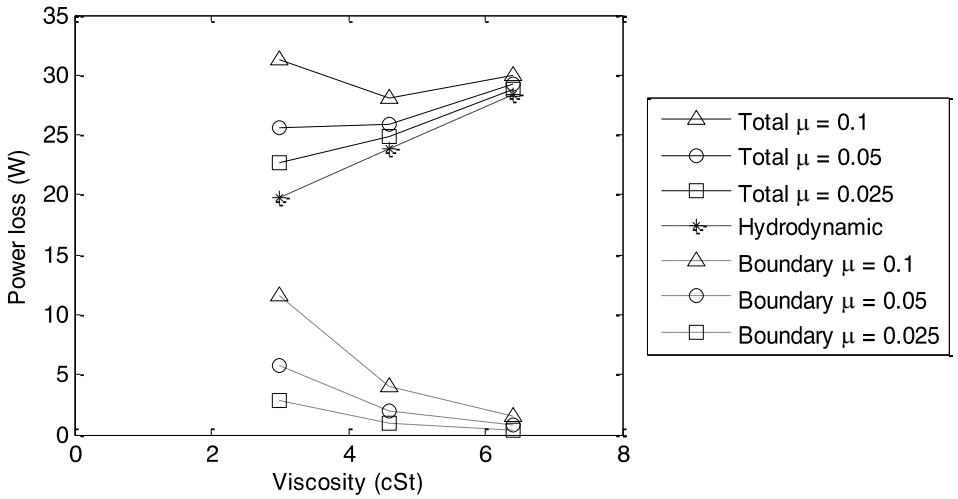

Figure 19. Variation in the predicted friction with changes in boundary friction coefficient (μ) at 22 Bar BMEP engine load and 2000 rev/min.

Current tribology simulations are not sufficiently powerful to predict the friction coefficient generated between the asperity contacts. Consequently, its value was specified. The model was sensitive to this assumption, because boundary friction became significant as the viscosity was lowered. Hydrodynamic friction continually lessened with reducing local viscosity. However, a concomitant increase in boundary

contact occurred, and the magnitude of friction in this regime depended on the friction coefficient defined following equation (20). Reducing the friction coefficient lowered the optimum viscosity for minimum friction. Figure 19 shows the results of total friction for several different friction coefficient values.

In practice, boundary friction behaviour can be varied using surface-active additives in the lubricant (i.e. friction modifiers, film-forming polymers and anti-wear) and by changing the bearing materials. Therefore, each of these parameters, along with surface finish and bearing geometry will affect the optimum lubricant viscosity. Such changes are very likely to occur (e.g. as components are updated during an engine's production life, due to 'running-in', normal wear processes and lubricant additive depletion). The performance variation over the engine's life presents an interesting lubricant engineering challenge, since the friction characteristics vary in use.

The sensitivity to friction coefficient indicates that with adoption of new bearing coatings (e.g. polymer bearings [76], [75]) the optimum bearing viscosity will reduce. Thus, enabling low viscosity lubricants to provide friction reduction.

3.4. The effect of VI in the big-end bearing

Three simulation matrices show the effect of VI on the predicted friction. Runs 1 to 5 (see Table 7) investigated the sensitivity of the model to predicted friction for a range of VIs at 6.4 cSt[9] KV100. Runs 6 to 9 and 10 to 13 also investigated this behaviour, but used 4.6 cSt and 3.0 cSt KV100 values respectively. In each group (e.g. Runs 1 to 5 were a group) the lubricants KV100 was kept constant but the KV40 was varied. The theoretical lubricants used in this part of the simulation were ideal monogrades (i.e. viscosity did not reduce due to the presence of shear stress).

[9] This value was equal to the KV100 of test lubricants used in the bearing wear testing programme reported by Taylor [78], [79].

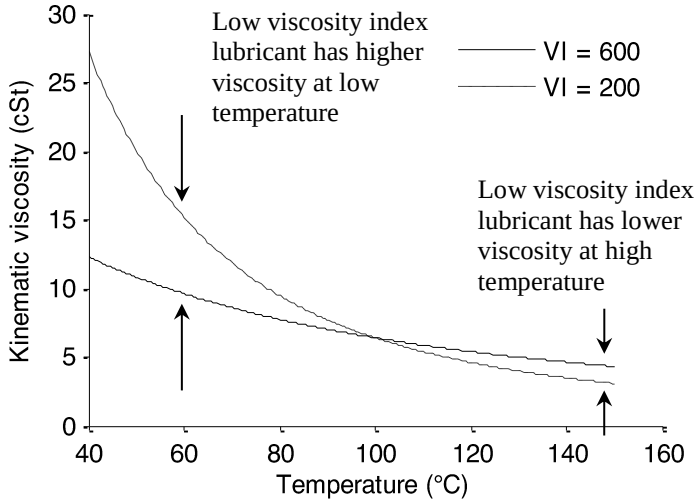

Figure 20. Kinematic viscosity variation with temperature for 600 and 200 VI lubricants.

Figure 20 shows the viscosity change for two lubricants having the same KV100 but different VIs. The lubricant with a lower VI exhibits higher viscosity above 100˚C and lower viscosity below 100°C. This behaviour is important, because in the simple model where all other contributing factors are ignored, the oil film temperature determines the lubricant viscosity and consequently will dictate where on the viscosity-temperature curve a given lubricant will operate. This characteristic provides another variable to engineer the lubricant's performance. Although, the limitations of the VI method (described in Section 2.5) must be understood prior to using it.

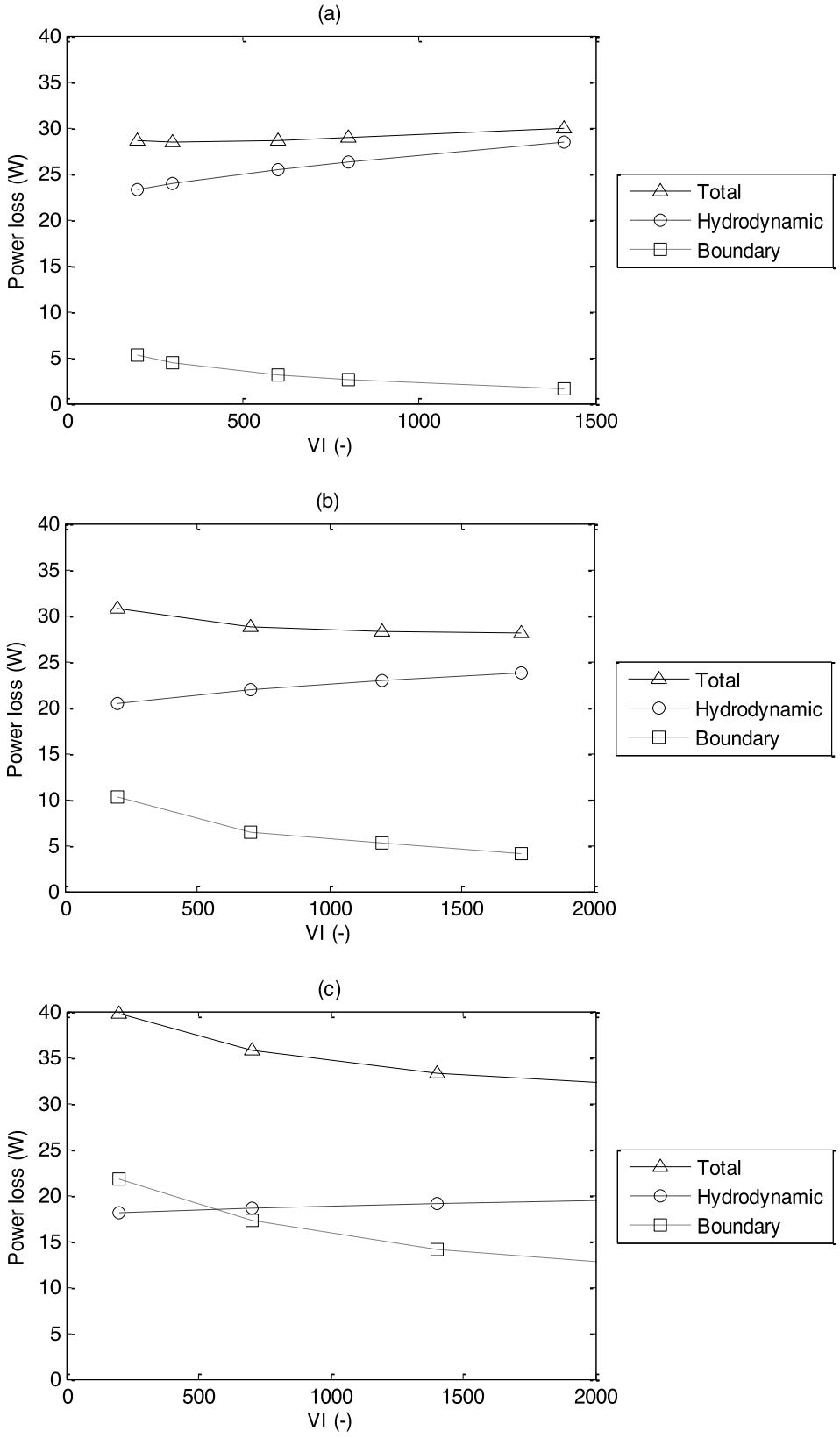

Figure 21. Variation of power loss with viscosity index (VI) for kinematic viscosities (KV) of (a) 6.4, (b) 4.6 and (c) 3 cSt at 100°C at 22 Bar BMEP engine load and 2000 rev/min.

3.4.1. Case 1: KV100 = 6.4 cSt, simulation Runs 1 to 5

Figure 21 shows the results from the runs where VI was varied. The bearing's optimum operating viscosity was simulated to be circa 4.6 cSt ($\mu = 0.1$). Thus, in Run 1,

the isoviscous viscosity was higher than the optimum identified so mechanisms reducing the viscosity should result in friction reduction. Since the lubricant temperature was increasing in the bearing due to frictional heating, and because its notional operation temperature was set to 120˚C, lowering VI was expected to provide this viscosity and friction reduction.

Figure 21 (a) shows results from Runs 1 to 5. As the VI reduced so did the total simulated friction loss. The smaller VI allowed the bearing's effective viscosity to reduce, proportional to the heat transfer and frictional heating in the bearing. This test case validated the hypothesis stated above by showing that, when the lubricant viscosity was greater than the optimum viscosity for the bearing, a lower VI could provide a net reduction in frictional power loss. The frictional power loss was predicted to decrease by 5.1% as the VI was reduced from 1409 to 300. This finding is significant. In lubricant development, technologists normally consider higher VI fluids to perform better than lower VI fluids [7], as they have lower viscosities during the warm-up phase of homologation test cycles like the New European Drive Cycle (NEDC). This low temperature benefit is important, but if technologists achieve high VI values, then these same fluids will increase the friction at more normal engine operating temperatures. Thus, following the conventional approach will degrade the real-world fuel economy performance of these lubricants, and will be a greater factor in legislative cycles like the World-wide harmonized Light duty Test Cycle (WLTC), due to replace the NEDC, because the warm-up period is a smaller portion of the overall cycle length. Equally, lubricant design for racing applications (where warm-up is not important) should not necessarily be focused on achieving high VI.

3.4.2. Case 2: KV100 = 4.6 cSt, Simulation Runs 6 to 9

In these simulations, the lubricant viscosity was equal to the optimum value found in Section 3.3. Thus, it was expected that reducing VI would correlate with a lowering

of the lubricant's effective viscosity and a friction increase. Figure 21 (b) shows the results from these runs. VI reduction correlated to friction increase, which was in line with the hypothesis. The frictional power loss was predicted to rise by 9.7% as the VI reduced from 1728 to 200.

3.4.3. Case 3: KV100 = 3.0 cSt, Simulation Runs 10 to 13

In these simulations, the lubricant viscosity was lower than the optimum for the bearing. Thus, it was expected that reducing VI would again correlate with a friction increase. Figure 21 (c) shows the results from these runs. VI reduction correlated to friction increase. A crossover between boundary contact and hydrodynamic friction losses occurred when the VI was equal to 575. The frictional power loss was predicted to increase by 26.8% as the VI was reduced from 1728 to 200.

3.4.4. Effective bearing viscosity

To compare the various simulation cases an 'effective viscosity' parameter was computed. Effective viscosity was calculated by taking the arithmetic mean of the viscosities reported by the model for each simulation node in the bearing. It provided a single parameter for the overall operational viscosity of the bearing system, but did not provide information on the minimum or maximum viscosity values.

Figure 22 plots the data above (Simulation Runs 1 to 13) against effective bearing viscosity. Similar to Figure 18, the bearing contact's optimum viscosity was circa 4.6 cSt ($\mu = 0.1$). Simulation Runs 1 to 13 showed that this value could be achieved either by varying the fluid's VI or KV100. Importantly, this graph shows that the optimum VI depended on the fluid's KV100.

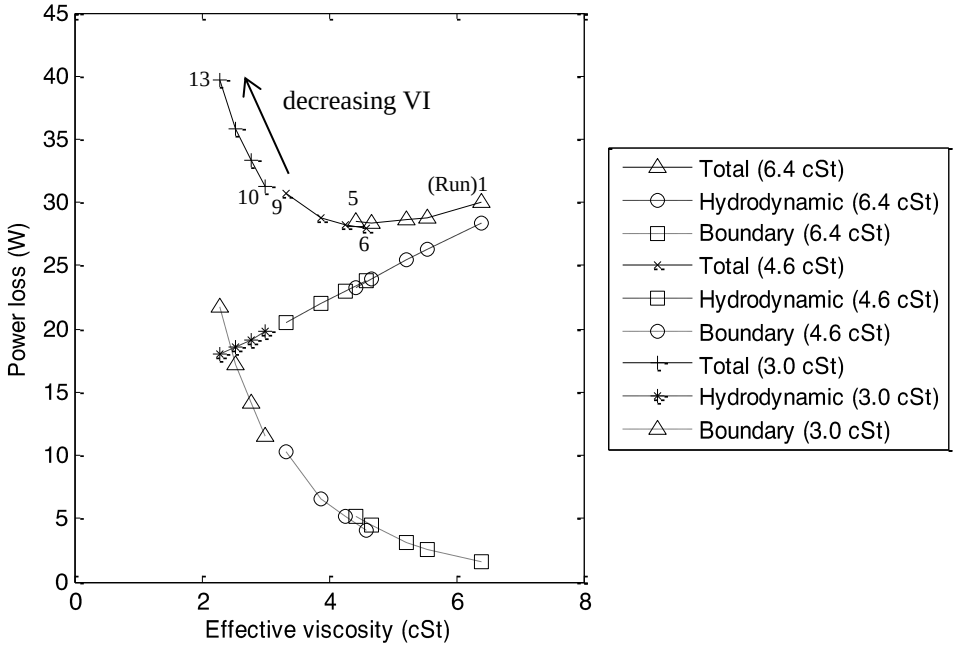

Figure 22. Frictional power loss against effective bearing viscosity for Simulation Runs 1 to 13 at 22 Bar BMEP engine load and 2000 rev/min.

The two simulation cases, which achieved the 'optimum' effective viscosity of 4.6 cSt, were Runs 4 (KV100 = 6.4 cSt, VI = 300) and 6 (KV100 = 4.6, VI = 1728 (isoviscous)). These are interesting simulation test cases, because the VI's importance can be analysed by comparing their results. The simulation output from Run 6 provided the lowest frictional power of all runs completed (28.0 W). However, the total power loss was only slightly greater in the low VI Run 4 (28.4 W), despite its KV100 being 1.8 cSt higher. This behaviour indicates that the performance of a very high VI fluid can be approached using a lower VI fluid, by tuning the KV100. The higher magnitude of boundary friction in Run 4 may indicate that the wear rates would be larger in the low VI case, which would be undesirable.

3.5. The effect of shear thinning in the big-end bearing

The presence of shear stress in the bearing, combined with the non-Newtonian behaviour of lubricant to these stresses, provided another opportunity to control viscosity reduction in the bearing. This correlation was investigated by predicting bearing friction changes using different shear viscosity profiles. The lubricants

evaluated were all thermally isoviscous (KV40 = KV100) to remove any confounding interactions from shear heating.

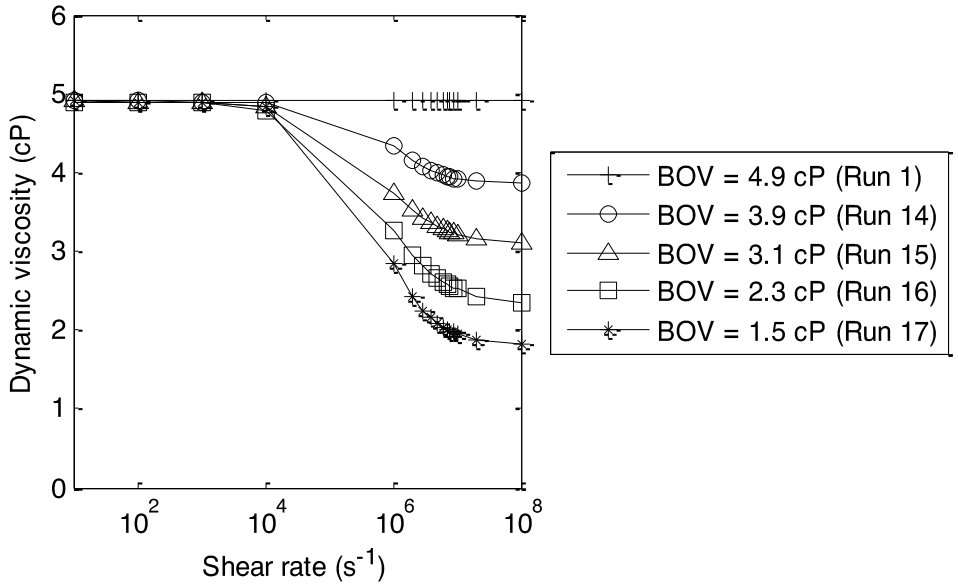

Figure 23. Shear viscosity profiles for Simulation Runs 1 and 14-17. BOV is the base oil viscosity.

For Runs 1 and 14 to 17 the shear viscosity profile was manipulated by varying the base oil viscosity[10]. Figure 23 shows the shear-viscosity behaviour of the lubricants. Each candidate demonstrated a slightly different viscosity change rate with altering shear rate (shown by the different gradients of the lines of shear rate below $1x10^7$ s^{-1}). This difference was necessary, since the starting viscosities (zero shear dynamic viscosity) were the same, but the final viscosities (infinite shear) differed.

For simulation Run 1, the zero-shear viscosity was higher than the optimum found for the bearing. Thus, it was anticipated that introducing the shear-viscosity dependency would reduce the predicted frictional power loss. Figure 24 plots the results from the shear-viscosity modelling activity undertaken to test this theory. Each result is plotted against fluid base oil viscosity, representing the maximum viscosity reduction achievable by shear thinning. As the base oil viscosity was lowered to 4 cSt, the total

[10] Base oil viscosity is a misnomer. Strictly speaking this is the viscosity of the non shear-thinning components of the formulation, which include the base oil and also some components in the lubricant additive package.

power loss lessened in line with the hypothesis. Reducing the base oil viscosity to below 4 cSt caused the friction to increase, which was attributed to the increased contribution from boundary friction to the total power loss.

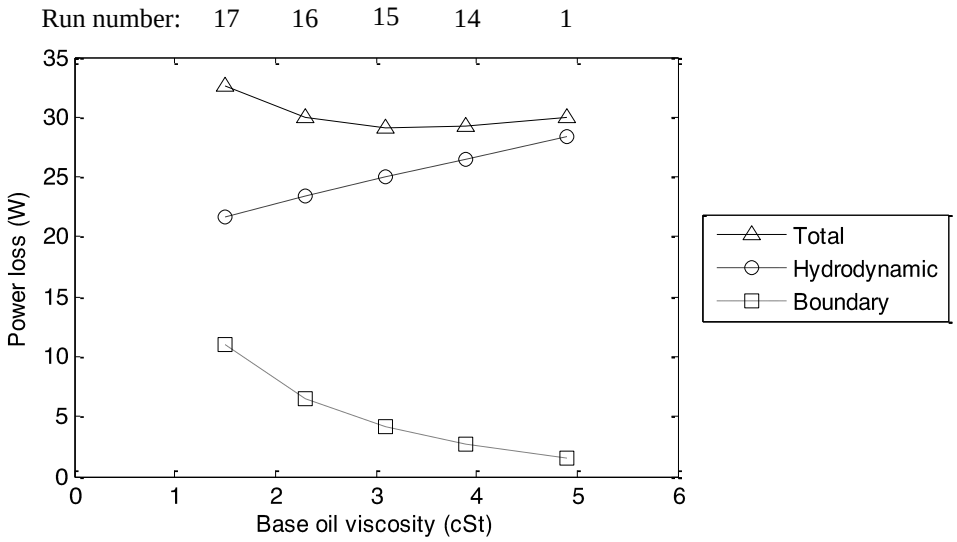

Figure 24. Frictional loss for Simulation Runs 1 and 14 to 17 over a range of base oil viscosities at 22 Bar BMEP engine load and 2000 rev/min.

Figure 26 shows the simulated shear response in a heat map format. The data shows the maximum shear rate predicted to occur in every location on the bearing throughout a full combustion cycle. The magnitude of the shear rates predicted by the simulation was high. Thus, the model predicted that the lubricant viscosity reduced to the base oil viscosity on the upper bearing shell during the combustion cycle. In all simulations, other than the non-shear-thinning case (Run 1), the oil viscosity in the sheared condition was lower than the bearing's 4.6 cSt optimum viscosity. Despite this, a reduction in total friction was predicted, since the shear rate varied spatially and temporally. Over the full bearing surface (and the combustion cycle), the effective bearing viscosity was above 4.6 cSt for many test cases, despite the notional base oil viscosity being low.

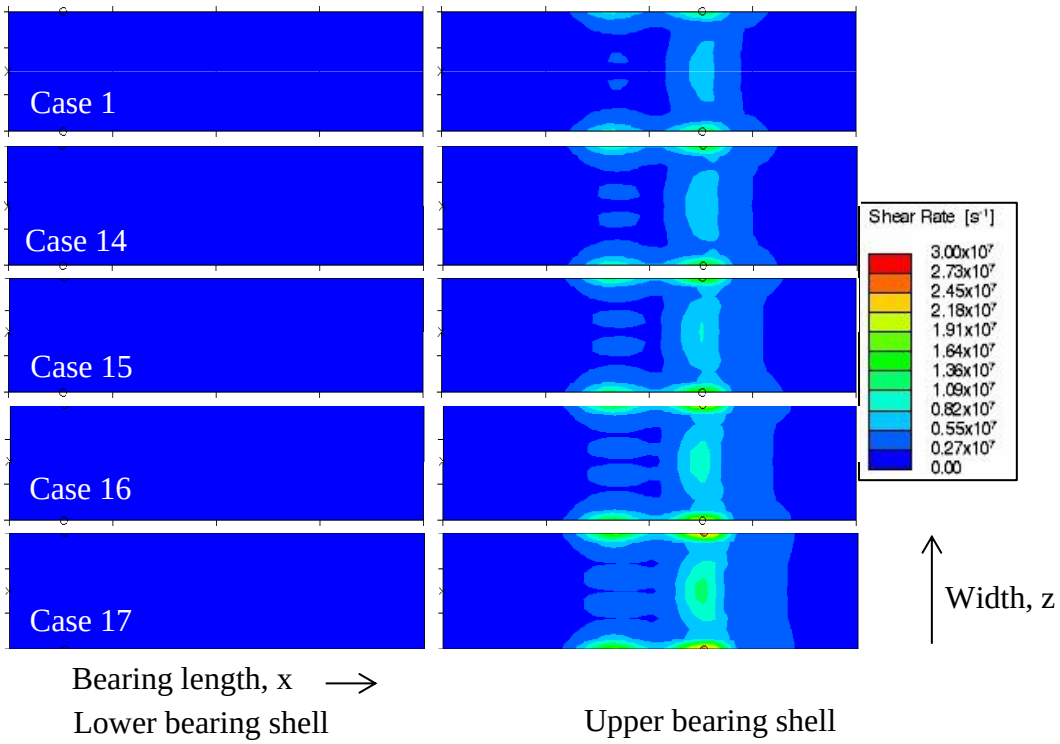

Figure 25 Location and magnitude of maximum shear rates predicted for Runs 1 and 14 to 17 at 22 Bar BMEP engine load and 2000 rev/min[v].

Figure 25 shows a concentration of high shear along the bearing's centreline due to the connecting rod distortion in this area during the combustion loading. The increases in predicted shear rate at the bearing shell's extremities are attributable to the lubricant's temperature rise across the bearing, resulting in reduced oil film thickness.

The results from these simulation runs indicate that when the lubricant viscosity is above optimum, the lubricant's shear-viscosity response can be used to reduce the total frictional power loss. The minimum frictional power achieved by lowering the base oil viscosity was 29.1 W and this occurred with a base oil viscosity of 4 cSt. This result was 2.8 % lower than the predicted total friction for Run 1 (6.4 cSt KV100, isoviscous), which generated 30.0 W of frictional power loss.

The improvement achievable by reducing base oil viscosity was lower than that simulated for the viscosity-temperature analysis in 3.4. Here, the shear-viscosity response is less significant than the temperature-viscosity effects. However, this effect

may not be reproducible in simulations with different bearing geometries, loading conditions or temperatures.

The shear rates in Figure 25 are mainly below $1x10^6$ s^{-1}, although some maxima are in the $3x10^7$ s^{-1} range. These ranges of shear rates are in the transition zone between the lubricants first and second Newtonian regimes (see Figure 4, Section 2.3). Thus, the performance of real lubricants in the non-Newtonian zone should be studied more fully. This sensitivity should be considered in future studies and may provide another variable to tune the lubricant performance (e.g. by selecting different viscosity modifiers).

3.6. The effect of lubricant density in the big-end bearing

Run 18 assessed the effect of lubricant density on predicted bearing friction. Table 8 shows Run 18's lubricant parameters, selected by varying those of Run 6.

Table 8. Density values used in each simulation.

Simulation Run	Density (kg/m^3)
1-17, 19	770
18	869 -0.61*T

where T is the temperature of lubricant contact in degrees Celsius.

Table 9 compares the results from Run 6 with those of Run 18. The lubricant used in Run 18 had a slightly higher density than that used in Run 6, which increased its dynamic viscosity. The higher viscosity increased the local oil film thickness, reducing boundary friction while increasing the magnitude of hydrodynamic friction simulated.

Table 9. Simulation results for density – temperature response simulation, Runs 6 and 18.

Simulation Run	6	18
Effective density (kg/m^3)	770	794
Effective viscosity (cSt)	4.6	4.8
Effective temperature (°C)	123.0	123.2
Hydrodynamic power loss (W)	23.8	24.2
Asperity power loss (W)	4.0	3.9
Total power loss (W)	28.0	28.1

These results indicate that lubricant density can be used as a variable to alter the viscosity in the bearing (e.g. by changing the base oil). The Reynolds equation (12) uses the dynamic viscosity (see Section 1). Thus, changing the density directly increased the dynamic viscosity, explaining the results. Moreover, the density change directly affected the resultant temperature rise. The mass in the control volume, the flow rate and the specific heat capacity (which varies with temperature) of the lubricant determine the temperature rise. Thus, the effect of reducing the lubricant density is non-trivial. In the simulation case investigated, increasing lubricant density increased total power loss. This result is attributable to the increase in effective bearing viscosity to above the optimum viscosity identified.

3.7. The effect of piezo-viscosity in the big-end bearing

Run 19 calculated the significance of the lubricant's piezo-viscosity behaviour. Table 10 shows the pressure viscosity coefficient (labelled α^*) values used in the model.

Table 10. Pressure viscosity coefficients used in each simulation run.

Simulation Run	α^*(GPa^{-1})
1-18	Disabled
19	10

Figure 26 shows the maximum hydrodynamic pressure in this contact, occurring at 30° after top dead centre on the firing stroke. At peak pressure (117 MPa) the lubricant viscosity increased by three times its atmospheric pressure value due to its piezo-viscosity behaviour (see Section 2.4).

To simulate the effect of varying the pressure-viscosity coefficient in isolation from other effects, Runs 13 and 19 were compared. In these runs, the KVs were below the optimum identified for the bearing. Including the lubricant piezo-viscosity model in the simulation reduced the predicted friction by 16%. Table 11 compares the results of

Runs 13 and 19. Changing the lubricant pressure-viscosity coefficient also increased the oil film pressure. Theoretically, this higher pressure could increase fatigue related wear in the bearing, although this is not a dominant form of wear in journal bearings [50]. The increase in viscosity that occurred increased minimum oil film thickness and reduced the maximum shear rate.

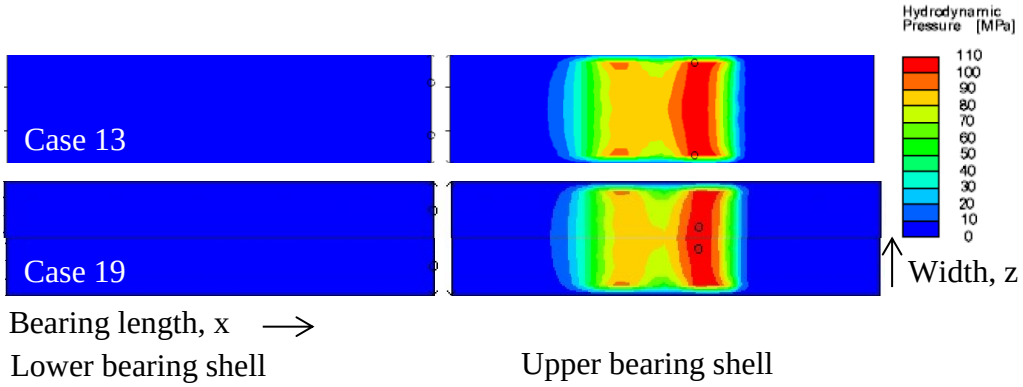

Figure 26. Hydrodynamic pressure area plots for simulation Runs 13 and 19 at 22 Bar BMEP engine load and 2000 rev/min[v].

Table 11. Simulation results for piezo-viscosity runs.

Simulation Run	13	19
Maximum hydrodynamic pressure over cycle (MPa)	112.6	117.4
Maximum shear rate over cycle (1/s)	$3.8x10^7$	$2.4x10^7$
Hydrodynamic friction power loss (W)	18.0	19.6
Boundary friction power loss (W)	21.9	13.9
Total power loss (W)	39.9	33.5

The lower friction predicted is attributable to a significant decrease in boundary regime friction caused by the higher local viscosity in the bearing contact. A small hydrodynamic friction increase was predicted due to local viscosity increase. This conclusion is significant as the lubricants' piezo-viscosity behaviour allows low viscosity lubricants, which under load behave like higher viscosity lubricants, to be used. The opportunity this piezo-viscosity behaviour offers is generally recognised. However, exploiting it to reduce the friction in the conformal contact of a journal bearing is novel.

3.8. Chapter 3 conclusions and recommendations

A simulation was built to predict friction in the big-end bearing of a 1.6 L 4-cylinder turbocharged gasoline engine. A comprehensive evaluation of previous work ensured the model was of high fidelity. Zhang and Gui [52] defined requirements to simulate friction in a journal bearing accurately. These parameters were improved by including: dynamic bearing profile calculations; bearing profile measurement after running-in; non-Newtonian lubricant behaviour; robust treatment of lubricant cavitation and an investigation of different boundary contact friction coefficients.

The simulation was validated by comparing the wear profile predicted by the model to the profile on worn engine components. A good agreement was found. A validation of the predicted and measured friction specific to this work was desirable, but was beyond the investigation's scope. Future work dedicated to developing a tool to measure bearing friction is recommended in order to advance the research reported here further.

An optimum kinematic viscosity of 4.6 cSt was established for the bearing by simulating the performance of a range of Newtonian lubricants with different kinematic viscosities. This optimum viscosity was relevant to the boundary conditions in the model (2000 rev/min engine speed, 22 bar BMEP, 120˚C). Any change in boundary conditions is likely to change the optimum bearing viscosity. An investigation into the optimum bearing viscosity under lower load conditions (e.g. the conditions more representative of vehicle homologation test cycles) is a worthwhile subject for future investigation. This analysis is likely to result in a lower calculated optimum viscosity.

The lubricant's non-Newtonian parameters were enabled independently so their contribution to lubricant performance could be understood. The model investigated response to variation in: VI; temporary shear; density; and piezo-viscosity.

The correlation between friction and lubricant VI was investigated using thirteen separate runs. Lubricants were defined by manipulating their KV40s for lubricants with fixed KV100s. The simulation was used to understand what value of VI was desirable for a lubricant in this bearing. The result was dependent on the lubricant's starting KV. Where the starting viscosity was above the optimum level for the bearing, a reduction in the VI reduced the friction the model predicted. This conclusion is significant, as when lubricants are developed, development technologists normally consider higher VI lubricants to be of a higher performance [7], as they have lower viscosities during the warm-up phase of homologation test cycles. While the low-temperature benefit is important, developing lubricants to achieve high VI values may lead to an increase in bearing friction at more normal engine operating temperatures. In the cases where the starting viscosity was at or below the optimum for the bearing, the simulation predicted that a higher VI reduced the bearing friction.

The magnitude of the shear rates predicted was high. Thus, the model predicted a reduction to the base oil viscosity when the simulation included shear-viscosity characterisation. A reduction in predicted bearing friction occurred when the lubricant shear-thinned. For the lubricants simulated, the zero shear viscosity was above the optimum identified for the bearing, explaining this effect.

The shear conditions predicted were mainly below the 10^6 s^{-1} shear-rate where lubricant high temperature high shear (HTHS) viscosity is normally measured. Thus, the sensitivity of the bearing (and other engine components) to variations in lubricant shear profile below the 10^6 s^{-1} shear-rate may be significant in understanding the performance of different lubricants. The shear viscosity behaviour in this shear-rate range largely depends on the viscosity modifier used in the formulation. Investigating the simulation's sensitivity to different profiles in this shear range would be interesting and is recommended as a future research project.

It was possible to change the predicted friction by varying the lubricant density. In the case reported, raising lubricant density increased total power loss. The result was attributed to an effective dynamic viscosity increase, to a greater magnitude than the bearing's optimum viscosity. A lubricant density reduction would in theory have provided a friction power loss reduction, but this case was not part of the test matrix.

The simulation was sensitive to piezo-viscosity, because the model predicted significant oil film pressures. Where lubricant viscosity was below the optimum, increasing the piezo-viscosity coefficient from 0 GPa^{-1} to 10 GPa^{-1} increased oil film thickness and reduced predicted bearing friction. Thus, lubricant technologists can optimise lubricant performance by varying the lubricant's piezo-viscosity behaviour.

The boundary regime friction coefficient was varied and this variable's importance to the predicted friction and lubricant behaviour was evaluated. This parameter was significant, as it directly affected the magnitude of boundary friction calculated. Interdependence was found between this parameter and the bearing's optimum lubricant viscosity. It was hypothesised that if the value changes (e.g. due to component surface finish varying during running-in, using different bearing materials or lubricant additives) then the optimum lubricant viscosity would also change. Thus, engine tests measuring friction or CO_2 emissions must be rerun, when surface finishes or metallurgies are changed.

Use of polymer bearing overlays in crankshaft bearing applications was found to be becoming more common. A survey of current literature, dedicated to the performance of polymer bearings, indicated that their boundary contact friction coefficients were lower than for bearings with more typical, aluminium alloy construction. The simulation showed that interdependence was present between the boundary contact coefficient of friction and the optimum bearing viscosity. Thus, these bearing types are likely to have

different (lower) optimum viscosities. Theoretically, the lower conductive heat transfer coefficients typical of polymers may reduce heat transfer into the lubricant from the bearing in big-end applications. This new thermal behaviour may mean that these bearings can allow further lubricant viscosity reduction. The current version of the simulation could not predict the effect that polymer bearings have on the oil film temperature, because a full thermal model was not included. For future research, it would be useful to develop the model to account for these effects. However, including this characterisation is unlikely to change the key conclusions from this research.

The journal and bearing's surface roughness was measured using a profilometer. This measurement occurred in the direction of motion for the surfaces, as the simulation was unable to account for the anisotropic surface roughness present. Work by other authors (e.g. Mishra and Rhanejat [59]) suggests that characterising the anisotropic surface roughness features can be significant to the oil film temperature prediction. Developing the code would be useful to include this effect. Theoretically, increased flow rates present in bearings with high axial roughness may improve cooling and lower optimum viscosity. These changes may help low viscosity lubricants' introduction.

3.8.1. Key findings:

- Manipulation of the lubricants' non-Newtonian characterisations allowed a model to predict their contribution to friction reduction.
- Where the starting viscosity was above the optimum level for the bearing, reducing the VI and introducing lubricant shear thinning reduced the friction the model predicted.
- Piezo-viscosity behaviour was found to be important in the bearing. Thus, lubricant technologists can optimise lubricant performance by varying the lubricant's piezo-viscosity behaviour.

4. Piston Friction

Base engine analysis, through simulation and rig testing, indicates that one area with significant potential to reduce engine friction is the piston-to-bore conjunction, due to the high friction in this area [82], [83], [84], [85], [86]. The losses in this zone can represent 20% to 50% of total engine friction [84], [85] [87]. Hydrodynamic friction is normally dominant when the piston speed is high [84] [88] [85] [89], provided good control of piston secondary motion exists. Other lubrication modes exist at different parts of the stroke (e.g. boundary and elastohydrodynamic occurs in the piston rings around the ring reversal points and because of high gas-pressure loading). These contact conditions occur following a transition through the mixed regime [11], [88]. The piston assembly operates with high relative surface speeds. Thus, small forces from friction multiply to give high frictional power losses. Simulation models designed to characterise behaviour here must be of a high fidelity for accurate results, since even small errors generate large power changes when the high piston speeds are considered.

Within this research, measurements from a motored engine test are compared with predictions made using Ricardo Software simulation packages, to understand the friction performance of two lubricants. The research uses the 0W-20 and SAE 8 lubricants defined in Section 2.1.1. The additives in each lubricant were different, but both included surface-active friction modifiers.

The 0W-20 formulation was a multigrade lubricant, including a synthetic viscosity modifier additive that caused its viscosity to vary with shear rate. To include this viscosity dependency in the model, the 0W-20 was tested using a high shear viscometer. Figure 4, in Section 2.3, shows the results from this testing.

4.1. Development of a validated piston friction simulation during warm-up

The NEDC's low temperature starting condition complicates the prediction of engine friction, since including temperature changes affects the lubricant viscosity, macroscopic surface profiles and resulting engine component clearances. Previous research in this area is scarce. Kimura and Murakami [89] evaluate the performance of different cooling jacket designs, comparing measured friction results to their simulation output. They conclude that knowing the differential thermal expansion between the piston and bore during warm-up is important to model the friction forces. However, lubricant effects were not their focus. Taylor [23] and Ma et al. [39] analyse the Mercedes-Benz M111 2.0 gasoline engine used in ACEA's M111 fuel economy test [18]. This test includes operation during warm-up, so their models must characterise the friction variation with temperature change. However, they provide little information to describe their model's approach to simulating friction changes during warm-up.

In the present research, a simulation model is built to allow friction prediction in the piston-to-bore zone during warm-up. Characterisation of various lubricant and component-level changes with temperature is undertaken to achieve a high fidelity simulation. The performance of the model is assessed by comparing the predicted and measured outputs at several temperatures using a motored engine rig.

4.2. Motored rig testing

A complete engine was installed into a motoring test cell for friction testing; Table 12 summarises the engine details. The engine was modified with pressure and temperature sensors, as is normal for this kind of testing, Figure 27 shows the test environment. The engine was connected to a regenerating alternating current (AC) dynamometer operating in motoring mode, with the test cell maintained at 293 K.

A teardown procedure was used, whereby the frictional torque of different parts of the engine subsystem were determined by removing engine components, measuring the resultant torque and completing a subtractive analysis. Two different engine build states were used: crankshaft and pistons and subsequently crankshaft-only tests.

Table 12. Engine specification.

Combustion system	Spark ignition
Engine type	4-cylinder, in-line
Stroke	85 mm
Bore	75 mm
Connecting rod length	141 mm
Peak power	80 kW
Compression ratio	10.5:1
Aspiration type	Natural

The cylinder head and timing drive were not present in either test. A dummy cylinder head, bolted to the engine block, replicated the normal static bore distortion from the cylinder head clamping loads. This component was manufactured with 60 mm diameter holes concentrically above each cylinder bore and vented to atmosphere, to minimise friction from pumping work above the piston crown.

Figure 27. Images of engine installation in the motored engine test.

Subtracting the friction measured using the crankshaft-only from that recorded using the crankshaft and pistons defined the friction contribution from the reciprocating group (piston assembly, big-end bearings and small-end bearings). Testing in this way meant it was not possible to deconvolve the work to overcome inter-bay pumping or big-end bearing friction from that to overcome piston assembly friction. The simulation

exercise included predictions for these quantities. The testing procedure used for the crankshaft-only runs did not include representative reciprocating loads from the piston and connecting rod inertiae, so the increase and change in bearing friction due to this approach was present as a noise factor in this experiment.

To mitigate the confounding effects from the engine oil circuit's changing permeability in its two build states (and associated oil pump drive torques), the standard pump was removed and an electronically-controlled externally-powered pump was fitted. The water pump load and friction from all other components ordinarily driven from the front-end accessory drive system were also removed.

Table 13. Variables controlled during the motored test work.

Test number	1	2	3
Lubricant temperature (˚C)	60	80	110
Coolant temperature (˚C)	60	80	95
Assumed liner and piston temperature in the model (˚C)	60	80	102.5
Engine speeds (rev/min)	600 – 6000		

To allow investigations to be completed at various temperatures, the test bed infrastructure included externally-powered heaters for the coolant and lubricant circuits. Table 13 shows the testing conditions. Tests were completed in a predefined, repeatable cycle. The lubricants were evaluated using the same procedures to remove experimental bias. A robust oil flushing procedure ensured lubricant carry-over effects were minimised. A design-of-experiments procedure allowed the test repeatability to be determined using multiple repeated runs.

4.2.1. Motored test results and discussion

Figure 28 shows the results for each temperature from the motored testing. The friction mean effective pressure (FMEP) of the piston-group components was calculated by subtracting the crankshaft-only drive torques from those which used the crankshaft and pistons, using:

$$\bar{P}_{\mathrm{f}} = \frac{4\,\pi\,(T_{\mathrm{CP}} - T_{\mathrm{CO}})}{V_{\mathrm{D}}} \tag{21}$$

where $\bar{P}_{\mathrm{f}}$ is the FMEP attributable to the piston-group, T_{CP} is the measured torque for the crankshaft and piston testing, T_{CO} is the measured torque for the crankshaft-only test and V_{D} is the swept volume.

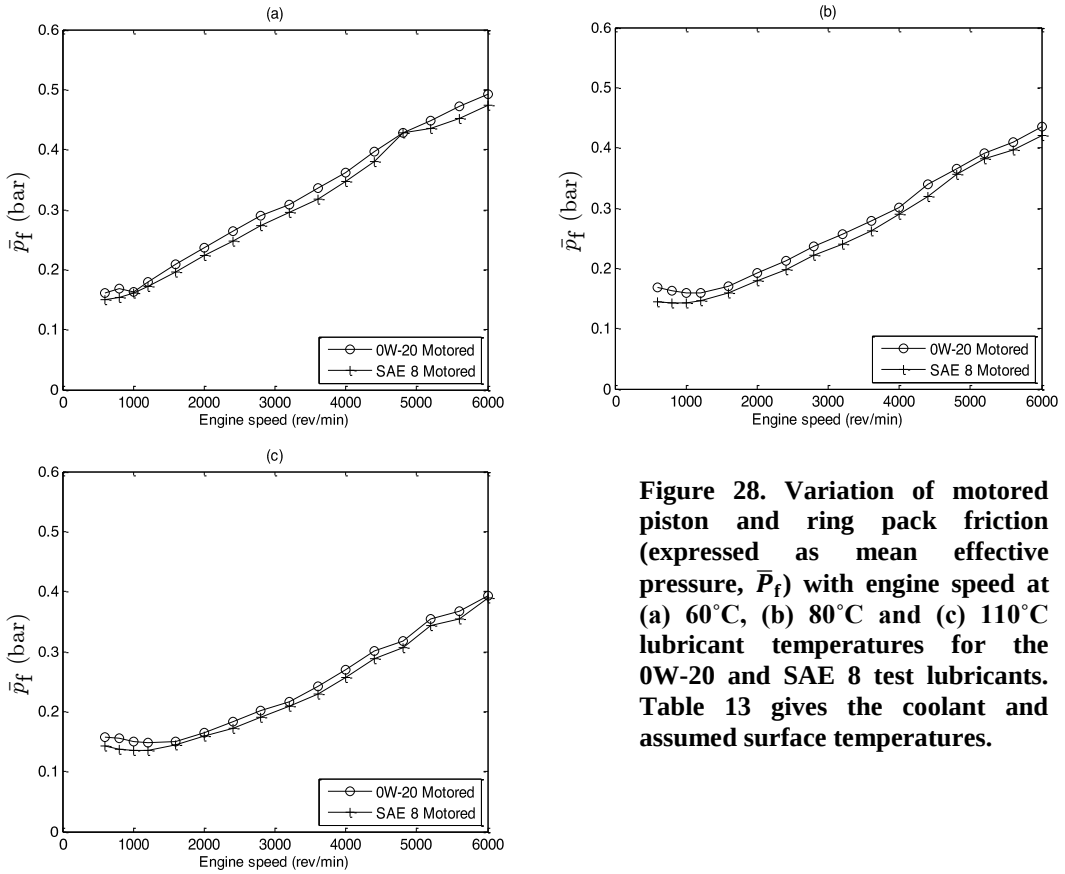

Figure 28. Variation of motored piston and ring pack friction (expressed as mean effective pressure, $\bar{P}_{\mathrm{f}}$) with engine speed at (a) 60˚C, (b) 80˚C and (c) 110˚C lubricant temperatures for the 0W-20 and SAE 8 test lubricants. Table 13 gives the coolant and assumed surface temperatures.

For each temperature condition, the FMEP increased monotonically with engine speed for all speeds above 1600 rev/min. A strong, approximately linear correlation with engine speed was measured. Using the SAE 8 reduced the FMEP. This behaviour suggested the systems were mainly operating in the hydrodynamic tribological regime, which is consistent with the expected behaviour during a motoring test.

At engine speeds below 1600 rev/min at 110°C, 1200 rev/min at 80°C and 1000 rev/min at 60°C, the FMEP significantly deviated from having a linear variation with engine speed. This behaviour became more pronounced and occurred further into

the engine speed range, as the temperatures were increased. This friction increase may indicate a transition into a condition where the boundary friction contribution had become relatively significant, possibly due to a lubricant film breakdown at lower surface speeds. Both lubricants exhibited similar behaviour. However, tests using the lower viscosity lubricant measured smaller FMEP values. This result is arguably peculiar given that the lower viscosity lubricant should transition into the boundary regime before the higher viscosity lubricant. However, it is probably due to the different additives in the lubricants affecting the friction magnitude.

4.3. Simulation tools and component characterisations

The Ricardo Software programs PISDYN and RINGPAK calculated the FMEP of the piston skirts, small-end bearings and rings. Ricardo's ENGDYN program calculated the losses at the big-end bearings. These models are described below.

4.3.1. Piston skirt and small-end bearing

The PISDYN program simulates the lubrication of the piston skirt and small-end bearings. The model predicts the true piston motion by adding the dynamic effects of the component elastic distortion and piston secondary motion onto the displacements calculated by considering only the kinematics of the crank-slider mechanism. This calculation was taken from Dursunkaya and Keribar [82], [83]. The model close-couples a prediction of the resulting lubrication and friction of the piston skirt and small-end bearings into the resulting motion of the system, while also considering the effects of these loads on the overall force balance [83], [90], [91].

4.3.1.1. Surface asperity characterisation within PISDYN

The Greenwood-Tripp model [67] calculated the friction due to asperity contact in the boundary and mixed lubrication regimes within PISDYN. It was assumed that the asperity peaks followed a Gaussian distribution. The asperities were characterised

using: mean summit height, *Zs*, and the standard deviation of summit height, σ. Figure 29 shows how these parameters were defined. Asperity density and radius of curvature measurements, defined in [92], were undertaken to complete the characterisation.

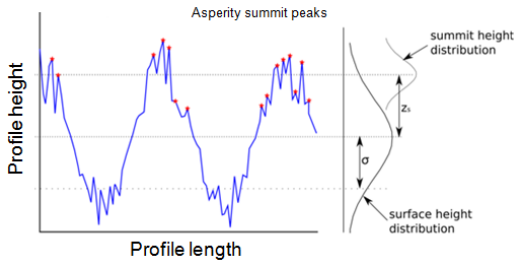

Figure 29. Surface characterisation (Reprinted with Permission from SAE International [93]).

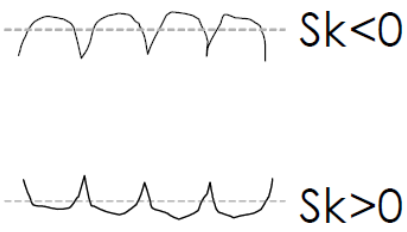

Figure 30. Surface profiles with positive and negative skew (Reprinted with Permission from ASME [85]).

The inclusion of this boundary friction model was important for the present research as other authors had cited the lack of such models as being significant sources of error. Nattrass and Davenport [94] compared simulation and motored tests that did not use an asperity contact model in the piston area. Their testing indicated boundary friction was critical for accurate friction prediction. Hanke et al. [95] completed simulation and fired engine testing showing that boundary friction occurred between the skirt and liner.

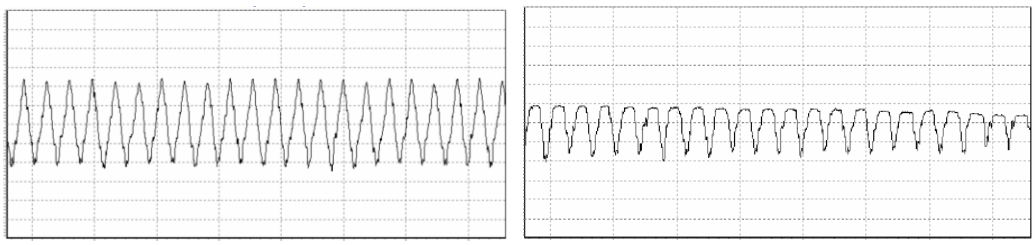

Figure 31. Roughness profile of a piston skirt. Left: as new. Right: following 15 hours of running (Reprinted with Permission from SAE International [92]).

An accurate characterisation of the surface is important when predicting asperity-to-asperity interaction. Thus, partially worn components from the test engine were measured. However, the characterisation model within PISDYN was imperfect since surface skewness and kurtosis were unaccounted for. Some authors consider that this characterisation is important. Tomanik [92] measured surface asperity features using white light interferometry. He states that engine surfaces are rarely Gaussian, due

to the running-in process. Figure 34 shows measurements of a piston skirt published by Tomanik [92]. The change in surface from Gaussian to non-Gaussian forms is apparent from his measurements. Jocsak et al. [85] also characterise the non-Gaussian surface geometry using a skewness factor; Figure 30 defines the form of positive and negative skew. Jocsak et al [85] find that reducing the skewness value generally results in a profile resembling that of a run-in surface (in which the tops of the sharpest asperities have been smoothed) and this change reduces boundary regime friction. Thus, the absence of this factor and potentially that of kurtosis, in the present work may cause over-prediction of asperity contact and boundary friction. Inclusion of these characteristics may improve the model's fidelity in its prediction of asperity-to-asperity interaction and indicates a key code development area for future study.

4.3.1.2. The characterisation of viscosity within PISDYN

The Vogel equation (4) was used by PISDYN to calculate dynamic, low shear, viscosity change with temperature. Viscosity variation with shear stress was calculated using the Cross equation (5). However, lubricant viscosity variation with pressure was not considered in the PISDYN program. Redressing this simplification may improve the model fidelity, should significant lubricant film pressures be predicted.

Lubricant compressibility was characterised using the lubricant bulk modulus:

$$\beta = \rho \frac{\mathrm{d}P}{\mathrm{d}\rho} \tag{22}$$

where β is the lubricant bulk modulus (N/m^2) which can be derived experimentally, ρ is the lubricant density and P is the pressure. Sensitivity studies completed by varying β demonstrated a minimal change in simulation output, but a significant reduction in program run time [91]. Consequently, this term was ignored in the analysis.

4.3.1.3. Characterisation of component profiles

Piston skirt and bore distortion from the nominal profiles was ignored by Carden et al. [90] who also used PISDYN, but including these effects in future models was cited as important to improve the model results. Thus, the present research simulated these effects. The change in skirt and liner profile was calculated using the Ricardo Software FEARCE finite element analysis (FEA) program. Distortions of the bore and skirt profiles due to assembly loads and thermal expansion were simulated.

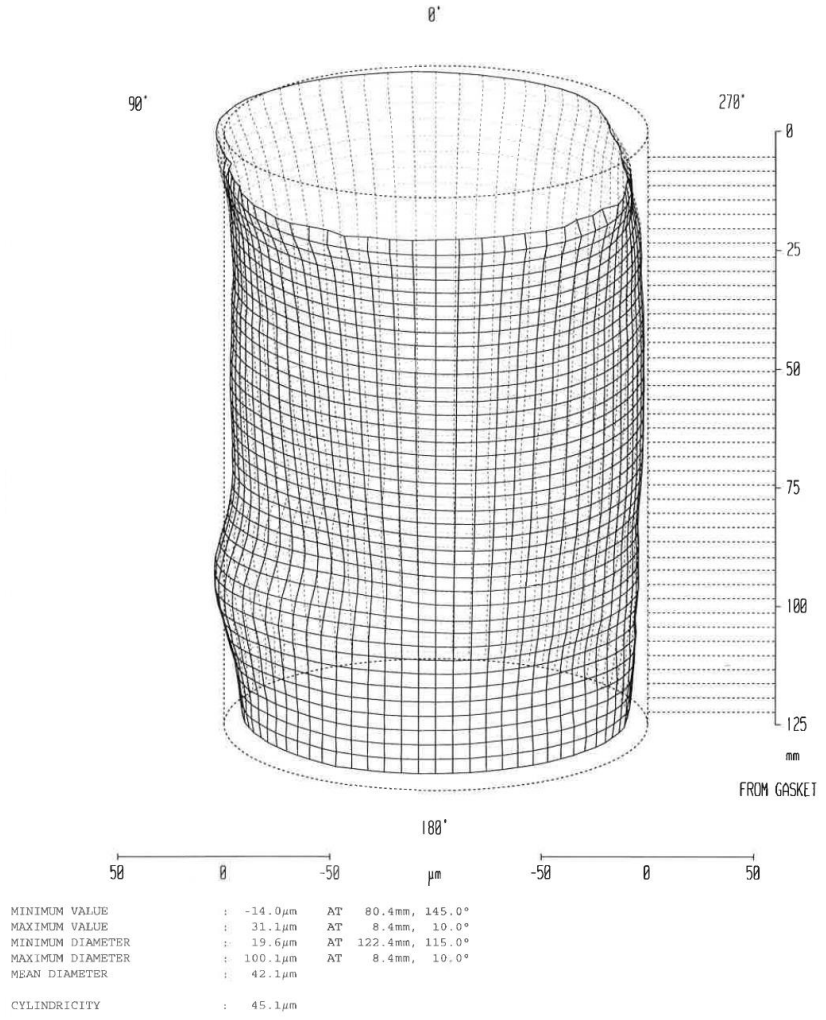

Figure 32. Measurement of the bore deviation from cylindrical for Cylinder 1.[¥]

The nominal bore profiles, including mechanical distortions, attributable to the cylinder head clamping loads, were measured using a 'dummy' cylinder head installed onto the block. Use of the tightening procedure defined by the manufacturer ensured the

correct clamping load and resultant distortions were present. The model incorporated the recorded axial and circumferential distortions. Figure 32 shows measurements from one cylinder. All bores were measured after soaking the block at 293 K for 24 hours.

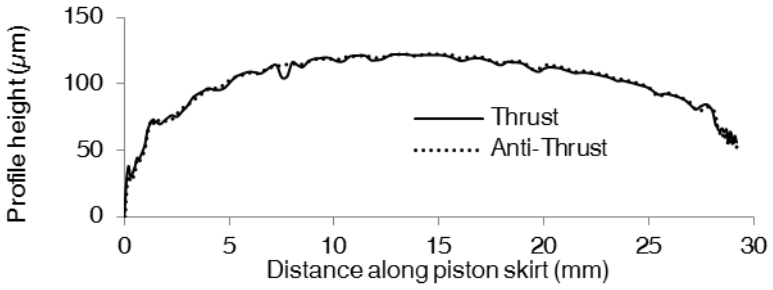

Figure 33. Measured piston skirt profile.

Figure 33 shows the piston skirt profile of a piston thermally soaked to 293 K, at the skirt's centreline. A finite element model adapted this cold profile to the hot shape. Laser scanning of the piston provided the input geometry for this finite element model.

Table 14. Measured surface parameters characterising cylinder bores and piston skirts.

	Summit mean height, *Zs* (microns)	Standard deviation summit height, σ (microns)	Asperity density ($1/m^2$)	Radius of curvature (microns)
Bore	0.313	0.168	$3.27x10^9$	102.3
Skirt	0.09	0.663	$9.72x10^9$	42.6

A surface profilometer measured the piston's surface finish. Table 14 shows the input values used. This data was generated by measuring used pistons.

4.3.2. Piston rings

The Ricardo Software program RINGPAK calculated the piston ring dynamics and friction. RINGPAK analyses: lubricant consumption due to evaporation, blow-by and throw-off; ring toroidal twist; the effect of bore distortion on ring conformance; lubricant transportation along the liner; mixed and hydrodynamic lubrication regimes on

the ring face and sides; axial and radial ring motion [96]. The simulation of each effect is fully coupled and integrated in the program.

The friction under hydrodynamic and boundary contact conditions is calculated using different subroutines in RINGPAK. Hydrodynamic friction is calculated using the Patir and Cheng average flow model [97], which includes surface roughness effects on hydrodynamic lubrication. The surface asperities were assumed to take a Gaussian distribution. A directional parameter was included to incorporate the effects of the generalised asperity shapes on the hydrodynamic flow prediction. The effects of lubricant cavitation in the tribological contact were also considered within RINGPAK.

Using a different proprietary program Taylor et al. [11] correlated oil-film-thickness prediction with measured values using laser fluorescence. They discuss the importance of including lubricant shear in the model and use the Cross equation (5). A significant (~30%) oil film thickness over-prediction, particularly at the first compression ring, occurred without it. Thus, the present work characterised this behaviour. The Vogel equation (4) characterised the viscosity variation with temperature.

The piston ring analysis does not include the effect of piston secondary motion, since this was ignored in RINGPAK. Other codes do include an allowance for this effect [95], suggesting this may be a key code development area. Viscosity variation with pressure was also left unmodelled, since the RINGPAK did not provide for its characterisation. Taylor et al. [11] included this effect in their model, but disabled it since its inclusion did not affect the results significantly. Thus, this simplification is believed to cause only a small error in the present model.

4.3.3. Characterisation of the piston rings' profiles

The ring face profiles were matched to measured data taken from the worn piston rings shown. A surface profilometer measured the surface roughness of the first and second compression rings. Figure 34 shows their forms. The small widths of the oil control ring prohibited its measurement, so a parabolic profile was assumed.

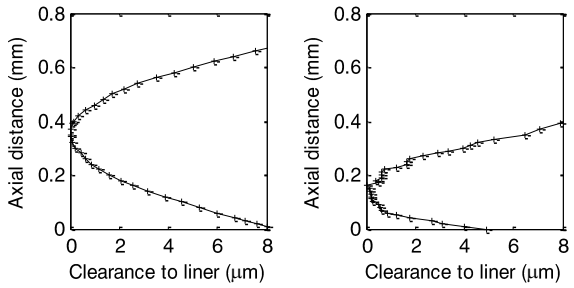

Figure 34. Measured profile from broken-in 1st compression ring (left), 2nd compression ring (right).

The procedure in BS ISO 6621-2:2003, Section 4.2.5.1, was followed to determine the spring stiffness in the piston rings. This standard describes the 'tape method' for determining tangential force of the rings as installed in the cylinder bore. Measurements of the ring end gaps at 293 K in the midstroke position of a partially worn cylinder liner set the installed diameter for the rings. Table 15 shows the mean results from four rings of each type.

Table 15. Measured ring tangential force results.

	Tangential force (N)	
Condition	New	Used
Top ring	**3.58**	Not available
Second ring	3.9	**3.55**
Oil control ring assembly	16.6	**14.1**

New and partially worn rings were measured to understand if any differences existed. The ring tension was lower on the worn components. However, it was not possible to determine if the variation in tangential force was attributable to a batch-to-batch variation or to the wear process, since the new and used components were not the same parts. Partially worn first compression rings were unavailable, so

only values obtained using new rings are reported. The model incorporated the results from the used second and oil control rings along with the results from the new top rings.

4.3.3.1. Piston ring surface roughness

Bolander et al. [88] describe a new ring-on-liner test method that includes an oil film thickness measurement. They compare results generated using this rig with predictions from a model. The correct characterisation of the non-Gaussian surface roughness distribution on this component was recommended. Including the roughness heights alone was said to be insufficient to describe the surface adequately.

Table 16. Measured surface parameters characterising the piston rings.

	Summit mean height, *Zs* (microns)	Standard deviation summit height, σ (microns)	Asperity density ($1/m^2$)	Radius of curvature (microns)
First ring outer face	0.064	0.066	$1.34x10^{10}$	62.8
Second ring outer face	0.159	0.541	$3.90x10^{9}$	60.2

The RINGPAK model developed in the present research characterised the ring and liner surfaces using the methodology described in Section 4.3.1, which included a comprehensive representation. However, a Gaussian distribution was again assumed for the asperity heights. Thus, boundary friction may also be overpredicted in the present ring pack model. Table 16 shows the input values.

4.3.4. Thermal boundary conditions

In the motored test work, the coolant and lubricant temperatures were controlled independently. The lubricant and coolant temperatures were the same at 60°C and 80°C, but at 110°C lubricant temperature, the coolant temperature was controlled to 95°C, since this setting more closely represented that of real engine usage. The piston temperature used in the model was 102.5°C, the arithmetic mean of the two set points.

4.3.5. Characterisation of the bearing and windage losses

The Ricardo Software program ENGDYN calculated the friction contribution from the big-end and crankshaft bearings. Chapter 3 describes the ENGDYN program. A simplified model was used, which assumed that the journals and bearings were rigid and operated in the hydrodynamic regime. The rotating and reciprocating motions of the crankshaft, pistons and connecting rods were calculated to define the bearing loading.

The crankshaft, connecting rod and piston inertiae were calculated using the computer-aided engineering program, SolidWorks. A laser scanning process defined the components' input geometry. The components' densities were determined by adjusting their values to match the calculated and measured masses.

A constant oil supply pressure of 3.5 bar gauge was applied at all speeds. The bearing model included an iterative thermal balance so that effective oil temperature was calculated from consideration of the oil supply temperature, flow rate and friction loss in the bearing at each speed. The viscosity models used within RINGPAK and PISDYN characterised the oil viscosity. However, the change in viscosity with pressure was also characterised using the Barus equation (defined in 2.4).

An empirical formula based on Ogawa's work [98] calculated crankcase pumping loss, which depended on crankshaft speed and inter-bay flow area. A coordinate measurement tool recorded an 11.5 mm désaxé offset between the crankshaft centreline and cylinder axes. The model included the effect of this offset on piston speed and loading.

4.4. Simulation results and comparison to measured values

Figure 36 plots the simulation results for each temperature. The simulation correctly ranked the lubricants and generally correlated well with the motored test results. The 60˚C simulation results are the least well correlated of those reported. As

engine speed increased, the difference between predicted and measured results increased. At 6000 rev/min friction was over-predicted by 18%. Lower and mid-engine speed results (e.g. 1500-3000 rev/min) were more closely correlated. At the lowest engine speeds, predicted friction was lower than measured. It was apparent that the simulation code did not correctly predict the friction increase at these low speeds.

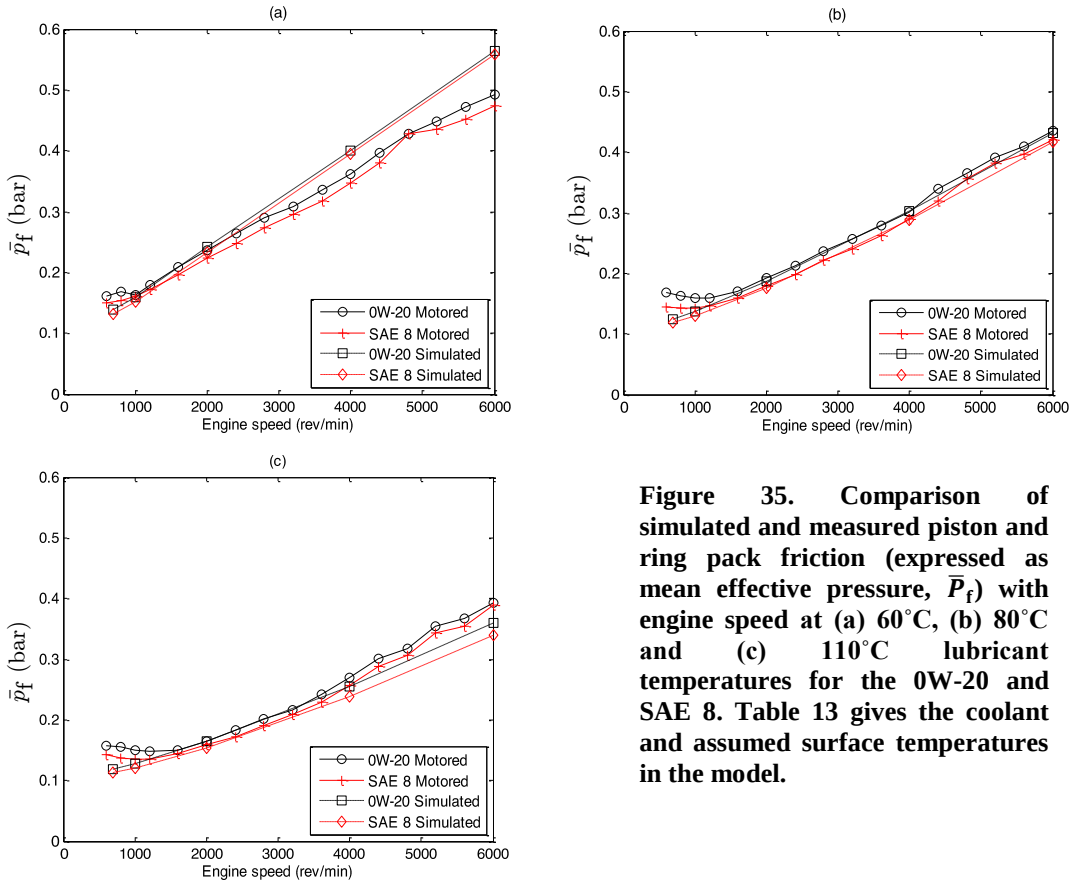

Figure 35. Comparison of simulated and measured piston and ring pack friction (expressed as mean effective pressure, $\bar{P}_f$) with engine speed at (a) 60˚C, (b) 80˚C and (c) 110˚C lubricant temperatures for the 0W-20 and SAE 8. Table 13 gives the coolant and assumed surface temperatures in the model.

The difference between measured and predicted friction was smaller at 80˚C, where a very good correlation was seen for most of the speed range. The simulation correctly predicted the frictional differences between each test lubricant at most speed cases and correctly ordered the lubricant results. Similar to the results at 60˚C, the simulation did not adequately predict the friction upturn at the lowest engine speeds.

The difference between measured and predicted friction was higher in the 110˚C test case than at 80˚C. However, the correlation was generally good and very close in

the mid-speed range. Like the other temperatures, the simulation did not predict the low speed friction upturn.

The difference between the measured and simulated friction at 60˚C may in part be due to the assumptions made with respect to the metal temperatures in this condition. The lubricant here is the highest viscosity of those tested. Thus, shear heating is significant. The boundary conditions input to the model assumed the metal surface temperature was the same as the temperature to which the coolant was controlled. For this high viscosity test, the assumption may be less valid. To investigate the model sensitivity to this boundary condition, repeat tests were completed using an assumed surface temperature of 65˚C. Figure 36 plots the results from this simulation.

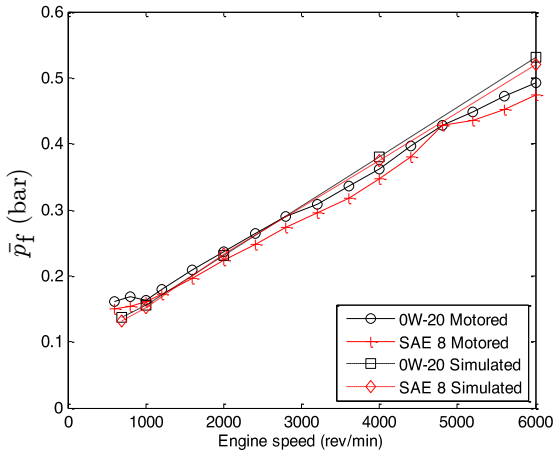

Figure 36. Predicted and measured test results using a metal surface temperature of 65˚C for the 0W-20 and SAE 8 test lubricant. Expressed as friction mean effective pressure, $\bar{P}_f$, versus speed.

The modification made to the surface temperature improved the correlation between the measured and simulated results, suggesting this may explain the differences reported. A deviation is still present, especially at 6000 rev/min, but the difference is much smaller than seen before. Rather than arbitrarily complete further simulation runs to improve the correlation between the measured and simulated results, further research is recommended to generate a more detailed thermal survey of the metal temperatures present in the test and to use these real values for further model refinement.

The friction deviation at each temperature for lower engine speeds warrants more consideration since the lubricant additive system appears to have a significant effect. Figure 37 breaks down predictions of the contributions of each factor modelled.

With decreasing engine speed, the model predicts a reduced contribution to friction from hydrodynamic losses. The surface speeds and loads within the component groups become smaller at low speed. Therefore, the measured friction increase is unlikely to be due to a reversal of this trend. Any increase in friction due to inter-bay pumping or big-end bearing friction is also unlikely. Thus, consideration must be given to boundary friction at the piston rings and skirt. Due to the loads present being very low, the piston skirt is not predicted to enter boundary contact conditions and no significant increase in piston secondary motion is predicted. The friction increase is more likely to be due to a change in the ring pack's frictional performance.

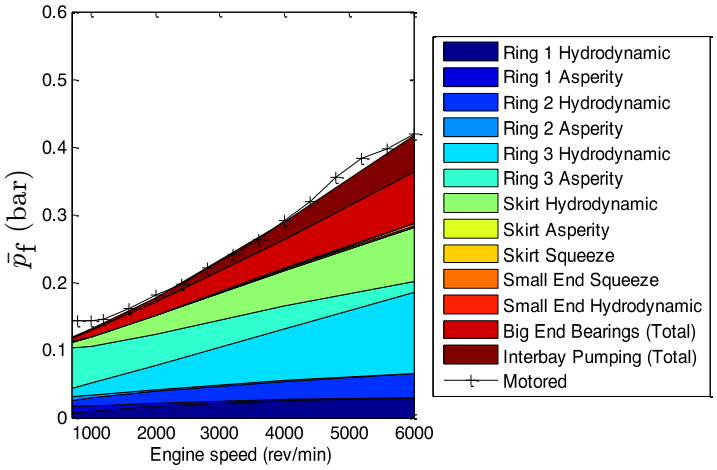

Figure 37. Predicted piston and ring pack friction and comparison to measured data for SAE 8 at 80˚C. Ring 1 is the first compression ring, Ring 2 is the second and Ring 3 is the oil control ring.

Similar low speed friction increase was also measured in motored testing by Taylor et al. [99] in the piston-to-bore, attributed to increasing boundary friction. Calabretta et al. [100] reported a similar discrepancy between simulated and measured results under low speed conditions. Their work used similar analysis techniques to the present research, but they simulated an engine valvetrain. Simulation accuracy was improved by including a variable friction coefficient under the boundary regime.

Applying a similar approach to improve the correlation of the models discussed in the present research, would require the asperity friction coefficient to vary as Table 17 describes.

Table 17. Variation in boundary friction coefficient required for correlation to motored results.

Engine speed (rev/min)	0W-20	SAE 8
700	0.15	0.13
1000	0.13	0.12
2000	0.1	0.1
4000	0.1	0.1
6000	0.1	0.1

The non-linear variation of the friction coefficient for boundary lubrication is unusual. Unlike the case studied by Calabretta et al. [100], a significant variation in the composition of tribofilms is unlikely given the similarity in contact loads between the high and low speeds. A tribometer was used to investigate whether this theoretical variation in friction coefficient was present in this conjunction. The TE77 Cameron Plint, High-Speed Reciprocating Rig (HFRR) and Mini Traction Machine (MTM) were available for this study.

4.5. Tribometer measurement of the boundary regime friction coefficient

Table 18 gives an overview of the three tribometers. The contact loads available covered a useful range. However, the surface speeds achievable with all the tribometers were below those occurring in the engine (e.g. a maximum piston speed of 1.3 m/s occurs at 270 rev/min for this engine). This limitation is undesirable, but since the piston velocity passes through zero at the end of each stroke, the rig does replicate some parts of the piston's motion. Clearly, even when the speeds are matched, a significant acceleration difference between the rig and the engine exists. This constraint will tend to reduce the similarity in the oil film fluid dynamics between the rig and engine.

Table 18. An overview of the three tribometers.

Feature / Rig	TE77	HFRR	MTM
Sample material	Sample from engine	Rig specific	Rig specific
Load range	5 – 500 N	0 – 10 N	0 – 75 N
Speed range	0 – 1.2 m/s	0 – 1.3m/s	-4 – 4 m/s
Motion type	Reciprocating	Reciprocating	Rotating
Contact type	Ring on liner	Ball on plate	Ball on disc

The reciprocating motions used in the TE77 and HFRR tribometers replicated the conditions in the piston-to-liner contact, which made them more desirable than the MTM, since its motion was rotational. The ability to install a section of piston ring and liner in the TE77 tribometer provided a benefit over other rigs, since the surface finish and metallurgy would be identical to the engine. Thus, the TE77 tribometer was used.

4.5.1. Rig set-up

A section taken from the first compression ring was mounted to a holding tool in the TE77 rig and loaded against a section cut from the engine liner. Figure 38 shows an overview of the test set-up, the liner section and piston ring holding tool. The liner section was taken from a used engine and the piston ring was taken from new stock.

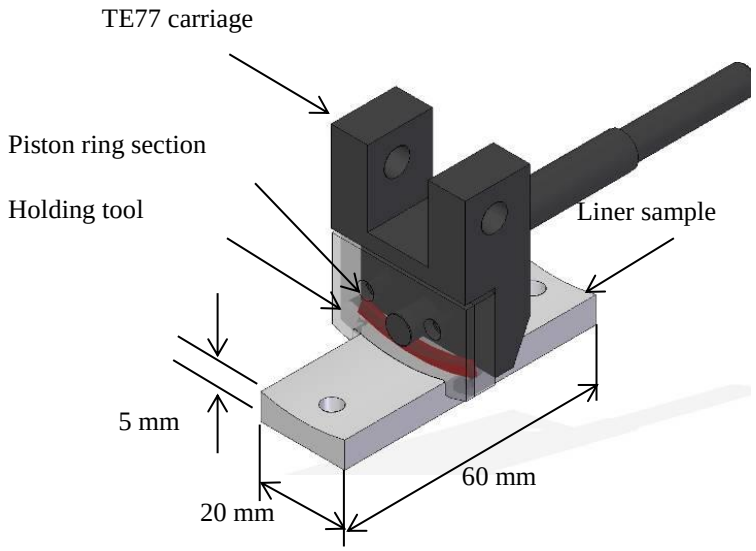

Figure 38. Model of liner sample and piston ring holder.

The contact pressure for the ring occurring in the engine was calculated using:

$$P = \frac{2F_T}{Dh} \tag{23}$$

where P is the contact pressure, F_T is the piston ring tangential force, D is the bore diameter and h is the thickness of the ring [101]. Combustion pressure loading was ignored since the TE77 rig test was used to replicate motored engine conditions.

The contact length used in the rig test was 10 mm. Thus, the load applied to the piston ring by the tribometer was set using:

$$F = \frac{2F_T l}{D} \tag{24}$$

where l is the piston ring contact length in the rig.

A contact force target of 0.95 N was arrived at using this equation. However, it was not possible to operate the rig at 0.95 N load, since the reaction force present to counteract the mass of the piston ring carriage exceeded this value. The lowest force that could be measured reliably was 5 N. This constraint meant that the rig could only be used to investigate friction coefficients, rather than the friction force magnitude in the motored engine. A matrix of contact loads from 5 N to 40 N was used to investigate the sensitivity of the rig output to this parameter.

4.5.1.1. Dynamics of the TE77

Figure 39 shows a schematic of the TE77 tribometer. A carriage mounts a liner sample on which the ring section is loaded and reciprocated. Plint [102] discusses the TE77 rig design as permitting two modes of operation: coupled and decoupled. In the coupled mode, the friction force transducer is mounted to the specimen carriage which is tied to the rig frame. The friction forces are reacted by the force transducer, which has a low stiffness compared to the specimen carriage mounts. In the decoupled mode, the freed specimen carriage can move relative to the machine frame. The friction forces are reacted by the transducer and elastomer stops at the end of the specimen carriage.

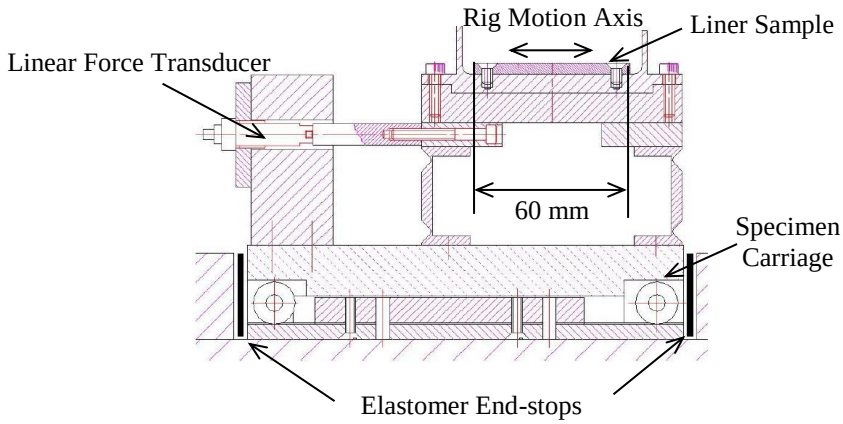

Figure 39. Schematic of TE77 rig. Reprinted (and Adapted) with Permission from Plint [102].

Operation in the decoupled mode is important at high speed to avoid gross vibrations of the machine body being transmitted into the liner sample and affecting the friction measurements. Decoupling is recommended for speeds over 20 Hz [102]. However, simply respecting this requirement is insufficient to avoid erroneous friction measurements. Plint [102] recommends reducing the stroke length when the rig uses high frequencies. Thus, two operation modes are possible: low frequency and long strokes or high frequency and short strokes.

4.5.1.2. Test set up investigation –TE77

Figure 40 shows friction coefficient results from 5 Hz friction tests, while Figure 41 shows the 25 Hz results and a range of loads. A high-speed acquisition system logged the friction force at a frequency of 22.5 kHz. The data plots the rig operation as if it occurred anticlockwise, although the rig reciprocated along a linear axis. The stroke start is at 7.5 mm displacement with a positive friction coefficient and the stroke end is at -7.5 mm. The friction coefficient is negative for the carriage motion from -7.5 mm to 7.5 mm. Data was recorded over 0.18 seconds, the maximum interval the rig permitted. Thus, part of the complete cycle was captured at 5 Hz with circa 4.5 complete cycles at 25 Hz. This limitation was addressed in later tests.

At 5 Hz and 5 N load, the friction coefficient varied from 0.03 to 0.4, but significant oscillations occurred (Figure 40). Increasing the load to 10 N reduced their

amplitudes. The friction coefficient varied from 0.15 to 0.2. Raising the load to 40 N reduced the amplitudes further. The friction coefficient varied from 0.11 to 0.13.

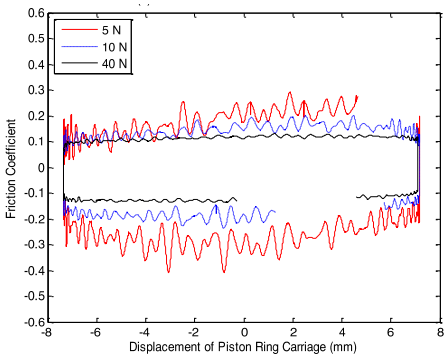

Figure 40. Results from TE77 procedure development testing using 0W-20 at 5Hz rig speed.

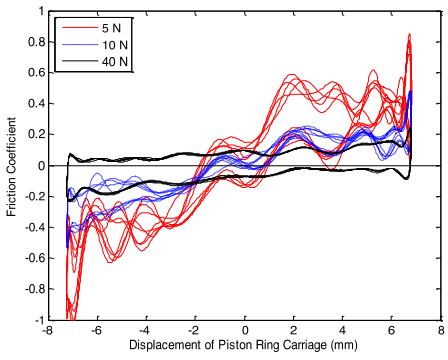

Figure 41 Results from TE77 procedure development testing using 0W-20 at 25 Hz rig speed.

Increasing rig speed to 25 Hz (Figure 41) caused the friction coefficient to vary abnormally. The friction coefficient oscillation increased, causing the friction force direction (and thus coefficient) to vary out-of-phase with the carriage motion. This behaviour does not follow logically, since it is impossible for the friction force to operate in the same direction as the carriage motion. These results were attributed to excitation of the specimen carriage by the machine body vibration that Plint describes [102]. After studying various frequencies, operation at 5 Hz was chosen.

Operating the machine using high-speed data recording equipment is not standard. Without this data, it would have been very difficult to explain the variation in mean friction coefficient ordinarily reported by the rig. Thus, using the high-speed data system is important for chemists and engineers developing new tests.

Elsewhere, Plint [103] discusses potential additional force measurement errors. He describes a plucking action at the start of each stroke causing the rig carriage to be excited and to vibrate at the natural frequency of its body and mounting stiffness. The plucking is caused by stiction between the ring and liner at the ring reversal point. This behaviour results in the transducer oscillating and can affect the measured friction

values. The oscillation decay rate is a function of the contact's damping coefficient. The present data exhibits this effect. The oscillation in friction coefficient output is likely to be due to the resultant vibration effect. Higher loads reduced the plucking noise and provided stable results, so a value of 40 N was used in the test work.

4.5.2. Test conditions

Testing used the 0W-20 and SAE 8 lubricants. Table 19 summarises the test conditions. Four tests were carried out to allow a repeat run on each lubricant. The ring and liner samples were changed for each experiment. Each test lasted 24 hours and there was a break-in procedure prior to operation at the target condition. Repeating set contact conditions periodically during the test allowed a check as to whether changes in the surface characteristics were occurring. No significant changes in friction took place.

Table 19. Testing conditions used in TE77 tribometer.

Test Number	Candidate	Contact load (N)	Rig speed (Hz)	Temperature (˚C)
1	SAE 8	40	5	60, 80, 102.5
2	0W-20			
3	0W-20			
4	SAE 8			

4.5.3. Results

Figure 42 shows the friction coefficients measured using the two lubricants. The mean friction values ranged from 0.10 to 0.11 for the SAE 8 and 0.11 to 0.12 for the 0W-20. The SAE 8 values reduced with rising temperature, probably due to its friction modifier's efficiency rising with temperature. The 0W-20 did not exhibit temperature sensitive behaviour.

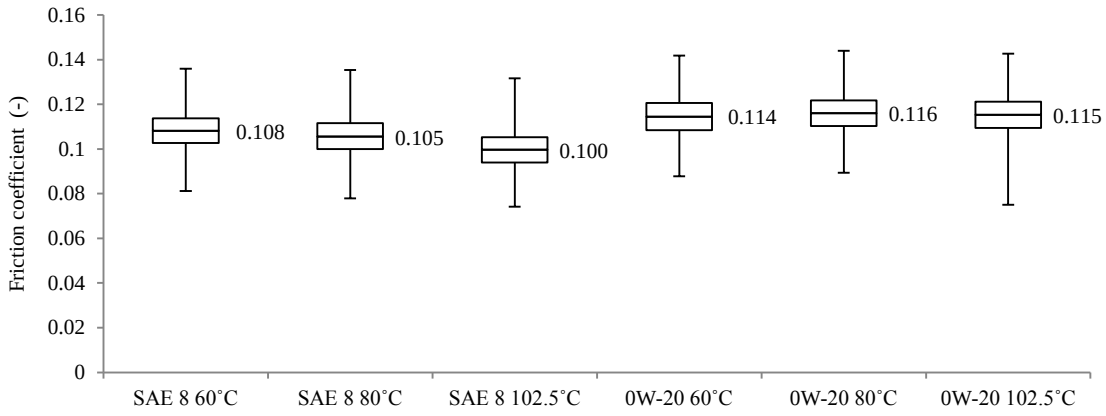

Figure 42. Boxplot showing friction coefficients from the tribometer. Upper and lower whiskers represent maximum and minimum values, upper and lower bounds of box represent 1st to 3rd interquartile range, mid line (and data labels) represents the mean value from test results.

These friction values are lower than those required in Table 17 to tune the engine model output. There was a small variation in results in each condition, but the first to third interquartile ranges were below 0.012 for each case. This spread is insufficient to achieve the values required to improve the model accuracy.

A large range from maximum to minimum friction values was present. Figure 43 plots the high-speed data for the cycles with 0W-20 at 5 Hz, 102.5˚C and 40 N, which showed the largest spread in friction coefficients. The high maximum and minimum friction coefficient values recorded on this lubricant occurred during an oscillation as the carriage passed between -3 mm and 4 mm on the return stroke. This data indicates the reported friction variation is likely to be due to a mechanical oscillation not a boundary friction change. Thus, it is unlikely that these extreme values are real.

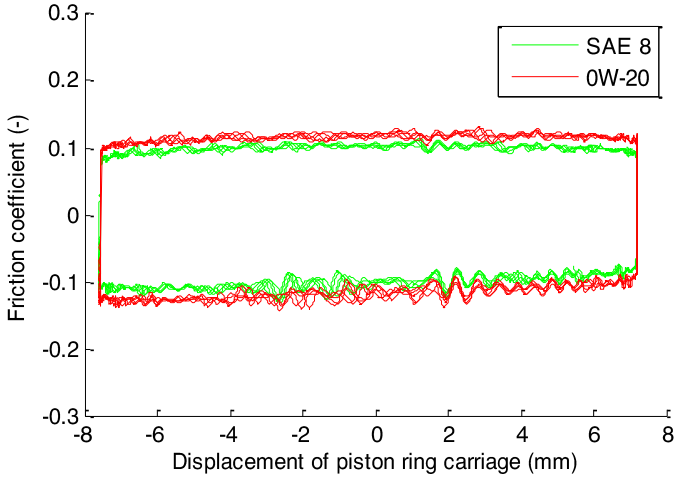

Figure 43. Results from the tests using 0W-20 at 5 Hz, 102.5˚C and 40 N load.

The test results showed that the friction coefficients measured by the rig were insufficient to achieve those required in Table 17. This conclusion indicates that the measured friction increase is unlikely to be due to incorrect characterisation of the boundary friction coefficient by the model. The test results cast doubt over the approach taken by Calabretta et al. [100] and may indicate that a more fundamental inaccuracy in the friction model exists. However, the exact ring-to-liner contact conditions could not be replicated, so it was not possible to establish this conclusion unequivocally.

Theoretically, the non-linearity at low engine speeds may be an attribute of the rig (e.g. a resonance in the drivetrain). Investigating the performances of the lubricants with friction modifier additives tested this hypothesis. Figure 44 shows the results from the SAE 8 compared to a 0W-20 including the friction modifier additive, molybdenum dithiocarbamate (MoDTC)[11]. At low speeds (e.g. below 1600 rev/min) the upturn in friction in the previous motored results disappeared. This change demonstrated the rig attributes were not at fault.

[11] MoDTC decomposes under the temperatures and pressures in the tribological contact to form a low friction tribo-layer of molybdenum disulfide.

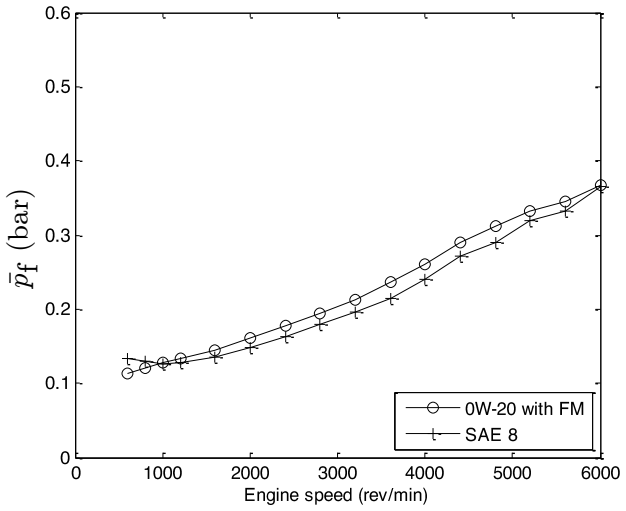

Figure 44. Motored piston and ring pack friction at 110˚C lubricant temperatures for a 0W-20 with friction modifier additive. Expressed as friction mean effective pressure, $\bar{P}_f$, versus engine speed.

Incorrect characterisation of asperity contact pressure could also result in incorrect prediction of boundary friction. The model's surface characterisation assumed a Gaussian distribution of the asperity peaks. This assumption was known to result in incorrect prediction of asperity friction, as discussed in Section 4.3.1. However, addressing this assumption by reducing the skewness value theoretically results in lower boundary friction predictions [85]. Thus, this factor's absence in the present work indicates that the boundary friction contribution is likely to be over-predicted and a more fundamental inaccuracy in the friction model may exist. The inclusion of these effects will tend to increase the model's error. However, correct characterisation is important. Further study (e.g. including oil film thickness and temperature measurement in this area) would be worthwhile to help understand this issue more completely.

4.6. Chapter 4 conclusions and recommendations

A simulation model was built to allow friction prediction in the piston-to-liner contact of a 1.6 L, 4-cylinder gasoline engine during warm-up. A motored rig test used a ‘teardown’ procedure to establish the friction contribution at various temperatures and its results validated the model.

The tool predicted the friction contribution from a conventional 0W-20 lubricant and a SAE 8 lubricant. The simulation’s results correlated well to the motored rig tests at medium to high engine speeds and above 80˚C. The tool correctly ranked the lubricants according to their motored frictional performance. At 60˚C the simulation tools significantly over-predicted measured friction at high engine speeds. Further simulation runs used an elevated metal surface temperature, improving the correlation. This discovery indicated that future work with non-intrusive surface temperature sensors placed along the block and in the piston assembly was important to tune the model.

The simulation predicted a lower friction level than that at low engine speeds (especially below 1200 rev/min). Tribometer tests showed the variation in boundary friction occurring in similar contact conditions was insufficient to account for the simulation error. The root cause of the model’s error was unconfirmed, but it was likely to be due to incorrect boundary friction characterisation. More research is required to understand these differences fully. The existence of this discrepancy means engineers using this model to predict lubricant performance under low speed conditions should be cautious and undertake a separate validation exercise. Unfortunately, these conditions are prevalent in homologation drive cycles like the NEDC and WLTC. The importance of the model’s error here is investigated using a vehicle model in Chapter 7.

To characterise the liner, skirt and ring surfaces, their asperity height distributions were assumed to be Gaussian, but a study of existing literature indicated that this assumption was unlikely to be valid. Joksack et al. [85] and Tomanik [92] suggest different surface characterisation methods to allow for the skewed nature of run-in engine components. Developing the code to permit inclusion of a skewness parameter is recommended for future work. Its inclusion is likely to reduce the magnitude of boundary friction, which will move the predicted values at low speed further from those measured. However, including this effect is important to improve the model fidelity.

The tribometer was used in a high-speed acquisition mode, which is atypical for testing of this type. Examination of the data recorded during the carriage's motion showed that the rig's settings were key to ensuring sensible friction results and that this could not be guaranteed without examining the rig's behaviour using high-speed data.

Predicting friction during warm-up was computationally intensive. The friction simulation tools required finite element models of both the piston and liner to calculate the components' surface profiles at each load, crank angle and temperature. Friction was predicted at three temperatures, but additional simulations would be required to allow investigation into this area's friction variation during warm-up on a drive cycle where a wide range of load and speed operating points are experienced by the engine. Using a high-powered computer to complete this characterisation is necessary. However, even with this capability significant work is required to set up and validate each of the cases required to characterise warm-up. Extending the model to account for combustion loading effects is also important.

Due to the limitations identified in this chapter, the model developed was not used in the vehicle level simulation work reported in Chapter 7. A separate piston-to-bore characterisation provided in the input values and is described in Section 7.1.4.

4.6.1. Key findings

- The model correlated well to a motored rig at medium to high engine speeds and above 80˚C. At 60˚C the simulation's over-predicting of friction at high engine speeds was attributed to incorrect selection of the thermal boundary conditions.
- The simulation under predicted friction at low engine speeds (especially below 1200 rev/min). The root cause of the model's error was unconfirmed, but was attributed to incorrect boundary friction characterisation.
- Prior to the simulation being included in a vehicle-level model a more complete validation exercise is required, including obtaining data from surface temperature thermocouples during the test work.

5. Variable displacement oil pumps (VDOPs) using low viscosity lubricants

Modern automotive engines use a pump and a network of galleries to supply lubricant to the engine components. The pump sits at the start of the main lubricant gallery. Its function is to pressurise the various passages and distribute the lubricant held in the engine sump. The oil galleries are a network of pipes that are drilled or cast into the engine structure [50]. Additional, smaller oil passages are located in the crankshaft, camshaft and connecting rods. These smaller conduits have a parasitic connection to the main oil system and draw lubricant on an intermittent basis or through other components, rather than having a dedicated line to the oil pump.

Figure 45 shows CAD images of a 4-cylinder passenger car engine's lubricant supply network. The engine structure is hidden to highlight the oil galleries. Lubricant supply channels are gold while main engine components are black.

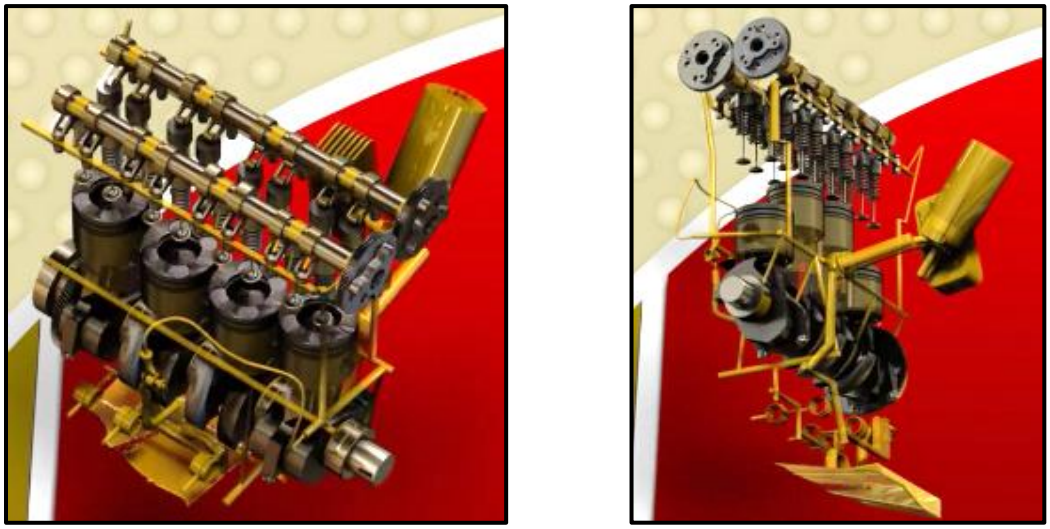

Figure 45. Engine CAD model exposing the oil galleries and main engine components by removing the engine structure.

Engine designers almost all specify that the pump is driven mechanically from the crankshaft and that it is based on one of a number of positive displacement designs [50], making the volumetric output from the pump proportional to the engine speed. The pump designs commonly used in automotive engines are trochoidal (gerotor), external

gear, and vane [104], [50]. These pumps are all positive displacement devices and variable output versions exist for each variant.

Oil gallery pressure depends on the oil flow rate from the pump, the resistance to flow in the circuit and outlet size. Lubricant exits the oil galleries by flowing from the clearances around the engine components and from lubricating orifices and cooling jets. Once the lubricant has exited the supply network, an arrangement of draining holes and channels directs it back to the sump reservoir. This pathway is unpressurised other than by airflows (e.g. the passage of blow-by gasses in the engine) and relies on gravity to return the oil to the sump.

Analysing this system is difficult, since the complicated network of passages connects to a plurality of components and orifices. The clearances in the oil circuit vary due to components' differential thermal expansion and engine wear, as well as dynamically due to elastic deflection during loading. Understanding the behaviour of clearances is important to ensuring the oil system lubricates the engine components adequately. Combining the orifice areas (and discharge coefficients) of each engine clearance enables approximation of the effective clearance for the entire oil circuit. This process is complex and usually achieved using a one-dimensional computational fluid dynamics model [105], [106], [107], [108] or empirical measurement. The flow rate through the effective oil gallery area is proportional to the oil circuit's permeability [109], or impedance, and the supply pressure.

Where the oil gallery's effective area is constant, the pressure is proportional to the flow rate:

$$\Delta P \propto \frac{Q^2 \rho}{2A^2} \tag{25}$$

where ΔP is the pressure drop in the oil gallery, Q is the oil flow rate, ρ is the fluid density and A is the combined orifice area of each oil exit port (e.g the bearing's and jet's effective oil exit areas).

Thus, without a regulator, the oil gallery pressure increases in proportion to the square of the engine speed. This effect is undesirable since, for an adequate volume of lubricant to be supplied at engine idle (or low) speeds, an excessive pressure will be produced at high speed. To avoid this scenario, a pressure relief valve is used to limit the maximum pressure [50]. This valve is also active when the lubricant viscosity is high (e.g. under cold start conditions). Pressure regulation occurs by discharging pressurised oil flow. Using this valve to relieve the surplus oil pressure is a source of inefficiency in the system due to the wasted work done by the engine driving the pump to deliver these excessive flows.

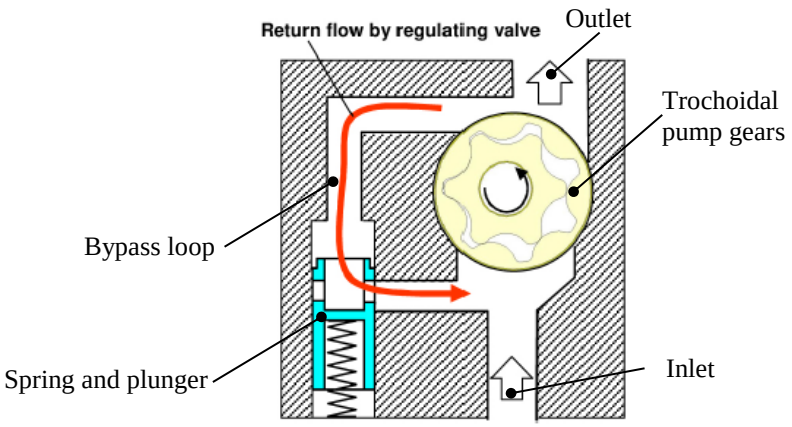

Figure 46. Design of pressure relief valve for trochoidal pump (Reprinted with Permission from SAE International [110]).

Figure 46 shows a trochoidal oil pump schematic with a pressure relief valve located inside the pump housing. The pressure-regulating valve returns excess lubricant to the pump inlet. Designing the bypass loop this way means the regulation pressure depends on lubricant viscosity. The regulated pressure is the sum of the control loop pressure drop and the pressure imposed by the spring and plunger. The pressure drop in the control loop becomes larger with increasing viscosity. Thus, the system can reach

undesirably high pressures [110]. Conversely, when this valve is active and the lubricant viscosity is reduced, a low control valve pressure prevails, potentially resulting in unsatisfactory lubrication of the components. This behaviour can result in a negative (high viscosity) and positive (low viscosity) impact on the pump load and, thus, friction.

5.1. Oil pump design specification

The oil pump design specification must account for extreme operating conditions, potentially resulting in the fitment of a pump that is too large for normal operation [106]. Typically, engine designers select the pump to ensure that:

1. A minimum oil pressure can be maintained under the condition of high oil temperature and low engine speed (e.g. 1 bar gauge at 140˚C lubricant temperature and idle) [98], [111], [104], [112]
2. Satisfactory oil pressure is maintained during operation with worn engine components (e.g. bearings) [50], [111]

A review of modern literature suggests the fitment of new hydraulically powered components, cooling jets, and cost engineering processes is also important in determining the specification of modern oil pumps.

Tightening emissions legislation has triggered the mainstream adoption of turbochargers as well as the use of hydraulically powered variable valve timing and lift (VVTL) systems. The oil flow these components require (and their minimum operational pressures) has increased the engine demand and, therefore, the size of modern oil pumps. Moreover, engine calibrators' requirement for VVTL systems to be operated lower in the engine speed range [110], [108] has increased the oil flow required at low engine speeds [104], [108], [110].

The trend toward higher engine power densities using turbocharging [113], [8] demands the fitment of piston cooling jets to aid heat transfer from the piston

under-crown [114]. Since these components need significant oil flow, their use has also increased the pump sizes specified [110].

Cost engineering processes can restrict the pump types available to the designer (e.g. increasing a pump's production volume allows economies of scale in the manufacturing and assembly process, encouraging a single pump design for a family of engines) [104], [50], [115]. This approach typically creates an oil pump with adequate performance in the family's largest engine, but is overcapacity for the smaller engines.

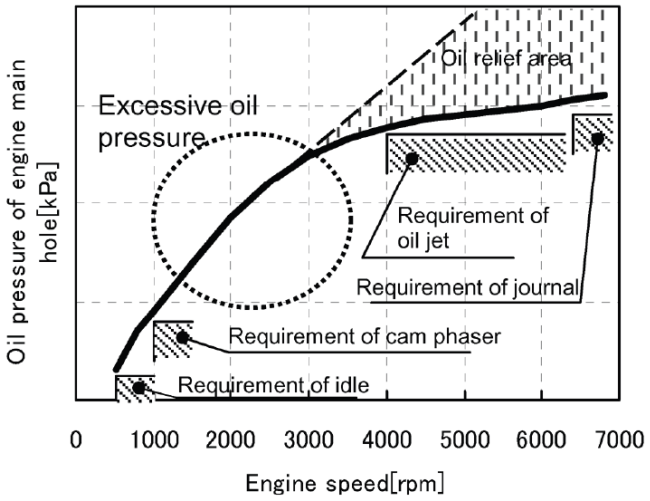

Figure 47. Engine oil pressure requirements (Reprinted with Permission from SAE International [116]).

Toyoda et al. [116] divide the pressure a contemporary automotive engine requires into four areas: idle, variable valve timing (and lift), piston cooling and bearing lubrication. Figure 47 shows pressure requirements for each operating condition and component. Over a significant part of the engine speed range (e.g. 1500 to 4000 rev/min), the oil pressure achieved by the fixed displacement oil pump is unnecessarily high. Thus, engine designers can reduce the parasitic load from the oil pump by lowering the oil pressure in this speed range. The power consumed by the oil pump can contribute 2.5% to 10% of the total engine friction [116], [98], [117]. Thus, engine designers are implementing pumps with a variable output capability to decouple

the increase in flow rate and system pressure from engine speed changes in these mid speed conditions [104], [109], [110], [112], [116], [118], [119], [120], [121], [122].

5.2. VDOP technology

Variable displacement oil pumps (VDOPs) are driven mechanically from the crankshaft, but independent or electrically-augmented mechanical systems control their volumetric output. Variable displacement versions of the three common pump types exist. However, the implementation of the variability differs for each pump design.

5.2.1. Trochoidal Oil Pump Design

Figure 48 shows a schematic of a variable outlet trochoidal pump. In low-pressure mode, a shuttle valve fitted within the pump body opens a relief hole that causes the discharge of oil at a low pressure. This action reduces the volume flow rate from the pump to the oil circuit, causing the circuit pressure to adopt a low value. In high-flow and high-pressure conditions, the shuttle valve moves and closes the relief hole, making the pump deliver maximum flow rate and causing the system pressure to be controlled at a high value.

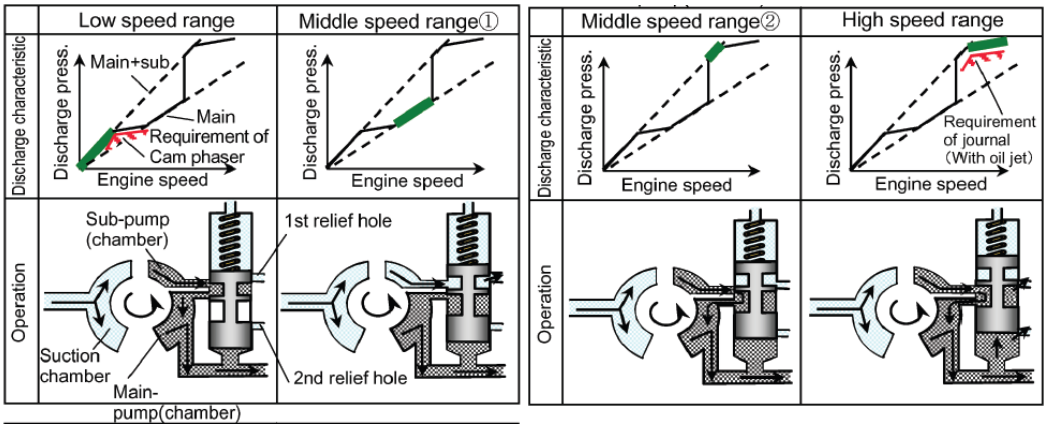

Figure 48. Variable output Trochoidal pump (Reprinted with Permission from SAE International [116]).

5.2.2. External Gear Oil Pump Design

Figure 49 provides a view of a variable output external gear pump. Moving a gear set axially in the pump controls the outlet flow rate by varying the pump's hydraulic efficiency. A two-stage pressure control valve limits system pressure. The oil pressure adopts a high value when the pump is in maximum displacement mode and a low value coincident with its minimum displacement position.

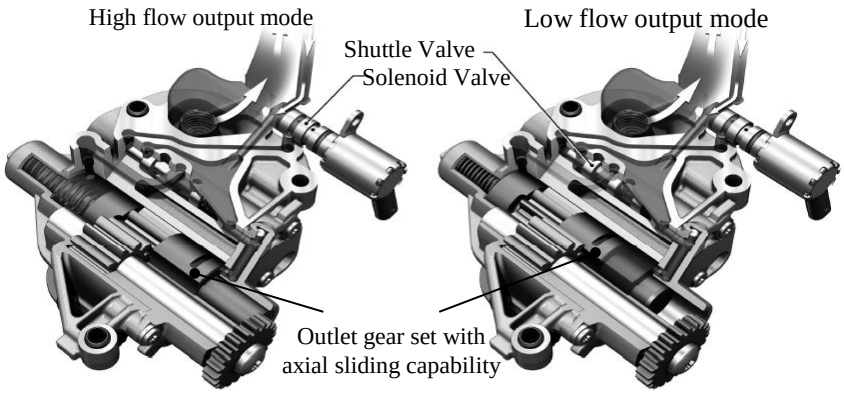

Figure 49. Variable output external gear pump (Reprinted with Permission from Aachen Colloquium [119]).

5.2.3. Vane Oil Pump Design

Figure 50 shows a schematic of a variable output vane pump. The movement of the control ring (decreasing output as the control ring moves left) within the pump controls the outlet flow rate by changing the eccentricity between the control ring and pump drive hub. The pressure control strategy is similar to the other pump designs.

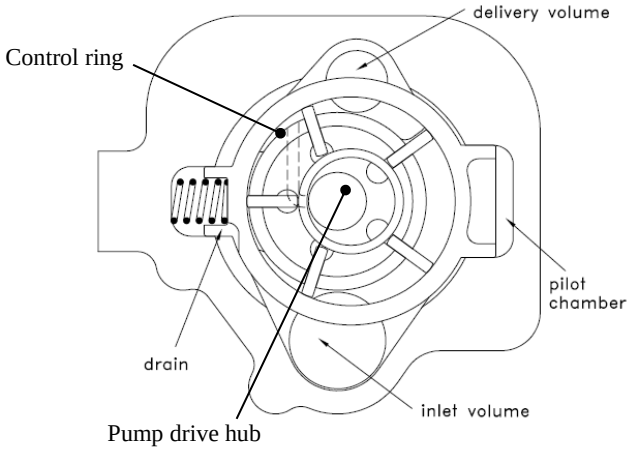

Figure 50. Variable output external vane pump (Reprinted with Permission from SAE International [122]).

5.2.4. Summary and implications for low viscosity lubricants

Each pump design has two notional flow rate conditions (high and low) [112], [116], [118], [119], [123]. This adjustability reduces the parasitic energy loss of driving the oil pump, by more closely matching volumetric output to the engine oil circuit's needs, reducing or eliminating relief valve losses [109]. CO_2 emission reductions of 0.5% to 3% are possible with variable displacement oil pumps on the NEDC [104], [112], [124].

The operation of the VDOP's requires a closed-loop control system and the signal in its control algorithm is the oil circuit pressure [111]. This approach ensures the oil gallery pressure is independent of the lubricant viscosity. However, low viscosity lubricants may be disadvantaged by this control system design, since the pump flow rate increases to achieve this pressure target. The power required to pump lubricant around oil galleries can be calculated using:

$$\dot{W}_{\mathrm{P}} = \dot{V}_{\mathrm{D}}\, P \tag{26}$$

where $\dot{W}_{\mathrm{P}}$ is the hydraulic power at flow rate $\dot{V}_{\mathrm{D}}$ delivered at gauge pressure, P.

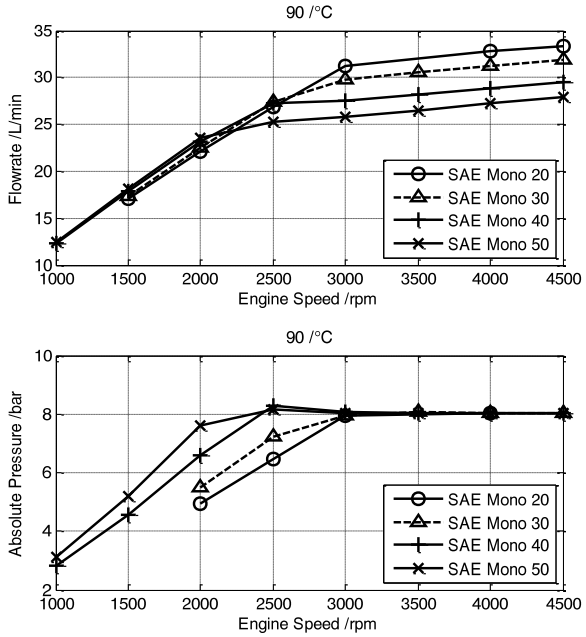

Figure 51. Simulated oil gallery pressure and flow rates for a 4 cylinder diesel engine and different lubricants (reproduced from Taylor [107]).

Thus, the theoretical power requirement for low viscosity lubricants is greater than for higher viscosity lubricants. This antagonistic interaction is significant when understanding low viscosity lubricants' performance. With older, fixed displacement pump designs, this behaviour did not occur. The frictional response to low viscosity lubricants was favourable at low engine speeds. Figure 51 shows the oil pressure variation with engine speed for a fixed displacement pump. The volumetric flow rate was similar for both viscosities. Therefore, when the relief valve was not active, the oil circuit pressure decreased as lubricant viscosity reduced. Following equation (26), this pressure change reduced the pump load.

The interaction between VDOPs and modern, low viscosity lubricants is undocumented in existing literature. Rundo and Squarcini [109] provide a comprehensive comparison of different lubricant pump types. They built a bespoke test rig to measure the performance of two fixed and one variable displacement pump, but did not consider the interaction between the pump and lubricant viscosity grade.

Burke et al. [120] and Meira et al. [98] did not investigate any system effects caused by changing lubricant viscosity grade.

Design analysis of variable displacement oil pumps, which considers how they behave with low viscosity lubricants, is important, since:

1. The prevailing trend is that modern engines use VDOPs [98], [111], [116], [118], [119], [120], [123]
2. Lower viscosity lubricant grades are being developed and implemented in modern engines [14]
3. The migration to VDOPs may reduce the CO_2 benefits achievable with low viscosity lubricants if the pump friction increases significantly

Therefore, the present research offers original analysis of the interaction between VDOPs and low viscosity lubricants.

5.3. VDOP performance with low viscosity lubricants

In theory, the interaction between lubricants and a VDOP can be investigated using engine tests, rig tests or through simulation. An evaluation of these options selected the correct methodology for this investigation.

5.3.1. Engine testing

The use of a full engine test was disregarded since this approach would have required an engine test facility with support from a manufacturer (to provide a test bed compatible engine controller). A full vehicle dynamometer does not need manufacturer support, so this approach was viable. However, measurement of the pump drive torque required development of a bespoke torque drive flange, adding significant challenges to the research.

5.3.2. Modelling

Mancò et al. [122] developed a mathematical model to simulate a VDOP. They achieved good accuracy at low engine speeds (Figure 52). However, the model performance was worse at higher engine speeds. The data that they published only allows a comparison between the simulation and measured data at one lubricant test temperature; it is not possible to understand the model's performance over the range of conditions found in a drive cycle. Moreover, Mancò et al. [122] only reported work completed using one lubricant, so it was impossible to understand what effect different lubricants had on their model's fidelity. Staley et al. [104] completed simulation and testing that investigates the regulation behaviour of a similar pump design. Their work indicates that the behaviour of this pump design was sensitive to oil viscosity. Mancò et al. [122] and Staley et al. [104] did not develop their models to include friction prediction, so the effect of changing lubricant viscosity on the pump load cannot be concluded from their findings.

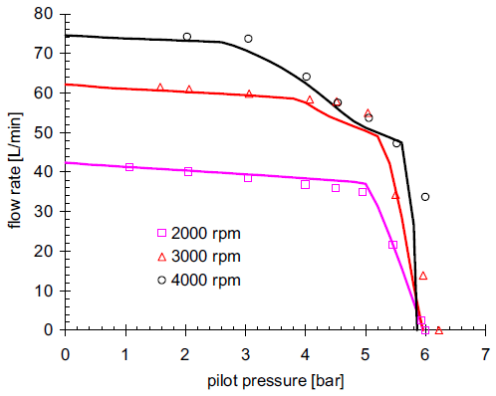

Figure 52. A comparison of the measured and simulated oil pump flow rates versus pressure for a variable displacement pump (Reprinted with Permission from SAE International [122]).

In previous research [107], a model was developed to simulate the lubricant circuit for a 4-cylinder, diesel, passenger car engine, using Mentor Graphics' FloMASTER program. The simulation's performance was assessed using two lubricants. The simulation used generic data (modified to account for the test engine's volumetric pump displacement) to characterise the trochoidal oil pump. A motored engine test was

completed and the measurements compared to the predicted flow rates and pressures. The pump model's inaccuracies limited the simulation's performance.

This previous model's limitations were addressed by building a new model, again using the FloMASTER program, but this time using the Ford 1.0 EcoBoost engine and including a detailed VDOP model. The flow paths and pump's porting design were numerous and complex. It was implausible to simulate the performance of each internal feature of the pump. Thus, a rig test was needed to improve the model accuracy. This requirement undermined the approach, as the model relied on input from empirical measurements. Discharge coefficients were defined using the measurements and used to improve the flow and pressure simulations. A comprehensive study was done, but comparing the measured and predicted results for flow rate and pressure showed differences that were significant relative to the anticipated lubricant effects (Figure 53 shows the predicted flow rate and pressure produced by the model). Another disadvantage was the substantial time it took to complete the project. This work is described more fully by Corbishley and OudeNijeweme [108]. No attempt was made to predict the friction in the pump during this research.

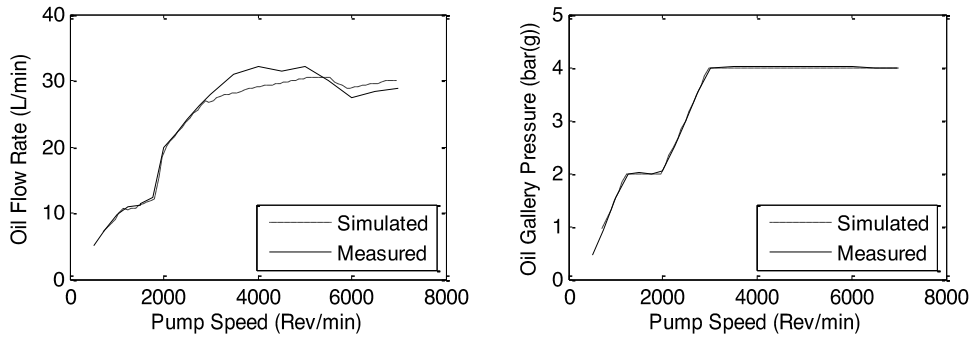

Figure 53. A comparison of the simulated and measured flow and pressure characteristics for a VDOP (adapted from [108]).

Fabiani et al. [125] and Mancò et al. [126] simulated a trochoidal pump design. They built bespoke simulation codes using the AMESim program. Despite significant work, differences of circa 9% between simulated and experimental results persisted in

their research. The accuracy achieved in their simulations is likely to be significant compared to the magnitude of difference anticipated by varying the lubricant viscosity grade. Mancò et al. [126] measured pump drive torques in their experimental work. However, they did not attempt to predict this parameter with their model.

5.3.3. Rig testing

Rundo and Squarcini [109] used a rig test methodology for their investigation. They tested and compared the drive torques for three pumps using the NEDC's speed and thermal boundary conditions. However, the rig was only able to achieve half of the heat input required to replicate the vehicle conditions. Thus, they could not reproduce the thermal profile synchronously with the pump speed trace. The test time was doubled and the accelerations halved to compensate for this limitation. The energy expended on the NEDC was calculated simplistically by summing their rig results and halving them. However, they do not present any work to validate the approach. In theory, this approach may be unreliable, since the pump's lower acceleration changes the fluid dynamics in the pump rotor while the test conditions did not account for temperature gradients in the pump.

5.4. Summary and selection of approach for VDOP characterisation

Many authors have attempted to develop high fidelity models for different oil pump types. The models have generally focused on predicting the pump's hydraulic performance at different flow rates and pressures. Published data showing the extension of these models to include a prediction of the resulting drive torque is scarce. However, the challenges in developing a high fidelity model to predict the hydraulic efficiency may mean that extending these to include a friction model is inappropriate.

Table 20. Key attributes of the Ford 1.0 EcoBoost engine.

Engine name	1.0 EcoBoost
Manufacturer	Ford
Displacement (litres)	0.999
Power (kW)	88
Torque (Nm)	170
Number of:	
Cylinders	3
Main bearings	4
Big-end bearings	3
Piston cooling jets	3
Camshafts	2
Variable valve timing units	2

Table 21. SHW Variable displacement oil pump specification.

Property	Value	Test condition
Volumetric displacement	11 cc/rev	1000 rev/min pump speed, 200 kPa discharge pressure, 90˚C lubricant temperature, 5W-20 lubricant
Drive gear ratio	19/21 (90% engine speed)	
Maximum measured flow rate with 5W-20	33 L/min	6000 rev/min pump speed, 400 kPa discharge pressure, 120˚C lubricant temperature.

Rig testing was chosen for this research. For a detailed assessment of drive torque changes with variation in speed, load and temperature, a pump was tested using a matrix of steady state conditions. The investigation measured the behaviour of a vane type VDOP with three different lubricant formulations. The VDOP used was taken from a Ford 1.0 EcoBoost engine [123]. Table 20 lists this engine's key attributes.

Table 21 lists the VDOP's key features. The engine used a two stage, oil pressure controlled, VDOP manufactured by Schwäbische Hüttenwerke GmbH.

Figure 54 shows the VDOP with the front cover removed. Figure 55 is a schematic of the pump. The VDOP comprised seven sliding vanes held by a drive hub, an inner guide rotor, an external control ring, pump housing and linear coil spring. The pump's volumetric output varied in proportion to the eccentricity between the control ring's centre and that of the inner guide rotor.

Figure 54. SHW VDOP oil pump fitted to the 1.0 Ford EcoBoost engine. The image shows the pump with the front cover removed[v].

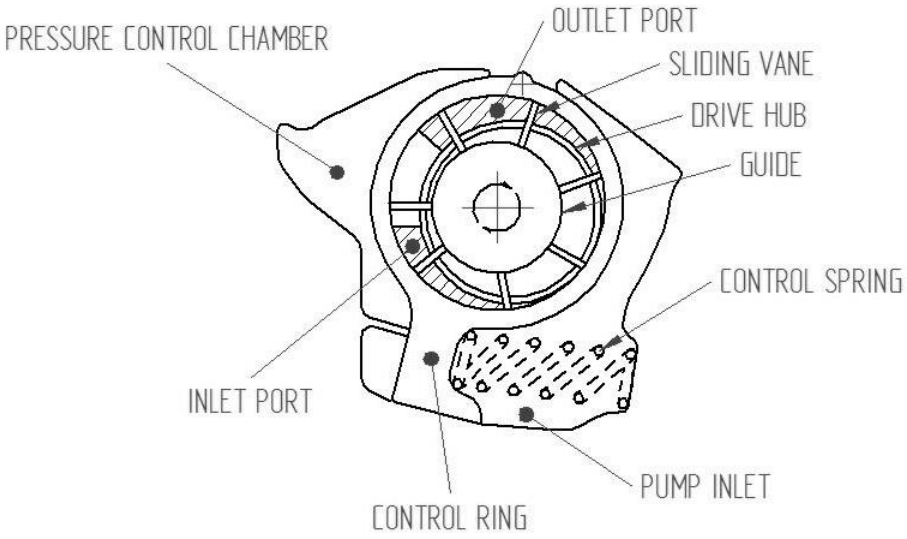

Figure 55. Simplified diagram of SHW VDOP, the pump rotates clockwise.

The drive hub and control ring formed a diverging volume, generating a depression in the inlet port when the drive hub rotated. This action drew oil into the space between the pump vanes and drive hub. At the outlet port, the drive hub and control ring formed a converging volume that forced the oil to exit the pump. The crankshaft drove the pump using a synchronous rubber belt.

An electrically-augmented shuttle valve controlled the pressure inside the pressure control chamber [108]. Algorithms in the engine control unit (ECU) determined this valve's movement. Therefore, the oil pressure varied at different operating conditions.

Figure 56 shows the oil gallery pressure recorded following testing using this pump. The pump pressure profile has four phases, similar to that of Arata et al. [110].

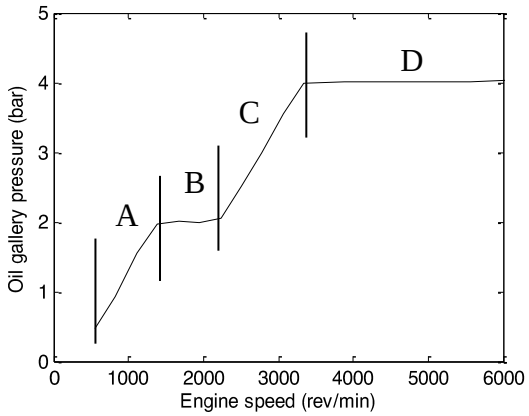

Figure 56. Measured variation of pressure with engine speed for SHW VDOP at 90˚C lubricant temperature.

Phase A: at low engine speeds, pump volumetric output was proportional to engine speed. The variable displacement function was suppressed. Increasing engine speed increased volumetric flow from the pump and oil gallery pressure. The control ring operated at maximum eccentricity, causing the pump to operate with maximum volumetric displacement for the pump rotational speed.

Phase B: at 200 kPa (gauge) gallery pressure, an engine control unit signal opened a solenoid to bring the oil gallery pressure to the shuttle valve. The force balance in the spool valve drove oil into the pressure control chamber, reducing the eccentricity from control ring to inner guide rotor. This action reduced the pump outlet displacement so the gallery pressure stayed at 200 kPa (gauge) independent of engine (and pump) speed.

Phase C: at the start of this phase, the control algorithm deactivated the control solenoid. This action reduced the control chamber pressure, causing the control ring to return to its high eccentricity position. The pump again operated in a proportional manner, until volume flow rate increased enough to cause an oil gallery pressure increase to 400 kPa (gauge).

Phase D: at 400 kPa (gauge), the same spool valve was used as in Phase B and it held the oil gallery pressure independent of engine speed. However, increased oil pressure in the pump control chamber again caused control ring movement. The resultant force balance on the valve created 400 kPa.

Changing the setting in the engine controller software enabled the pump calibration to be altered. Thus, differences between these measurements and those in engines with a different engine calibration are possible.

5.4.1. Oil pump testing rig

Figure 57 shows a schematic of the bespoke test rig built for the present research. The experimental rig comprised a heated lubricant sump and associated thermal control unit, a motor drive, torque flange and flexible shaft coupling, an electronically-augmented variable restrictor and a flow meter.

The heated lubricant sump was circa 10 litres and equipped with an electronic thermal control unit to maintain the lubricant temperature (T_{tank}) at 20˚C, 90˚C and 120˚C. An automatic data logging system recorded pressures and temperatures during the test at the pump inlet (T_{in}, P_{in}) and outlet (T_{out} and P_{out}). The electronically-augmented variable restrictor limited the flow rate in the circuit. Immediately after this valve, a turbine flow meter measured lubricant flow rate. The flowmeter was recalibrated at each temperature and with each lubricant tested.

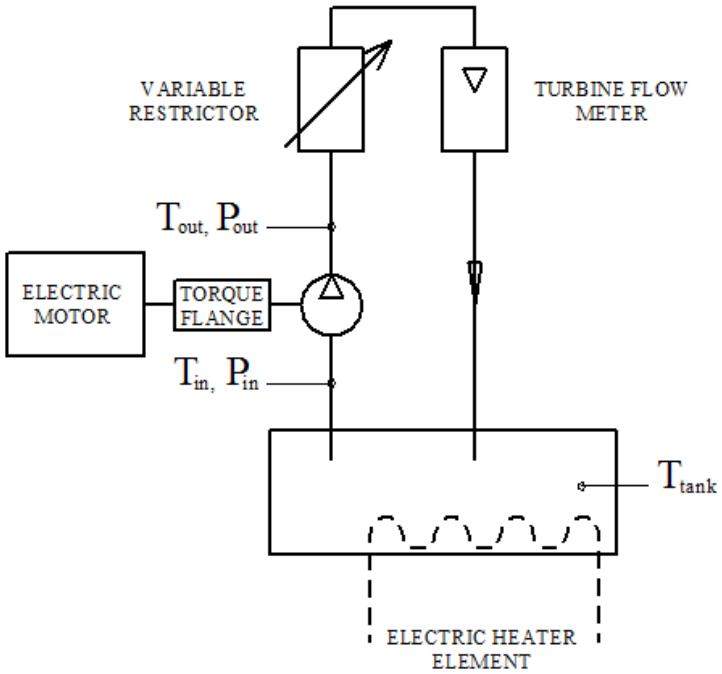

Figure 57. Oil pump experimentation schematic, where T_x represents a temperature measurement position and P_x represents a pressure measurement position.

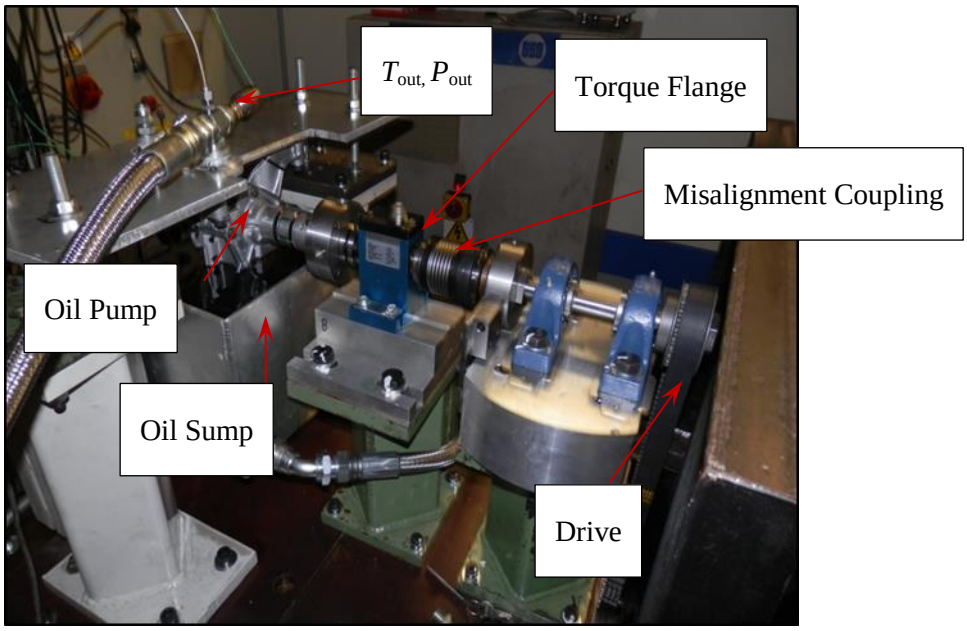

Figure 58. Oil pump testing rig[v].

An electric motor powered the oil pumps, by driving their input shafts using a toothed, synchronous, rubber belt. Pillow block type bearings were fitted between the drive belt and pump inlet to isolate the pump from the belt tension forces. A misalignment coupling was installed between the drive belt and torque meter. A torque

flange close to the pump measured drive torque. Pump speed was measured at the electric motor using a shaft encoder.

Table 22. Oil pump experimentation target control accuracy.

Variable	Target accuracy
Pump speed	± 3 rev/min
Temperature	± 1°C

Figure 58 shows the test rig. Table 22 shows the target variance for each of the key controlled variables.

5.4.2. Torque measurement

A Kistler Staiger Mohilo rotational torque transducer, with an output range of 0 Nm to 50 Nm, was used to measure drive torque. The anticipated drive torque for the pumps was less than 5 Nm (the lower end of the transducer range). Testing confirmed the accuracy and repeatability of the instrument within the range of expected torques.

5.4.2.1. Accuracy

The torque transducer output a voltage of 0 V to 5.003 V, corresponding to a torque range of 0 Nm to 50 Nm. The test system converted the voltage into a torque reading. A linear correlation was established by applying known torques to the transducer and recording the voltage output. Table 23 shows the results from this testing. A similar calibration process was undertaken daily to establish the size of the offset, and these values were subtracted from the measurements.

Table 23. Data used in torque meter calibration.

Applied torque (Nm)	Measured torque (Nm)	Offset (Nm)
0	0.09	0.09
2	2.08	0.08
4	4.09	0.09
5	5.09	0.09
4	4.1	0.1
2	2.09	0.09
0	0.09	0.09

5.4.2.2. Repeatability

Loading and unloading the torque transducer with three masses attached to a lever arm investigated the repeatability of its output, 140 tests were completed over three days. Measurements were taken during loading and unloading to see if hysteresis was present. Table 24 shows the results. The maximum torque error that occurred was 0.007 Nm, at 1 Nm notional torque. The maximum standard deviation was 0.004 Nm. No significant hysteresis effects occurred.

Table 24. Summary of results from torque meter repeatability testing.

Test order	Mean torque (Nm)	Maximum error from mean (Nm)	Standard deviation (Nm)
1	0.003	0.003	0.002
2	0.136	0.005	0.003
3	0.155	0.005	0.004
4	1.012	0.007	0.004
5	0.156	0.006	0.003
6	0.137	0.004	0.003
7	0.003	0.003	0.002

5.4.3. Lubricants

Rig testing used the lubricants defined in 2.1.1. The 0W-20 provided baseline performance for the pump. The 5W-30 and SAE 8 were used to assess the effect on pump friction of using older, high viscosity and modern, low viscosity lubricants.

5.5. VDOP rig testing

The location of the feedback loop to control the flow rate and pressure output for this pump complicated the measurement. During operation on the engine, the pump's internal mechanism held outlet pressure at the notional oil gallery pressures of 200 kPa (gauge) and 400 kPa (guage) (Figure 56). However, the pressure signal for the regulation was located after the oil filter and coolant-to-lubricant heat exchanger, so the pump outlet pressure was higher than these values. Figure 59 shows a process diagram, illustrating the pressure control loop. The magnitude of the pressure drop was measured

by building a subsystem test including the oil filter and cooler assembly. The pressure drop varied from 10 kPa to 40 kPa, for the range of oil flow rates present on the NEDC[12].

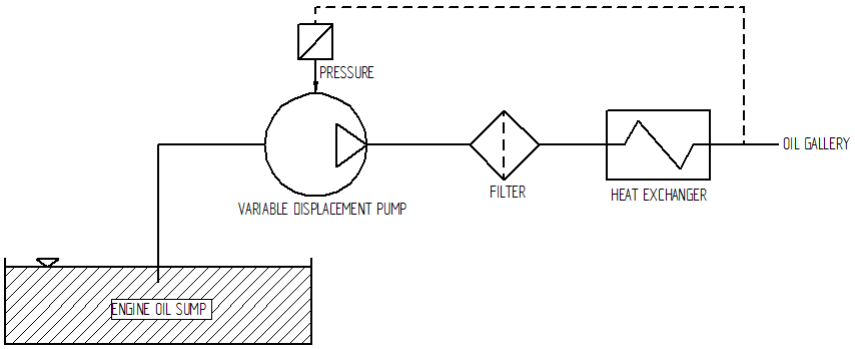

Figure 59. Schematic of VDOP operation.

Given these values were small, and to simplify the test, the pump outlet pressure was controlled to 200 kPa (gauge) and 400 kPa (gauge). These values approximated to the minimum pressures seen at the pump outlet during controlled pressure operation. This approach precluded direct assessment of pump torque demand for this engine, but allowed pump performance to be isolated from the effects of the oil cooler and filter assembly.

In some conditions (e.g. if the pump speed was too low), the pump was unable to achieve the target pressure. When this happened, the pump operated in an open-loop manner and the rig recorded the pressure achieved. Further complications occurred since the pump could achieve the specified outlet flow rates at different speeds, by varying the rig's effective orifice diameter. Thus, a matrix of pump speed and orifice sizes was used. For broad coverage of pump performance, the orifice diameter was varied to reach oil flow from 5 L/min to 30 L/min in 5 L/min increments at each pressure. To evaluate the effect on efficiency due to lubricant viscosity and pump temperature changes, tests used three lubricant temperatures at 20˚C, 90˚C and 120˚C.

[12] Engine test bed measurements showing the pressure variation across the oil filter and cooler assembly during the NEDC are analysed in section 5.8.4.

5.6. Results

5.6.1. Performance of 0W-20 at 90˚C with a variation in flow rate

Figure 60 shows outlet pressure variation, oil flow rate and calculated efficiency for pump speeds from 1000 rev/min to 6000 rev/min. These results were taken with the pump in a notional 200 kPa (gauge) backpressure condition using the 0W-20 lubricant at 90˚C.

Figure 60 (a) shows that at 5 L/min and 90˚C, the pump controlled the outlet pressure to between 215 kPa (gauge) and 230 kPa (gauge) at all pump speeds tested. As the flow rate was increased, the pump could not achieve the target output and pressures for all conditions. The pump's ability to achieve the flow rate improved with increasing pump speed, indicating that low outlet pressure could be attributed to pump speed being too low. When the drive speed was over 3000 rev/min, the pump could achieve the notional oil pressure for every flow rate in the test matrix. Increasing flow rate caused a small reduction in the outlet pressure at every pump speed tested. This behaviour is likely to be due to the flow rate changing the force balance on the pump control ring and, thus, the pump output. Theoretically, this balance change could have been due to a reduction in inlet chamber pressure or to the internal viscous forces on the control ring increasing. This effect is analysed by comparing the performance of different lubricants in Section 5.6.3.

Figure 60 (b) plots the pump outlet flow rate over the speed range tested. The maximum flow rate the pump reached at 1000 rev/min was 10.8 L/min. Thus, the lines on the graph converge at 1000 rev/min. As pump speed was increased, the maximum flow rate rose to 21.7 L/min at 2000 rev/min and 30.3 L/min over 3000 rev/min.

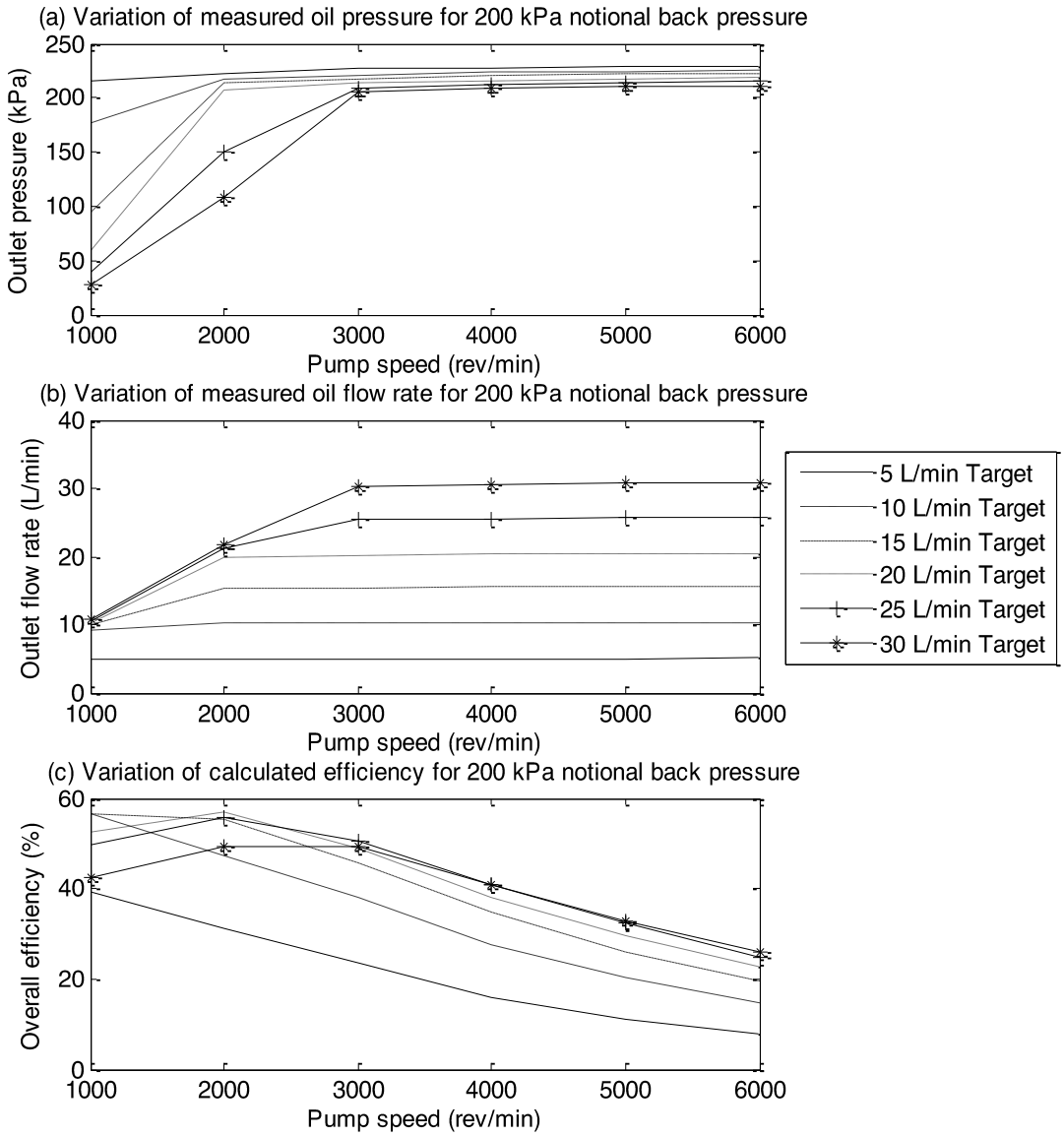

Figure 60. VDOP test results at nominal 200 kPa (gauge) backpressure, 90˚C for 0W-20.

Figure 60 (c) plots the overall pump efficiency, calculated as the ratio of the delivered fluid power level to the mechanical power needed to drive the pump using:

$$\eta = \frac{V_{\mathrm{D}}\, P}{T_{\mathrm{P}}\omega} \tag{27}$$

where η is pump total calculated efficiency, V_{D} is measured volumetric flow rate, P is outlet pressure, T_{P} is measured pump drive torque and ω is measured pump speed.

Above 3000 rev/min, increasing speed reduced the pump's total efficiency in all test conditions. This behaviour is unavoidable with this pump design, as with rising speed the mechanical losses increase (roughly proportional to the speed squared) and

the volumetric output automatically reduces, to meet pressure control requirements. Thus, these two variables interact to reduce the pump's net efficiency. Equivalent output flow rate was achieved, but with higher losses.

Using a variable speed pump (e.g. from an electronic drive [127]) could avoid this reduction in efficiency. However, the net energy consumption, including the efficiency of generating electrical energy to power the pump, must be included in the testing work with these systems (Ribeiro et al. [127] ignore this efficiency loss).

Below 3000 rev/min the shape of the calculated efficiency graph depended on oil flow rate. When the pump was operated at 5 L/min and 10 L/min, the calculated efficiency reduced with speed. Under these test conditions, the pump achieved the 5 L/min and 10 L/min target flow rates throughout the speed range tested. This behaviour indicated that the variable displacement system was in control of the flow rate throughout the speed range, explaining the observed variation in efficiency. Under test conditions that demanded a flow rate greater than 15 L/min, an increase in total pump efficiency was measured at low pump speeds. The pump operating at maximum output (in order to achieve the demanded flow) and the suppression of the variable displacement system caused this behaviour. For each flow rate above 3000 rev/min, the oil pump moved into an output-controlled mode.

The 5 L/min test case's peak efficiency was 39% at 1000 rev/min. The efficiency for the 10 L/min and 15 L/min test cases, at 1000 rev/min was 57%, the highest value recorded. The pump's total efficiency reduced to 29% for 30 L/min at 6000 rev/min and to 8% for 5 L/min using the same conditions. Speed and flow rate were key in determining the pump's operating efficiency.

5.6.2. Performance of 0W-20 with a variation in flow rate and temperature

Figure 61 shows the pump performance at 5 L/min and 30 L/min using the 0W-20 lubricant at 20˚C, 90˚C and 120˚C. When the rig was set to 5 L/min flow rate, a significant increase in outlet pressure occurred with rising temperature (Figure 61(a)). This behaviour occurred at all speeds. A correlation with temperature here may indicate that low viscosity lubricants operate at higher pump outlet pressures in this pump design. However, variation in internal pump clearance due to differential thermal expansion may have contributed to this effect. Data recorded from the other lubricant formulations is discussed below.

The pump outlet pressure performance at 30 L/min followed similar behaviour to that at 5 L/min, when the pump speed was over 3000 rev/min. However, the outlet pressure change was marginally smaller (maximum difference of 38.4 kPa versus 51.1 kPa in the 5 L/min tests). At lower speeds, the outlet pressure for the 90˚C and 120˚C cases was similar, but markedly different behaviour was measured at 20˚C, where an outlet pressure increase occurred at low pump speeds. The performance change at 20˚C was speed-dependent as the pump transitioned from an uncontrolled to a controlled flow rate at circa 3000 rev/min. Below 3000 rev/min, the variable outlet strategy was not active. Thus, the 20˚C high viscosity lubricant achieved the same flow rate as higher temperature tests. The higher viscosity with the same notional flow rate increased the pressure in the circuit. This effect was less pronounced at 90˚C and 120˚C, since lubricant viscosities were more similar. Above 3000 rev/min, the outlet control system was active for this 20˚C test, causing a small outlet flow rate and pressure reduction.

Figure 61(b) shows the measured flow rate for each pump test condition. Flow rate was a controlled parameter in this test. Thus, the lines are overlaid for most test conditions. The pump operated in a closed-loop control mode at a 5 L/min flow rate.

The pump was in open-loop control mode below 3000 rev/min, when the flow rate was increased to 30 L/min, and achieved the demanded output above this speed. The measured outlet flow rate was independent of temperature, indicating that any leakage within the pump was insignificant to the pump performance in these test conditions.

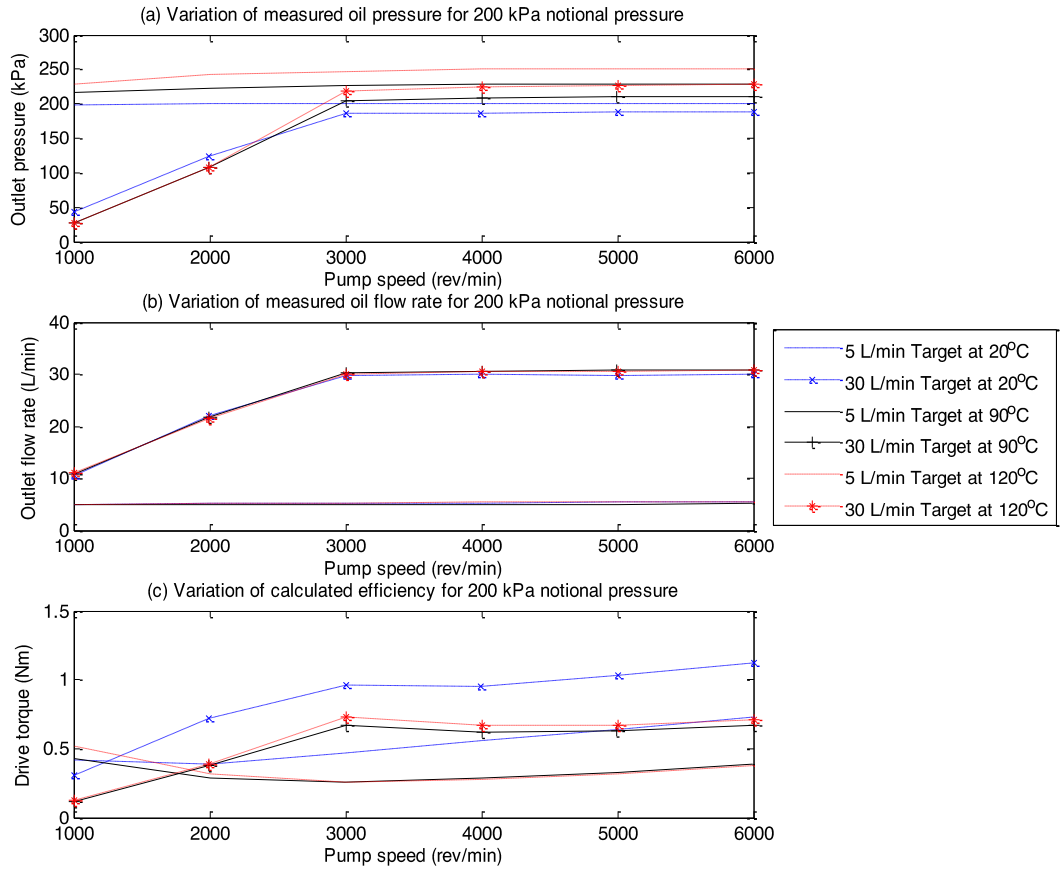

Figure 61. VDOP results at notional 200 kPa (gauge) pressure at 20˚C, 90˚C and 120 ˚C for 0W-20.

Figure 61(c) shows the measured pump drive torque. At 5 L/min the drive torque varied with pump speed, despite its outlet pressure remaining approximately constant. As pump speed increased, the drive torque initially reduced to a minimum (2000 rev/min at 20˚C and 3000 rev/min at 90˚C and 120˚C) then increased. This behaviour may indicate the pump frictional surfaces transitioning between friction regimes, (e.g. a transition from boundary to mixed friction – 2000 rev/min at 20˚C and 3000 rev/min at 90˚C and 120˚C) then to a mainly hydrodynamic regime at high pump speeds. The divergence between the friction curves measured at 90˚C and 120˚C is

consistent with a larger contribution from boundary regime friction in the higher temperature, lower viscosity case. Oil film thickness would need to be measured to conclude if this transition were occurring. Arata et al's work [110] corroborates the theory that boundary friction is present in VDOP designs. They report high asperity contact levels resulted in control ring and vane tip wear [110], indicating that surface-active additives, such as friction modifiers, may reduce the friction present in VDOPs.

At 30 L/min demand flow rate, the measured drive torque showed different behaviour to that at 5 L/min. In the high flow condition, the drive torque initially increased to a pump speed of 3000 rev/min before decreasing. The increase in drive torque here was coincident with rising pump outlet pressure, explaining the higher pump load. As the pump speed increased beyond 3000 rev/min, the drive torque initially decreased, reaching a minimum at 4000 rev/min, and then rose. This behaviour was similar to that measured at 5 L/min, indicating that the transition between the lubrication regimes was speed, load and temperature dependent. The pump drive torque was higher at 120˚C. The lower lubricant viscosity and increased boundary friction at this temperature, alongside the higher outlet pressure, explains this torque increase.

The measured torque during the 20˚C test showed the pump friction was significantly larger than in the higher temperature test cases for most conditions. This result is likely to be due to an increase in viscous friction from pumping the higher viscosity lubricant.

5.6.3. Pump performance at 200 kPa (gauge) back-pressure for each lubricant

Figures 62(a to i) shows pump performance at 5 L/min and 30 L/min with each test lubricant. All the tests used the 200 kPa (gauge) back-pressure setting. Figures 62(a), (b) and (c) show the outlet pressure variation at each test temperature. The outlet

pressure achieved by the pump depended on the lubricant viscosity. The lowest viscosity lubricant tested, SAE 8, caused the pump outlet pressure to increase by 21 kPa (9%) compared to the 5W-30 when tests were completed at 120˚C and 5 L/min flow rate. The outlet pressure rose with increasing temperature and with reducing lubricant viscosity. The outlet pressure variation between the lubricants was minimal at 20˚C and 5 L/min. This behaviour was unexpected since the lubricants' viscosities were still significantly different at this temperature. The pump's response indicated that the outlet pressure depended on both lubricant viscosity and pump temperature.

Figures 62 (d), (e) and (f) show outlet flow rate variation at each temperature. The maximum outlet flow rate was a controlled parameter and so varies little. In all test conditions, the pump achieved a 5 L/min output. However, a performance difference was measured at 30 L/min. The 5W-30 flow rate was significantly lower than measured when testing the 0W-20 and SAE 8 at over 2000 rev/min. The reduced outlet flow here may be due to the viscous forces inside the pump causing the control ring to adopt a low output condition. This phenomenon is largely unreported, but recognised by some component designers [108] since it can also cause poor lubrication performance during low temperature vehicles tests.

The pump performance at the notional 30 L/min showed only a small sensitivity to the lubricants at 90˚C. The flow rate for the SAE 8 lubricant at 120˚C was poorly controlled, resulting in the pump output exceeding the notional value by 3 L/min.

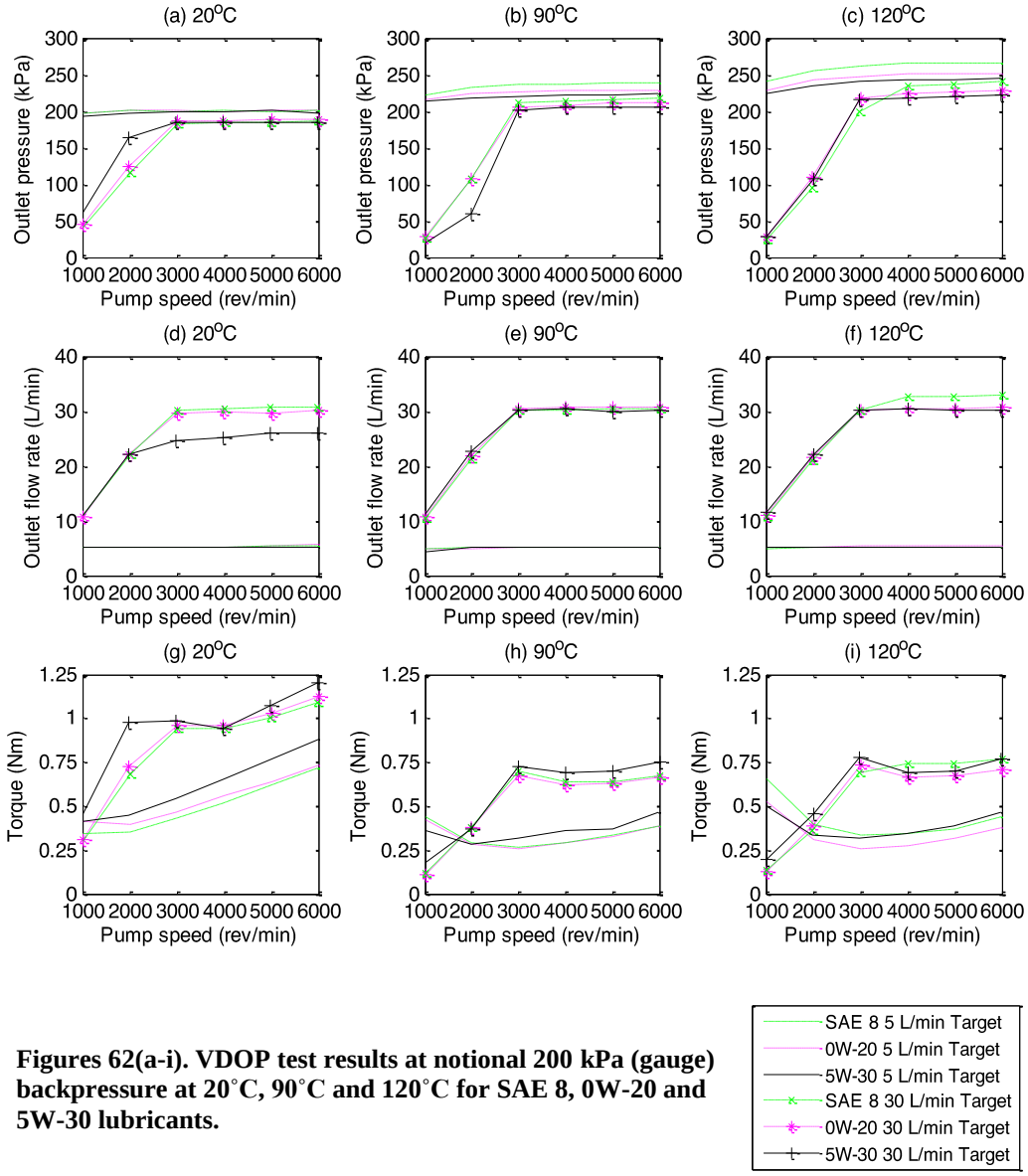

Figures 62(a-i). VDOP test results at notional 200 kPa (gauge) backpressure at 20˚C, 90˚C and 120˚C for SAE 8, 0W-20 and 5W-30 lubricants.

Figures 62(g), (h) and (i) show the drive torque variation at each temperature. The test results at 20˚C showed the pump drive torque was highest with the highest viscosity lubricant and lowest with the lowest viscosity lubricant. This behaviour indicates that losses due to hydrodynamic friction were dominant in this condition. At 5 L/min, as the pump speed was increased, the drive torque values for SAE 8 and 0W-20 converged. The pump outlet pressure and flow rate did not vary with pump speed. Thus, the drive torque variation is probably due to the 0W-20's viscosity reduction as pump speed increased (e.g. because of temporary shear viscosity reduction).

The pump behaviour at 90˚C was similar for all lubricants tested. At 1000 rev/min and 5 L/min, pump drive torque was lowest for tests using 5W-30, arguably due to increased oil film thickness and an associated reduction in asperity friction with this lubricant. At higher pump speeds, the 5W-30 drive torque requirement was higher than that for the 0W-20 or SAE 8. This behaviour corroborated the hypothesis that the 5W-30 was operating in the hydrodynamic friction regime.

The test results at 120˚C showed an increase in drive torque from the 90˚C test. This occurrence may have been due to an increase in friction. However, the pump's higher outlet pressure will have also contributed to the increased load. The 5W-30's superior performance measured at 90˚C and 5 L/min was not replicated in this higher temperature test. The kinematic viscosities for the 5W-30 and 0W-20 lubricants were more similar at 120˚C (Table 2), explaining their similarity in frictional performance. The divergence in their performance with increasing pump speed, and lubricant shear rate, may be due to their different shear viscosity behaviours. At 5 L/min and 1000 rev/min, the highest friction occurred with the SAE 8. This result is likely to be due to both a rise in boundary regime friction and the increased magnitude of the outlet pressure. The higher friction torque at the low pump speeds was greater than the increase in outlet pressure, suggesting that the rise in boundary friction was significant.

5.6.4. Pump performance with different lubricants at 400 kPa (gauge) backpressure

Figures 63(a to i) shows pump performance at 5 L/min and 30 L/min with each lubricant at the higher outlet pressure of 400 kPa (gauge). Figures 63(a), (b) and (c) show outlet pressure variation at each temperature. Similar to at 200 kPa (gauge), outlet pressure rose with temperature and reduction in lubricant viscosity.

The pump outlet pressure was circa 50 kPa below the target pressure at 20˚C. The same rise in pressure with increasing temperature and reducing lubricant viscosity was observed. The pressure increased by 80 kPa between 20˚C and 120˚C with SAE 8. This behaviour compares to the variation of 73 kPa at the notional 200 kPa (gauge) condition.

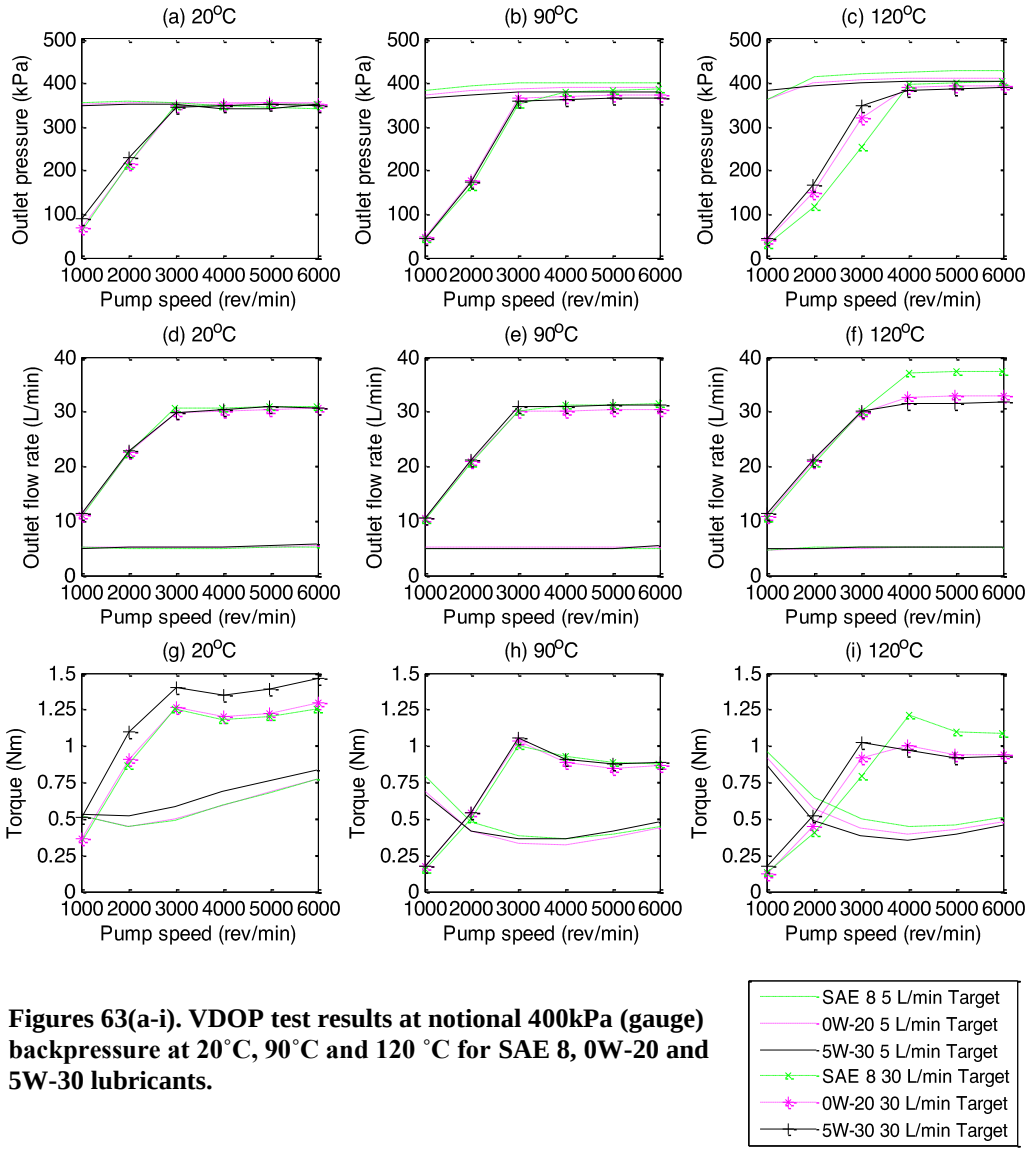

Figures 63(a-i). VDOP test results at notional 400kPa (gauge) backpressure at 20˚C, 90˚C and 120 ˚C for SAE 8, 0W-20 and 5W-30 lubricants.

The pump outlet pressure followed similar behaviour to that in the 200 kPa (gauge) condition at 90˚C. However, the pump performance at 120˚C differed. At 5 L/min the outlet pressure for SAE 8 and 0W-20 was initially lower than for 5W-30, until the pump speed was increased to over 2000 rev/min. This behaviour was unexpected and could not be explained. The pressure curve shape for SAE 8 and 0W-20 is similar to that in

the 200 kPa (gauge) tests, indicating it was the 5W-30 that introduced the change in behaviour.

Figures 63(d), (e) and (f) show the flow rate variation. As per the testing methodology, maximum outlet flow rate was a controlled parameter. The pump's performance was broadly similar to that at 200 kPa (gauge).

At 20˚C, the 5W-30's performance did not deviate from the other lubricants. The flow rate reduction in the 200 kPa (gauge) test was not replicated. The pressure balance on the pump control ring differed here, thus it did not influence the control ring position. At 120˚C, the SAE 8 was badly controlled and the pump output exceeded the notional value by 7 L/min, producing an undesirable effect on the torque measurements. The other flow rates were well controlled.

Figures 63(g), (h) and (i) show that the drive torque was higher in tests using the 400 kPa (gauge) outlet pressure setting. This behaviour was expected and follows logically from the increased pump work required to supply lubricant at this higher pressure. The graph shape follows a similar form to at 200 kPa (gauge), validating the conclusion that the pump friction surfaces transitioned between the different tribological regimes.

5.7. Summary of VDOP performance

Testing at both low (200 kPa (gauge)) and high (400 kPa (gauge)) outlet pressures showed that the pump interaction with the lubricants was similar. The pump outlet pressure rose with increasing temperature and reducing lubricant viscosity. This pressure sensitivity was greater at higher temperatures and caused the theoretical pump load to increase for low viscosity lubricants. However, the pump drive torque did not increase when testing low viscosity lubricants. This behaviour was unexpected and may be due to increased efficiency in the pumping process concurrent with a reduction in

viscous friction, a reduction in friction between the moving surfaces in the pump or a change in volumetric efficiency. These factors were confounded in testing and could not be separated. All these effects are likely to have contributed to the lower torque values.

5.8. VDOP performance in an engine

Rig testing established the pump's performance in isolation from the engine. However, the rig results did not allow direct comparison of the lubricants' performance, since each lubricant's test conditions were the same. This approach did not account for the flow rate increase that occurs when reducing lubricant viscosity. Equally, in rig testing the simulated lubricant circuit permeability was adjusted manually to achieve the target flow rate. This condition was held constant and pump speed was varied. Controlling the rig in this way replicated the behaviour of the oil circuit in a steady-state condition, but did not account for transient behaviour, such as the operation of variable valve timing systems or the intermittent activation of piston cooling jets. Measurement of oil flow rate in the engine was beyond the scope of this rig test. Thus, the flow and pressure measurements used were from a separate research study where lubricant development work was undertaken using a Ford 1.0 L EcoBoost engine test. The pump fitted to this engine was the same design of VDOP as used in the rig test.

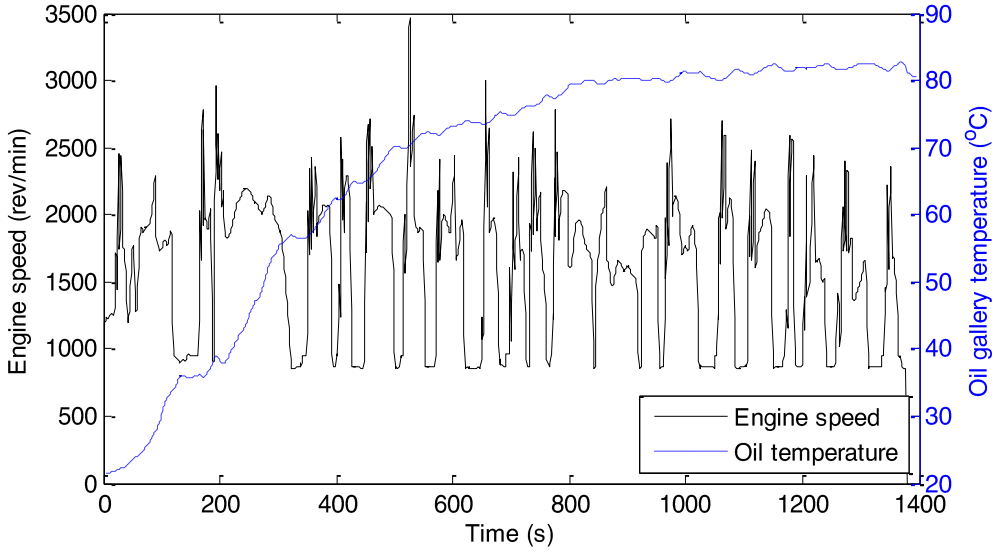

Figure 64. Summary of engine speed and oil temperature for Ford 1.0 L EcoBoost test.

Figure 64 shows the variation in engine speed and oil temperature for the tests using this procedure. The test cycle is based on the United States Environmental Protection Agency (EPA) Urban Dynamometer Driving Schedule (UDDS) – also known as the 'FTP 72' cycle. The tests replicated those found driving in urban environments. This test's scope is comparable to the NEDC, although the speed and loads differ [128]. The test cycle included measurements during warm-up.

Table 25. Summary of test lubricants.

	0W-20		5W-30		SAE 8	
Lubricant code	A1293P /176A	E1218P /040A	A0940P /069A	E1218P /041A	E0966A /005A	E1218P /053M
Test Type	Rig	Engine	Rig	Engine	Rig	Engine
KV120 (cSt)	6.1	6.1	6.6	7.2	3.8	5.3
KV100 (cSt)	8.5	8.9	9.7	10.6	5.4	7.5
KV90 (cSt)	10.3	10.9	12.1	13.3	6.6	9.2
KV40 (cSt)	36.7	47.5	55.0	64.0	26.0	38.0
KV20 (cSt)	77.2	115.0	137.3	165.2	60.4	89.6

An oil flow meter was installed by modifying the oil circuit between the oil filter and cooler assembly and the engine oil gallery. The flow meter was a turbine type, but was not calibrated for each lubricant. Thus, the values only indicate the flow rate.

The lubricants used in this testing were different to those in the rig test project. Table 25 summarises the differences in viscosity between these test lubricants. Oil flow measurements for each viscosity grade tested using the rig were recorded. However, the engine test lubricants had higher kinematic viscosities.

5.8.1. Engine testing results

Figure 65 shows measured variation in oil flow and gallery pressure for the three lubricant viscosity grades. The oil flow rate was low at the start; before getting larger in the warm-up phase (roughly 0 to 800 seconds). The increasing oil flow correlated with the lubricant viscosity reduction caused by the engine and lubricant temperature

increase. Oil flow rate rose and fell with engine speed. Thus, the transient engine speed in this test cycle caused the oil flow rate to appear noisy.

Lowering the lubricant viscosity grade increased the oil flow rate in the engine. As the lubricant viscosity reduced, the oil pump flow rate increased to keep the pressure target set by the pump control algorithm. Oil gallery pressure increased through the test as the temperature rose, which replicated its behaviour in the rig testing work. Reducing the lubricant viscosity increased oil gallery pressure, also similar to the behaviour in the rig testing. Towards the middle of the test (e.g. after 430 seconds) the oil gallery pressure was at times lower with the low viscosity lubricants. This behaviour was not replicated on the test rig. These low pressure events correlated with the engine running at its idle speed of 860 rev/min (774 rev/min pump speed) – a lower speed than tested in the rig phase.

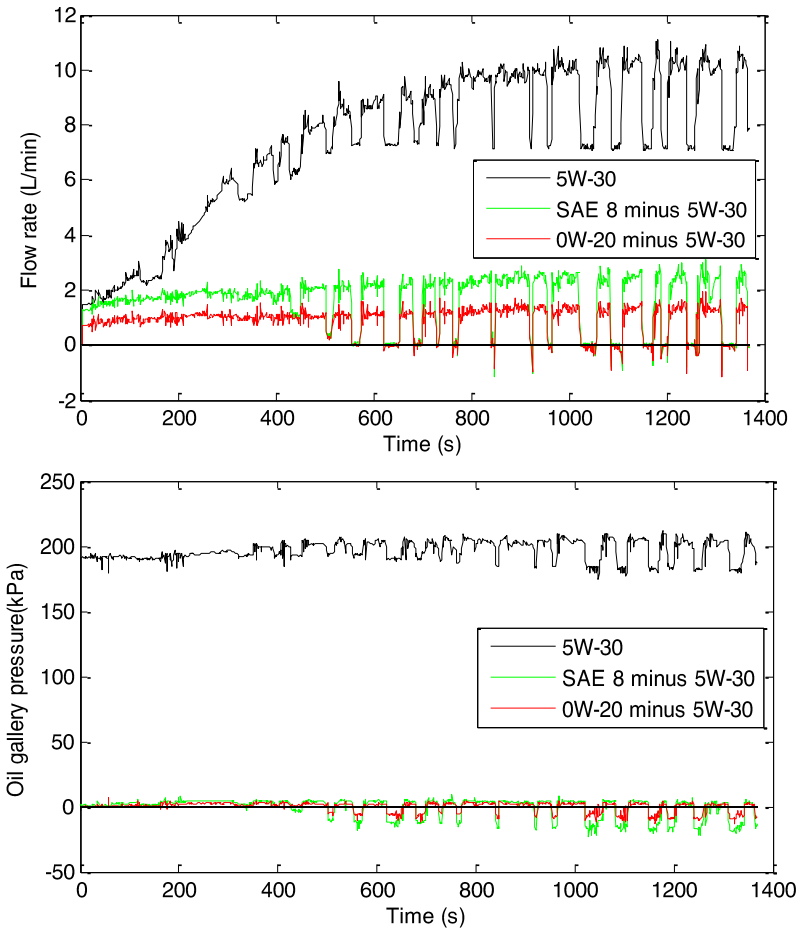

Figure 65. Oil flow rate and oil gallery pressure during engine testing using 1.0 L EcoBoost engine with three lubricants.

The oil flow rate increase varied in the test due to the lubricants' different temperature-viscosity behaviour. Comparing the 5W-30 and 0W-20, the flow rate increased by 0.7 L/min at the start and by 1.5 L/min at the end of the test by reducing the viscosity. This change equates to an increase of 50% and 14% respectively. The difference in flow rate from 5W-30 to SAE 8 was 1.3 L/min at the start and 2.7 L/min at the end, equating to an 86% and 26% increase respectively.

5.8.2. Calculated effect on oil pump drive torque

To determine the significance of lubricants viscosity differences on the pump drive torque, calculations were undertaken using the data collected at four discrete points. The results showed that oil pump temperature, and the associated lubricant viscosity difference, was significant in determining if reducing lubricant viscosity lowered or increased drive torque. This analysis is described below.

5.8.3. 0W-20 and SAE 8 at 20˚C

Figure 66 shows the percentage change in pump drive torque for the 20˚C conditions with a notional 5 L/min flow rate as well as the predicted effect of increasing oil flow rates. The drive torque at the higher oil flow rate was calculated using:

$$T_{\mathrm{P}} = \frac{V_{\mathrm{D}}\, P}{\eta\omega} \tag{28}$$

where the theoretical flow rate was between 5 L/min to 10 L/min, the pump total efficiency was calculated by interpolating between the efficiencies measured on the rig at each flow rate. A similar approach was taken for flow rates between 10 L/min and 15 L/min. The outlet pressure was taken from the values at 5 L/min. Using this calculation, the increase in oil outlet pressure due to the reduction in lubricant viscosity was considered. However, the oil pressure rise due to the increasing oil flow rate was not included.

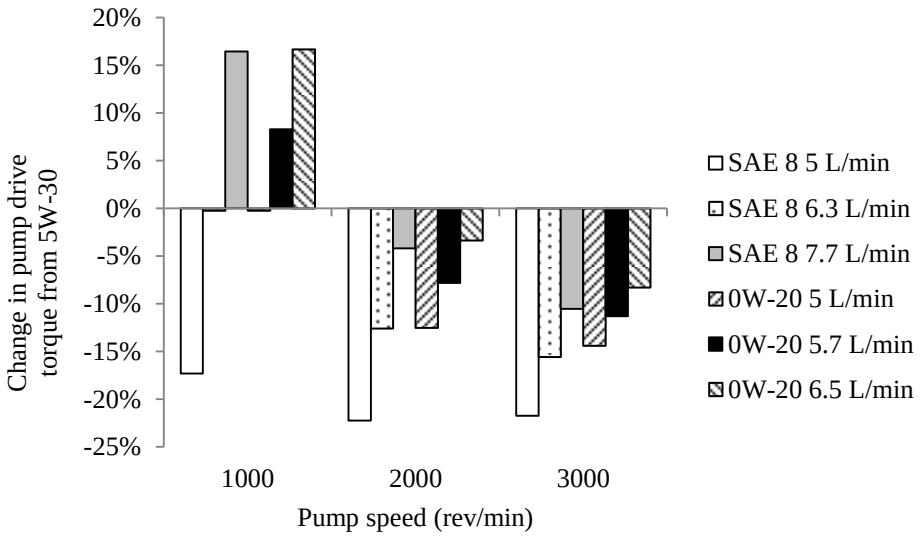

Figure 66. Change in pump drive torque at 20 ˚C, 5 L/min notional flow rate and 200 kPa (gauge) backpressure.

Using maximum and minimum flow changes from the engine test allowed assessment of the torque sensitivity to the increased oil flow rate. The calculations showed that increasing oil flow rate from 5 L/min to 6.3 L/min for SAE 8 caused the pump drive torque to increase to the same level as in the tests at 5 L/min with 5W-30. When the flow rate was increased to 7.7 L/min an increase in pump drive torque of 15% was predicted, consistent with the hypothesis that lower viscosity lubricants increase pump drive torque. However, as the pump speed was increased, the pump's higher efficiency with this lower viscosity lubricant compensated for the increase in flow rate. Thus, the total pump torque was predicted to reduce in these higher speed conditions.

The behaviour of the 0W-20 was calculated at oil flow rates of 5.7 L/min and 6.5 L/min. These flow rates are smaller than those in the SAE 8 calculations, but consistent with the smaller increase in oil flow in the engine tests. When the oil flow rate was increased to 5.7 L/min, an increase in pump drive torque from the 5W-30 baseline of 8% was predicted. Increasing flow rate to 6.5 L/min increased drive torque by 17% at 1000 rev/min. As pump speed increased, the greater pump efficiency using 0W-20 compensated for oil flow rate increase, resulting in a net drive torque reduction.

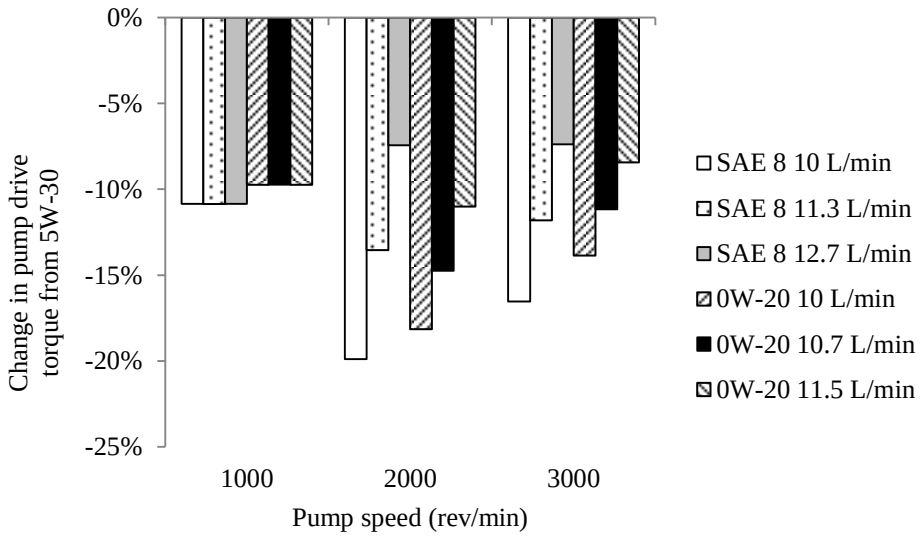

Figure 67. Change in pump drive torque at 20˚C, 10 L/min notional flow rate and 200 kPa (gauge) backpressure.

Figure 67 shows percentage change in pump drive torque at 20˚C and 10 L/min. The results show drive torque reduction in all conditions using low viscosity lubricants.

At 1000 rev/min, the increase in demanded oil flow rate did not change the pump drive torque, since the pump maximum displacement was insufficient to reach the set point. If this condition were to exist in an engine, the low viscosity lubricant would also achieve a lower oil pressure, resulting in further drive torque reductions. Satisfactory operation of the engine's pressure sensitive components would have to be confirmed. At higher engine speeds, the drive torque reduced when testing using the lower viscosity lubricants. The increase in pump efficiency was greater than the loss associated with the increased flow rate. Consequently, the calculated pump drive torque reduced.

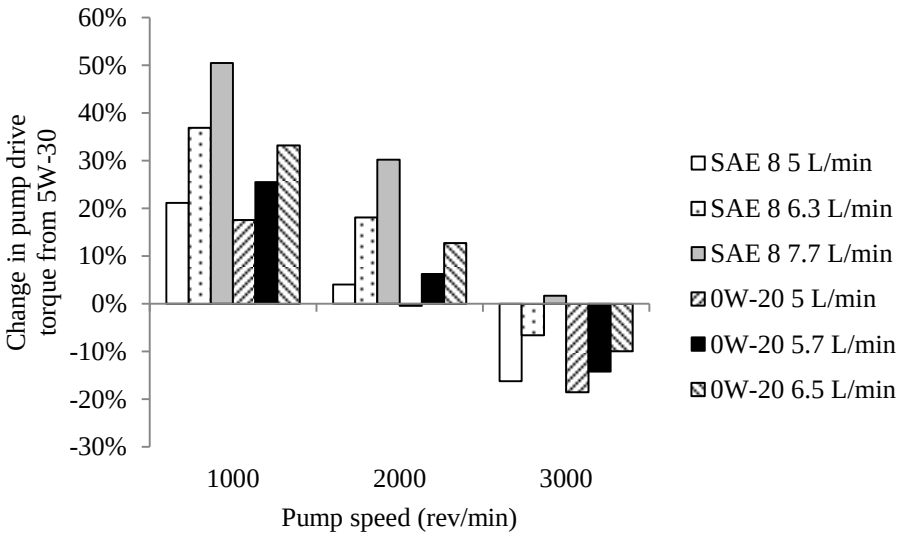

Figure 68. Change in pump drive torque at 90˚C and 5 L/min notional flow rate and 200 kPa (gauge) backpressure.

Figure 68 shows the percentage change in pump drive torque at 90˚C with a notional 5 L/min flow rate. At 1000 rev/min, the results indicate that the lower viscosity lubricants caused an increase in pump drive torque. The pump efficiency was highest when tests used 5W-30 at 1000 rev/min, explaining why there was no benefit associated with the low viscosity lubricants. Theoretically, adding friction modifiers could improve the performance of low viscosity lubricants in this test condition. At 2000 rev/min, the drive torque also increased with reducing oil viscosity, although performance improved compared to at 1000 rev/min. The calculated efficiency was similar for each lubricant (between 30.9% and 31.4%). Thus, the greater oil flow rate increased the pump drive torque. At 3000 rev/min, the low viscosity lubricants caused the pump to operate at a greater efficiency. With the exception of the 7.7 L/min flow condition, using the SAE 8 lubricant the increase in pump efficiency was greater than the rise in flow rate. Hence, the drive torque was predicted to reduce with low viscosity lubricants.

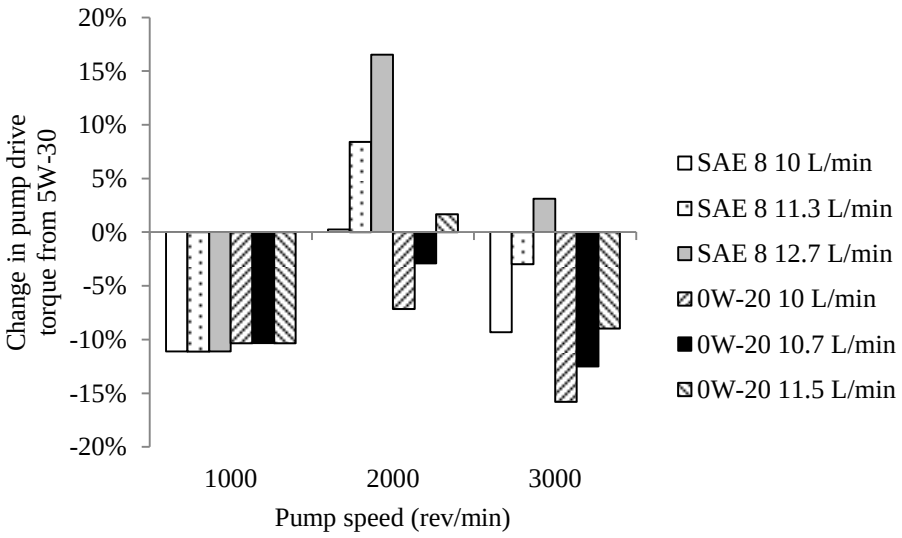

Figure 69. Change in pump drive torque at 90˚C and 10 L/min notional flow rate and 200 kPa (gauge) backpressure.

Figure 69 shows the percentage change in pump drive torque at 90˚C with a notional 10 L/min flow rate. At 1000 rev/min, the measured drive torques reduced when testing the low viscosity lubricants since the pump output could not achieve the demand flow rate. As the pump speed increased to 2000 rev/min, the performance of the low viscosity lubricants worsened. The low viscosity lubricants reduced pump torque at the 3000 rev/min condition except for the high flow rate condition using the SAE 8.

The test results showed that whether a low viscosity lubricant provided a net increase or decrease in drive torque was dependent on pump speed, lubricant viscosity and flow rate. However, the simplification made in the testing where the oil filter and cooler assembly losses were ignored was revisited to ensure that this had not confounded the results. This re-evaluation was necessary since the pressure control signal used by the oil pump sat after the oil filter and cooler assembly (see Section 5.5). Thus, the pump outlet pressure was higher than the gallery pressure in normal operation. In theory, the pump outlet pressure could have differed across lubricants, dependent on the pressure drop via this intermediary system.

5.8.4. Effect of the oil filter and cooler assembly

Engine test data measured the oil filter and cooler's effect on the oil pump's outlet pressure. Pressure transducers were installed before the oil filter and cooler assembly and in the oil gallery. Modifications extended the engine oil circuit to allow the fitment of the oil flow meter and test bed controlled oil cooler, so the reported pressure drops were slightly larger than on the standard engine due to these components.

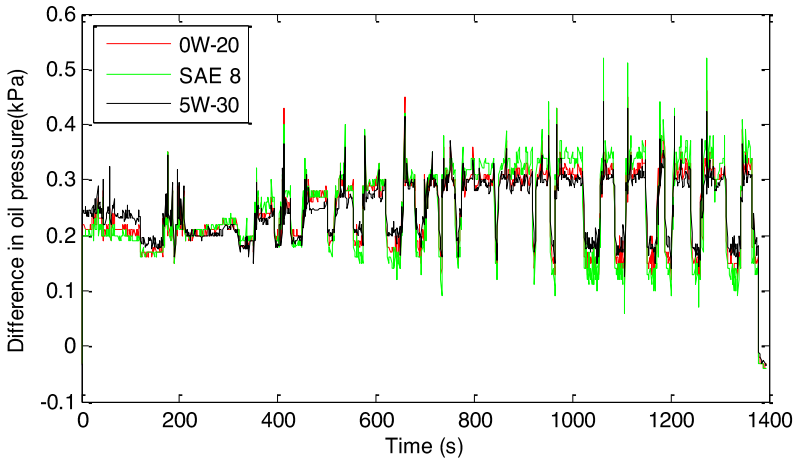

Figure 70. Pressure difference across oil filter and cooler assembly measured using the Ford 1.0 L EcoBoost engine dynamometer test.

Figure 70 shows the difference in oil pressure across the oil filter and cooler for the three lubricants in the engine dynamometer testing phase. The data shows that the outlet pressure for each lubricant was similar. At the test start, when lubricant viscosities were high and flow rates were low, the pressure drop reduced by circa 5 kPa with SAE 8 compared to 5W-30. As the temperature and flow rate increased, the low viscosity lubricant's behaviour depended on the oil gallery pressure. Under high oil gallery pressure, the pressure drop increased slightly (circa 5 kPa) as the lubricant viscosity was reduced. Under low oil gallery pressure (e.g. when the engine returned to idle), the pressure drop decreased slightly (circa 5 kPa) as the lubricant viscosity reduced. This small variation is unlikely to increase the torque output significantly.

5.8.5. Operation in the high output pressure mode

Figure 71 shows drive torque variation with a 5 L/min notional flow rate and at 20˚C. Figure 72 shows the variation at a 10 L/min notional flow rate. Increasing pump delivery pressure reduced the low viscosity lubricants' performance throughout the engine speed range for 5 L/min and 10 L/min notional flow rates in comparison to that seen in the 200 kPa (gauge) tests. The increase in drive torque reduced as pump speed increased, except at 10 L/min and 1000 rev/min pump speed where drive torque was lower than expected for the 5W-30 (discussed in 5.6.4).

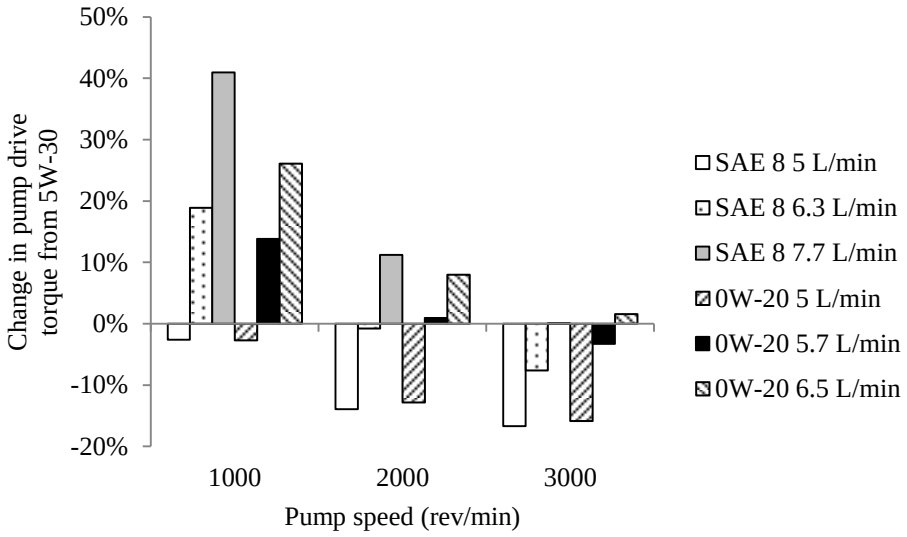

Figure 71. Change in pump drive torque at 20˚C and 5 L/min notional flow rate.

Figure 73 shows drive torque variation at 90˚C with 5 L/min notional flow rate. Figure 74 shows the variation at 10 L/min notional flow rate. Increasing pump delivery pressure worsened the performance of the low viscosity lubricant throughout the engine speed range (except for at 1000 rev/min and 90˚C where the pump displacement was at it maximum condition), demonstrating similar behaviour to that found in the 20˚C tests.

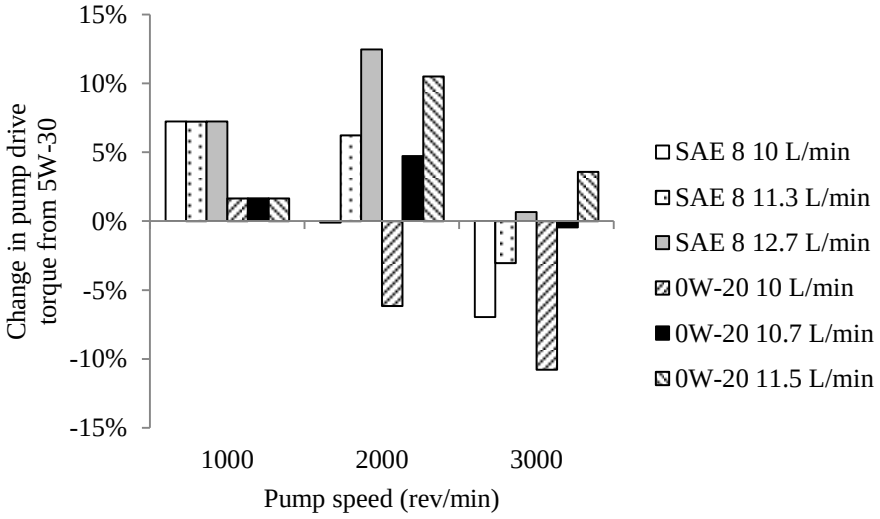

Figure 72. Change in pump drive torque at 20˚C, 10 L/min notional flow rate and 400 kPa (gauge) backpressure.

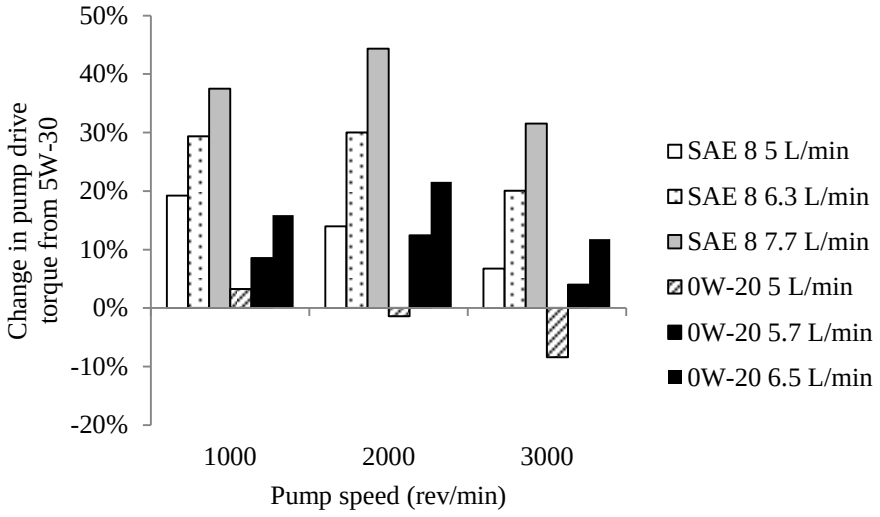

Figure 73. Change in pump drive torque at 90˚C and 5 L/min notional flow rate.

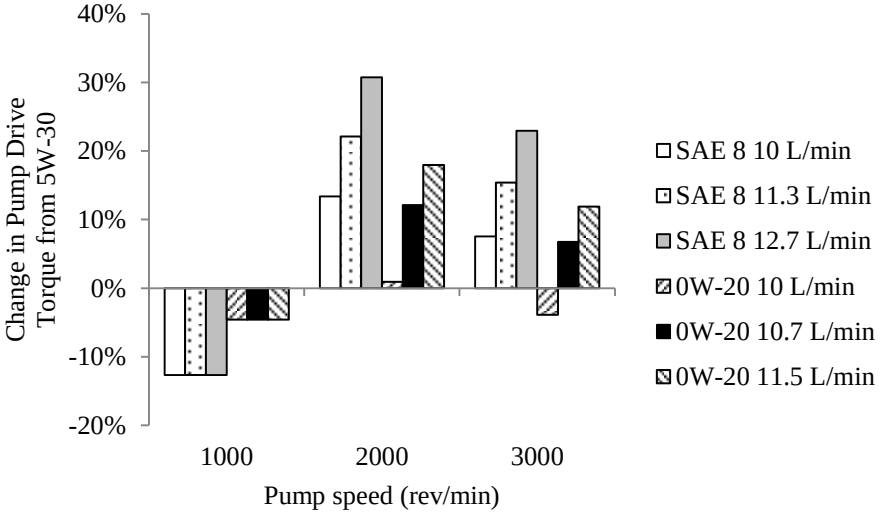

Figure 74. Change in pump drive torque at 90˚C and 10 L/min notional flow rate.

5.9. Chapter 5 conclusions and recommendations

Modern engine designers are choosing VDOPs and lower viscosity lubricants are being introduced. Existing literature does not document the interaction between VDOPs and low viscosity lubricants. The potentially antagonistic interaction between these components warranted investigation.

VDOPs have reduced vehicle CO_2 emissions by between 0.5% and 3% on the NEDC. However, the CO_2 benefit is not the only reason designers choose to implement these pumps. The adoption of other new components has increased the engine's oil flow requirements (e.g. hydraulically powered variable valve timing systems and piston cooling jets). Using these components lower in the engine speed range has become increasingly common, adding to low speed flow requirements. VDOPs achieved the higher flow rate requirements of these systems at low engine speeds, without resulting in significant oversupply at high engine speeds.

VDOPs need a control strategy to vary pump output. Typically, their control systems target a predefined oil gallery pressure and govern the pump output using electronically-augmented or mechanical systems. Since oil gallery pressure is a function of oil flow rate and viscosity, an interaction between the lubricant viscosity and pump output is evident using these pumps. To achieve the predetermined oil pressure, the oil flow rate increases as lubricant viscosity reduces. Thus, it was hypothesised that reducing lubricant viscosity caused a greater oil pump load due to this increase in required oil flow rate. Since using low viscosity lubricants may increase the parasitic load from VDOPs, this behaviour marks an important research area. An investigation was completed in the present research to substantiate this hypothesis.

Engine testing, simulation and rig testing were evaluated for quantifying the effect low viscosity lubricants have on a VDOP's drive torque. Rig testing was chosen. A

Ford 1.0 L EcoBoost engine's VDOP was fitted to a bespoke rig test to investigate the performance change different lubricants caused. The pump was tested using oil flow rates from 5 L/min to 30 L/min (in 5 L/min increments), three lubricants, 5W-30, 0W-20 and SAE 8, and three temperatures, 20˚C, 90˚C and 120˚C. The test found that pump pressure, speed and flow rate were significant in deducing the pump's operating efficiency and performance.

Tests measured pump outlet pressure and drive torque at various oil flow rates. The oil pressure from the pump reduced as the flow rate increased. This effect was attributed to the flow forces internal to the pump changing the force balance between the guide spring and outlet pressure. The pump's outlet pressure also increased as the oil viscosity grade was lowered; this effect increased as pump temperature rose. An increase in outlet pressure of 21 kPa (a 9% increase over the 5W-30) occurred when testing the SAE 8 low viscosity lubricant at 120˚C, 5 L/min and 200 kPa (gauge) backpressure. This pressure increase augmented the theoretical load for the low viscosity lubricant compared to that needed for higher viscosity lubricants. In theory, this behaviour could be tuned out of the pump by respecifying the guide vane control spring's stiffness, to improve the performance with low viscosity lubricants.

The oil pump's total efficiency was calculated, varying from 8% to 57% at 90˚C for 0W-20 across the flow rates tested. Significant pump efficiency variation was an unavoidable design feature, since the crankshaft directly drove the pump. Achieving an oil flow reduction was only possible by reducing the pump displacement. The frictional losses that increased with pump speed occurred simultaneously with low output. At key points in the test matrix (e.g. high flow rate and low speed) the pump could not achieve the pressure target. Pump outlet pressure grew with pump speed. The flow rate increase was linear, suggesting the pump variable displacement control was not active.

The torque measurements indicated a transition between friction regimes depended on speed, load and temperature in the oil pump. Oil film thickness must be quantified to validate this conclusion. Other authors report tests where vane tips [110] and guide rings on similar pump designs suffered wear, corroborating the theory that there was boundary regime friction in this test. This conclusion indicates that using surface-active additives, like friction modifiers, could reduce mechanical losses in this component.

Oil flow was also measured on a 1.0 L Ford EcoBoost engine over a UDDS using a fired engine dynamometer test. The SAE 8 increased the flow rate by 1.3 L/min (86% increase) at low temperature and 2.7 L/min (25% increase) at high temperature compared to the 5W-30's values.

The effect on pump drive torque at 5 L/min and 10 L/min was evaluated using data from the rig test. The flow rate increase when the engine used low viscosity lubricants was accounted for by simulating the drive torque present at higher flow rates.

Including increased oil flow rates with low viscosity lubricants caused an oil pump drive torque increase, but did not always increase the calculated net drive torque. The pump's higher efficiency using low viscosity lubricants offset the flow rate increase. A total drive torque reduction was predicted for many 20˚C runs. A drive torque reduction (relative to the high viscosity lubricant) occurred as pump speed increased and was attributed to decreased hydrodynamic friction from lower viscosity lubricants.

The effect on predicted pump drive torque of lowering oil viscosity was less favourable as oil temperature rose and pump outlet pressure increased. The oil pump's response to low viscosity lubricants depended on the oil flow rate, pump speed, temperature and outlet pressure variation. Thus, behaviour may vary with engine tests on different drive cycles or real world usage. Simulating the pump performance over a drive cycle is left for completion in a full vehicle model (see Chapter 7).

At low pump temperatures, the mechanical losses were dominated by viscous friction increase. Thus, reducing lubricant viscosity allowed a significant drive torque reduction. The efficiency variation at very low flow rates was not measured. However, at flow rates lower than those measured in these tests, it is likely that the greater efficiency from a lower magnitude of viscous friction will become increasingly significant. Knowledge of this behaviour and the exact increase in flow rate is key to concluding whether low viscosity lubricants provide a net benefit or penalty in low speed and low temperature conditions prevalent in test cycles such as the NEDC.

5.9.1. Key findings:

- A variable displacement oil pump was mounted to a rig to test the hypothesis that its friction increases when pumping low viscosity lubricants (due to a concomitant increase in oil flow rate).
- The low viscosity lubricant's increased oil flow rates did not always increase the net drive torque. The pump's higher efficiency using low viscosity lubricants offset the flow rate increase in many conditions.
- The effect on predicted pump drive torque caused by lowering the oil viscosity was unfavourable as oil temperature rose and pump outlet pressure increased. The oil pump's response to low viscosity lubricants depended on the oil flow rate, pump speed, temperature and outlet pressure variation.

5.9.2. Recommendations for further work

To conclude the effect on the pump drive in a low temperature low speed drive cycle, a fuller rig testing matrix with a greater refinement of oil flow rate increments and oil temperature changes is needed. The rig results could be improved by adding to the test points (e.g. 1 L/min increments from 0 L/min to 15 L/min). The pump's speed range should also be lowered to measure pump behaviour at engine idle speed.

The pump's performance under transient testing conditions was not evaluated. An advantage of developing an engine test or more complex rig test would be the inclusion of any effects due to rapid speed changes and thermal transient conditions.

Published data showing a simulation-based approach that predicts pump flow rate, pressure and torque is scarce. Developing such a tool is recommended as it may provide unique insight into the modern oil pump performance with low viscosity lubricants.

Evaluation of oil pump performance in the engine is complicated since a number of interdependencies exist. If a more refined simulation is developed, then a model of oil flow rate variation in the engine will be needed, using a program like Flowmaster. This approach would allow the oil flow rate variation to be predicted for different lubricant viscosities. However, characterisation of the transient flow rate needs of the variable valve timing drive may complicate this approach. The lubricant temperature variation due to change in oil flow rate also needs to be assessed, since this will affect the results.

The present research focuses on the performance of a single vane-type VDOP. The interaction between lubricants and other variable output pump designs (e.g. trochoidal and external gear pumps) requires study to identify broader conclusions. Due to the differing designs of these pumps their frictional behaviour is likely to differ, which may affect the conclusions presented in this investigation.

6. Lubricant thermal management

The procedure used to measure the tailpipe CO_2 emissions, for new vehicles being homologated in Europe, is the NEDC Type I test. The protocol requires that the vehicle be preconditioned to between 293 K and 303 K prior to the test starting [129]. Because of this thermal boundary condition, the exhaust gasses emitted during vehicle and engine warm-up are included into the measurements completed and, since the speed and load ratings in the test are low, the engine and transmission systems spend a significant portion of the test time warming up [130]. Frequently the lubricant temperature does not reach a steady-state level in the test. In fact, for this cycle, it is common to measure increasing lubricant temperature throughout the duration of the test (Figure 75).

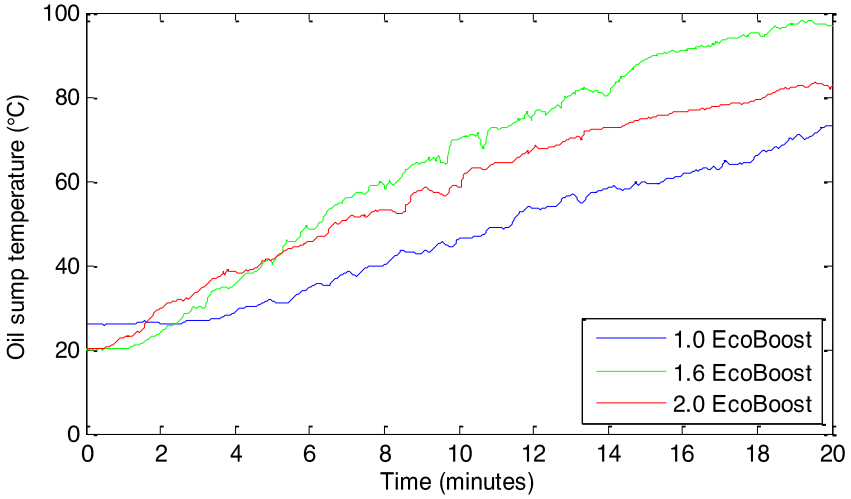

Figure 75. Lubricant temperatures measured in the sump for three passenger car engines when tested over the Type I NEDC from a cold (20˚C to 26˚C) start. (1.0 EcoBoost data taken from engine test bed, 1.6 and 2.0 EcoBoost taken from chassis dynamometer testing. All tests replicated the NEDC using the loading profile from a Ford Focus vehicle model.)

The low average torque produced by the engine in order to meet the road load demanded by the NEDC means that frictional losses are relatively large and, therefore, make a significant contribution to the measured tailpipe CO_2 emissions. High levels of engine friction during cold start conditions are the dominant reason for increased fuel consumption during warm-up [45], [46], [131]. Slow rates of lubricant temperature increase cause this poor efficiency to persist for a significant part of the cycle. The high

friction in this condition can be attributed to a significant increase in lubricant viscosity and a reduction in some component tribological contact clearances at low temperatures, which tend to increase the hydrodynamic friction in the engine. Notable components that do not follow this trend are aluminium alloy pistons in cast iron cylinder bores. Lubricant pumps can also operate at significantly higher drive torques, dependent on the design adopted, adding to the engine parasitic loading (see Chapter 5).

The variation in lubricant viscosity with temperature change can be calculated using the Vogel equation (4). Since this viscosity equation follows a logarithmic increase with reducing temperature, a large amount of hydrodynamic friction can be present in the engine during the low temperature start conditions of the NEDC. Consequently, systems that can reduce lubricant viscosity and, therefore, this hydrodynamic friction, are worthy of investigation.

The hot-cold factor describes the percentage change in the vehicle's tailpipe CO_2 emissions when the NEDC is started with the vehicle in a cold condition (e.g. 293 K to 303 K), compared to the CO_2 emissions when the same cycle is completed with the engine fully warmed up. The hot-cold factor can be calculated using:

$$\emptyset = \mathbf{100}\left(\frac{\boldsymbol{m_c}}{\boldsymbol{m_h}} - \mathbf{1}\right) \tag{29}$$

where $\emptyset$ is the hot-cold factor (%), m_c is the mass of CO_2 emitted during a cold start NEDC and m_h is the mass of CO_2 emitted during a hot-start NEDC.

This simple calculation can usefully be completed to allow a first pass interpretation of the magnitude of improvement that can be made by implementing thermal management systems. Kunze et al. [132] indicate a typical hot-cold factor of 10% for a 3.0 L gasoline engine. The work reported by Zammit et al. [45] indicates a hot-cold factor of 5.4% for a 2.4 L diesel engine. Reverault [133] reports between 7% and 12% for diesel passenger car engines. Therefore, the opportunity to improve vehicle

efficiency during warm-up is significant. However, these values must be interpreted with caution since the increased fuel consumption is not solely attributable to an increase in friction in the engine for the low temperature start case. Significant differences exist because of the higher start-of-test thermal energy in the hot case (reducing heat losses from the combustion event) and variations in the engine fuelling calibration (e.g. due to catalyst light-off strategies). The large differences between the engines reported in the work above are also attributable to the adoption of different thermal management strategies, such as electric water pumps and split cooling systems. Using integrated exhaust manifolds combined with these technologies can also impact the warm-up of the engine significantly.

Lubricant temperature increase occurs because of the conversion of mechanical energy to thermal energy in the lubricant due to friction and heat transfer from the combustion process. These losses are both sources of inefficiency in the system since, following the Second Law of Thermodynamics, the net heat transfer between the engine and the test chamber environment is increased. Thus, processes that reduce the heat transfer increase the system's efficiency. To understand these results, the heat transfer from the system as a whole must be considered. The heat transfer from the sump may increase (e.g. due to preheating of the lubricant), but the complete system heat transfer may reduce due to the smaller parasitic loads, resulting in a reduced fuelling rate.

Due to the relative importance of warm-up in the test cycle, advanced thermal management systems are an important research area. A worthwhile reduction in CO_2 emissions can be made at a relatively low cost [8].

6.1. Thermal management approaches

The opportunities to influence lubricant viscosity during warm-up using thermal management can be divided into five main categories:

1. Thermal energy storage (to store the lubricant thermal energy from previous vehicle use or the preconditioning cycle)
2. Active heat input via:
    a. engine coolant, using coolant-to-lubricant heat exchangers
    b. electrically powered heating elements
    c. exhaust heat recovery
3. Reducing the lubricant thermal mass
4. Insulating the oil sump

For the purposes of this investigation 1, 2a, 2b and 3 are considered. Insulating the oil sump (4) was not considered due to the complexities of installing the insulation without dismounting the vehicle from the chassis dynamometer between tests. Exhaust heat recovery (2c) was beyond the scope of the present work. However, Zammit et al. [45] report work evaluating the opportunity presented by this technology.

6.1.1. Thermal energy storage (1)

This section considers the effect of storing the lubricant thermal energy from previous vehicle use. The scarcity of literature dedicated to, or focused on, this area is probably due to technical challenges associated with implementing this technology into vehicles. Ideally, the fitment of a remote reservoir and transfer pump is required.

Kunze et al. [132] built and validated a 1D simulation to investigate the potential fuel economy impact of actively heating or storing thermal energy from previous engine runs. No practical realisation of this strategy is presented, although a suggestion is made that it could be achieved using a heat accumulator or via the use of electrical energy

storage. In the simulations reported, a fuel consumption improvement of 1.6% is predicted. This forecast uses a 90˚C input boundary condition for the lubricant temperature and a test vehicle preconditioned to 20˚C prior to the NEDC start. Kunze et al. [132] completed an experiment to validate the model. However, the tests' repeatability was too poor to determine measured fuel economy variation with statistical certainty. The effect of the engine temperature change on the fuelling calibration algorithm was not fully understood and was cited as a potential noise factor.

Following Kunze et al's work [132], Andrews et al. [8] made calculations to understand the amount of energy required to increase the temperature of a 10 L volume of oil from 25˚C to a predicted end of test temperature of 80˚C. These simplistic calculations indicate circa 2 MJ is needed, equivalent to approximately 12.5 gCO_2/km. The energy added to the lubricant ordinarily occurs due to inefficiencies in the system (friction and heat transfer). The conversion of chemical energy in the fuel to heat occurs coincidentally with useful work on the test cycle. It remains a valid indication of the magnitude of the effect. However, the number obtained by Andrews et al. is an overestimate of the magnitude of the energy required to heat the lubricant used in more modern passenger car engines, because the lubricant volume assumed in the calculation is relatively high. The energy requirement to heat the lubricant can be obtained, using:

$$Q = m\, c_v\, \Delta T \tag{30}$$

where m is the mass of lubricant being heated; c_v is the specific heat capacity for the lubricant at constant volume; ΔT is the change in temperature of the lubricant and Q is the energy input required to effect the temperature increase.

Table 26 shows that by using values representative of a more modern engine the energy requirement is about 0.7 MJ, which is equivalent to approximately 4.7 gCO_2/km.

This calculation uses a mean value for the specific heat capacity and density, since they vary slightly with temperature.

Table 26. Parameters assumed for lubricant temperature rise and resulting energy requirement.

Volume of lubricant (L)	5.1
Density at 20˚C (kg/m^3)	849
Density at 90˚C (kg/m^3)	806
Mean density (kg/m^3)	828
Mass of lubricant (kg)	4.3
Specific heat capacity (J kg^{-1} K^{-1}) @20˚C	2232
Specific heat capacity (J kg^{-1} K^{-1}) @90˚C	2502
Mean specific heat capacity (J kg^{-1} K^{-1})	2367
Lubricant temperature difference (K)	70

Energy input (MJ)	0.70
Equivalent mass of gasoline @43 MJ/kg	0.017
Equivalent CO_2 (gCO_2/km)	4.7

The calculated energy input required to increase the lubricant temperature still represents a significant portion of the total CO_2 emitted by modern vehicles (~130 gCO_2/km) and warrants further investigation. However, even if this energy could be delivered to heat the lubricant without being debited from the drive cycle (e.g. through externally powered heating elements used with plug-in electric hybrids) then the actual CO_2 reduction in the cycle would not be 4.7 gCO_2/km. All of the system's complicated energy flows must be considered when interpreting the net effect on tailpipe CO_2 emissions. Three large interdependencies exist:

(1) Heat flow into the lubricant occurs due to the combined effect of frictional heating and heat transfer from the combustion process. If the lubricant temperature is elevated, the lubricant viscosity will be reduced and accompanied by a hydrodynamic friction reduction. This reduced friction load then directly causes a decrease in frictional heat input to the lubricant and will reduce the engine's indicated work, fuelling rate and heat transfer from combustion. The reduced fuel input will then cause a reduction in engine warm-up rate.

(2) The elevated lubricant temperature earlier in the test cycle will increase lubricant-to-test-chamber heat transfer so some of this energy will be transferred quickly.

(3) Heating the lubricant mechanically (via friction) is inefficient due to the engine's low thermal efficiency. Hence, reducing the engine's load would magnify the CO_2 improvement.

To interpret the net effect theoretically, a full thermal model is required. For this investigation, empirical measurement establishes the behaviour.

6.1.2. Active Heat Input (2a, b)

6.1.2.1. Coolant – Lubricant Heat Exchangers (2a)

Hess et al. [134] broadly describe the fitment of a coolant-to-lubricant heat exchanger and the interaction this has with an electrically-powered coolant pump in a 6-cylinder BMW group engine. They highlight that in their design the coolant pump is deactivated during parts of the engine warm-up phase, resulting in limited coolant flow through the coolant-to-lubricant heat exchanger. Therefore, theoretically there is no beneficial heat transfer to the lubricant at this stage in the test. Zammit et al. [135] offer a similar insight when discussing the design of a modern 2.4 L diesel engine. In their investigation, the coolant-to-lubricant heat exchanger was isolated from the main coolant supply until the coolant temperature reached 70˚C. This coolant temperature rise took 4 minutes 40 seconds at operating conditions of 2000 rev/min and 3 bar BMEP when tests using the engine preconditioned to 20˚C were conducted. In their design, a thermostatic valve controlled the bypass operation.

Andrews et al. [130] describe testing completed to quantify the effect on warm-up of fitting a coolant-to-lubricant heat exchanger in a passenger car engine. Their paper

reports research work completed before 2007 and uses 5W-50 and 15W-50 viscosity grade lubricants no longer relevant to current mass market passenger car engines. The general physical principles the paper presents remain relevant. However, the impact on lubricant viscosity of increasing the lubricant temperature will probably be lower with modern, lower viscosity formulations. The claimed specific fuel consumption improvement attributable to the fitment of a coolant-to-lubricant heat exchanger was 8% over the first 6 minutes of warm-up, but the test did not use the NEDC. The lack of up-to-date information relating to the performance of coolant-to-lubricant heat exchanger systems suggests this system warrants further research (see 6.4.2).

6.1.2.2. Electrically powered heating elements (2b)

Theoretically, thermal energy input to the lubricant could be achieved by using an electrical heating element powered by the engine electrical system. However, the indicated engine efficiency (~30% for a gasoline engine on the NEDC) combined with the generator efficiency (<60%) [136] means this is probably not useful.

6.1.2.3. Reducing the lubricant mass (3)

The hypothesis that engine CO_2 emissions will reduce by removing a portion of the lubricant mass from the engine suggests that due to lower total engine mass, the engine temperature will rise, and the lubricant viscosity will reduce more quickly. Table 27 shows the energy saving potentially achievable by reducing the engine's lubricant fill volume, which is based on an oil reduction of 2.6 kg (3.1 L) from a 4.3 kg (5.1 L) original fill mass. These simple calculations indicate a potential saving of 2.9 gCO_2/km. For a vehicle with 130 gCO_2/km emission on the NEDC this represents a theoretical 2.2% saving, although the exact magnitude achieved will differ in practice since the reduced lubricant mass will change the engine system heat transfer to ambient. To achieve this theoretical reduction in CO_2 emissions the true minimum running level also

needs to be established whereby engine oil pressure is not negatively affected, e.g. even under dynamic driving conditions, which is beyond the scope of this investigation.

Table 27. Calculation parameters used to assess the energy saving associated with reducing the lubricant fill volume by 3.1 litres.

Standard oil fill volume (L)	5.1
Reduced oil fill (L)	2.0
Reduction in oil fill (L)	3.1
Mean density (kg/m^3)	828
Reduction in lubricant Mass (kg)	2.6
Mean Specific heat capacity (J kg^{-1} K^{-1})	2367
Temperature difference (K)	70

Energy input (MJ)	0.43
Equivalent mass of gasoline @43 MJ/kg	0.010
Equivalent CO_2 (gCO_2/km)	2.88

Theoretically, the oil sump capacity can be divided into three key volumes:

(1) a volume to fill the oil galleries and oil drain-back path (which is a function of the engine and lubricant temperature and engine speed)

(2) a volume to allow for the movement of the oil in the sump during dynamic vehicle motion (a function of the vehicle acceleration and sump design) and for buoyancy driven deaeration

(3) a volume to achieve the oil drain interval (a function of oil consumption and oil degradation)

Conceptually, opportunities exist to remove a portion of volume (2) and volume (3) in order to achieve a reduction in CO_2 during warm-up. The amount of volume (2), which can be used, depends on the driving conditions and the response rate of the control system to rapidly reintroduce the oil in order to avoid loss of oil pressure.

The lubricant has a relatively high specific heat capacity compared to the engine's metallic parts. Consequently, a small reduction in lubricant mass has the same effect on the engine's mean specific heat capacity as a large reduction in metallic mass. By comparing the specific heat capacities of the 2.6 kg of lubricant with those of the engine components, this reduction becomes equivalent to removing 6.7 kg of aluminium or

13.2 kg cast iron. These values are large compared to the engine mass (~100 kg) and would be hard to achieve without major engine modifications.

Andrews et al. [130] discuss lubricant mass reduction during engine use, although the potential benefit is not quantified. Their hypothesis is that a split sump pan would allow preferential use of hot returning oil in contrast to using colder oil sitting lower in the sump pan. A volume of twice the oil in the lubrication circuit is arbitrarily suggested for the split, although no justification is provided for this value.

Zammit et al. [45] use simulation to consider lubricant mass reduction. The specific details of the test engine are not shared (e.g. lubricant formulation, fill volume) and the modelled benefit of reducing lubricant mass is compounded with the simulated effect of fitting a novel lubricant-cooled Exhaust Gas Recirculation (EGR) heat exchanger. The predicted benefit of both systems was 0.83% with 20% reduction in lubricant mass and 1.08% improvement with 40% reduction in lubricant mass (the predicted fuel economy benefit due to the fitment of the EGR system in isolation from other variables was reported as 0.63%). The simulations used a cold-start NEDC.

Simulation-based work by Reverault et al. [133] includes variable sump volume analysis. The lubricant volume is reduced to 40% then 20% of the original fill level. The research concerns predicted fuel economy improvements for drive cycles completed on a diesel hybrid vehicle. Tabulated fuel economy improvements are not reported. However, the diagrams indicate that a maximum fuel economy improvement of circa 5% was attributed to reduced oil sump volume (20% of original volume) and circa 3.5% when simulations used 40% of the original volume.

Chisaki et al. [137] assess a split sump fitted to the Toyota “D4-D” 2.0 L 4-cylinder diesel engine. Their design features a false wall in the sump that traps part of the lubricant fill, causing the engine to warm-up using a reduced portion of the sump fill

volume. Figure 76 shows a schematic of the system fitted to the D4-D engine including oil volume measurements taken from a sump removed from a vehicle. Chisaki et al. state this unit achieves a 0.8% fuel consumption reduction. The system design compounds the effects of reducing the lubricant volume warmed up with the false wall's insulating properties. Tests using the oil pan fitted with the false wall achieved up to 6 K increase in lubricant temperature (measured in the inner sump). Interestingly, some of this thermal benefit is measured late in the test cycle, so one might reasonably assume that fuel consumption differences persisted throughout.

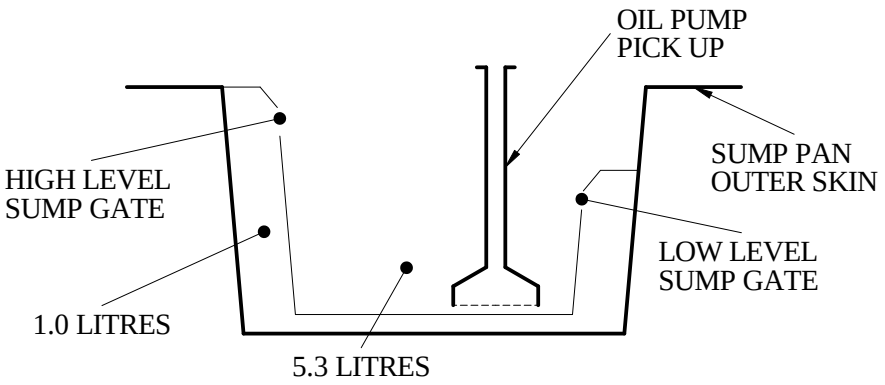

Figure 76. Schematic cross section of Toyota split-sump system. (Oil volume measurements taken from 2012 MY Toyota Avensis with D4-D engine).

Law et al. [138] discuss a split sump design in a 4-cylinder 2.4 L swept volume diesel engine application. They report the effect on fuel consumption and lubricant temperature in the oil gallery and at the pick-up pipe for three different sump designs. The reduction in friction mean effective pressure (FMEP) was not large enough to draw statistically significant conclusions for the room temperature start (17˚C to 20˚C) case at 15 mg/stroke fuelling. Engine starts at a lower soak temperature of -10˚C provided a statistically significant ~10% reduction in FMEP. Figure 77 reproduces a schematic from [138] showing one of the split sump designs. The bulk lubricant volume was introduced to the running oil volume using a thermostatic valve triggered to open at 70˚C.

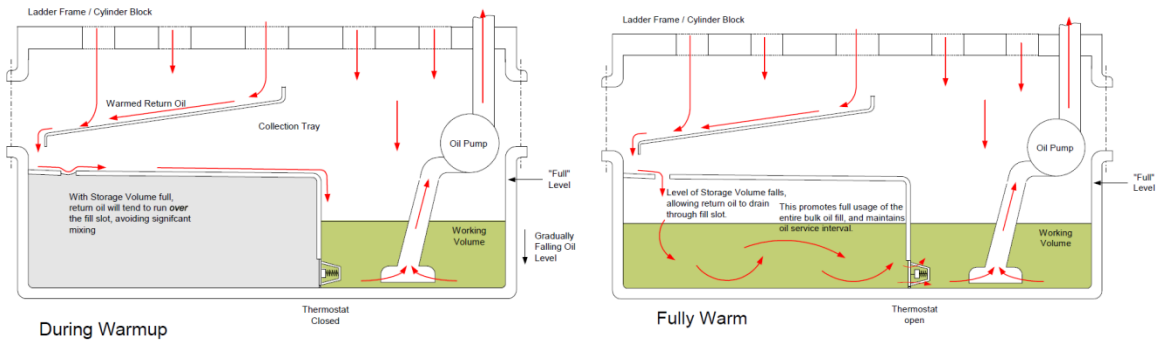

Figure 77. Schematic of sump design tested by Law et al. (Reprinted with Permission from IMechE [138]).

Each of the designs had the same basic operating principles:

(1) The oil flow returning from the engine was preferentially directed towards a shielded volume around the oil pick up tube.

(2) A significant portion of the sump volume was segregated from the running volume using a false wall arrangement.

The differences in the design were in the approach to and construction methodology selected for the inner sump walls.

6.1.3. Heat transfer in the oil galleries and engine components

The lubricant temperature reaching the engine's tribological contacts is key to interpreting the potential success of lubricant thermal management systems. However, many authors do not consider it. Kunze et al's [132] 1D lumped mass simulation approach fails to assess it. Zammit et al. [45] consider it at a subsystem level by investigating the effect of preheated lubricant entering the main bearing lubricant supply for a 2.4 L diesel engine. Their results indicate that heat transfer between the lubricant and engine surfaces (e.g. oil galleries, bearing shells and journals), significantly reduces the temperature of the lubricant reaching the tribological contact zone. Their experimental set-up increases lubricant supply temperature by 20 K, 45 seconds after the test start. The lubricant quickly reduces to 15 K above engine temperature before entering the main gallery. A modest 5 K temperature increase in the bearing oil film was

measured. A 10% bearing friction reduction (the difference in total cumulative energy dissipated in the bearing with and without preheating) is measured during warm-up using hot lubricant. They suggest ways to mitigate heat loss. However, heat transfer in the bearing (through the bearing shell, into the engine block and then the journal) is greatly influential and reducing this requires significant engine modification.

Roberts et al. [139] completed a bench-top investigation to quantify the effect of insulating parts of the oil gallery to minimise heat transfer from the lubricant to the engine structure during warm-up. Their work shows this approach reduces temperature loss from the lubricant and offers benefits, although no assessment is made on the effect of tailpipe CO_2 emissions. The design's transferability to a real engine is uncertain because of the simplifications made in the test rig (which simulates an engine oil gallery using a single 16 mm internal diameter tube of 380 mm length) and the practical complexities associated with insulating the oil gallery.

6.2. Summary and plan for further work

Existing literature discusses various approaches to understanding the benefit of increasing lubricant warm-up rate. However, key differences exist in the magnitude of measured results. Rapid engine design and lubricant technology advances over the past decade mean that historic work now relates to old engine technology and uses outdated lubricant viscosity grades. The literature usefully contextualises potential benefits, but it is impossible to assess what effect thermal management of lubricant mass can have on modern vehicles' tailpipe CO_2 emissions. The present research assesses how significant the lubricant volume filled into the sump is to engine warm-up rate.

In the work reviewed, no practical solution has been suggested for achieving lubricant preheating or heat storage from previous engine running. For dry-sumped engines, where the lubricant reservoir is ordinarily positioned remotely from the engine,

the way to install a lubricant thermal management system is more obvious. For wet-sumped engines an external reservoir with a transfer pump would be required. To allow an interpretation of how important lubricant preheating or heat storage is to reducing tailpipe CO_2 emissions, tests are included in the present work.

To determine the feasibility of heat storage, the heat transfer from an insulated, remotely-mounted oil tank is modelled. This simulation tests the capabilities of different insulation designs to maintain the lubricant temperature after engine shutdown.

The experiments focus on: Thermal energy storage (1); coolant-to-lubricant heat exchangers (2a); reducing lubricant mass (3); reducing lubricant viscosity. The latter variable was added since thermal management systems attempt to achieve a portion of low viscosity lubricants' friction reduction at low temperature, by reducing viscosity via temperature rise. Comparing the performance of a high viscosity lubricant with thermal management to a low viscosity lubricant without was interesting to interpret the relative importance of thermal management and viscosity grade reduction.

6.3. Vehicle testing using two vehicles mounted to chassis dynamometers

To evaluate the response of tailpipe CO_2 to these variables, a suite of tests was completed on conventional wet-sumped engines. Two test vehicles were selected and installed into climatically-controlled, rolling road dynamometers. The facilities were equipped to analyse exhaust emissions, monitor temperature and pressure sensors and to log data. Table 28 describes the vehicles and test facilities.

Table 28. Description of test vehicles and pertinent test facility information.

Vehicle identification	1		2
Test vehicle	Ford Focus		Ford Focus
Engine	1.6 L EcoBoost		2.0 L EcoBoost
	4-cylinder		4-cylinder
	Turbo-charged		Turbo-charged
Vehicle model year	2011		2013
Location of testing	Facility 1	Facility 2	Facility 1
Ambient temperature	293-313K		293-313K
Driver	Robotic	Human	Robotic
Test cycle	NEDC		NEDC
Fuel	Gasoline		Gasoline

6.4. Vehicle CO_2 emission changes from lubricant thermal management

A test matrix using two test vehicles mounted onto chassis dynamometers was used to assess the effect on tailpipe CO_2 emissions caused by varying lubricant mass during NEDC tests. Thermal preconditioning of the vehicle to 293 K allowed assessment of the effect on tailpipe CO_2 emissions during vehicle warm-up. Both overnight thermal soak and 'forced' cool down preconditioning procedures were used interchangeably; a robust statistical assessment for experimental bias was completed to ensure that this approach did not affect the test results. All test vehicles were operated in a similar manner and were essentially unmodified except for adding temperature and pressure probes as per standard practice for testing in this manner.

6.4.1. Lubricant thermal energy storage (1) – Preheating

The effect on tailpipe CO_2 emissions caused by preheating the lubricant mass during NEDC tests was assessed. An external oil bath heated the lubricant fill during the vehicle soak period. For safety, a remotely-operated gravity drain line was installed. This pipe introduced the oil directly into the sump prior to the engine start process. Figure 78 shows an overview of the test facility. Initiation of the filling process occurred just prior to the test start using an electrically-actuated flow valve, activated by the test control system. A time delay allowed the oil to flow into the sump. Thus, some of the lubricant temperature was lost between the oil bath and vehicle due to heat

transfer in the flexible tube and thermal conduction after the lubricant reached the engine.

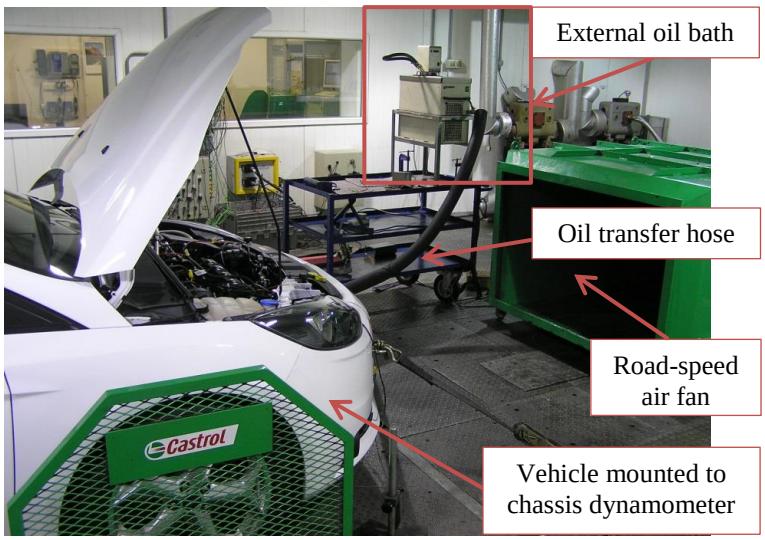

Figure 78. Installation overview for lubricant preheating test work.

Any benefit to engine friction reduction caused by increasing the engine structure temperature during the filling process will have been compounded in the results and may have augmented the CO_2 reduction measured. Block contact thermocouples were installed on the engines' outside surfaces to measure their temperatures during the tests.

6.4.2. Coolant-Lubricant heat exchanger (2a)

The effect of bypassing the coolant-to-lubricant heat exchanger was determined by installing a bypass loop on the coolant side and experimenting using the standard oil volume, preheating, and the reduced lubricant volume tests. This installation was chosen so that the pressure drop was retained in the lubricant system. A small reduction in coolant pump load was present during these tests due to this design.

6.4.3. Reducing lubricant mass (3)

The hypothesis tested in this section was that decreasing the engine lubricant volume during warm-up would:

- Reduce the lubricant thermal mass (reducing the thermal energy required to achieve a significant lubricant viscosity decrease)
- Increase the pump inlet temperature, since the hot lubricant returning from the engine would cool less due to mixing in the sump
- Reduce the engine system's thermal mass

The tests aimed to assess the effect on measured CO_2 emissions of varying the lubricant volume filled into the engine in isolation from other test variables. However, because the change in oil fill varied the oil height in the engine some confounding factors were present (e.g. varying interbay breathing area, oil deaeration time).

Prior to the test start it was determined if lubricant sump height could be maintained by (1) changing the sump between tests or (2) blocking out sections in the sump. These options were not tested as: (1) would require uninstalling the test vehicle from the chassis dynamometer between tests, fitting the sump and reinstalling the vehicle, which could introduce significant bias into test results (e.g 1.5% due to vehicle alignment changes) [140]; (2) would require significant sump modification.

Consequently, the lubricant height in the sump was allowed to change simultaneously as the oil volume in the sump reduced. The response of two variables was assessed: reduction in lubricant mass and increasing interbay breathing area. In the testing, these two variables were compounded and could not be deconvolved. The predicted effect on vehicle tailpipe CO_2 emissions due to interbay pumping area changes was simulated using a proprietary vehicle simulation tool (described generically in [93]). This model indicated that the absolute magnitude of interbay

pumping losses were insignificant (<0.05% CO_2) in the NEDC for a typical four cylinder 1.6 L passenger car engine, so this effect was ignored.

The effect of reducing lubricant sump height on the drive torque of any second-order balancer shafts (if fitted) is thought to be insignificant, but has not been formally assessed and will confound the results. Similarly, the confounding effect caused by interaction with any other sump-mounted components is included in the results.

Engine friction or durability effects due to an increased level of entrained air in the lubricant were not assessed. Theoretically, the amount of entrained air will increase coincidentally with the reduced oil volume, due to a reduced residency time for the lubricant in the sump. The effect on oil gallery pressure due to reduced lubricant mass was analysed to investigate if lubricant supply pressure decreased, since this could augment CO_2 emission reduction by lowering the pump's parasitic load. Assessing engine durability effects would require more tests, but was beyond the scope of the present research.

6.4.4. Lubricants used in test programme

Each test used fresh lubricant, although always of the same formulation. Tests used the 5W-30(R) and SAE 8 lubricants defined in Section 2.1.1.

6.5. Chassis dynamometer test results

Vehicle 1 was tested at two different chassis dynamometer facilities. The unmodified vehicle was tested at Facility 1 to generate baseline data. It was then modified to add a coolant bypass loop around the coolant-to-lubricant heat exchanger before being tested at Facility 2 for the remainder of the programme. The test conditions between the two facilities were broadly the same, excepting the use of a robotic driver at

Facility 1 and a human driver in Facility 2. Table 29 summarises the test conditions used and the running order for the baseline tests on this vehicle.

Table 29. Description of testing running order for Vehicle 1, Facility 1.

Test name	Fill volume (L)	Start oil temp (˚C)										*n*
Reference	4.1	20	x						x			x	3
Hot fill (50˚C)	4.1	46		x						x			2
2.0 L cold	2.0	20			x		x						2
2.0 L hot (60˚C)	2.0	64				x		x					2
Hot fill (80˚C)	4.1	78									x		1

x indicates a test position; chronological order is left to right and *n* refers to the number of tests completed in each test condition.

6.5.1. Vehicle 1 – Facility 1, unmodified

Figure 79 shows the vehicle response to the test variables, assessed as CO_2 in gCO_2/km over the NEDC. The CO_2 variation measured during the reference tests was relatively large compared to the response of the test variables and only a small number of reference runs was completed. Thus, the test results could not be separated from the mean of the reference population to a statistical significance of at least 95% confidence. Figure 80 shows the results as percentage change from the mean of the reference runs.

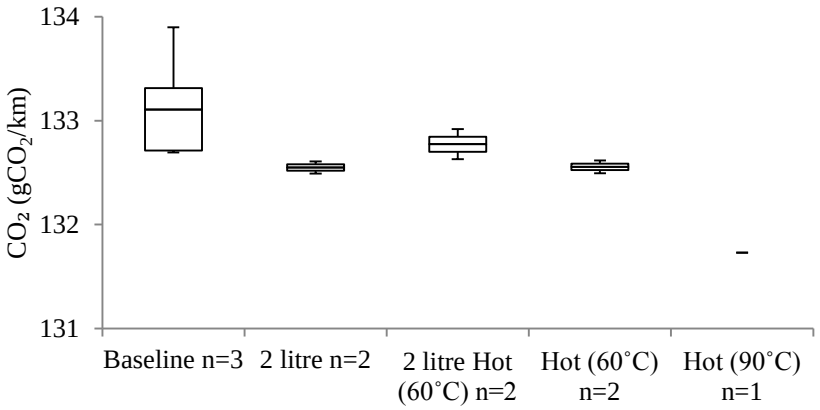

Figure 79. Boxplot showing fuel economy results from Vehicle 1 chassis dynamometer testing. Upper and lower whiskers represent maximum and minimum values, upper and lower bounds of box represent 1st to 3rd interquartile range, mid line represents the mean value from test results.

6.5.1.1. Lubricant thermal energy storage (1) – Preheating

The measured results show that preheating the lubricant before starting the NEDC reduced the CO_2 emitted. The response was assessed using two start temperatures, 60˚C and 90˚C, and Figure 80 shows the relative reduction in measured CO_2. The mean difference in CO_2 emissions was 1.04% where the lubricant was preheated to 90˚C, and 0.41% for the 60˚C case. The mean results could not be separated using statistical processes from the mean of the reference population to 95% confidence.

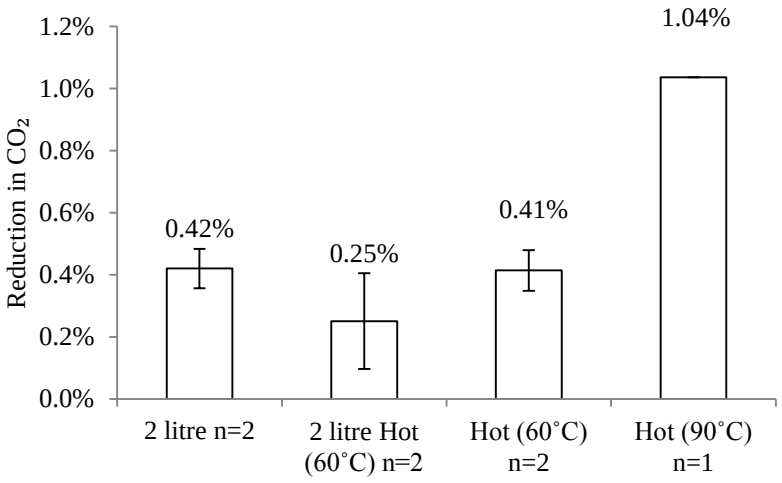

Figure 80. Results presented as percentage reduction from baseline performance. Error bars represent upper and lower bounds of one standard deviation from the mean.

Figures 81 (a) and (b) show the differences in lubricant temperature and calculated kinematic viscosity at the oil gallery. Preheating the lubricant caused a significant reduction in viscosity early in the test. The difference in lubricant temperature initially increased, probably due to the oil pump temperature rising. The temperature difference then increased to a maximum before steadily reducing for the rest of the test. A significant temperature loss of 40 K where the lubricant was preheated to 60˚C and a loss of 60 K in the 90˚C preheating case was measured between the sump and oil gallery.

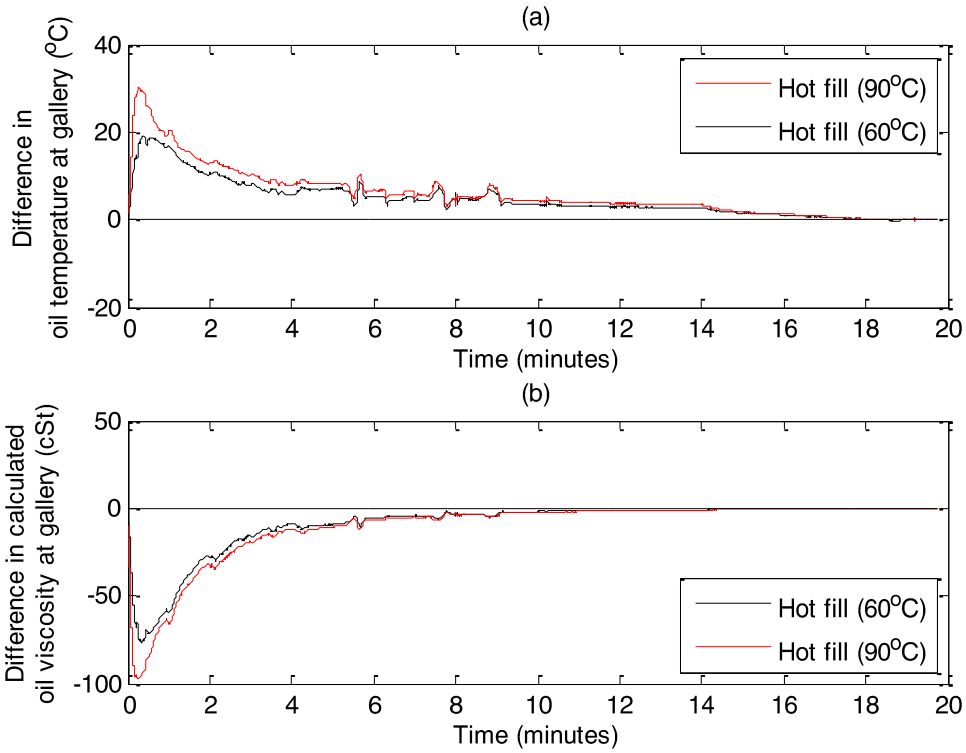

Figures 81(a-b). Difference in lubricant temperature (measured at the gallery) and calculated lubricant viscosity for the preheated fills using Vehicle 1. Calculated as: reduced fill volume - unmodified reference.

The largest difference in lubricant viscosity occurred 18 seconds into the test when the reduction in relative CO_2 emissions was also greatest (2.9% lower than the reference, using the combined CO_2 emissions of the first two ECE 15s[13] in the NEDC and the 90˚C preheating case). The lubricant viscosity reduction persisted throughout the test, allowing a reduction in tailpipe CO_2 emissions to be measured until relatively late in the test (circa. 17 minutes).

6.5.1.2. Reducing the lubricant mass (3)

Reducing the fill mass to 1.7 kg (2.0 L), a 1.8 kg (2.1 L) reduction, decreased the tailpipe CO_2 emitted by 0.42% for the non-preheated case, and by 0.25% when the reduced oil fill was preheated to 60˚C. These results could not be separated from the mean of the reference population with statistical confidence to 95% certainty.

[13] The ECE-15 is the Economic Commission for Europe urban driving cycle. The NEDC comprises four elementary urban drive cycles (ECE-15's) followed by one extra urban drive cycle (EUDC).

Figure 82 shows the oil gallery temperature variation and calculated viscosity for the reduced fill test condition without preheating. The oil gallery temperature difference was circa 2 K, corresponding to a maximum reduction in calculated kinematic viscosity of approximately 10.5 %. The temperature difference is smaller than in the Vehicle 2 testing (reported below) or Chisaki et al's [82] work. The smaller benefit here is probably due to the confounding insulation effects in Chisaki et al's [82] work and the smaller reference sump volume in this new test case. Vehicle 1 demonstrated a slightly lower hot-cold factor than Vehicle 2 (8% versus 8.7% respectively), which is likely also to reduce its sensitivity to thermal management systems.

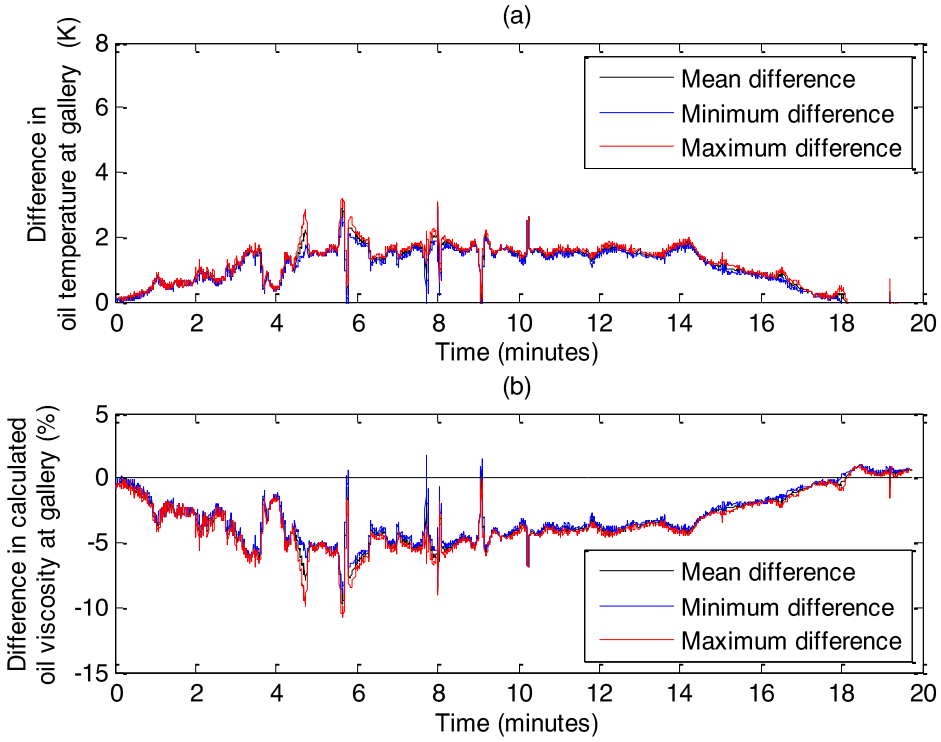

Figure 82. Difference in lubricant temperature (measured at the gallery) and calculated lubricant viscosity for the 2.0 L volume fill using Vehicle 1. Calculated as: Reduced volume fill – Unmodified reference.

In both tests, the lubricant temperature trace was very repeatable, as shown by the maximum and minimum difference lines in Figure 82. This result may indicate that the oil fill volume variation provides a repeatable effect, although more test runs are required to prove this unequivocally.

The slightly lower reduction in CO_2 values seen for the reduced mass hot-fill test (preheating to 60˚C) does not follow logically. The CO_2 emission results for the first two ECE 15 cycles (the first two repeated speed profiles in the NEDC) confirmed that the hot fill initially provided a greater CO_2 reduction than the non-preheated, low fill test. The reduced volume with preheating to 60˚C test, reduced the CO_2 emissions by 2.4% compared to the reference in the first two ECE 15 cycles. The comparable result without preheating was 1.8%. Thus, this result was attributed to the test's repeatability.

6.5.2. Vehicle 1 – Facility 2, modified

After initial tests, Vehicle 1 was modified to bypass the coolant-to-lubricant heat exchanger from the coolant circuit then sent to Facility 2 for more chassis dynamometer testing. Table 30 shows the test result matrix for this work. Three reference tests were first completed to establish the vehicle's stability in the new facility. These reference measurements were taken with the vehicle in standard configuration (without the bypass) and using overnight soak thermal preconditioning for the chamber and vehicle. A bypassed reference position was established and retained for the rest of the tests.

Table 30. Description of test running order for Vehicle 1 at Facility 2.

Test Name																																*n*
Reference	x	x	x																													3
Bypassed cooler				x	x		x							x	x	x	x				x		x				x					x		x	12
Bypassed cooler forced						x		x														x		x				x					x		6
2.0 L cold (Byp.C.)									x		x		x																	x			x			5
2.0 L cold (Byp.C.) forced										x		x		x																	x		x	x				6
4.1 L Hot (Byp.C.)																			x	x	x																3
SAE 8 forced																										x	x	x									3

x indicates a test position; chronological order is left to right; *n* refers to the number of tests completed; "forced" refers to tests completed using forced cool chamber preconditioning, all other tests used overnight soak thermal preconditioning and

"Byp.C" refers to tests completed with the coolant-to-lubricant heat exchanger bypassed on the coolant side.

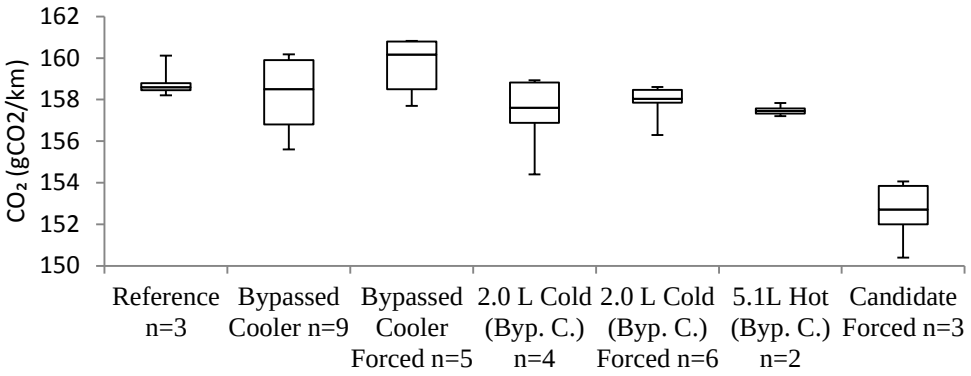

Figure 83. Boxplot showing fuel economy results from Vehicle 1 chassis dynamometer testing at Facility 2. Upper and lower whiskers represent maximum and minimum values, upper and lower bounds of box represent 1st to 3rd interquartile range, mid line represents mean value from results.

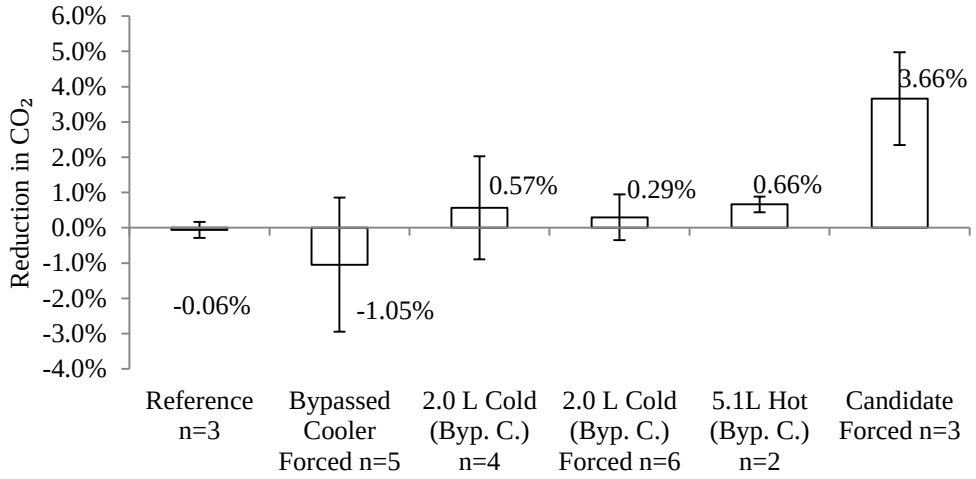

Figure 84. Results presented as percentage change from bypassed cooler test case. Error bars represent upper and lower bounds of one standard deviation from the mean.

Testing used forced cool-down and overnight soak preconditioning interchangeably, as shown in the test descriptors in Table 30. Analysis of results showed differences between these conditioning strategies, so the results are reported separately.

Figure 83 shows the vehicle response to the test variables, assessed as CO_2 in gCO_2/km emitted whilst completing the NEDC. The variation in measured CO_2 for repeat test runs in the same test conditions was relatively large. Thus, only the mean result for the low viscosity candidate tests could be separated from the mean of the bypassed cooler data set with statistical confidence to 95%.

Figure 84 shows the results as percentage change from the mean of the bypassed cooler data runs.

6.5.2.1. Coolant – Lubricant heat exchanger (2a)

Comparing the mean tailpipe CO_2 emitted in the unmodified and bypassed cases showed that bypassing the coolant-to-lubricant heat exchanger increased tailpipe CO_2 emissions by 0.06%. However, these results could not be separated from each other with statistical confidence to 95% certainty. The test results from the forced cool preconditioning strategy showed the bypass increased tailpipe CO_2 emissions by 1.05%. The difference in results from the overnight soak and forced cool preconditioning cycles was unexpected. It is also within the repeatability of the results from this test sequence so it is not possible to determine if this was a real effect. Analysis of temperature traces at the test start did not demonstrate any significant differences.

The tests' repeatability here is worse than was reported in [140] where values of 0.5% repeatability were targeted, but the actual value achieved is not reported, despite following the same protocols. The test vehicle may have introduced random errors or errors not directly attributable to the test variables. Alternatively, the lower temperature of the tests completed in [140] could have triggered the use of a more repeatable warm-up calibration.

The lubricant temperature difference between the reference and bypassed cooler test cases measured at the oil cooler outlet (Figure 85) was more repeatable than the CO_2 results. The repeatability of these results was worse than during the previous testing. However, this is predominantly due to a slightly poorer control of test start temperature in Facility 2 (although it is within the acceptable tolerance for vehicle type approval testing).

Figure 85 shows the temperature traces for these tests results. This graph shows that bypassing the coolant-to-lubricant heat exchanger had little effect during the initial part of the test (0 to 5 minutes), but then caused a reduction in lubricant temperature. The repeatable temperature spike at 5 minutes 20 seconds is likely to be attributable to the thermostat opening and a flow of cold coolant entering the heat exchanger. Bypassing the coolant-to-lubricant heat exchanger had little effect on the end of test lubricant temperature. During the latter test phase, the lubricant temperature approached that of the coolant, so there was little temperature difference to drive any significant heat transfer. Thus, the inclusion or removal of the heat exchanger had a negligible effect on the lubricant temperature under these conditions.

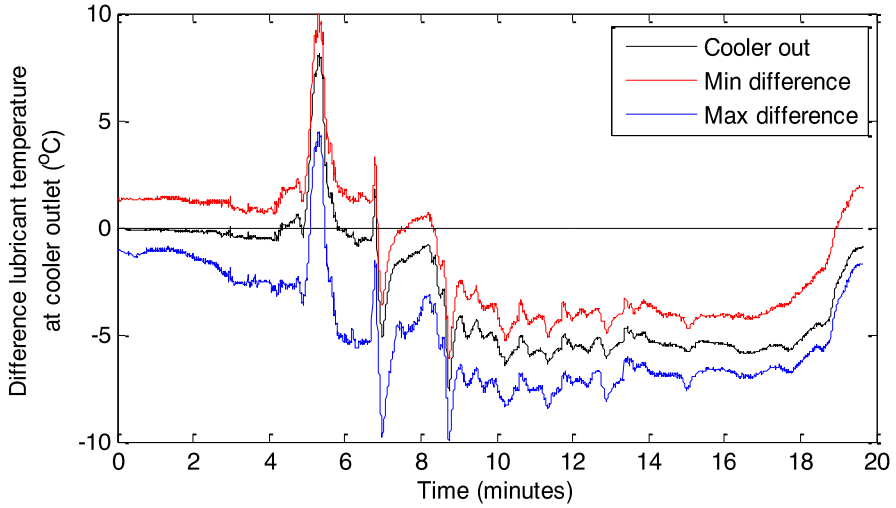

Figure 85. Difference in lubricant temperature due to the bypassing of the coolant-to-lubricant heat exchanger. Calculated as Oil Gallery Temperature (Bypassed) – Oil Gallery Temperature (Reference).

The remainder of the analysis of results from this test matrix uses the coolant-to-lubricant heat exchanger bypassed test, including overnight soak, and 5W-30(R) lubricant as the "reference" condition. All of the test variables are compared to the performance of this test case in the following paragraphs.

6.5.2.2. Lubricant thermal energy storage (1) – Preheating

The effect on emitted CO_2 caused by introducing hot lubricant into the sump prior to the test start was assessed in two runs during this testing sequence. A single test was completed with the lubricant preheated to 110˚C. However, a significant amount of the lubricant temperature was lost filling the lubricant into the sump due to the test infrastructure. Therefore, two further tests were completed at a 150˚C preheat temperature. These are the reported data points. It is recognised that it is unrealistic to expect the lubricant temperature to be this high following the requisite vehicle soak period for a homologation cycle without implementing an active lubricant heating system. However, at the test data points are useful to interpret the magnitude of the potential CO_2 reduction. Importantly, the test start lubricant temperatures were also significantly lower, owing to heat losses in the test bed oil transfer system and heat transfer to the engine block. The magnitude of engine structure temperature increase was measured using block contact thermocouples. The temperature increase that occurred probably contributed to the measured reduction in tailpipe CO_2 emissions.

Mean tailpipe CO_2 emissions reduced by 0.66%, when the lubricant was preheated to 150˚C compared to the reference tests with the cooler bypass in place (and using overnight soak thermal preconditioning). However, the data points could not be separated from the population of reference mean to a statistical confidence level of 95%.

Figures 86 (a) to (c) show the lubricant temperature and viscosity differences measured at the oil gallery caused by preheating the lubricant before the test start. Introducing hot lubricant into the sump caused a significant decrease in calculated lubricant viscosity throughout the majority of the test cycle. The peak temperature difference measured at the oil gallery was 53 K, which corresponded to a reduction in (calculated) lubricant viscosity of 87%.

The relatively modest mean improvement in CO_2 is surprising given the relatively significant change in calculated viscosity measured under test conditions. Zammit et al. [135] reported significant lubricant temperature loss due to heat transfer between the lubricant and engine structure, since the engine is colder than the lubricant in the test's early phase. This behaviour probably also occurred in the present research. Thus, the lubricant temperature reaching the components needs further consideration and may partially explain the modest CO_2 reduction measured.

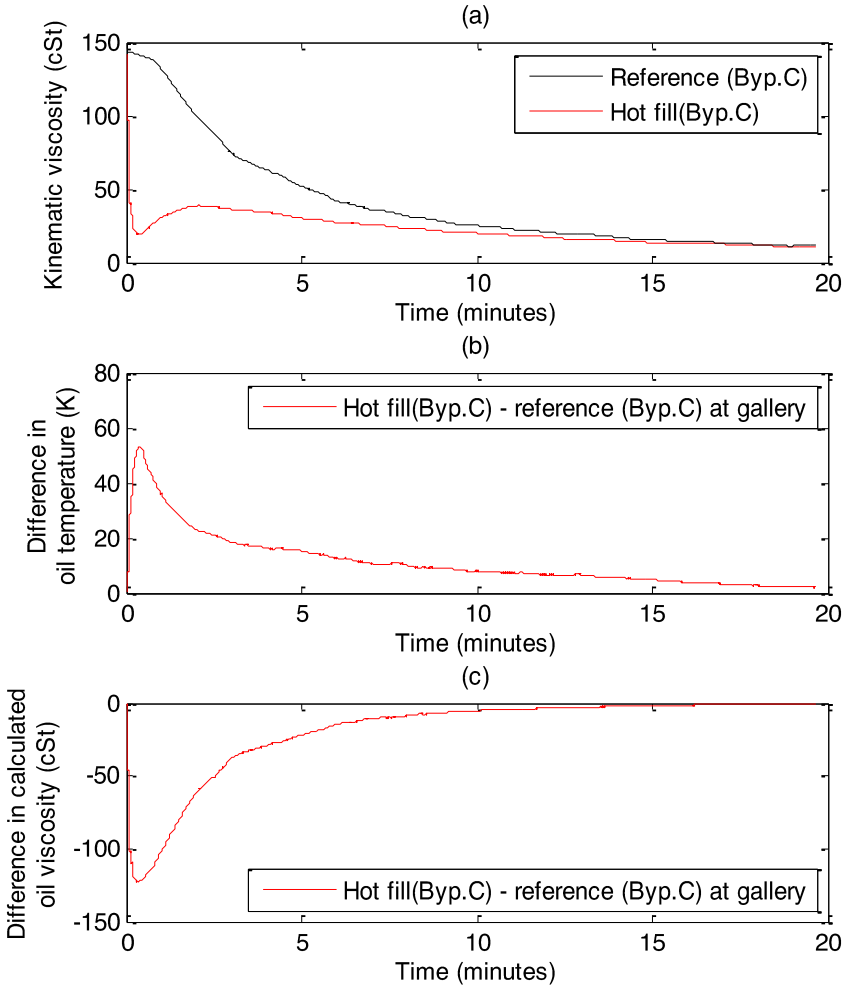

Figures 86(a-c). Calculated kinematic viscosity for hot fill (150°C) and reference tests and calculated difference in lubricant temperature and viscosity for the cases where the lubricant was preheated. Calculated as: mean of test data – mean of bypassed cooler (Byp.C) reference.

In this test programme, it was impossible to instrument the engine components internally, but additional instrumentation was added externally to allow result interpretation. Surface contact thermocouples were positioned on the block externally at

two locations (nominally low and high locations) to measure engine temperature differences. An extra thermocouple was added into the cylinder head oil drain-back path to measure the returning oil temperature. Figures 87 (a to c) show the readings from these thermocouples.

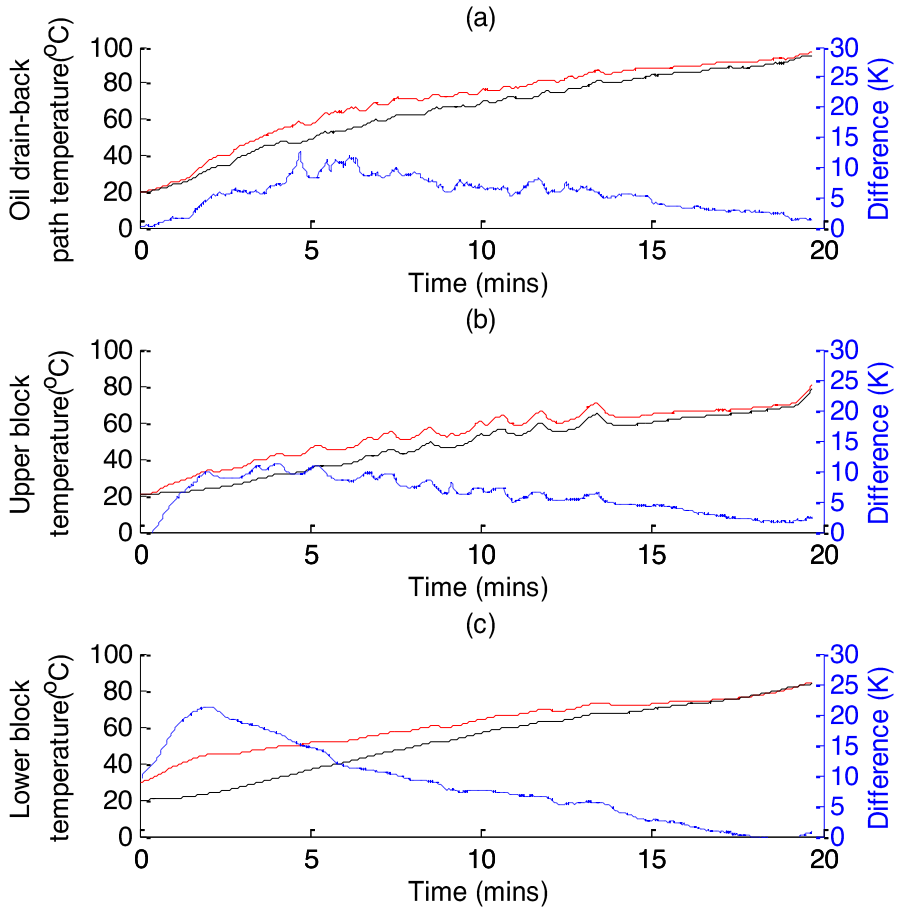

Figures 87(a-c). Temperatures and calculated difference in cylinder head drain-back path oil temperature (a), mid-height (b) and lower (c) external block contact temperature for the preheated (150°C) and non-preheated fills using Vehicle 2.

Heat transfer from hot lubricant to the block structure, between the time the lubricant was added to the sump and the test cycle started, increased the lower block temperature by 9 K. This temperature difference increased in the test's initial phase, probably due to increased heat transfer with the lubricant flowing around the structure, and caused the test to be run at an elevated temperature at all points in the test cycle.

The external temperature measured at the cylinder head, labelled as upper block temperature, showed a more damped response to the energy input from the lubricant,

with a peak difference of 11 K, occurring 4 minutes into the test cycle. The engine's significant thermal mass compared to the lubricant significantly reduced the lubricant temperature even with a high initial lubricant filling temperature.

The oil drain-back path temperature was measured, as this was thought to be a useful indicator of the lubricant temperature reaching the engine components. Theoretically, the lubricant temperature here should include any detrimental heat transfer from the lubricant to the engine structure, since this location is furthest from the oil pump. The cylinder head also generally operates at a lower oil flow rate than the reciprocating group feeds, so has greater opportunity for temperature loss. However, the component feed temperatures cannot be directly inferred from this measurement, because the lower viscosity and higher temperature lubricant will shear heat less in the moving components. The dependency of the lubricant temperature on the shear heating tends to bring preheated and non-preheated temperature traces measured at the drain-back path closer together than might actually exist in the tribological contact.

The oil drain-back path temperature indicates that the higher lubricant temperature is maintained throughout the test cycle and closely follows the cylinder head structure temperature after the test start (circa 6 minutes) once equilibrium is established between the initially hotter lubricant and cooler structure. Thus, arguably the heat addition to the lubricant mainly acts to increase the engine structure temperature.

6.5.2.2.1. Effect on engine oil gallery pressure

Figures 88 (a to c) show the average oil pressure and the calculated differences for the reference and hot fill tests. Preheating the lubricant caused the oil gallery pressure to reduce. The oil pressure difference was greatest when road speed reduced to zero and the engine returned to idle. A reduction in pumping work probably resulted from the

lower oil pressure, contributing to reduced tailpipe CO_2 emissions. The oil viscosity reduction will also have reduced the viscous losses and improved the pump's efficiency.

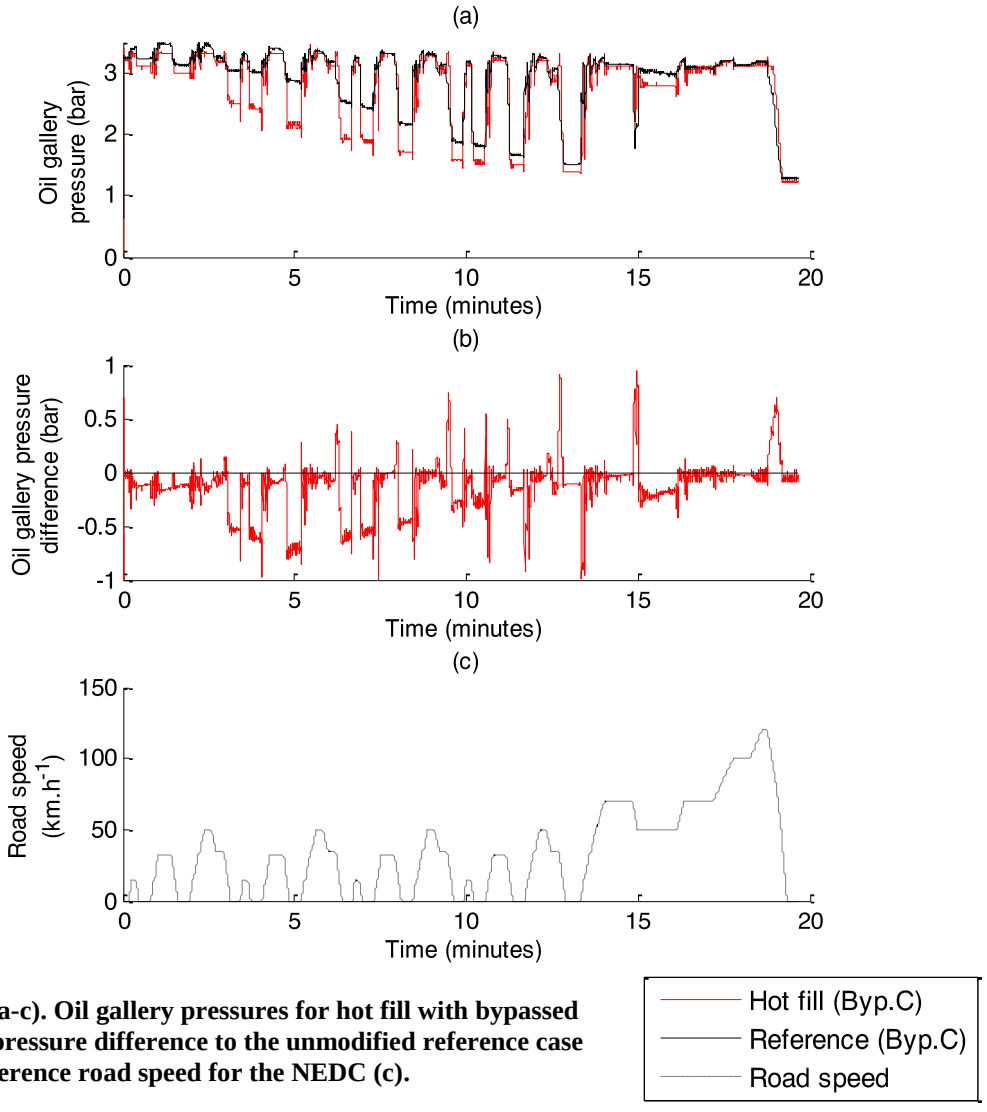

Figures 88 (a-c). Oil gallery pressures for hot fill with bypassed cooler (a), pressure difference to the unmodified reference case (b) , and reference road speed for the NEDC (c).

An oil pump's response to changing viscosity is discussed more completely in Chapter 5, although this engine has a different pump design to that which was tested. Since this component is positioned between the oil sump (where the oil is hottest) and the oil gallery, the lubricant's temperature inside is higher than that measured at the gallery. Therefore, benefit from viscosity reduction is probably more significant in the oil pump than would be concluded if the gallery temperatures were assumed to be present in the pump.

6.5.3. Reducing the lubricant mass (3)

Decreasing the fill mass by 1.8 kg (2.1 L) to 1.7 kg (2.0 L) reduced the tailpipe CO_2 emitted by 0.57% for the overnight soak case and by 0.29% when forced cooling was used, compared to the mean of the overnight soak bypassed cooler cases. These results could not be separated from the mean of the reference results with statistical confidence to 95% certainty.

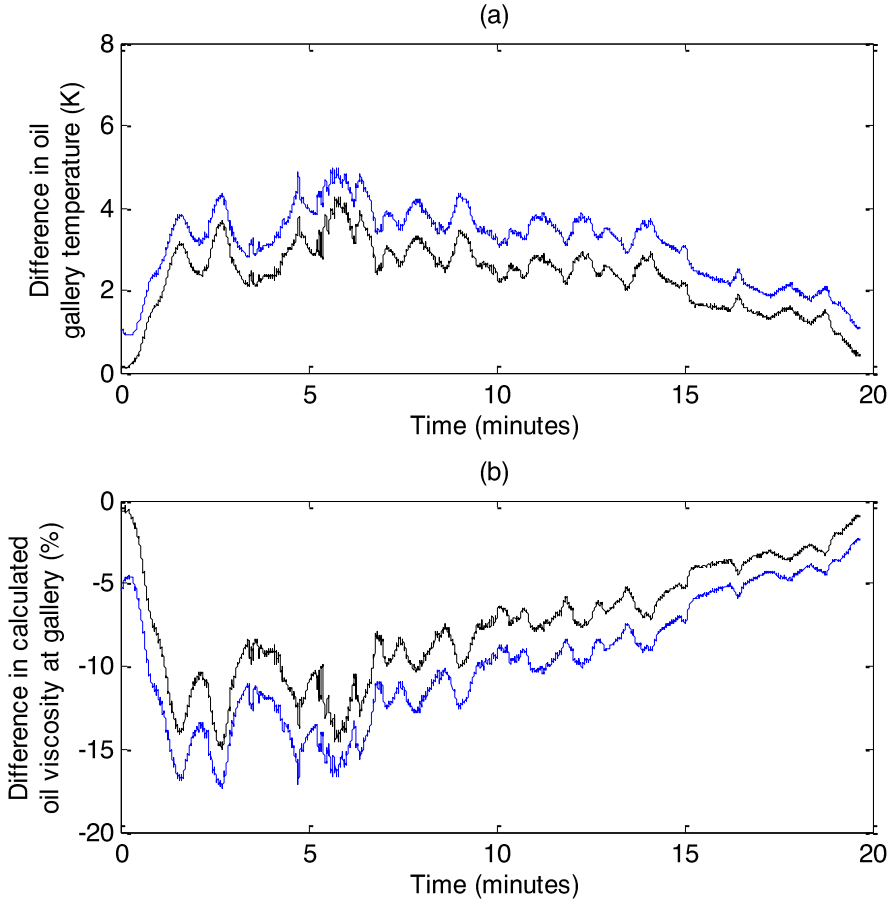

Figures 89 (a-b). Difference in lubricant temperature measured at the gallery (a) and calculated lubricant viscosity (b) for the 2.0 L volume fill using the Vehicle 1. Calculated as: 2.0 L volume fill - Unmodified reference.

Figures 89 (a) and (b) show the variation in oil gallery temperature and calculated viscosity for the reduced fill test condition without preheating. The maximum oil gallery temperature difference was circa 4 K, corresponding to a 15% calculated kinematic viscosity reduction during the test's early phases (17% with forced cooling, driven by

the different starting temperature). This viscosity reduction is larger than in the initial test cases when the coolant-to-lubricant heat exchanger was fitted. Therefore, designers attempting to achieve a thermal benefit should consider strategies to include the bypass. Equally, using the coolant-to-lubricant heat exchanger later in the test, when the coolant temperature exceeds the lubricant temperature could provide an additional benefit, to improve the CO_2 performance using low lubricant fill levels beyond those reported here.

6.5.4. Reducing the lubricant viscosity grade

A mean CO_2 reduction of 3.7% was measured during tests where the SAE 8 was used, which is consistent with the expected performance for this lubricant. Figures 90 (a) to (c) show the difference in calculated lubricant viscosity at the gallery for the SAE 8 and 5W-30(R) from the 2.0 L and preheated tests. The SAE 8 operated with a significantly reduced viscosity throughout the test cycle, with the exception of a crossover, measured at 2 minutes 40 seconds for the hot fill case, which was calculated using the gallery temperature. However, this hot fill benefit reduced when the lubricant reached the tribological contacts in the engine, due to heat transfer with the cooler engine surfaces, as shown by the viscosity calculated using the cylinder head drain back temperature. Figures 90 (a) to (c) show that the most significant viscosity reduction was measured using the SAE 8. The size of improvement anticipated by using low oil fills and hot oil fills with the 5W-30(R) can be assessed approximately by comparing these viscosity traces. The CO_2 reduction would be expected to be greatest when using the SAE 8 (which is consistent with measurements) followed by the 5W-30(R) hot fill and then the reduced oil fill tests.

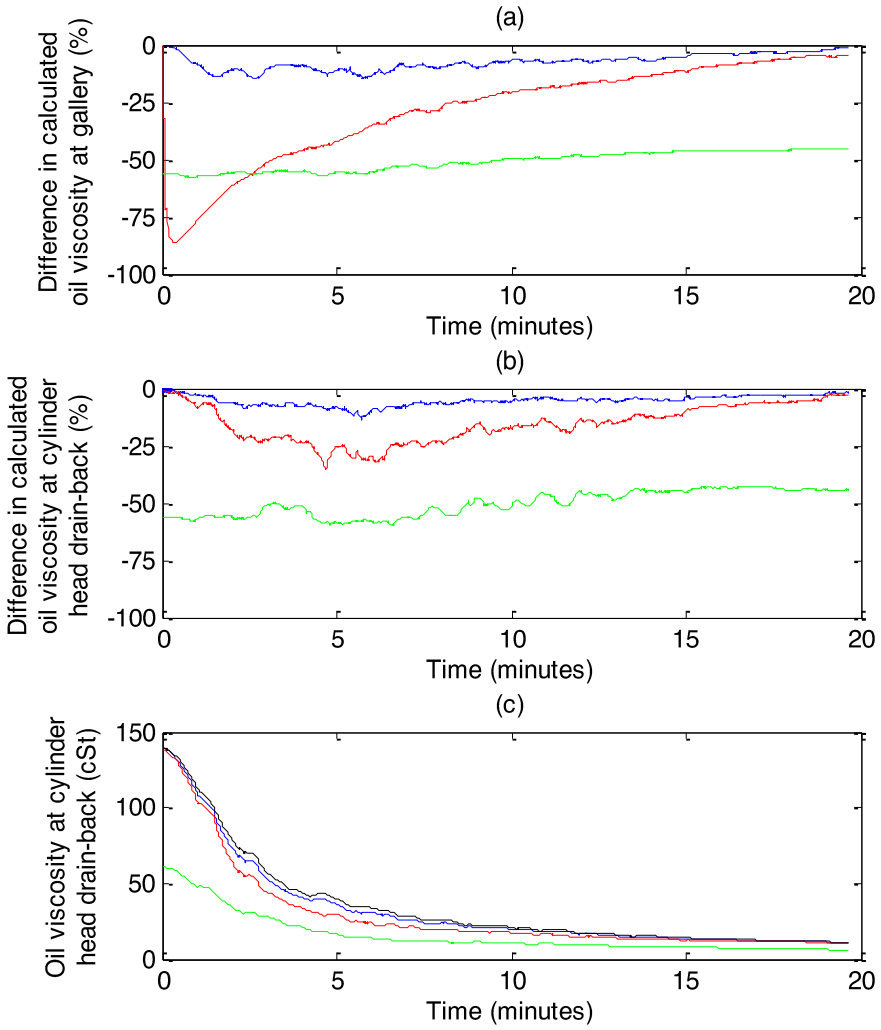

Figures 90 (a-c). Difference in calculated lubricant viscosity at the gallery (a), at the cylinder head drain-back path (b) and absolute viscosity for the preheated, reduced oil fill using 5W-30(R) and SAE 8 at full fill volume for Vehicle 1 (c).

6.5.5. Vehicle 2, unmodified

Investigations into the same test variables were conducted using Vehicle 2 to allow interpretation of how significant the engine type was to the results found. Table 31 summarises the test conditions and running order.

Table 31. Description of testing running order for Vehicle 2, Facility 1.

Test Name	Fill Volume (L)	Start Oil Temp (˚C)																			*n*
Reference	5.4	20	x	x	x	x								x	x					x	x	8
2.0 L Cold	2	20					x	x	x		x											4
2.0 L Hot (70˚C)	2	73								x		x										2
3.0 L Cold	3	20														x	x	x	x			4

x indicates a test position; chronological order is left to right and *n* refers to the number of tests completed in each test condition.

No assessment was made of the effect of preheating the lubricant, in isolation from lubricant mass changes, so only the effect of varying the lubricant mass is reported.

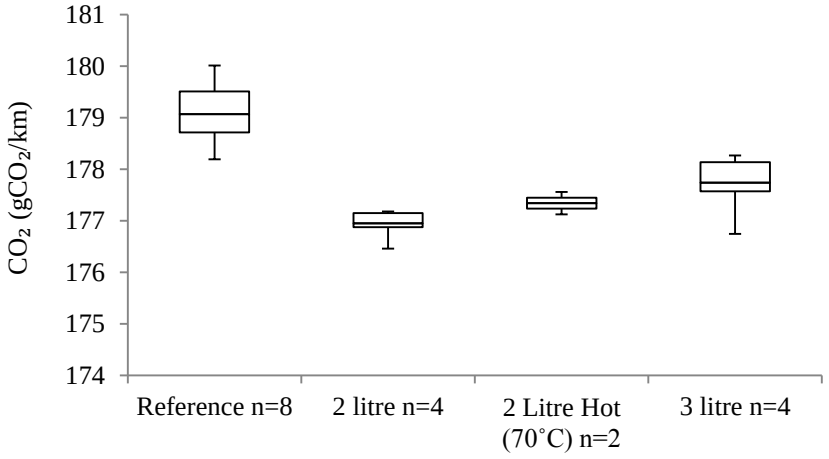

Figure 91. Boxplot showing fuel economy results from 2.0 L Gasoline testing with Vehicle 2 chassis dynamometer testing. Upper and lower whiskers represent maximum and minimum values, upper and lower bounds of box represent 1st to 3rd interquartile range, mid line represents the mean from the test results.

Figure 91 shows the vehicle's response to test variables, assessed as CO_2 in gCO_2/km over the NEDC. The CO_2 variation is expressed as percentage change from the reference results in Figure 92.

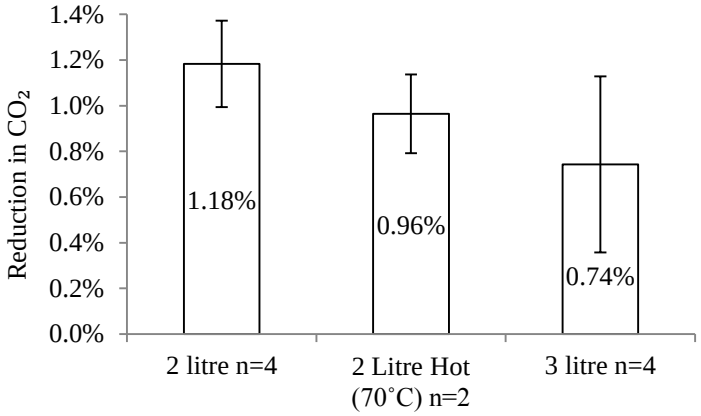

Figure 92. Results for tests completed with Vehicle 2 presented as percentage change from baseline performance. Error bars represent upper and lower bounds of one standard deviation from the mean.

Decreasing the fill mass to 1.7 kg (2.0 L) reduced the tailpipe CO_2 emitted by 1.18% for the non-preheated case and by 0.96% when the reduced oil fill was preheated

to 70˚C. The test results could be separated from the results of the reference to 95% confidence and can be considered as statistically significant. However, the lower value obtained when the lubricant was preheated is directionally against expectation.

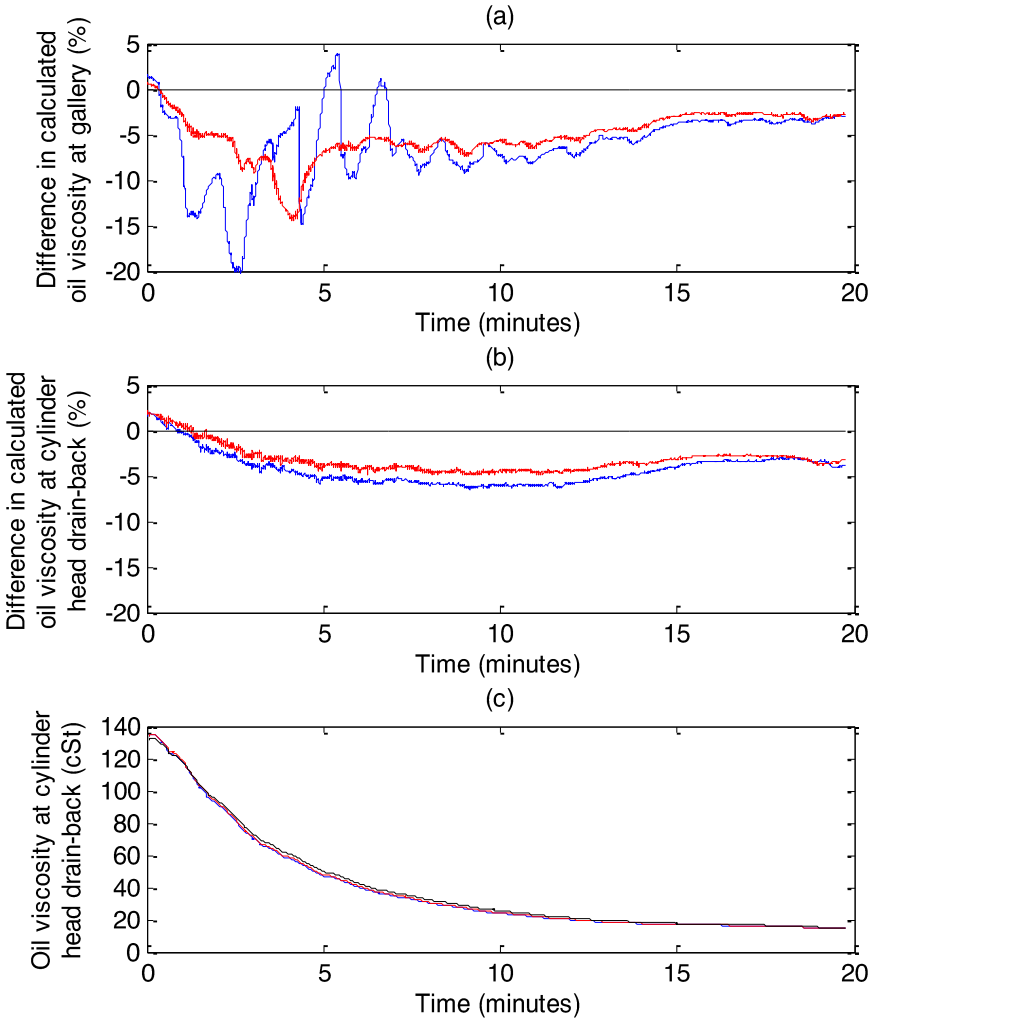

Figure 93(a-c). Difference in lubricant viscosity between reference (5W-30(R)), 2.0 L and 3.0 L fill tests at gallery (a), at the cylinder head drain-back (b) and lubricant viscosity, calculated from the mean of the gallery temperature measurements for Vehicle 2

Figure 93 shows the calculated lubricant viscosity at the gallery overlaid with the calculated viscosities from the two low oil fill cases. The variation in calculated oil viscosity at the gallery for the low fill cases demonstrates a similar magnitude of effect as seen in the Vehicle 1 tests (Figure 82) although the trace is less stable. Examination of the oil pressure indicated that the 2.0 L fill was causing some oil gallery pressure fluctuations in the test cycle. These variations may have reduced the oil flow rate for the

low fill test case. The oil pressure variability may also have contributed towards the reduction in CO_2 measured, due to a reduced pumping workload with aerated oil. The oil pressure was unaffected in the 3.0 L fill test cases.

The greater tailpipe CO_2 reduction for this engine is peculiar given the similar thermal response (and hence viscosity reduction) of the two vehicles. Examining the engine post-test demonstrated it was fitted with second-order balancer shafts mounted onto the main bearing ladder and thus sitting beneath the oil fill line. More investigation is needed to understand these components' frictional response with respect to oil level and establish whether these contributed to the CO_2 reduction measured.

6.6. Summary of test results

A suite of tests was completed using two modern vehicles to assess the impact of: i) preheating the lubricant to simulate thermal energy storage systems, ii) reducing the lubricant mass and iii) reducing the lubricant viscosity. Testing was also performed to understand the interaction of these test variables with coolant-to-lubricant heat exchangers, since the peculiar situation of this testing approach meant that the lubricant temperature exceeded the coolant temperature at key points in the test.

Cold start tests completed using the NEDC showed that the tailpipe CO_2 reduced by 0.41% when lubricant preheated to 60˚C was added to the sump immediately prior to the test start and by 1.04% for the test cases when lubricant preheated to 90˚C was added. The results could not be separated from the population of the mean results to a statistical significance of greater than 95% confidence. Test cases where the preheated lubricant was added very hot (150˚C) with the oil cooler bypassed showed a CO_2 reduction of 0.66% in comparison to the reference case (which also had the coolant-to-lubricant heat exchanger bypassed). These data points could not be separated from the population of reference mean to a statistical confidence level of 95%.

Each test using lubricant preheating recorded a significant loss in lubricant temperature between the oil sump and oil gallery. This result suggests there was significant heat transfer occurring between the lubricant and engine structure and that the lubricant temperature at the tribological contacts should not be directly inferred from the gallery temperature. A thermocouple in the cylinder head oil drain-back path gave the lubricant temperature after the lubricant had passed through the oil gallery. This thermocouple's measurements indicated that the oil drain-back path temperatures for preheated cases were higher throughout the test cycle. They closely followed the cylinder head structure temperatures after the test's initial phase, circa 6 minutes, once equilibrium was established between the initially hotter lubricant and cooler structure. It was concluded that the heat addition to the lubricant primarily increased the engine temperature. A similar conclusion was found when reducing the lubricant mass.

The frictional response of the lubricant pumps was not reported. However, it can be concluded that this component sees greater lubricant temperature variations, and thus viscosity change, than other engine components, since it sits between the sump and gallery thermocouples, which both showed increased lubricant temperatures during testing. Whether this component provides a net increase or reduction in friction depends on its design and control strategy (see Chapter 5).

A reduction in tailpipe CO_2 was measured when tests were completed with lower oil volumes. The theoretical benefit associated with an oil fill reduction of 3.1 L was 2.2%. Between 0.3% and 1.2% CO_2 reduction was measured when the oil mass was varied. The lower measured values in comparison to the calculated values may be attributable to an increased amount of heat transfer from the engine during the warm-up phase for the test cases where the lower fill volumes were used. A maximum reduction in viscosity of 15% occurred when tests were completed with reduced oil fills.

An assessment investigated whether fitting the coolant-to-lubricant heat exchanger in these tests reduced the effect of lubricant thermal management systems, due to the peculiar condition of lubricant temperatures being higher than the coolant temperature. Bypassing the coolant-to-lubricant heat exchanger increased tailpipe CO_2 by between 0.06% and 0.99%. A different response was found when the vehicle was preconditioned using overnight soak versus forced cooling strategies, but this could not be explained. However, the results could not be separated from the population of the reference mean to 95% confidence. A greater lubricant viscosity reduction occurred when tests had a reduced oil volume and the coolant-to-lubricant heat exchanger was bypassed. The combined effect of isolating the coolant-to-lubricant heat exchanger for the test's initial phase and introducing it when the coolant temperature was higher than the lubricant temperature was not assessed. However, it warrants further investigation and may augment the effect attributable to lubricant mass reduction. The interaction with switchable coolant pumps and thermostats is also worthy of separate study.

A greater tailpipe CO_2 reduction was found with Vehicle 2 than Vehicle 1 when lubricant mass was removed from the sump. Oil pressure fluctuations in the Vehicle 2 test, where the oil volume was reduced to 2.0 L, may have contributed to the CO_2 reduction measured, owing to reduced oil pump parasitic loading. Further investigation would be required to prove this conclusion. Repeat tests completed with Vehicle 2 at a slightly greater oil fill volume showed a tailpipe CO_2 reduction of 0.74%. This CO_2 reduction was surprising given the relatively small variation in lubricant viscosity measured here (5% reduction). This result could indicate that the response was augmented due to an interaction with the warm-up calibration, a reduction in the parasitic loading from the second-order balancer shafts or friction in the oil pump.

Generally, the repeatability of the results was not large enough to allow the effect of the test variables to be separated with statistical confidence to 95%. Any future work

should be completed with greater emphasis on improving this repeatability (e.g. using a transient engine dynamometer capable of reproducing drive cycle speeds and loadings).

A low viscosity lubricant reduced tailpipe friction by 3.7% compared to a reference case (both tests were undertaken with the coolant-to-lubricant heat exchanger bypassed). The results of this testing could be separated from the results of the reference to a statistical certainty of more than 95% confidence. Using the calculated kinematic viscosity as an indicator, it was anticipated that the tailpipe CO_2 reduction would be greatest using the low viscosity lubricant followed by the hot fill and then the reduced oil fill tests. This effectiveness ranking agreed with the trend of the results reported.

6.7. Lubricant thermal management of an external oil reservoir

The tests showed that lubricant thermal management strategies could provide a worthwhile contribution to the reduction of vehicle CO_2 emissions. However, systems that achieve these benefits (e.g. via lubricant heat storage) are scarce. Singh et al. [141] evaluated a range of thermal management approaches for passenger car engines. They have predicted that vehicles will be fitted with oil heat storage tanks by 2020. The increasing focus on reducing tailpipe CO_2 emissions means that thermal management systems are attractive to manufacturers, if cost-effective systems are developed.

The acceptability of lubricant preheating, or thermal storage systems for use in the NEDC is governed by the United Nations Economic Commission for Europe requirements laid out in Regulation 83 [129]. This document describes the thermal preconditioning procedure that vehicles must undergo prior to completing a Type I NEDC. The regulation states: “before testing, vehicles shall be kept in a room in which the temperature remains relatively constant between 293 K and 303 K. This conditioning shall be carried out for at least six hours and continue until the engine oil temperature and coolant, if any, are within ±2 K of the temperature of the room.” Thus,

systems designed to retain the lubricant thermal energy during the preconditioning procedure must ensure that lubricant temperature is maintained for at least 6 hours and that derogation is achieved regarding the location of the oil temperature measurement probe. Achieving a derogation here seems credible, given that any system purposefully designed to store the lubricant thermal energy would provide a real world benefit in vehicle usage beyond the NEDC. The lack of a maximum soak time specification may cause more significant issues. The acceptability of any thermal management systems that would cause the vehicle CO_2 emission response to depend on the duration of the preconditioning would also need to be assessed.

The introduction of the World-wide harmonized Light vehicles Test Procedure (WLTP)[14] for the measurement of tailpipe CO_2 emissions in 2017 means that this new cycle's requirements must also be considered when assessing implementation of oil thermal management systems. Two thermal boundary conditions are currently proposed for use in the WLTP [142]. The European Commission ambient test temperature is proposed to be 287 K, but this is 296 K for the other non-European United Nations member states for whom the procedure carries over the same soak time criteria as the NEDC. However, the tolerance of the vehicle soaking area ambient temperature has been reduced to 296 K ± 3 K, from 293 K to 303 K used previously. The regulation requires that the lubricant temperature be within 296 K ± 2 K [143]. The test protocol that shall be used by European member states has not yet been defined. Defining this regulation forms part of Phase 2 development due to conclude by 2018.

The reduction in temperature range for the vehicle from between 293 K and 303 K for the NEDC to 290 K to 299 K may result in a slightly lower starting temperature for

[14] The WLTC is a test cycle prescribed in the WLTP

the engine and lubricant. However, the exact difference will depend on the set point previously selected by the test facility.

6.7.1. Simulation of a lubricant heat-storage system

A lubricant heat-storage system's ability to retain lubricant temperature during the soak period was simulated using the computer program COMSOL. A form factor for the heat-storage reservoir was taken from the author's patent design registration for an engine component [144]. Figure 94 includes a schematic of this reservoir. This component locates the lubricant remotely from the engine (e.g. replacing a dry-sump tank in a vehicle). Simulations were performed to conclude the efficiency of different tank insulation designs and the inclusion of supersaturated chemicals (commonly referred to as phase change materials) into the insulation layer.

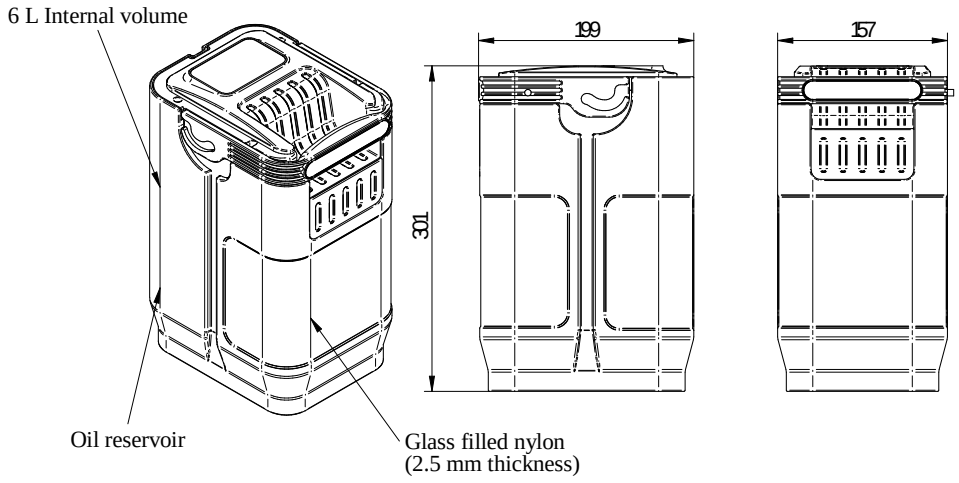

Figure 94. Form factor for remote oil reservoir used in thermal simulation study. All dimensions in millimetres.

The lubricant's starting temperature was 90˚C. It was assumed that vehicle preconditioning cycles run prior to the soaking period would result in temperatures at least this high.

6.7.2. Baseline simulation and validation test

A reservoir, manufactured using a Selective Laser Sintering (SLS) process, was installed into an environmental test chamber to allow validation of the simulation output. The reservoir was filled with 5 L of 5W-30 lubricant and a single 'K' type thermocouple was positioned in the centre of the oil volume. A data logging system recorded the temperature measured by the probe at a frequency of 0.1 Hz. Increasing the chamber's ambient temperature to 100˚C elevated the oil and reservoir temperatures. This condition was retained until the oil temperature (measured using the thermocouple) read 95˚C. The chamber temperature was then set to 20˚C and recordings were stated when the oil temperature reached 90˚C. The thermal boundary conditions chosen for this test are more severe than those on the vehicle, since the real under-bonnet temperature is higher owing to heat rejection from the other engine components. However, this condition was selected to allow a simple initial evaluation of the system performance.

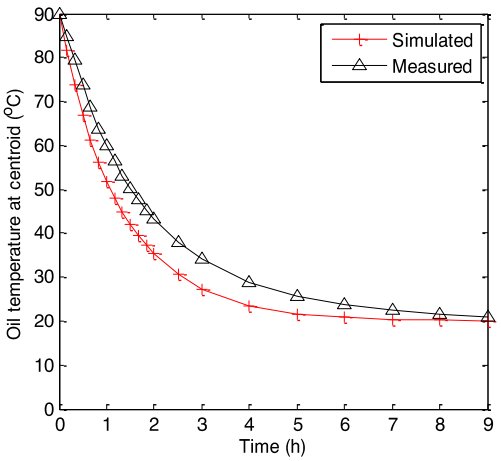

Figure 95. Measured and simulated results of cooling test with oil reservoir positioned in 20˚C ambient chamber.

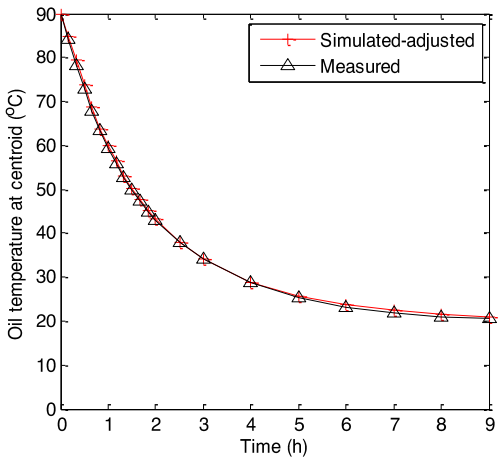

Figure 96. Comparison of measured and adjusted simulated results.

Figure 95 shows the temperature the probe measured and the values achieved using the simulation. The predicted cooling rate was faster than achieved in testing, which was attributed to the selection of the heat transfer coefficient between the reservoir and

the chamber being too high. This coefficient was adjusted to reduce the simulation error. Figure 96 shows results with the adjusted coefficient. Reducing the heat transfer coefficient improved the simulation's accuracy.

The simulation and testing results showed that the bulk oil temperature cooling curve approximated to an exponential decay and reached the requisite 22˚C condition for acceptability to start the NEDC within 4 hours 24 minutes of the soak condition start. At 6 hours in, the lubricant temperature was 20.8˚C, indicating that simply mounting the oil reservoir remotely from the engine would be insufficient to provide any increase in lubricant temperature following the mandatory soak period. The heat transfer to the chamber was large, so further simulations were completed to predict the benefit that could be achieved by installing insulation onto the reservoir.

6.7.3. Insulation simulation

The validated simulation predicted the performance of three insulation types that were wrapped around each surface of the reservoir design. The effect on oil temperature of 5 mm and 15 mm insulation thickness was simulated. The performance of an insulating air gap and the performance change caused by filling this void with polystyrene and a silica aerogel were assessed. These three options cover a range of installation costs from very low (additional plastics required to provide the air gap) to approximately £0.10 per litre for the polystyrene and £25 per litre for the aerogel systems. The volume of a 5 mm insulation layer was approximately 1.5 L and this increased to 4.5 L where the insulation thickness was increased to 15 mm.

6.7.3.1. Results

Figure 97 summarises the predicted mean oil temperature after 6 hours of cooling for these simulation runs. The uninsulated reference case achieved an end of soak period temperature of 20.8˚C. This temperature increased for each case that included insulation. Adding a 5 mm insulation filled with air was predicted to increase the oil temperature to 37˚C, while 15 mm raised the temperature to 55.6˚C after 6 hours.

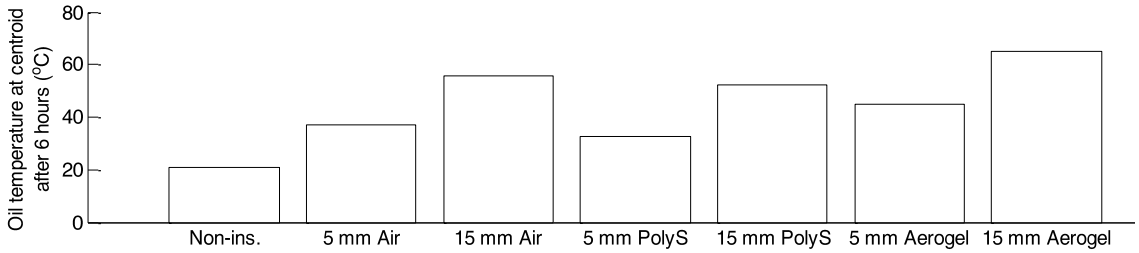

Figure 97. Predicted mean oil temperature following a 6-hour thermal soak. Where "ins." Is insulated and "PolyS" is Polystyrene.

Filling the insulation gap with polystyrene was predicted to result in oil temperatures of 32.9˚C and 52.3˚C for the 5 mm and 15 mm cases respectively, after 6 hours. The predicted temperatures were lower than those when the cavity was filled with air. This poorer performance was attributable to the increased thermal conductivity of the polystyrene compared to air and the reduction in thermal resistance between the reservoir and the chamber resulting from this change. The polystyrene was simulated to inhibit buoyancy driven heat transfer in the insulation void, but this benefit was smaller than the degraded performance due to conductive heat transfer through the insulation.

The predicted oil temperature for the case where the insulation was constructed from a 5 mm thick silica aerogel layer was 45˚C. Increasing the insulation to 15 mm thickness increased the predicted end of test temperature to 65˚C. Figure 98 shows the simulated test start and end thermal profile for the 15 mm thick silica aero gel simulation. The end of simulation run image shows that a temperature gradient was

predicted to occur between the centre of the reservoir and the wall. This behaviour was present in each of the simulations and indicates that the oil temperature fed to the engine could be maximised by drawing lubricant from the centre of the tank.

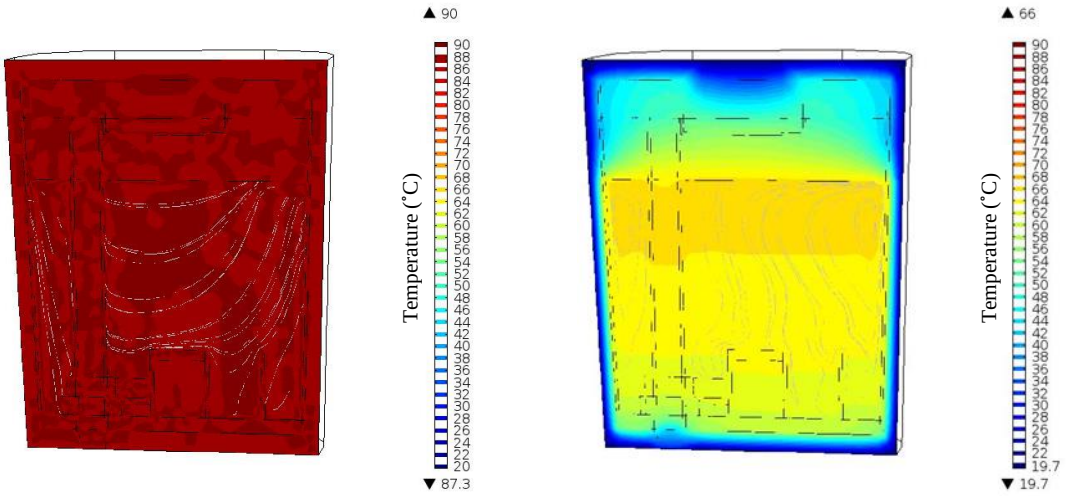

Start of simulation condition: 0 hours End of simulation condition: 6 hours

Figure 98. Cross section through the reservoir showing a two dimensional heat map of the predicted temperature for the 15mm thick silica aero gel insulation case.

The chassis dynamometer testing demonstrated that a reduction in CO_2 emissions of 0.4% was possible when the lubricant temperature was preheated to 60˚C (Section 6.5.2.2). Thus, this simulation work shows a heat storage system can be used to provide this benefit. The higher starting ambient temperature in the under-bonnet location will also increase the oil temperature that this system could achieve in practice.

6.7.4. Simulation of phase-change material

The simulation predicted the effect on oil temperature caused by substituting insulation material for phase-change material (PCM). The PCMs were simulated to release latent thermal energy when changing from liquid to solid during cooling. Schatz [145] investigated a system using a similar heat storage technology. However, he did not explore the system's applicability to store the engine lubricant. His invention focused on using latent heat for cabin or engine coolant warming.

The effect of insulating the reservoir with two chemicals was simulated. A wax with a transition temperature of 68˚C and a supersaturated sodium acetate solution were chosen. The activation temperature for the sodium acetate solution was 50˚C. The time during the cool-down at which the PCMs provided heat input differed by following this approach.

6.7.4.1. Results

Figure 99 summarises the predicted mean oil temperature after 6 hours of cooling, for the models that included PCMs. The results from two sets of simulations are included. Initially the effect of adding the PCM to the outside of the reservoir was modelled. The results from this uninsulated testing were poor, so the effect of insulating the PCM blanket using a low cost 5 mm air barrier was also investigated. The predicted lubricant temperature increased for all of the simulated cases that included PCMs.

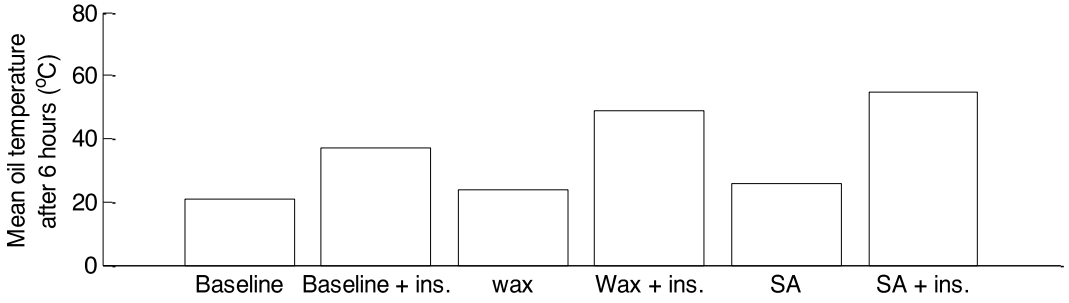

Figure 99. Predicted mean oil temperature following a 6-hour thermal soak. Where "ins." refers to the simulations that included 5 mm of insulation and "SA" refers to the Sodium Acetate PCM.

Adding a wax PCM blanket was predicted to increase the mean oil temperature to 24˚C. Insulating this PCM layer with 5 mm of air raised the temperature to 49˚C after 6 hours. The performance of the sodium acetate PCM exceeded that of the wax. The simulation predicted that wrapping a sodium acetate PCM blanket around the reservoir resulted in a mean oil temperature of 26˚C after 6 hours. Adding 5 mm of air insulation to this PCM's outer surface increased the mean oil temperature to 55˚C.

The simulation results showed that after a 6-hour soak, insulating the reservoir with PCMs could increase the oil temperature. The efficacy of the PCMs increased when a 5 mm air insulation layer was added to the outer surfaces. The maximum mean oil temperature predicted was lower than that which could be achieved with the best performing 15 mm thick layer of silica aerogel insulation. A study that combined both a PCM with a silica aerogel material was not completed, since the cost of installing both of these solutions was prohibitive in practical applications. Whilst this approach may seem sensible, it should be noted that the phase transition temperature occurring in the PCM limits the maximum potential temperature achieved by the phase change material.

6.7.4.1. Vehicle application

The simulations were simple. Thus, no account was made for thermal conduction through the reservoir's mounting features or through the fluid connections to the engine. Both of these effects are likely to increase the heat transfer rate from the oil. The models are a useful indicator for the system's performance potential. However, establishing the system's behaviour with a higher accuracy requires a more complex test or higher fidelity model. If the reservoir is positioned under-bonnet a significant amount of residual heat will probably be present in the other engine bay components, so the local temperature of the reservoir walls is likely to be higher than simulated.

6.8. Chapter 6 conclusions and recommendations

Many researchers focus on thermal management, due to the typical warm-up profile of vehicles on the NEDC and the favourable cost-benefit ratio often presented. An assessment of existing research indicated that thermal management opportunities arising from managing lubricant thermal mass needed updating.

A testing programme investigated the effect of different thermal management strategies for the engine lubricant. Reducing the oil volume during the engine warm-up

phase resulted in higher engine oil temperatures. Thermocouples installed onto the outside surfaces of the engine block and cylinder head showed that the engine temperature increased along with the higher oil temperatures. Measurements of engine exhaust emissions during the test showed that reducing the lubricant volume present during the warm-up phase decreased the CO_2 emitted. Reductions in CO_2 emissions of between 0.4% and 1.2% were achieved by lowering the oil volume from 5.1 L to 2.0 L during tests using the NEDC. The tests' repeatability was insufficient to measure CO_2 differences that were statistically significant to greater than 95% confidence levels. Further work is needed to measure CO_2 emission differences using a more accurate process (e.g. by using an engine dynamometer capable of reproducing drive cycle speed and load profiles). Developing a system that achieves the CO_2 emission reduction caused by lowering the oil volume in this way should be the basis of further study.

Two vehicles were used in the testing matrix; each of which demonstrated a different magnitude of CO_2 reduction when the oil volume was varied. This behaviour was expected and attributable to the different thermal management systems already in the engines. The engine loading parameters used on the chassis dynamometer were the same for each vehicle, but the engines' swept volumes were different. Thus, the BMEPs in the engines were not the same, and this change in loading is likely to have contributed to dissimilar reductions in CO_2 emissions. The transferability to other engines of the results in this research is non-obvious because of the large range of engine thermal management strategies in modern engines, the different engine materials and masses used and the variation in loading caused by differences in engine swept volume and vehicle design. Prediction of the benefit that lubricant thermal management systems can provide could be achieved through the development of a thermal simulation model. Testing could also be undertaken if an engine or vehicle was available.

Investigations were completed to establish the significance of preheating lubricant prior to starting the NEDC. The results from this testing were used to predict the change in engine performance caused by fitting an external oil reservoir capable of retaining the lubricant temperature over the NEDC and WLTC mandatory 6-hour soak period. Measurements completed during the testing procedure showed that reductions in tailpipe CO_2 emissions of between 0.4% and 1.0% were possible by flowing oil into the engine, just prior to the test start, at 60˚C and 90˚C respectively.

The capability of an oil storage reservoir to retain the lubricant's thermal energy during the 6-hour soak period was established using a simulation. A thermal model of the reservoir was built and validated by completing an experiment to measure the reservoir's cool down rate in an environmental chamber. The simulation showed it was possible to reduce the heat transfer from the lubricant to the test chamber, during the vehicle soak period by adding insulation to the reservoir. Installing a 15 mm thick layer of silica aerogel insulation to the reservoir resulted in a mean oil temperature of 65˚C, based on a starting temperature for the lubricant of 90˚C. Thus, combining an insulated oil reservoir and a control system to introduce the lubricant into the engine prior to starting could achieve a CO_2 emission reduction of greater than 0.4% on the NEDC, for the engine tested. The simulation used a simple fixed temperature assumption for the ambient temperature surrounding the oil reservoir. This simplification meant that the testing conditions might have been more severe than would occur in a practical application, because they did not include any heat rejection from adjacent components in the engine bay. The measurement of the temperature in a suitable under-bonnet location would allow a greater refinement in the simulation. It is recommended that this thermal study be completed, so that the simulation fidelity can be increased.

The performance change due to installing phase change materials in the insulation volume of the external reservoir was investigated using the thermal model. The model's

results showed that the oil temperature increased when a layer of these materials was added to the reservoir. Adding an insulating air layer to the outside of the phase change material greatly increased the predicted mean oil temperature after 6 hours. The maximum predicted mean oil temperature achieved using phase change materials was 55˚C. This temperature was lower than achieved using the best performing insulation design. The combination of an insulation that performed well with a phase change material is likely to increase the ability of the phase change material to maintain a high lubricant temperature for a longer duration. However, the maximum temperature achievable depends on the temperature that the transition from the liquid to the solid states occurs at for the phase change material.

The NEDC was used to complete all testing work in the present research. This cycle was appropriate to understand the potential of thermal management of the lubricant to current emissions' legislation. However, the planned migration to the WLTC during September 2017 means that further work is required to establish the performance on this new cycle. The WLTC's higher load and longer duration are two key factors that are likely to reduce the impact of lubricant thermal management. Some authors [141] predict that modern engines will still include lubricant thermal management systems, so an investigation into the thermal behaviour of engines on the new test cycle would be worthwhile.

6.8.1. Key findings:

- A chassis dynamometer testing programme investigated the effect of different thermal management strategies for the engine lubricant.
- Reductions in CO_2 emissions of between 0.4% and 1.2% were achieved by lowering the oil volume from 5.1 L to 2.0 L and by between 0.4% and 1.0%

when the oil was preheated to 60˚C and 90˚C respectively prior to the test start. The tests were completed using the NEDC.

- Simulation of an external oil reservoir with insulation showed that a viable system to achieve the oil preheating benefits existed.

7. Vehicle level simulation

The component-level assessments in Chapters 3 to 5 gave insight into causal factors contributing to friction reduction in various engine subsystems. However, understanding the contributions to CO_2 reduction of these components at a vehicle level requires close-coupling and exercising of the models over a drive cycle. This chapter develops such a holistic model and uses it to gain additional understanding into some of the effects examined earlier at a component level.

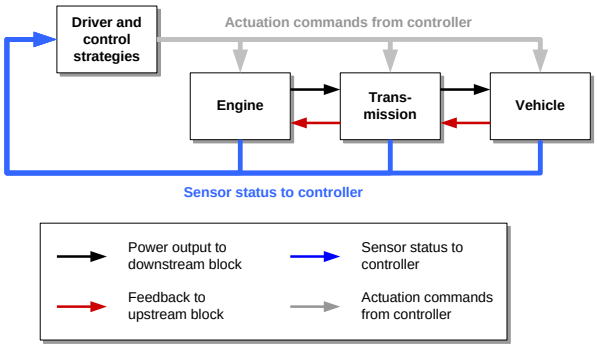

Figure 100. Block model of the V-SIM control structure.[¥]

The Ricardo Software program V-SIM is a vehicle parametric modelling tool that simulates engine behaviour in a drive cycle (e.g. fuel consumption and CO_2 emissions). MathWorks' software packages MATLAB and Simulink provide the operating environment for V-SIM. A forward-facing driver model inputs the desired vehicle speed, mass, aerodynamic drag, rolling resistance and road gradient to calculate an ideal torque at the vehicle wheels. The driver control model manipulates the demanded engine load and vehicle retardation levels (simulated throttle, gear and brake pedal positions) to achieve this ideal torque, after accounting for the instantaneous engine and powertrain losses. The driver model uses a proportional, integral and derivative function to control its outputs. Heath and Mo [146] describe an early version of this tool. This simulation approach allows closer simulation of real vehicle behaviour on the drive cycle [146].

Figure 100 summarises the simulation structure. The user inputs data defining the base engine performance, such as brake specific fuel consumption (BSFC), the torque variation with engine speed, engine mass and inertia. The model calculates fuel consumption using the BSFC values and the predicted engine speed and torque. It uses the performance characteristics of a 1.6 L turbocharged gasoline engine. Bespoke subroutines were developed to predict the effect of different lubricants on a theoretical engine. The parasitic loads were increased or decreased dependent on the friction models' outputs. Vehicle retarding force was defined using an equation of the form:

$$F = \frac{1}{2}\rho C_{\mathrm{d}} A V^2 + C_{\mathrm{r}} m\mathrm{g} + X F_{\mathrm{b}} \quad (31)$$

Where: ρ is air density, C_{d} is the coefficient of the vehicle body's drag, A is the vehicle frontal area, V is the vehicle velocity, C_{r} is the coefficient of rolling resistance, m is vehicle mass, g is the constant of gravitational acceleration, X is the braking force fraction and F_{b} is the maximum braking force achievable to retard the vehicle.

Table 32 summarises the input values used in this equation. The vehicle retarding force, F, sets the engine load along with the contribution from engine friction changes, vehicle acceleration and angular acceleration of the driveline inertiae.

Table 32. Properties used in V-SIM model.

Property	Value
C_{d} (-)	0.33[15]
A (m^2)	2.29[15]
C_{r} (-)	0.011
m (kg)	1,467[15]
F_{b} (N)	10,000

The vehicle model includes a manual gearbox and the gear ratios from a 5-speed Durashift gearbox fitted to a Ford Focus. The values used for gears 1 to 5 were 3.58,

[15] Data from Ford Focus [147]

2.04, 1.41, 1.11 and 0.88 respectively. The driveline friction variation with warm-up or in different gear positions was not characterised. A constant efficiency of 95% was assumed for the gearbox and final drive.

7.1. Friction calculation approach

The BSFC input values included losses from engine friction, since a dynamometer-mounted engine generated this data. A 5W-30 lubricant was used, but this work was not completed during the present research, so exact details of the lubricant are unknown. To assess the engine performance improvement from lubricant engineering, the friction for the 5W-30 (described in Table 2, Section 2.1.1) was simulated and the difference between these results and other lubricant results was added to or removed from the engine torque demand. The engine friction variation during the warm-up process was accounted for by modelling the lubricants' friction magnitudes at various temperatures.

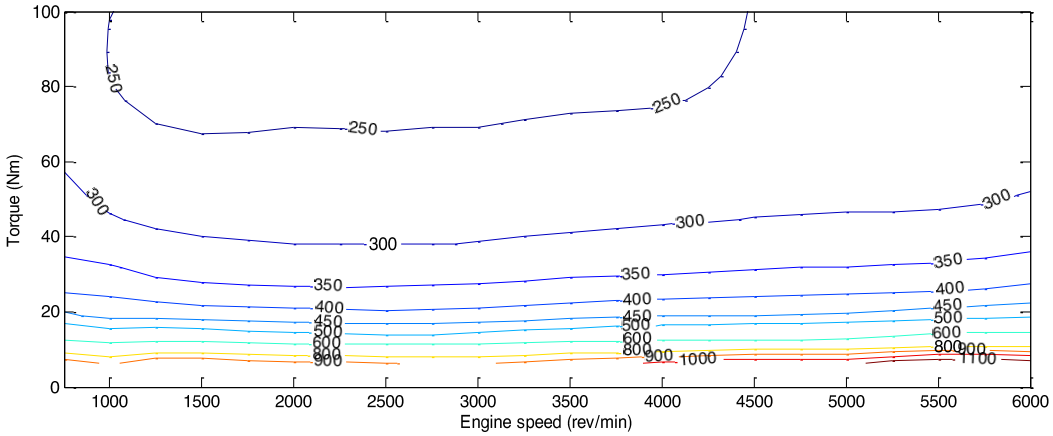

Figure 101. Specific fuel consumption (g/kWh) data used within the vehicle model.

Oil temperature rise was defined as an input to the model, taken from empirical measurements on each drive cycle for each lubricant. Chapter 6 describes the vehicles used to generate this data. The heat flux variation in each component that typically occurs during warm-up was not accounted for. Extending the model to assess this behaviour is recommended for its future development. The BSFC increase resulting

from the requirement to raise the exhaust gas enthalpy by delaying the combustion phasing to 'light-off' the exhaust catalysts was not characterised.

7.1.1. Friction models

The matrix of friction results was generated outside V-SIM model and characterises FMEP variation with engine speed, loads and temperatures. Table 33 summarises the 132 conditions used. The FMEP values comprise empirical and simulated results. Linear interpolation was used to obtain the FMEP values at the engine operating points visited on the cycles modelled.

Table 33. Conditions used in FMEP simulation.

BMEP (bar)	2, maximum (defined by the full-load line)
Engine speed (rev/min)	500, 1000, 1500, 2000, 2500, 3000, 3500, 4000, 4500, 5000, 5500
Oil and coolant temperature (˚C)	20, 30, 40, 60, 80, 100

Calculated FMEP values accounted for valvetrain and engine bearing losses. A semi-empirical model characterised piston-to-liner losses. An empirical model characterised oil pump losses.

7.1.2. Valvetrain friction

The Ricardo Software program VALDYN calculated valvetrain friction. This program is a multi-body dynamics code that calculates friction at the cam-tappet and tappet-bore interfaces. Friction in the camshaft bearings was calculated separately, (see Section 7.1.3). Losses between the valve stem and guide and stem seal were ignored.

A model of a Ford ZETEC cylinder head was used, as a simulation existed from a previous research activity [148]. The valvetrain design used direct acting bucket followers with hydraulic lash adjusters. The predicted contact conditions included significant contributions from boundary regime friction and elastohydrodynamic behaviour.

7.1.2.1. Valvetrain friction calculation

Elastohydrodynamic shear stress was calculated using:

$$\tau = \begin{cases} \mu \dfrac{V}{h} & \text{for } \tau \leq \tau_0 \\ \tau_0 + \varsigma P & \text{for } \tau_0 < \tau \leq \tau_{\mathrm{L}} \\ \tau_{\mathrm{L}} & \text{for } \tau > \tau_{\mathrm{L}} \end{cases} \tag{32}$$

where τ is shear stress, μ is local dynamic viscosity, V is the relative velocity between the cam and follower, h is oil film thickness, τ_0 is the Eyring[16] stress, ς is the rate of change of shear stress with pressure, P is the oil film pressure and τ_{L} is the limit shear stress.

This equation was taken from Zhu and Taylor's work [149]. Evans and Johnson's work [150] set the lubricant values. The relative velocity at the contact patch was calculated based on the camshaft lobe's surface speed and the follower's rotational speed. Comparing the simulation output to the measurements of Mufti and Jeffries [151] validated the rotational speeds at the follower (although they used a different cylinder head design). Integrating the shear stress over the contact region allowed a prediction of the friction force and multiplying this value with the radius from the camshaft centreline gave the torque at the crankshaft using:

$$T = \int_0^x \int_0^y \frac{1}{2} \tau r \, \mathrm{d}x \mathrm{d}y \tag{33}$$

where r is the radius of the contact from the camshaft centreline, x is the dimension across the width and y is the dimension along the length of the contact patch.

Timing drive losses were included and assumed to be independent of lubricant temperature, viscosity or engine load. Data from motored tests set these values.

[16] The Eyring stress, τ_0, is relevant under fluid shear conditions and marks the limit of Newtonian flow (shear stress proportional to velocity (see Equation (15)) and a transition into a linear 'Eyring' flow (shear stress proportional to log(γ) where γ is the strain rate). This flow condition exists until the limit shear stress, τ_{L} , is reached [150].

Boundary friction on the camshaft was calculated using Greenwood and Tripp's model [67] and this was converted to a torque at the crankshaft using the equation:

$$T = \frac{1}{2}\,\eta r W_{\mathrm{a}} \tag{34}$$

where W_{a} is asperity contact load and η is the friction co-efficient in boundary contact.

7.1.2.2. Valvetrain friction results

Figure 102 summarises the predicted friction at 20˚C and 100˚C for the SAE 8 and 5W-30 lubricants. Over 1000 rev/min the SAE 8 reduced the total friction at 20˚C, owing to a hydrodynamic friction reduction. The predicted friction increase below 1000 rev/min was caused by an increase in boundary contact between the cam and tappet due to the low entrainment velocity and high contact pressures in this condition. As the temperature was increased, the performance of the SAE 8 worsened due to low oil film thicknesses and consequent high boundary friction magnitudes. Whether a low viscosity lubricant provided a benefit or deficit in FMEP depended on temperature and engine speed.

The calculated hydrodynamic friction variation did not follow the expected pattern of increasing FMEP with speed. This behaviour was due to:

1) Shear rates increasing with engine speed causing a shear thinning of the 5W-30 oil, and the oil transitioning into a limiting shear stress (see equation (32)). The viscosity variations with pressure and shear for the lubricants are given in Sections 2.3 and 2.4

2) A reduction in contact load due to the valve and follower dynamics at high speed. This dynamic behaviour reduces contact stress during part of the cycle, since the inertia of the valve assembly acting against the spring load becomes significant at high speeds

The hydrodynamic friction change between the SAE 8 and 5W-30 at 20˚C was small, suggesting the friction was insensitive to this parameter, and that the optimum viscosity for this contact was high (e.g. 60 cSt)[17]. The relative hydrodynamic losses reduced with temperature for each lubricant due to the decreased viscosity.

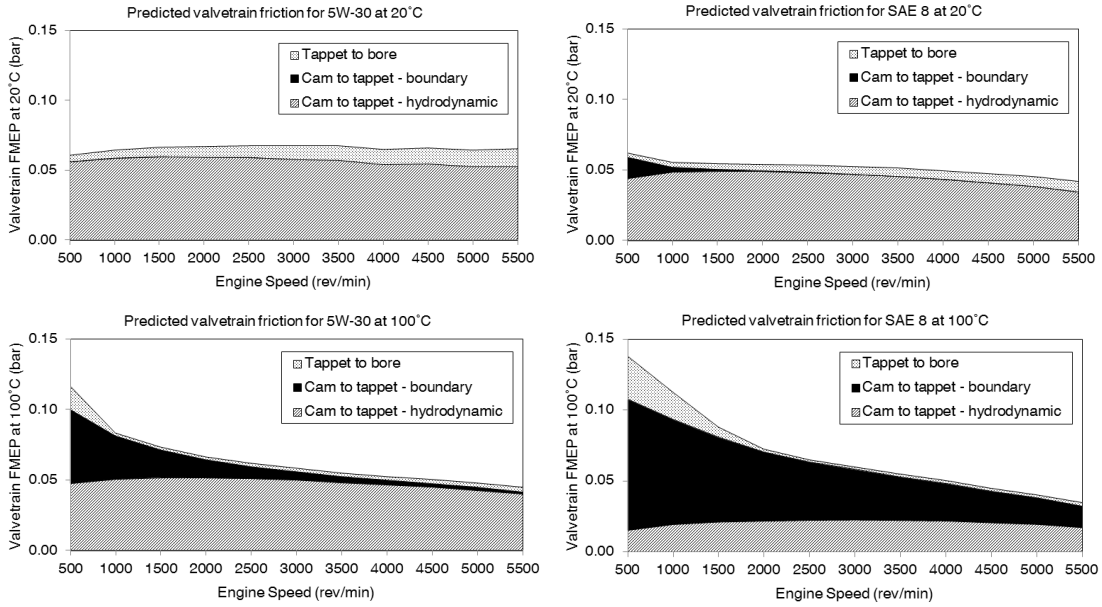

Figure 102. Friction prediction for the Ford ZETEC valvetrain.

The NEDC and WLTC both transition from low to high lubricant temperatures during warm-up. Lubricant viscosities shift from high to low values due to this temperature change. The friction contribution to the total fuel burnt in homologation drive cycles like the NEDC and WLTC also varies from a high magnitude in the cold phase to lower magnitudes at higher temperatures. Thus, the ability for a low viscosity lubricant to provide a friction reduction in the valvetrain area and engine is not obvious. This relationship is investigated using the V-SIM model later in this chapter.

The valvetrain model in the present research assumed that friction was independent of engine load. In reality, a small loading increase occurs due to increasing cylinder pressure at high engine loads when the exhaust valve opens. This simplification

[17] High magnitudes of Hertzian contact stress mean that the pressure-viscosity coefficient has a more significant impact on the friction in this area than low pressure and low shear viscosity values [148].

probably led to a small error in the simulation. A minor oil film temperature rise is also likely in practice due to thermal conduction from the combustion chamber via the valve stem. This behaviour was not characterised.

7.1.3. Bearing friction

Ricardo's ENGDYN program simulated the contribution of bearing losses to overall engine friction. As described in Chapter 3, friction at the big-end bearings was calculated using an EHD model. Main bearing friction for the same 1.6 L 4-cylinder gasoline engine was calculated using ENGDYN. However, the mobility method was used, which assumed the bearings' housings and journals were infinitely stiff, circular and operated in the hydrodynamic regime.

The same mobility approach calculated the friction present in the camshaft bearings, using the geometry and contact conditions present in the Ford ZETEC cylinder head. The increased loading present in the first camshaft bearings due to tension from the timing drive system was not characterised.

The thermal balance calculation used in ENGDYN assumed that all the friction in the contact generated heat rise in the lubricant [152] and the bearing and journal temperatures were equal to the coolant temperature. These assumptions are oversimplified, since heat conduction from hot components (such as the pistons) occurs. This approach probably caused under-prediction of the lubricant viscosity decrease and overestimation of the bearing friction.

7.1.4. Piston friction

Friction in the piston and liner conjunction was modelled using the Ricardo Software simulation program FAST. This tool uses a semi-empirical approach to resolve the friction magnitude. A tabulated approach was used whereby the results from

a number of motored engine tests were correlated to allow prediction of the friction under the engine conditions simulated in this test. The BMW/PSA group 1.6 L 4-cylinder gasoline engine used in defining the big-end bearing model provided the input values for this simulation. Completing the simulation using this approach was necessary due to the limitations identified in Chapter 4 (e.g the requirement to validate the thermal boundary conditions, the models high simulation run times and the inaccuracies occurring at low engine speed). FAST could not deconvolve hydrodynamic and boundary regime friction losses. Consequently, developing this simulation to include higher fidelity characterisation in this area of the engine is recommended for future research.

7.1.5. Oil pump

The results from the experimentation in Chapter 5 defined the oil pump's FMEP. This model characterised the change in load due to lubricant viscosity changes. Operation at 200 kPa (gauge) pressure was assumed for all conditions.

7.1.6. Oil temperature rise

Manipulating the temperature profiles input into the model allowed the CO_2 emission reduction achieved by improving lubricant warm-up rates to be characterised. The temperature rise data reported in Chapter 6 defined these inputs. A lower temperature rise was used for the SAE 8, since this was recorded in the experimental work.

7.1.7. Alternator

The engine included an alternator to convert mechanical rotational to electrical energy to power the ancillary systems. The load this component requires was included in the model by inputting empirically derived alternator efficiency measurements at a

range of engine speeds. The alternator mean efficiency was approximately 50%. A constant auxiliary load of 280 W was assumed for the operation of the engine's electrical system.

The effect of lubricant preheating using an electrical element was simulated by assuming that electrical energy stored in the battery powered the heating element prior to the engine start. The model assumed that the energy depleted was returned via the alternator during the drive cycle. The torque demand change was found by calculating the resultant crankshaft load including the alternator's conversion efficiency.

7.1.8. Crankcase pumping and sealing

Crankcase pumping and windage losses were calculated following a similar approach to that in Chapter 4. A crankcase pumping area of 0.005 m^2 was selected. The magnitude of this loss was assumed to be independent of lubricant temperature, viscosity and engine load. This assumed independence from load is likely to be the largest simplification here, since the crankcase gas dynamics change with blow-by flow rates, which vary with load. Applying a constant small torque to the crankshaft allowed losses from seal friction to be included. The value used was calculated by scaling friction measurements from empirical data.

7.1.9. Fuel pump and other ancillaries

A simple empirical model predicted the load attributable to the direct injection fuel pump. This model interpolated the friction magnitude, based on fuel flow rate, between measurements at high and low flow rates.

The model included losses from the front-end accessory drive. A speed-dependent calculation, based on empirical data, defined the friction in this system. A static tension

of 350 N was assumed. The losses from driving an air conditioning pump were also included, but were unaffected by the lubricant.

7.2. Drive cycles

The performance of the SAE 8 and 5W-30 lubricants was evaluated using the NEDC and WLTC. Figure 103 provides an overview of the speed traces for the NEDC and WLTC.

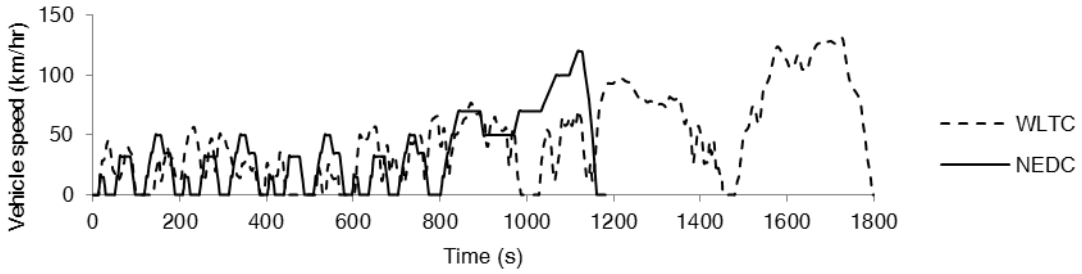

Figure 103. Comparison of vehicle speeds defined by NEDC and WLTC.

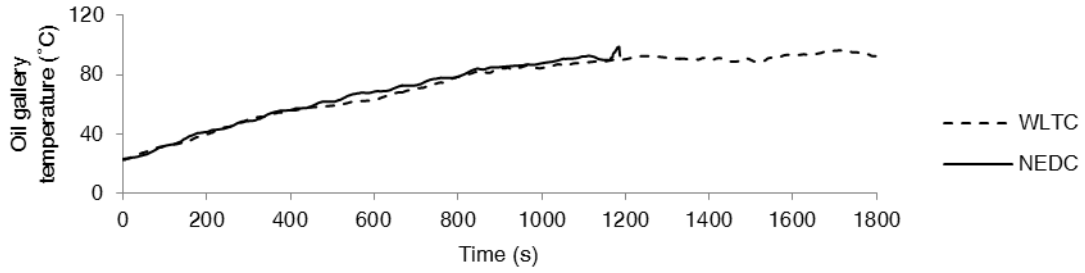

Figure 104. Comparison of measured oil gallery temperatures using NEDC and WLTC taken from Ford PUMA 2.2 L diesel engine mounted to an engine dynamometer using 5W-30(R).

The WLTC is 50% longer in duration and covers twice the distance of the NEDC. The higher mean vehicle speed and accelerations in the WLTC caused the engine to operate at a greater mean load. However, Figure 104 shows that the oil gallery temperatures for both the NEDC and WLTC are broadly similar. The longer duration of the WLTC proportionally reduced the time spent below fully warmed-up running temperatures and reduced the impact of the warm-up period on the distance-corrected CO_2 emissions.

Table 34. Comparison of NEDC and WLTC attributes.

Cycle	NEDC	WLTC
Duration (s)	1200	1800
Distance (km)	11.0	23.3
Mean vehicle speed (km/hr)	33.6	46.5
Max vehicle speed (km/hr)	120	130
Total time at zero vehicle speed (s)	261	227
Max acceleration (m/s^2)	2.10	2.25

Table 34 compares the key drive cycle attributes for the NEDC and WLTC. The absolute and relative times with the engine at idle are reduced using the WLTC. This change may be important when considering the lubricants' contribution to friction reduction since, at idle, the fuel combusted is all wasted to overcome engine friction. This change also alters the contribution to CO_2 reduction from stop-start systems.

7.3. Validation of the vehicle level simulation

Ricardo Software validated basic versions of V-SIM and routinely demonstrated 2% to 3% error in predicting vehicle fuel consumption during hot-start drive cycles. The model's performance is normally worse when simulating cold-start cycles where accuracy is typically 3% to 5% [153]. Using V-SIM, Heath and Mo [146] achieved 0.9% error when modelling a Volkswagen Golf with a diesel-electric hybrid powertrain over the NEDC and 1.9% with a Mercedes Sprinter 2.9 L 90 kW diesel engine. However, their plots comparing simulated and measured instantaneous fuel consumption values show larger errors. Work by Goodfellow et al. [154] discusses using V-SIM to model a diesel hybrid vehicle. Comparing the predicted fuel consumption on the NEDC to values reported for a vehicle homologation test validated their model. An error of 1% was achieved. Lyu and Rogers [155] describe a V-SIM model and provide data showing predicted and measured fuel consumption. A close correlation is found by the end of their real-world cycle simulation (1.7% error), but at times the error reached 5%. Few details of their vehicle or engine are provided.

The output from the model in the present research was validated by comparing the predicted CO_2 emissions to homologation values reported for similar vehicles. Running the model using the 5W-30 on the NEDC resulted in a predicted CO_2 emission of 153.3 gCO_2/km. The result published for the Ford Focus 1.6 EcoBoost Stop-Start (150PS) was 137 gCO_2/km and 155 gCO_2/km for the Peugeot 308 1.6 THP 156. The stop-start system on the Ford Focus was not a feature of the model and will have contributed to the homologated CO_2 emissions being lower than those the simulation predicted by 4% to 5%. It was not possible to compare the output of the model to measured values directly as the subsystems simulated in the present work were taken from a number of different engine designs. No actual vehicle or engine was available for this purpose.

The predicted friction using the SAE 8 was 149.1 gCO_2/km, representing a 2.8% CO_2 reduction relative to the 5W-30. A measured reduction of 3.7% was recorded during work on a similar engine type with the same lubricants (see Chapter 6), which may indicate the model underpredicts the lubricants' differences.

The predicted CO_2 emissions on the WLTC were 148.0 gCO_2/km for the 5W-30 and 145.1 gCO_2/km for the SAE 8, representing a 1.93% CO_2 reduction. No published data was available to validate this result. Changing from the NEDC to the WLTC was predicted to lessen the lubricant's ability to reduce CO_2 emissions by 31%.

7.4. Results

Table 35 compares key parameters for the NEDC and WLTC calculated with the model using the lubricant temperature profiles in Figure 5. Over the WLTC the engine operated with a slightly higher mean and maximum speed compared to the NEDC. However, this change was small and depended on the assumed gear shift strategy. The time-averaged FMEP reduced by 0.02 bar, which was attributed to the net effect of

longer operation at high oil temperatures in the WLTC, concomitant operation at low viscosity, and higher friction from increased engine load. The time-averaged BMEP increased significantly from 1.88 bar on the NEDC to 3.82 bar on the WLTC. The higher vehicle speeds and resultant engine loads increased the proportion of fuel burnt to overcome the vehicle drag in comparison to that used to overcome engine friction on the WLTC, and explains the smaller percentage reduction in CO_2 emission from using the SAE 8 on this cycle.

Table 35. Comparison of simulation results for NEDC and WLTC.

Cycle	NEDC	WLTC
Cycle-average engine speed (rev/min)	1637	1696
Maximum engine speed (rev/min)	3415	3723
Cycle-average FMEP (bar)	0.81	0.79
Cycle-average BMEP (bar)	1.88	3.82
Contribution of lubricant-related friction to CO_2 emissions (%)	8.7	6.3

The lubricant-related engine friction in Table 35 was calculated by running the model with the friction losses from the piston assembly, bearings and valvetrain set to zero. It should be noted that the losses in the oil pump were not removed, as it was not possible within the model to deconvolve friction losses from the pump's hydraulic efficiency. This analysis showed that the contribution from lubricant-related CO_2 emissions was 8.7% on the NEDC and reduced to 6.3% on the WLTC. These numbers provide a theoretical boundary to the maximum benefit that could be attained through lubricant engineering (ignoring oil pump and warm-up effects) for this virtual engine and vehicle combination. However, the full magnitudes of these benefits are unachievable in practice since they rely on the elimination of all friction. This analysis indicates that adopting the WLTC will reduce the potential benefit from lubricant engineering by around 28% compared to the NEDC.

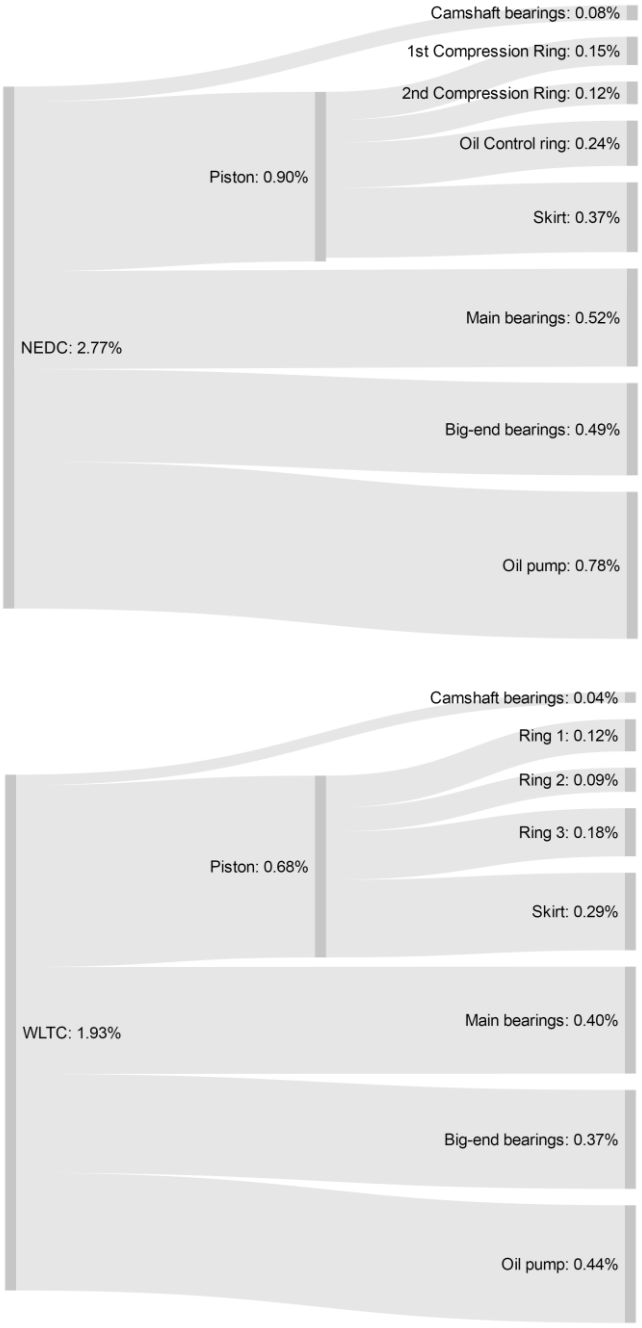

Figure 105. Sankey diagram showing contribution to CO_2 reduction from engine subsystems when operating on the SAE 8 in comparison to the 5W-30 for the NEDC and WLTC.

Figure 105 shows the absolute contribution to friction reduction from the various engine subsystems when operating on the SAE 8 compared to the 5W-30. The results were generated by completing simulations using the FMEP values from the 5W-30 instead of those calculated for the SAE 8, for each of the components in turn (e.g. to evaluate the contribution to CO_2 reduction from the camshaft bearings, the FMEP values calculated using the 5W-30 were applied instead of those for the SAE 8). The difference in model output indicated the effect of this change to the subsystem's FMEP.

The contribution from the valvetrain was removed since this was negative for both cycles. Sections 7.4.1 and 7.4.2 explain this behaviour.

Summing the results for each component generated a higher theoretical total CO_2 reduction than was measured when the SAE 8 was used throughout the engine. This difference was due to the change in engine efficiency, with small changes in load, being non-linear. Therefore, the data included in Figure 105 was generated by summing the components' individual contributions to CO_2 reduction and calculating their proportional contributions to the total CO_2 reduction when the SAE 8 was used throughout the engine.

As Chapter 4 anticipates, Figure 105 shows the piston-to-bore conjunction as the dominant contributor to lubricant-related friction on the NEDC and WLTC. The next biggest contributors were from the oil pump, main and big-end bearings, indicating that friction reduction here remains key to lubricant development on both drive cycles.

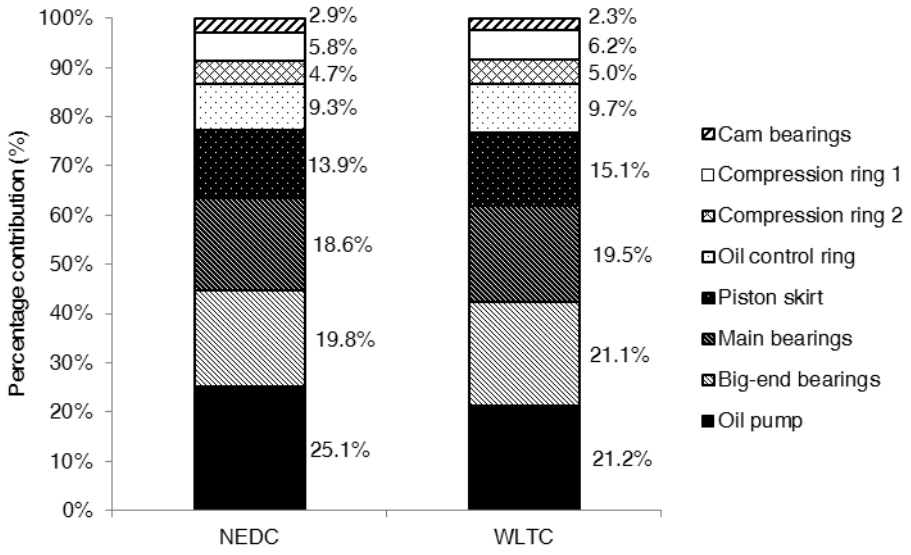

Figure 106. Relative contribution to lubricant-related friction reduction on NEDC and WLTC between SAE 8 and 5W-30 lubricants.

Figure 106 shows the percentage contribution to lubricant-related friction reduction from different engine parts on the NEDC and the WLTC. The contributions from each

component were similar on the two cycles. The benefit from the oil pump reduced, due to the engine's operation at higher speeds toward the end of the cycle when the lubricant viscosity was low. The tests in Chapter 5 showed that the performance of the SAE 8 here was worse at high temperatures and engine speeds.

7.4.1. Calculated valvetrain friction - NEDC

Figure 107 shows the predicted friction during the NEDC for the 5W-30 and SAE 8 in the camshaft lobe-to-tappet contacts; Figure 107 (a) shows the friction contribution from the camshaft lobe-to-tappet; Figure 107 (b) shows the magnitude of boundary friction; Figure 107 (c) shows the variation of lubricant viscosity and engine speed with time in the test.

At the test start, predicted friction in the camshaft lobe-to-tappet contact reduced with the SAE 8 lubricant. Yet, as the SAE 8 viscosity reduced, due to lubricant temperature rise, the simulation predicted that the friction was at times higher than that with the 5W-30 (e.g. after 100 seconds). This behaviour became dominant later in the cycle, indicating that the low viscosity lubricant did not consistently provide friction reduction. The predicted friction for the SAE 8 was high when engine speed was low and oil temperature high, causing high friction at idle conditions. However, when the engine was not idling, the SAE 8 performance was similar to the 5W-30. Thus, an idle-stop system would be likely to reduce the SAE 8's detrimental effects in this valvetrain.

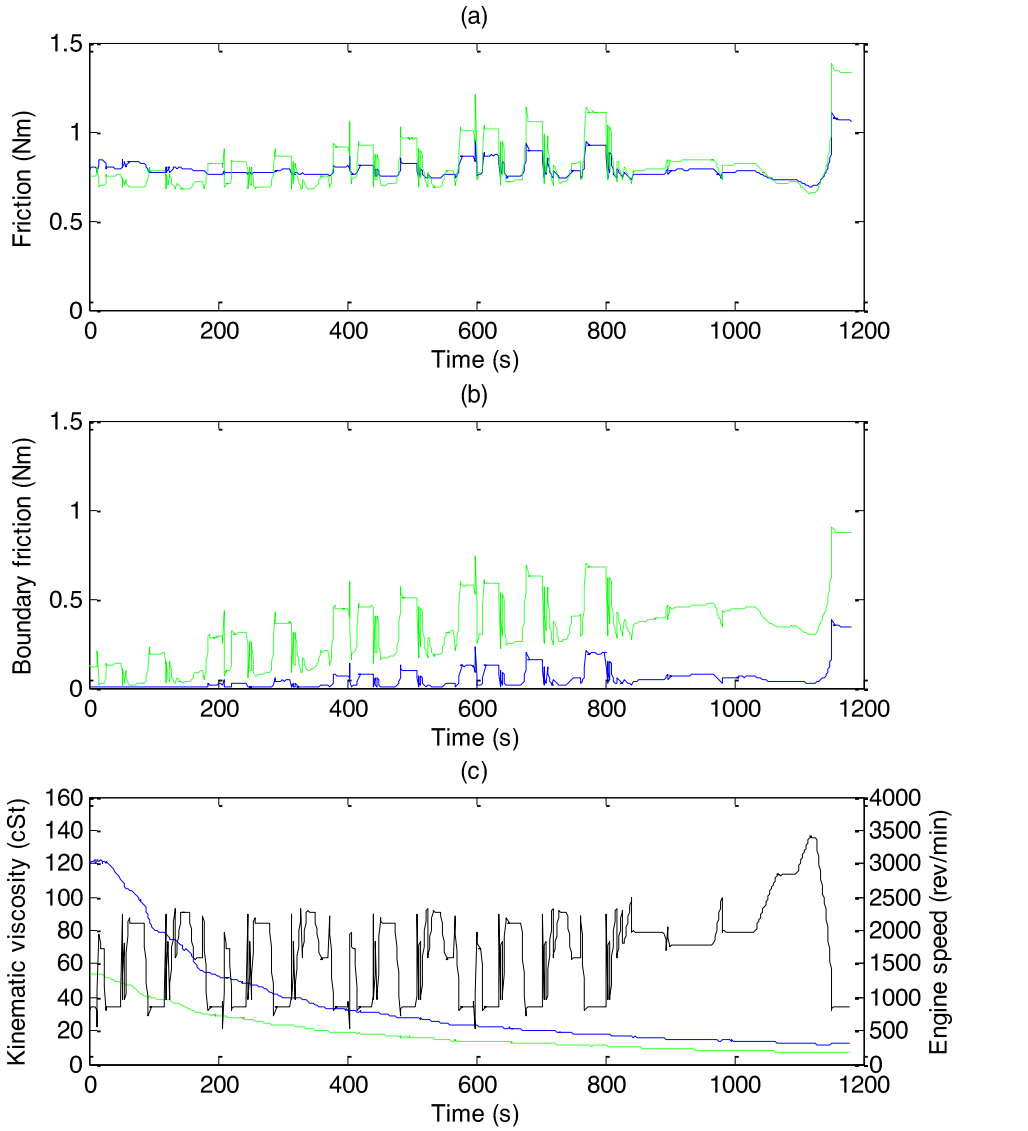

Figure 107(a-c). Valvetrain friction simulation during NEDC. Simulated friction torque at valvetrain (a), contribution from boundary friction to torque (b) and calculated oil viscosity and NEDC road speed (c).

Figure 107 (b) shows high magnitudes of predicted boundary friction with the SAE 8. This loss became dominant as lubricant viscosity reduced and offset the friction reduction from lower hydrodynamic losses. This behaviour explains the change in the SAE 8's performance relative to the 5W-30.

7.4.2. Valvetrain friction – WLTC

Figure 108 shows the predicted valvetrain friction during the WLTC for the 5W-30 and SAE 8. Figure 108 (a) shows the friction contribution from the camshaft lobe-to-tappets, while Figure 108 (b) plots the calculated boundary friction at this

conjunction and Figure 108 (c) shows the variation of lubricant viscosity and engine speed.

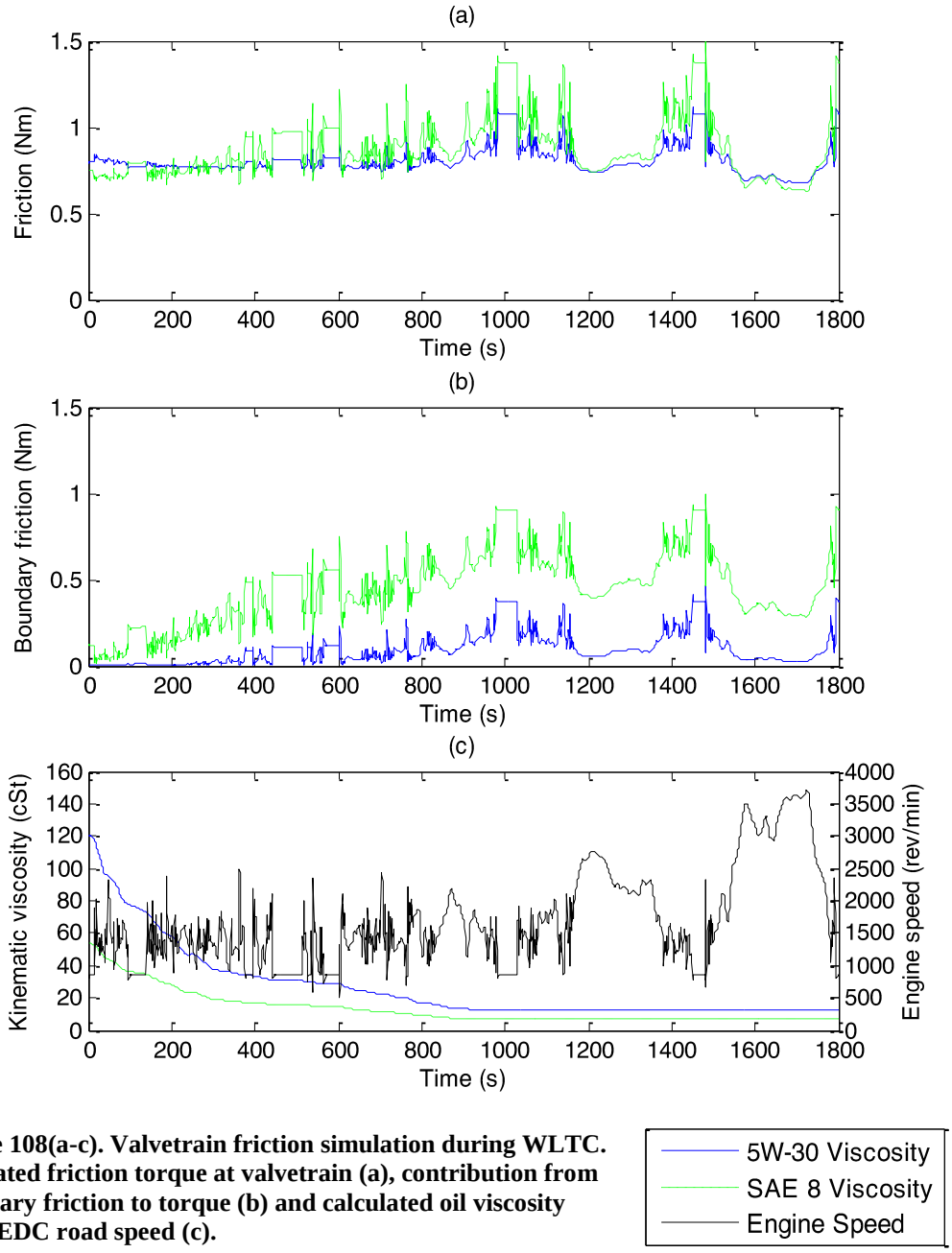

Figure 108(a-c). Valvetrain friction simulation during WLTC. Simulated friction torque at valvetrain (a), contribution from boundary friction to torque (b) and calculated oil viscosity and NEDC road speed (c).

Similar to on the NEDC, the SAE 8 was predicted to increase valvetrain friction from about 100 seconds after the test start on the WLTC. The higher mean temperature on the WLTC caused the SAE 8's performance to be poorer for longer than with the NEDC. However, this cycle's fewer idle periods reduced the SAE 8's detrimental effects. An idle-stop system could provide a theoretical reduction in the SAE 8's

disbenefit, but the contribution would be lower due to the smaller proportion of idling time on the WLTC.

7.4.2.1. Valvetrain summary

The optimum viscosity level for this component was high. Consequently, using a very low viscosity lubricant here was predicted to increase engine friction and CO_2 emissions. However, the net effect of this change was small. Table 36 shows the results from theoretical simulations where the frictional losses for the 5W-30 replaced those for the SAE 8 in the camshaft-to-lobe and tappet contacts. The simulation showed that the SAE 8's poor performance caused a 0.004% CO_2 debit on the NEDC and 0.044% on the WLTC. These results are likely to be within the simulation's error tolerance due to the simplifications made in the model.

Table 36. Reduction in CO_2 emissions caused by using the 5W-30 in camshaft-to-tappet contact in a model otherwise simulating friction using the SAE 8.

Simulation	Drive Cycle	Condition	Reduction in CO_2 emissions
1	NEDC	5W-30 lubricant in camshaft lobe to tappet contact	0.004%
2	WLTC		0.044%

Table 37. Reduction in CO_2 emissions caused by setting boundary friction to zero in the camshaft-to-tappet contact for a model otherwise using simulating friction using the SAE 8.

Simulation	Drive Cycle	Condition	Reduction in CO_2 emissions
1	NEDC	Boundary friction removed form SAE 8 FMEP	0.43%
2	WLTC		0.47%

The results indicate a significant contribution from boundary friction in the camshaft lobe-to-tappet contacts. Theoretically, changing the local lubricant viscosity here could influence this behaviour (e.g. by using base fluids with a higher pressure-viscosity coefficient, film forming additives such as zinc dialkyldithiophosphates (ZDDP) and surface-active viscosity or friction modifiers). An upper-bound estimate of the ability of these approaches to improve the SAE 8's performance was simulated by removing the boundary friction contribution from the total valvetrain friction in the model for this lubricant. Table 37 shows that the SAE 8's

performance can theoretically be improved on the NEDC by 0.43% and on the WLTC by 0.47% using this approach. Thus, these results suggest film-forming and surface-active additives can provide worthwhile contributors to friction reduction in direct acting valvetrains on the NEDC and WLTC. Furthermore, the models indicate that the ability of lubricant additives to reduce CO_2 emissions is greater as the viscosity is reduced, particularly in direct acting valvetrains.

7.4.2.2. Quantifying the benefits of the split-lubrication approach

Nattrass and Davenport [94] investigated a Ford ZETEC engine's response to different lubricant additives and lubricant viscosity changes. They modified the lubrication circuit to allow the cylinder head to operate with a different lubricant to that used in the crankcase. They only present data in hot conditions (93˚C gallery temperature), so it is impossible to understand the net effect of these changes on cold-start drive cycles. They identified significant contributions from boundary regime friction in the valvetrain by measuring FMEP reduction when surface-active additives reduced the boundary friction coefficient. Engine friction modelling (using a proprietary code) validated their findings. No assessment was made to understand if a split-lubrication approach could benefit engine design. However, the present research assesses the value of using a split lubrication system to reduce friction by coupling the predicted contribution from camshaft lobe-to-tappet friction with the losses at the camshaft bearings. Table 38 shows the results.

Table 38. Reduction in CO_2 attributable to cylinder head and crankcase operation on different lubricants.

Simulation	Drive Cycle	Condition	Change in SAE 8 CO_2 benefit
1	NEDC	Valvetrain using 5W-30, crankcase using SAE 8	-0.07%
2	WLTC		-0.01%

A simple split-lubrication design was modelled using the higher viscosity 5W-30 lubricant in the valvetrain and the lower viscosity SAE 8 lubricant in the crankcase.

These simulation results show an increase in overall valvetrain friction. Hence, predicted CO_2 emissions rose by 0.07% on the NEDC and 0.01% on the WLTC. This rise occurred because the hydrodynamic friction increase in the camshaft bearings offset the benefit from reducing the small boundary friction level in the camshaft lobe-to-follower contact. Thus, the benefits of split-lubrication designs are not obvious.

It is still theoretically possible for a split lubrication approach to reduce net friction (e.g. if a tailored valvetrain lubricant causes detrimental behaviour elsewhere in the engine). Theoretically, the additives required to reduce friction in the valvetrain can increase the lubricant's high shear viscosity so a beneficial approach could be to separate the oil circuit to prevent this compromise. Nattrass and Davenport [94] validate this hypothesis experimentally. They reported poor whole engine performance due to using an additive to reduce friction in the valvetrain. Therefore, if an optimum valvetrain lubricant causes detrimental behaviour elsewhere in the engine, a split lubrication approach could reduce overall friction. However, the impact of needing an additional oil pump must be understood to conclude if a net benefit is realisable. This investigation is important because the potential friction reduction contribution of split lubrication systems is small compared to the extra friction required to drive an additional pump for this separate circuit.

7.4.3. Bearing behaviour

The relatively low predicted loads on the NEDC and WLTC meant boundary friction was minimal in the connecting rod bearings for the 5W-30 and SAE 8. In the analysis for the main and camshaft bearings, the mobility method was used, ignoring boundary friction. Thus, the friction predicted by the bearing model was lowest for the SAE 8 in all conditions.

Table 39. Reduction in CO_2 emissions from the baseline attributable to the use of the SAE 8 in the engine bearings.

Drive cycle	Component	Contribution to friction reduction
NEDC	Camshaft bearings	0.08%
	Main bearings	0.52%
	Big-end bearings	0.49%
WLTC	Camshaft bearings	0.04%
	Main bearings	0.40%
	Big-end bearings	0.37%

Table 39 summarises the calculated friction difference between the 5W-30 and SAE 8 in each bearing system. The friction reduction contribution from the main bearings was highest, followed by the big-end bearing and camshaft bearings. This ranking was anticipated since the load in the cycles was low and the model engine included five main bearings but only four big-end bearings. The low friction contribution from the camshaft bearings is partially explained by the lower rotational speed (half engine speed), smaller bearing diameters and assumption of hydrodynamic operation. The overall percentage friction reduction was circa 40% lower with the WLTC owing to the higher mean BMEP in this cycle.

7.4.4. Piston friction

Table 40 summarises the friction difference between the 5W-30 and SAE 8 in each component in the piston assembly. The friction reduction contribution of the SAE 8 from the skirts was highest, followed by the oil control ring, first compression ring and second compression ring.

Table 40. Reduction in CO_2 emissions from the baseline attributable to SAE 8 in piston assembly.

Drive cycle	Component	Contribution to friction reduction
NEDC	1st compression ring	0.15%
	2nd compression ring	0.12%
	Oil control ring	0.24%
	Piston skirt	0.37%
	Total	*0.90%*
WLTC	1st compression ring	0.12%
	2nd compression ring	0.09%
	Oil control ring	0.18%
	Piston skirt	0.29%
	Total	*0.68%*

7.4.5. Piston friction behaviour at low engine speeds

Figure 109 (a) shows the predicted friction in the piston rings and skirt for temperatures from 20˚C to 100˚C and engine speeds from 500 rev/min to 5500 rev/min. Similar to the model behaviour in Chapter 4, FMEP was predicted to become smaller with reducing engine speed at each temperature and that the increase in friction at low speed was not found.

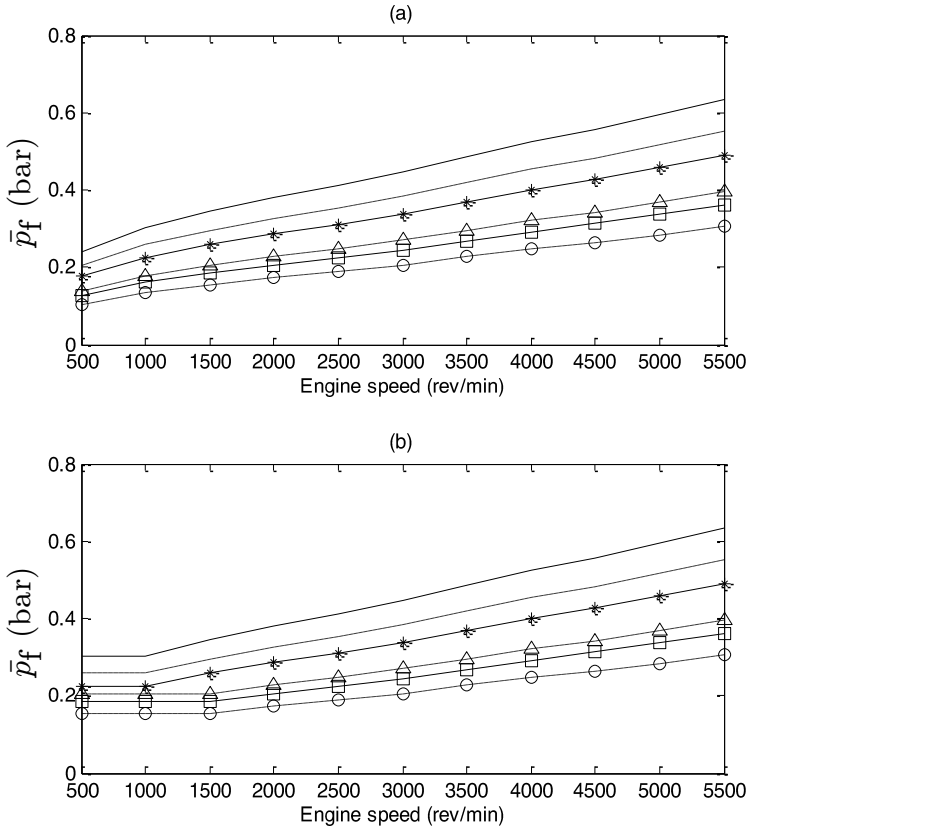

Figure 109. Predicted friction (expressed as mean effective pressure, $\bar{P}_f$) at the piston rings and skirt for 5W-30 at 2 bar BMEP load (a). Modified friction values used in sensitivity study (b).

Modification of the calculated friction magnitudes below 1500 rev/min allowed investigation of the importance of model inaccuracy in this area. Figure 109 (b) shows the modified FMEP values used for the 5W-30. A similar approach calculated modified FMEP values for the SAE 8. By making this change to the model for both lubricants,

drive cycle CO_2 emissions were increased by 0.05% on the NEDC and 0.02% on the WLTC, indicating the impact of the model's incorrect characterisation here is small.

7.4.6. Oil pump

The measured drive torque of the oil pump for the 5W-30 and SAE 8 from Chapter 5 was included in the model. The rig data only included measurements at 20˚C, 90˚C and 120˚C. However, the oil temperatures on both the NEDC and WLTC were below 90˚C. Thus, to permit a simple model to be built, the friction values between 20˚C and 90˚C were calculated by linear interpolation. This simplification should be reviewed when more pump data is available.

The oil flow rates at each engine speed and lubricant viscosity were unknown. Consequently, the flow rate was varied to understand the model's sensitivity to this parameter. In each case the oil flow rate was correlated linearly to oil temperature (e.g. low oil flow rates at 20˚C and high flow rates at 90˚C). The reference case assumed that the 5W-30 operated with an oil flow rate of 5 L/min at 20˚C and 10 L/min at 90˚C. Operation in the low-pressure mode of the lubrication system was simulated, as per the measured performance on the UDDS (see Chapter 5). This assumption may not be valid for the WLTC, but can only be modelled once the pump control strategy has been set.

Table 41. Reduction in CO_2 emissions from the baseline due to different oil pump flow rates.

Drive cycle	Lubricant	Flow rate at 20˚C (L/min)	Flow rate at 90˚C (L/min)	Reduction relative to 5W-30 5 L/min to 10 L/min flow
NEDC	SAE 8	5	10	1.13%
	SAE 8	**5**	**15**	**0.78%**
WLTC	SAE 8	5	10	0.69%
	SAE 8	**5**	**15**	**0.44%**

Table 41 shows the predicted CO_2 reduction due to operating the pump with the SAE 8 and 5W-30 lubricants for a range of flow rates. The model was sensitive to the assumed oil flow rate. Simulating the SAE 8 performance with the same oil flow rate as

the 5W-30 resulted in a 1.13% CO_2 reduction. The dynamometer testing in Chapter 5 indicated that the SAE 8's lower viscosity increased the oil flow rate. Thus, comparing the SAE 8's friction at higher flows is more likely to represent its real performance. Increasing the oil flow rate to 15 L/min at 90˚C caused the CO_2 benefit to reduce to 0.78% on the NEDC and 0.44% on the WLTC. The true variation in oil flow rate in the engine testing work (using the UDDS) was small (e.g. 2 L/min increase for the SAE 8). Thus, the net benefit achievable is likely to sit between these two test conditions. However, further refinement to the model is needed to establish this conclusion unequivocally. The predicted CO_2 reduction for the WLTC was lower than the NEDC, indicating the cycle change contributed to a reduced difference between the lubricants. Chapter 5's hypothesis that low friction lubricants cause friction increase in the oil pump, due to their higher flow rates, was not confirmed in the present research. The improved mechanical efficiency of the pump when using the SAE 8 compensated for the increase in flow. The results indicated that the oil pump contributed to reduced CO_2 emissions when using the SAE 8.

7.4.7. Thermal management – reducing the lubricant mass

Table 32 shows the model results for reducing oil fill volume by 3.1 L (from 5.1 L to 2.0 L) and preheating the lubricant to 90˚C. The simulated results were smaller than found experimentally in Chapter 6.

Table 42. Reduction in CO_2 from the baseline of each lubricant without thermal management.

Drive Cycle	Condition	SAE 8	5W-30
NEDC	3.1 L reduction in lubricant fill	0.10%	0.18%
WLTC		0.06%	0.09%
NEDC	Preheating to 90˚C	0.32%	0.86%
WLTC		0.23%	0.36%
NEDC	367 W additional net alternator power	-5.6%	-5.8%
WLTC	244 W additional net alternator power	-3.2%	-3.1%

Drive cycle CO_2 emissions were predicted to reduce by 0.1% on the NEDC and 0.06% on the WLTC for the SAE 8. The 5W-30's performance was better – CO_2

emissions reduced by 0.18% on the NEDC and by 0.09% on the WLTC. The smaller values here compared to those found in testing are likely to be due to the simplifications in the warm-up model (e.g. SFC map taken at a single temperature). In each modelled condition, the predicted benefit was greater with the 5W-30 lubricant, owing to its higher viscosity and rate-of-change of viscosity than the SAE 8. The higher load and longer length of the WLTC meant the relative predicted performance of each strategy in Table 11 was worse on this cycle.

7.4.8. Thermal management – preheating the lubricant

For the SAE 8, the simulation predicted CO_2 reductions of 0.32% on the NEDC and 0.23% on the WLTC with preheating. In the same conditions, the 5W-30's higher viscosity led to a predicted benefit of 0.86% on the NEDC and 0.36% on the WLTC. Chapter 6, Section 6.1.2.3 calculated the energy required to heat the lubricant to 90˚C was 0.44 MJ. Assuming the battery was depleted by this amount prior to the engine starting, and that no heat loss occurred during the oil warming, an additional alternator load of 367 W is required to recharge the battery in the NEDC. A value of 244 W is required for the WLTC, due to the longer cycle duration. The additional alternator loading required for these charging rates was simulated. The results showed an increase in CO_2 emissions of 5.8% for the 5W-30 and 5.6% for the SAE 8 on the NEDC and 3.1% on the 5W-30 and 3.2% for the SAE 8 on the WLTC. Thus, adopting this approach is unlikely to provide a net CO_2 benefit. Theoretically, a smart charging strategy could reduce this penalty (e.g. by only charging in areas of low SFC). However, the mean brake power required on the NEDC was 5.1 kW on the NEDC and 5.3 kW on the WLTC. Thus, the additional alternator loading (0.66 kW for the NEDC and 0.44 kW for the WLTC) is significant and any smart-charging strategies are unlikely to achieve net friction reduction. Passive approaches, such as insulation, should

be a preferred option, provided the legislative and packaging issues cited in Chapter 6 can be resolved.

7.5. Chapter 7 conclusions and recommendations

A simulation modelled the frictional behaviour of a 5W-30 and a SAE 8 lubricant on cold-start drive cycles using the Mathworks software packages MATLAB and Simulink and Ricardo's V-SIM program. CO_2 emissions were calculated from the predicted fuel consumption. The results from component level friction simulations were added to the torque required to propel the vehicle. A map of the engine's SFC determined the instantaneous fuel consumption rate at this torque. Engine speed was deduced from drive cycle speed traces, using predefined gear change points and a forward-facing driver model.

A Ford ZETEC cylinder head model was used to set the friction contribution from the valvetrain. Engine bearing models were characterised using simulations of the PSA group EP6 1.6 L engine. A fully compliant model of the big-end bearings was used, so that any boundary regime friction in these components due to elastic deformation was included. Models of the main and camshaft bearings assumed hydrodynamic operation. The piston assembly's contribution to friction was calculated using a semi-empirical model based on the same PSA group EP6 1.6 L engine. Losses in the oil pump were taken from the Ford 1.0 L EcoBoost engine using the empirical measurements in Chapter 5.

The simulated vehicle CO_2 emissions were 153.3 gCO_2/km and 149.1 gCO_2/km for the 5W-30 and SAE 8 respectively on the NEDC and 148.0 gCO_2/km and 145.1 gCO_2/km for the SAE 8 on the WLTC. Setting the friction calculations to zero in the model predicted the relative magnitude of CO_2 emitted to overcome friction. The

model predicted friction-related CO_2 emissions were 8.7% on the NEDC and reduced to 6.3% on the WLTC.

The simulation predicted that an SAE 8 lubricant would provide an overall CO_2 reduction compared to the same cycle using a 5W-30. The SAE 8 reduced emissions by 2.8% on the NEDC and 1.9% on the WLTC. The smaller benefit on the WLTC indicates that engineers and chemists should expect the contribution of friction reduction from low friction lubricants to reduce on this cycle. A component-level analysis indicated that the percentage contributions to friction reduction from each engine area were broadly the same on both cycles. A small reduction in friction contribution from the oil pump was predicted, due to the longer duration of operation at high oil temperatures on the WLTC.

Investigating the SAE 8's performance in the valvetrain showed friction was not always lower with this lubricant. Friction increased under the conditions of high oil temperature, due to the reduced viscosity, and low engine speed. A significant contribution from boundary regime friction caused this effect, because the oil viscosity was too low to prevent part of the contact load being reacted by asperity-to-asperity interaction. Investigations showed that the addition of film-forming additives (or other additives capable of reducing friction in the boundary contact conditions) could achieve 0.4% further benefit from the SAE 8 in the NEDC and 0.5% on the WLTC, if they eliminate the boundary friction. The high contribution of friction during engine idle periods indicated that idle-stop systems (now commonplace) could reduce the SAE 8's negative friction performance in the valvetrain, if these two technologies were co-adopted.

The model assessed the potential benefit of separating the valvetrain and main engine lubrication circuits. Using a 5W-30 lubricant in the valvetrain and the SAE 8 in

the crankcase caused a net CO_2 increase. However, the use of a split-lubrication approach is worthy of further research (e.g. if valvetrain-specific lubricants are developed, since these could cause detrimental performance elsewhere in the engine). The net effect including additional oil pumps was not studied, but would be essential to assessing the merits of split-lubrication.

The model uses a direct acting valvetrain. High levels of boundary friction occur in this design due to the sliding nature of the contact. The model's extension to represent the behaviour of low friction follower coatings (e.g. diamond-like-carbon) or to test the roller-finger-followers valvetrains many passenger cars use would be useful. Including this valvetrain design in the model would likely alter the predicted performance of this engine area, as overall valvetrain friction may reduce [100].

The big-end bearing model did not show any significant contribution from boundary friction in either drive cycle. Hence, friction was reduced by lowering the lubricant viscosity. Boundary friction was ignored in analysing the main and camshaft bearings. Thus, lowering lubricant viscosity reduced the friction here.

The simulation indicated that the friction reduction at the piston-to-liner conjunction contributed 0.9% of the total reduction on the NEDC and 0.7% on the WLTC. It was impossible to separate the contributions to FMEP from boundary and hydrodynamic friction, as the model did not calculate these separately. The tool's development to use the piston friction simulation from Chapter 4 is recommended for further research.

The piston friction model did not predict the upturn in FMEP at low engine speeds measured using Chapter 4's motored rig test. A simulation run assessed the importance of this inaccuracy as being circa 0.05% on the NEDC and 0.02% on the WLTC.

The model predicted that the VDOP contributed 0.8% to the friction reduction on the NEDC and 0.4% on the WLTC. The limited data points from the experimental phase and the lack of true oil flow rates and pressures means further work is needed to characterise the pump performance unequivocally. Thus, the validity of these results should be confirmed once this extra data is available.

The oil temperature traces during warm-up were varied to be consistent with the values in Chapter 6. This change allowed the model to simulate the effect on CO_2 emissions from varying lubricant mass. When the SAE 8 was used with a 3.0 L reduced oil fill, the model predicted a CO_2 reduction of 0.1% on the NEDC and 0.06% on the WLTC. Using the 5W-30 increased these values to 0.2% and 0.1%. The lower predicted benefit from this simulation was due to the simplifications made to characterise engine warm-up. Developing the model to include a subroutine to predict the engine temperature rise at each component is recommended for further research. An understanding of the variation in specific fuel consumption during the warm-up process is also needed to improve the model fidelity.

The simulation predicted the contribution to friction reduction from lubricant preheating. The largest CO_2 reduction was 0.9%, when the 5W-30 was preheated and run on the NEDC. Preheating the lubricant using electrical energy from the vehicle battery, then replenishing this during the test cycles, showed that CO_2 emissions increased by circa 5% on the NEDC and 3% on the WLTC due to the high alternator load. Thus, it is recommended that lubricant preheating be achieved by storing the lubricant temperature using an insulated reservoir.

7.5.1. Key findings

- The model predicted that the opportunity for lubricants to lower friction reduced by 28% when using the WLTC compared to the NEDC.

- Valvetrain friction increased when using an SAE 8 under the conditions of high oil temperature and low engine speed, owing to increased boundary friction compared to a 5W-30. An incremental 0.4% benefit from the SAE 8 in the NEDC and 0.5% on the WLTC could be achieved by lowering its boundary regime friction magnitude in the (direct acting) valvetrain.
- The simulation indicated that when moving from an SAE 8 to a 5W-30: friction reduction at the piston-to-liner conjunction contributed 0.9% of the total reduction on the NEDC and 0.7% on the WLTC, and a variable displacement oil pump contributed 0.8% to the friction reduction on the NEDC and 0.4% on the WLTC.

8. Conclusions

Low friction lubricants continue to provide manufacturers with a cost-efficient contribution to the reduction of vehicle CO_2 emissions. The absolute magnitude of the benefit that can be achieved remains small compared to other technologies. However, engine designers must combine the improvements of several technologies to meet their targets and, thus, reducing CO_2 by addressing engine friction is worthwhile.

Lowering the lubricant viscosity grade offers the easiest potential route to CO_2 reduction. Recently, SAE J300 (the classification defining lubricant viscosity grades) was updated to include low viscosity SAE 16, 12 and 8 grades. These changes facilitated the introduction of new low friction lubricants to the marketplace.

By showing how the lubricant properties affect the performance of both individual components and the whole engine system, this study highlighted the importance of developing the lubricant and engine alongside one another. Lubricant specification controlling bodies continue to focus on lowering fuel consumption and CO_2 emissions using outdated test procedures and old engine technologies (e.g. with first productions of some standard test engines dating back 10 to 20 years). This practice presents a challenge and co-engineering presents a viable solution. Development engineers are free to market lubricants not governed by specifications and, by co-engineering tailored lubricants with manufacturers, high performance levels are achievable.

Some researchers have used co-engineering successfully. However, their approaches rely on empiricism based on expensive test programmes (e.g. mounting an engine to a dynamometer and running hundreds of tests). This process is time-inefficient and makes it difficult for the scientist to understand why a lubricant's composition achieves low friction. Moreover it may be holding back low friction

lubricant development, since the contribution to friction reduction (or increase) from different engine subsystems is not known.

Lowering viscosity causes some components to transition into higher friction areas of the Stribeck curve (e.g. boundary contact), but the possibility exists for this process to occur whilst the friction for the engine as a whole reduces. This behaviour is hard to detect and, once significant friction increase occurs, may be attributed to the identification of the engine's optimum viscosity grade. Understanding the engine's behaviour in more detail provides the opportunity to improve its performance by locating these components and co-engineering the lubricant and engine to permit operation with lower viscosities. This study has shown the benefits which can be achieved by using this philosophy.

Modern tribological simulations are able to predict the friction occurring between lubricated engine surfaces. Engineers use these models during engine design, but few use them to design lubricants. The present research shows the power of using engineering models, combined with rig, engine and chassis dynamometer tests to understand low friction lubricant performance. The knowledge gained within the present investigation will help to engineer the next generation of lubricants and the model informs the design requirements for new engines.

A full vehicle model, built in Simulink, determined the contribution to CO_2 reduction achieved by using a SAE 8 engine lubricant compared to a 5W-30 on drive cycles. Chapter 7 described this work. Research dedicated to characterising the key engine subsystems defined the inputs to this model. This work included building tribological models of the bearings (Chapter 3) and pistons (Chapter 4). A rig test determined the behaviour of a variable displacement oil pump (Chapter 5) and opportunities for lubricant thermal management were investigated using a chassis

dynamometer (Chapter 6). The lubricants' behaviours were assessed using each sub-model prior to the vehicle level simulations.

Low friction lubricant performance in hydrodynamic bearings was evaluated using a detailed bearing model. A review of existing literature determined the factors considered in the model's construction. Parametric studies based on the lubricants' non-Newtonian viscosity characteristics investigated the correlation with friction. An isoviscous lubricant with a viscosity of 4.6 cSt achieved the minimum friction in the bearing. By starting with lubricants with kinematic viscosities higher than this value it was possible to improve lubricant performance by lowering viscosity index (VI) and introducing shear-thinning. Conversely, lubricants with lower starting viscosities required higher VI values and more shear-stable lubricants.

The model predicted high oil film pressures (e.g. 117 MPa), which caused the lubricant viscosity to increase locally by 300% due to piezo-viscosity effects. Thus, the lubricants' different piezo-viscosity coefficients were characterised and used to show that friction could be reduced where the lubricant's starting viscosity was below the bearing's optimum value. A review of existing research indicated that lubricant engineering using piezo-viscosity effects in conformal bearings was novel.

Similar research established that changing the lubricant density correlated with bearing friction changes. Raising the lubricant density increased the lubricant's dynamic viscosity (for a given kinematic value) and caused the effects discovered. This correlation was undocumented in existing research. Manipulating the density of the base oil (e.g. including using non-standard, high density, fluids such as polyalkylene glycols) are a practical way of achieving this lubricant engineering benefit.

The calculations underpinning the VI test method were discovered to provide misleading results for the SAE 16 and lower viscosity grades. However, a review of

existing literature indicates that researchers continue to use this metric to interpret the performance of low friction lubricants. The prevailing trend is the specification of lower viscosity lubricants. Thus, the discoveries made in the present research are relevant and important. Using the lubricant viscosity at the start of the test (e.g. its kinematic viscosity at 20˚C) was a suitable alternative to VI.

Friction in the piston-to-bore conjunction was investigated using a tribological model and motoring rig test. The model correctly predicted the friction magnitudes for 0W-20 and SAE 8 lubricants. The thermal boundary conditions specified changed the results (but not the lubricant's rankings) significantly. An increase in friction was measured at low engine speeds (e.g. below 1200 rev/min), but this was not predicted by the model. The root cause of this inaccuracy was investigated using a ring-on-liner tribometer. The friction coefficients identified in this testing did not account for the differences between the simulated and measured friction at low speed. Thus, a more fundamental error in the model's characterisation of boundary friction was identified.

The piston friction model's characterisations were complex and computationally intensive – achieving a robust model required comprehensive empirical validation. Even with the detailed work completed in the present research, differences between the measured and simulated friction levels existed. Consequently, a simplified model was used in the vehicle simulations conducted in Chapter 7.

A rig test determined the behaviour of a modern oil pump with 5W-30, 0W-20 and SAE 8 lubricants. The vane-type variable displacement oil pump (VDOP) from the Ford 1.0 L EcoBoost engine was used. A potentially antagonistic interaction between this pump's control system and low viscosity lubricants was identified, since engine designers specify a target for the oil gallery pressure when using VDOPs. Thus, lowering the viscosity causes the VDOP to operate at higher flow rates to satisfy their

pressure requirements. Analysis indicated that this interaction could increase pump parasitic power demand when using low viscosity lubricants, because equivalent gallery pressure is achieved with greater oil flow. This interaction was undocumented in existing research and warranted investigation.

Rig testing established that the pump's total efficiency increased as the lubricant viscosity was lowered. This improvement was prevalent at low temperature (where the viscosity differences between the lubricants was greatest). Engine testing determined the differences in flow rate occurring during a cold-start urban-style driving cycle. Whether the pump contributed to friction reduction or increase depended on the temperature and oil flow rate. The results from this pump testing were built into the vehicle-level model described in Chapter 7 to allow its predicted performance on the New European Drive Cycle (NEDC) and World-wide harmonized Light duty Test Cycle (WLTC) to be understood. The improved mechanical efficiency of the pump when using the SAE 8 compensated for its increased flow rate and the results indicated that the oil pump contributed to reduced CO_2 emissions when using this lubricant.

Lubricant thermal management systems were investigated during the dynamometer testing in Chapter 6. The cold-starts used in the NEDC and WLTC caused the lubricant viscosity to be much higher (10 to 20 times) than its value when the engine is fully warmed-up. This viscosity increase caused a concomitant increase in lubricant related engine friction. A review of existing literature indicated that the opportunities arising from managing the lubricant thermal mass required updating.

Chassis dynamometer tests established the correlation between CO_2 emissions and the volume of oil in the engine. Reductions in CO_2 emissions between 0.4% and 1.2% were achieved on the NEDC by lowering the oil volume from 5.1 L to 2.1 L. However, the poor repeatability of the testing did not allow these results to be separated from

those of the unperturbed case to greater than 95% statistical certainty. Heating the engine oil remotely and adding this to a cold vehicle prior to test start allowed investigation of the opportunities offered from lubricant preheating. CO_2 reductions of between 0.4% and 1.0% were identified, using a cold-start NEDC with 5W-30 preheated to 60˚C and 90˚C respectively. A significant oil temperature loss between the sump and the engine components was found using a thermocouple placed in the cylinder head drain-back path. The recordings from this probe along with probes placed on the engine block led to the conclusion that lubricant thermal management strategies primarily increase the base engine temperature (and, thus, decrease friction). The oil pump temperature was not measured, but its friction is likely to be more acutely affected by lubricant preheating since it is proximal to the sump.

The performance of a novel external oil reservoir was simulated to understand its insulation properties. The model assumed that a fluid management system removed hot lubricant from the engine following engine running. The model predicted the temperature loss from the reservoir during the mandated 6-hour soak periods of the NEDC and WLTC. An oil temperature of 65˚C at the end of the soak period following a prior test was achieved by installing insulation to the reservoir and indicated a method to achieve the preheating CO_2 benefits identified.

The subsystem models, rig, engine and dynamometer tests were incorporated into a whole vehicle simulation in Chapter 7. The model predicted that an SAE 8 lubricant reduced CO_2 emissions by 2.8% on the NEDC and 1.9% on the WLTC. The contribution of different subsystems to these values was assessed at a component level so it was possible to understand how the SAE 8 achieved its benefits. This form of quantification of the CO_2 reduction was novel and provided insight impossible to gain by following the traditional co-engineering processes.

The simulation was used to complete a theoretical investigation where the friction contributions from the engine components were set to zero, allowing the magnitude of CO_2 attributable to lubricant-related friction to be understood. The model predicted lubricant-related CO_2 emissions were 8.7% on the NEDC and reduced to 6.3% on the WLTC. These results indicate that the planned adoption of the WLTC in September 2017 will reduce the potential contribution to CO_2 emission reduction from lubricants by 28%.

A direct-acting valvetrain model (built outside the present research) was included in the vehicle simulation. The SAE 8 lubricant's friction in this system was not always lower than recorded using the 5W-30 lubricant. High contributions from boundary friction indicated that the use of additives capable of changing the tribofilms here could achieve up to 0.5% further CO_2 reduction with the SAE 8.

8.1.1. Key findings:

- The thesis establishes that lubricant engineering provides a viable method to inform the development of lubricants that can reduce CO_2 emissions in drive cycles.
- Deficiencies in the calculation of the Viscosity Index (VI) method were uncovered. Limitations for its use when developing low friction lubricants were established and a viable alternative method was proposed.
- A simulation model established the engine components' contributions to CO_2 emissions reduction caused by lowering the lubricant viscosity grade from 5W-30 to SAE 8 in the NEDC and WLTC.

9. Recommendations for further work

The present research establishes the viability of a combined modelling and testing approach to lubricant engineering. During the investigation, opportunities to improve the models further have been identified:

1. A review of existing literature was unable to identify any correlation studies between simulated and measured bearing friction. Further study dedicated to this area (e.g. model validation using a bearing friction rig) would provide worthwhile validation of the model's output.
2. Shear rates between the first and second Newtonian regimes were identified in the bearing model in Chapter 3. Comparing the behaviour of different viscosity modifiers between these shear rates would provide useful insight to establish if their performance differences here are significant.
3. A higher fidelity approach to simulating the heat flows in Chapter 3's bearing model would improve its accuracy. Theoretically, this development would also allow lubricant engineering to focus on the impact of polymer-coated bearings and their changes in bearing heat transfer.
4. Improvement of Chapter 4's piston model requires the addition of surface temperature sensors into the test engine to define the test's thermal boundary conditions more robustly.
5. The significant run times, complexity and need to validate at each condition precluded using the piston model in the vehicle simulation. Development of this model is recommended since it would allow the contribution from boundary friction in the cycle (and the opportunity for lubricant additives to reduce it) to be understood. A research programme focused on this activity is likely to require significant resources. Extension of this model to account for engine load changes should also be undertaken.

6. A friction increase at low engine speeds (below 1200 rev/min) indicated that Chapter 4's characterisation of piston friction here was inaccurate. The vehicle model established the impact of this error was small. However, research is needed to establish the root of this miscalculation since the model cannot reliably predict the contributions of boundary friction on drive cycles until this issue has been resolved.
7. The pump testing discussed in Chapter 5 established the performance of 5W-30, 0W-20 and SAE 8 lubricants. A greater number of temperatures, along with smaller increments in flow rate and outlet pressures should now be characterised to allow the behaviour of this pump in drive cycles to be established unequivocally.
8. Extension of the programme to include characterisation of other pumps, such as external gear and trochoidal designs, would allow assessment of pump specific attributes to be disentangled from those applicable more generally.
9. Chassis dynamometer testing in Chapter 6 was unable to determine the contributions to CO_2 emission reduction attributable to various lubricant thermal management systems to 95% statistical confidence. Repeating the tests using an engine dynamometer should improve the test accuracy and is recommended for future study. Care must be taken with this approach to ensure that the test conditions are thermodynamically similar to the vehicle (e.g. selecting appropriate test cell ventilation fan speeds, correct installation of test bed cooling systems, and incorporating a representative gearbox).
10. The transferability of the measurements found in the present research to other engine designs is unknown (e.g. those including integrated exhaust manifolds, lower engine masses, stop-start systems and active thermal management

systems). A research programme dedicated to investigating these effects with a greater number of vehicles would provide valuable insights.

11. The temperature rise existing when the engine warms-up was input to the simulation, using measured values. Thus, these values were not affected by predicted friction changes. Extending the model to include a thermal simulation would allow the effect of changing engine friction to be included in the model (e.g. slower rates of warm-up when friction is reduced) and would allow novel insight into the significance of this interaction. However, it is recognised that full characterisation of engine warm-up in a vehicle drive cycle is challenging.

The inclusion of the items identified above would improve the fidelity of the overall approach used in this study. Extending the simulation to include other engine designs (e.g. a selection of valvetrain, piston and bearing systems) would allow its use in predicting the impact of different technology changes on the lubricant's ability to reduce CO_2. This capability would provide important insight for co-engineering discussions and could focus engineers' research to develop low friction lubricant and engine designs.

10. References

[1] Davison, E. and Haviland, M., "Lubricant Viscosity Effects on Passenger Car Fuel Economy," SAE Technical Paper 750675, 1975.

[2] Tanaka, H., Nagashima, T., Sato, T., and Kawauchi, S., "The Effect of 0W-20 Low Viscosity Engine Oil on Fuel Economy," SAE Technical Paper 1999-01-3468, 1999, doi:10.4271/1999-01-3468.

[3] Manni, M. and Florio, S., "An Experimental Evaluation of the Impact of Ultra Low Viscosity Engine Oils on Fuel Economy and CO2 Emissions," SAE Technical Paper 2013-01-2566, 2013, doi:10.4271/2013-01-2566

[4] Tamoto, Y., Kido, M., and Murata, H., "Possibilities of Ultra Low Viscosity Fuel Saving Gasoline Engine Oil," SAE Technical Paper 2004-01-1936, 2004, doi:10.4271/2004-0

[5] An, F., Gordon, D., He, H., Kodjak, D., Rutherford, D. "Passenger Vehicle Greenhouse Gas and Fuel Economy Standards: A Global Update," The ICCT. 2007. Accessed 09-08-2016. Available from: http://www.theicct.org/sites/default/files/publications/PV_standards_2007.pdf

[6] King, J. "The King review of low-carbon cars, Part I: the potential for CO2 reduction," HM Treasury. 2007. ISBN-13: 978-1-84532-335-6.

[7] Seeman, M., Lauterwasser , F., Smolenski , D., Liu, B. "Megatrend Fuel Economy: How to Optimize Viscosity with VI Improvers," 24th Aachen Colloquium Automobile and Engine Technology 2015.

[8] Ernst, C.S., "CO2 Reduction potentials for passenger cars until 2020," Management Summary 113510, Institute fur Kraftfahrzeuge, Aachen December 2012.

[9] Taylor, R. I., Coy, R. C., "Improved fuel efficiency by lubricant design: a review," 1999. Proc Instn Mech Engrs Vol 214 Part J. J01499.

[10] Gangopadhyay, A., Sorab, J., Willermet, P., Schriewer, K. et al., "Prediction of ASTM Sequence VI and VIA Fuel Economy Based on Laboratory Bench Tests," SAE Technical Paper 961140, 1996, doi:10.4271/961140.

[11] Taylor, R., Brown, M., Thompson, D., and Bell, J., "The Influence of Lubricant Rheology on Friction in the Piston Ring-Pack," SAE Technical Paper 941981, 1994, doi:10.4271/941981.1-1936.2010-01-2286.

[12] Bickerstaffe, S., "By the numbers," Automotive Engineer, January-February 2012. Pg 18-19.

[13] Unattributed. "Rewriting the formulation rule book," Available from www.shell.co.uk. Accessed 10/August/2016.

[14] Covitch, M., Brown, M., May, C., Selby, T. et al., "Extending SAE J300 to Viscosity Grades below SAE 20," SAE Int. J. Fuels Lubr. 3(2):1030-1040, 2010, doi:10.4271/2010-01-2286.

[15] SAE J300 Jan 2015. "Engine Oil Viscosity Classification," SAE International, 400 Commonwealth Drive, Warrendale, PA 15096-0001, USA. Available at www.sae.org

[16] Stribeck R., "Die wesentlischen Eigenschaften der Gleit- und Rollenlager," Zeitschrift des Vereines deutscher Ingenieure 1902; 46(37):1341-1348 (pt I).

[17] Stambaugh, R.L. and Kinker, B.G. “Chapter 5: Viscosity Index Improvers and Thickeners,” Chemistry and Technology of Lubricants, 3rd edn., Pages 153-183. C Springer Science+Business Media B.V. 2010. Doi: 10.1023/b105569_5

[18] ACEA “European Oil Sequences,” 2012. Available at www.acea.be. Accessed 12-2014.

[19] Engine Oil Licensing and Certification System. API 1509 Seventeenth edition, September 2012. Available at www.api.org. Accessed 6-8-2015.

[20] Taylor, R.I., Mainwaring, R., Mortier, R.M. “Engine lubricant trends since 1990,” Proceedings of the Institution of Mechanical Engineers, Part J: Journal of Engineering Tribology. Volume 219. Issue 5. Pages 331-346

[21] ASTM D7589-10, “Standard Test Method for Measurement of Effects of Automotive Engine Oils on Fuel Economy of Passenger Cars and Light-Duty Trucks in Sequence VID Spark Ignition Engine,” American Society for Testing and Materials, 2010.

[22] CEC L-54-T-96, “Fuel Economy Effects of Engine Lubricants (MB M111 E20),” the Coordinating European Council, 2008.

[23] Taylor, R.I., “Engine friction: the influence of lubricant rheology,” 1997. Proceedings of the Institution of Mechanical Engineers, Part J: Journal of Engineering Tribology. Volume 211. Issue 3. Pages 235-246.

[24] Devlin, M., Lam, W., and McDonnell, T., "Critical Oil Physical Properties that Control the Fuel Economy Performance of General Motors Vehicles," SAE Technical Paper 982503, 1998, doi:10.4271/982503.

[25] Moore, A., "Influences of Lubricant Properties on ASTM Sequence VI and Sequence VI-A Fuel Efficiency Performance," SAE Technical Paper 961138, 1996, doi:10.4271/961138.

[26] Styer, J. and Guinther, G., "Fuel Economy Beyond ILSAC GF-5: Correlation of Modern Engine Oil Tests to Real World Performance," SAE Int. J. Fuels Lubr. 5(3):1025-1033, 2012, doi:10.4271/2012-01-1618.

[27] Kamil, M., Rahman, M, M., Bakar, R, A., “An integrated model for predicting engine friction losses in internal combustion engines,” International journal of automotive and mechanical engineering. Volume 9. Page: 1695-1708. 2014.

[28] Shimada, Y., Abou, S., Okita, K., and Chuubachi, M., "Development of Friction Prediction Procedure and Friction Reduction Technologies for New Nissan HR and MR Engines," SAE Technical Paper 2006-01-0618, 2006, doi:10.4271/2006-01-0618.

[29] Shayler, P., Christian, S., and Ma, T., "A Model for the Investigation of Temperature, Heat Flow and Friction Characteristics During Engine Warm-Up," SAE Technical Paper 931153, 1993, doi:10.4271/931153.

[30] Goenka, P., Paranjpe, R., and Jeng, Y., "FLARE: An Integrated Software Package for Friction and Lubrication Analysis of Automotive Engines - Part I: Overview and Applications," SAE Technical Paper 920487, 1992, doi:10.4271/920487.

[31] Patton, K., Nitschke, R., and Heywood, J., "Development and Evaluation of a Friction Model for Spark-Ignition Engines," SAE Technical Paper 890836, 1989, doi:10.4271/890836.

[32] Sandoval, D. and Heywood, J., "An Improved Friction Model for Spark-Ignition Engines," SAE Technical Paper 2003-01-0725, 2003, doi:10.4271/2003-01-0725.

[33] Thring, R., "Engine Friction Modeling," SAE Technical Paper 920482, 1992, doi:10.4271/920482.

[34] Crane, M. and Meyer, R., "A Process to Predict Friction in an Automotive Valve Train," SAE Technical Paper 901728, 1990, doi:10.4271/901728.

[35] Dowson, D. and Higginson, G.R., "Elastohydrodynamic Lubrication, SI Edition," Pergamon Press, Ltd., Oxford, England, 1977, pp. 55.

[36] Goenka, P.K., Meernik, P.R., "Lubrication Analysis of Piston Skirts," SAE Technical Paper 920490, 1992.

[37] Taylor, R. I., Coy, R. C., "Improved fuel efficiency by lubricant design: a review," 1999. Proc Instn Mech Engrs Vol 214 Part J. J01499.

[38] Taylor, I., "Lubrication, Tribology & Motorsport," SAE Technical paper.2002 doi:2002-01-3355

[39] Ma, H., Dixon, R., Mainwaring, R., "Innovations in Fuel Economy and Sustainable Road Transport: Demonstrating the fuel economy potential of passenger car motor oils," (C1321/006). Woodhead Publishing Limited. IMechE 01/01/2012: pp 89-69

[40] ASTM D5293, "Standard Test Method for Apparent Viscosity of Engine Oils and Base Stocks Between –10 °C and –35 °C Using Cold-Cranking Simulator," Available at https://www.astm.org/Standards/D5293. Accessed 11-5-2015.

[41] ASTM D445, "Standard Test Method for Kinematic Viscosity of Transparent and Opaque Liquids (and Calculation of Dynamic Viscosity)," Available at https://www.astm.org/Standards/D445.htm. Accessed 11-5-2015.

[42] ASTM D4683, "Standard Test Method for Measuring Viscosity of New and Used Engine Oils at High Shear Rate and High Temperature by Tapered Bearing Simulator Viscometer at 150 °C," Available at: https://www.astm.org/Standards/D4683. Accessed 11-5-2015.

[43] Private communication with the SAE J300 steering committee. 1-5-2012.

[44] Zuidema, H. H. "The performance of lubricating oils," Second Edition. pp 34-38, Reinhold publishing corp. New York 1959

[45] Zammit, J.P., Shayler, P.J. and Pegg, I., "Thermal Coupling and Energy Flows between Coolant, Engine Structure and Lubricating Oil during Engine Warm-up," IMechE/ SAE Int Conf VTMS 10, Paper C1305/053, 2011.

[46] Shayler, P., Christian, S., and Ma, T., "A Model for the Investigation of Temperature, Heat Flow and Friction Characteristics During Engine Warm-Up," SAE Technical Paper 931153, 1993, doi:10.4271/931153.

[47] Cross, M., M., "Rheology of non-Newtonian fluids: a new flow equation for pseudo plastic systems," Journal of Colloid Science. 1965, 20, Pages 417-437.

[48] Zakarian, J., "The Limitations of the Viscosity Index and Proposals for Other Methods to Rate Viscosity-Temperature Behavior of Lubricating Oils," SAE Int. J. Fuels Lubr. 5(3):1123-1131, 2012, doi:10.4271/2012-01-1671.

[49] ASTM D2270-10 “Standard Practice for Calculating Viscosity Index from Kinematic Viscosity at 40 °C and 100 °C,” Available at: https://www.astm.org/Standards/D2270.htm.Accessed 7-3-2011.

[50] Manning, J., “Internal combustion engine design,” 2012 Ricardo Uk Limited. Print ISBN 978-0-9573292-0-1.

[51] Harnoy, A., “Bearing Design in Machinery,” Engineering Tribology and Lubrication. 2003 Marcel Dekker Inc. Print ISBN: 978-0-8247-0703-3

[52] Zhang, X.J., Gui, C.L. “An intelligent system for Tribological Design in Engines,” Elsevier 2004. Print ISBN 0 444 51756 1.

[53] Carden, P., “Survey of bearing technology: Main and Big-end bearings for gasoline passenger car engines,” BP internal report. RD.11/113901.2. 2011.

[54] Reynolds, O., “On the theory of lubrication and its application to Mr. Beauchampt Ower's experiments, including an experimental determination of the viscosity of Olive Oil,” Philosophical Transactions of the Royal Society of London, Vol. 177 (1886), pp. 157-234.

[55] Booker, J. F., “Dynamically Loaded Journal Bearings: Mobility Method of Solution,” J. Basic Eng 87(3), 537-546 (Sep 01, 1965). doi:10.1115/1.3650602

[56] Gulwadi, S. and Shrimpling, G., "Journal Bearing Analysis in Engines Using Simulation Techniques," SAE Technical Paper 2003-01-0245, 2003, doi:10.4271/2003-01-0245.

[57] Stachowiak, G.W., and Batchelor, A.W. “Engineering Tribology,” Fourth Edition. Saint Louis, US: Butterworth-Heinemann, 2013.

[58] Taylor, O., “Taiho bearings rig testing phase I,” BP internal report. GLT-230111

[59] Mishra, P.C. and Rahnejat, H., “Tribology of big end bearings,” in Rahnejat, H (Ed.), Tribology and dynamics of engine and power train, Woodhead Publishing, Cambridge, UK, 2010 ISBN: 978-1-84569-361-9

[60] Galera, L., Souza Rodrigues, A., "Optimization of Lemon Shape Big End Profile Connecting Rod under Engine Operation in Elastohydrodynamic Regime," SAE Technical Paper 2014-36-0309, 2014, doi:10.4271/2014-36-0309.

[61] Uehara, S. and Peixoto, V., "Influence of Surface Finishing on Bearing Performance," SAE Technical Paper 2006-01-2893, 2006, doi:10.4271/2006-01-2893.

[62] Choi, J., Kim, S.S., Rhim, S., Choi, J.H., “Numerical model of journal bearing lubrication considering a bending stiffness effect,” Journal of vibroengineering. September 2012. Volume 14, issue 3. Section 824. ISSN 1392-8716

[63] Conway-Jones, J. M., Martin F. A., and Gojon R., “Refinement of engine bearing design techniques,” Tribology International, 24 (2), 1991, pp. 119-127

[64] Knoll, G., Umbach, K., “Lubricant effect on mixed friction of slide bearings,” MTZ Worldwide, Mar 2010, pp48-53.

[65] Knoll, G. “Simulations- und versuchsgestütztes Auslegungsverfahren hoch beanspruchter Motorgleitlager,” MTZ worldwide. October 2007, Volume 68, Issue 10, pp 18-20

[66] Chittenden, J, R., “Measurement of bearing surface parameters for crank pin and shells.” University of Leeds, School of Mechanical Engineering. Order number: STC245682, Job reference: RD0033RJC. September 2010.

[67] Greenwood, J.A. and Tripp, J.H., “The contact of two nominally flat rough surfaces,” Proceedings of IMechE, 185, pp625- 633, 1970. 20484.

[68] Allmaier, H., Priestner, C., Reich, F.M., Priebsch, H.H., Forstner, C., Novotny-Farkas, F., “Predicting friction reliably and accurately in journal bearings-The importance of extensive oil-models,” Tribology International 48 (2012): 93-101

[69] Boedo, S., “Practical tribological issues in big-end bearings,” Tribology and Dynamics of Engine and Powertrain, Woodhead Publishing, Cambridge, UK, 2010. ISBN: 978-1-84569-361-9.

[70] Sato, k., Makino, K., Machida, K., “A Study of Oil Film Pressure Distribution on Connecting Rods Big Ends,” SAE Technical Paper 2002-03-04, 2002, doi: 10.4271/2002-01-0296

[71] Mohammadpour, M., Rahmani, R., and Rahnejat, H., "The Effect of Cylinder De-Activation on Thermo-Friction Characteristics of the Connecting Rod Bearing in the New European Drive Cycle (NEDC)," SAE Technical Paper 2014-01-2089, 2014, doi:10.4271/2014-01-2089.

[72] Taylor, R. I., “The inclusion of lubricant shear thinning in the short bearing approximation,” Proceedings of the Institution of Mechanical Engineers, Part J: Journal of Engineering Tribology. 1997. Volume 213. Issue 1. Pages 35-36.

[73] Deconninck, B., Delvigne, T., and Videx, G., "Air-X, an Innovative Device for On-line Oil Aeration Measurement in Running Engines," SAE Technical Paper 2003-01-1995, 2003, doi:10.4271/2003-01-1995.

[74] Maassen, F., Koch, F., and Pischinger, F., "Connecting Rod Bearing Operation with Aerated Lube Oil," SAE Technical Paper 981404, 1998, doi:10.4271/981404.

[75] Chitose, T., Kamiya, S., Kabeya, Y., and Desaki, T., "Friction and Wear Reduction of Engine Bearings with Solid Lubricant Overlay," SAE Technical Paper 2014-01-0955, 2014, doi:10.4271/2014-01-0955.

[76] Achim, A., Prefot, M., Wilhelm, M. “Crankshaft bearings for engines with start-stop systems,” MTZ 1212010 Vol 71., pp22-25.

[77] Leetch, D., “Analysis of composition of bearing overlay material,. BP internal report IAR249. 31/March/2009.

[78] Taylor, O. “Bearing wear in downsized engines,” BP internal report, GLT-2011-01.

[79] Taylor, O. “Test development for the measurement of bearing wear in running engines– report II,” BP internal report, GLT-2012-04

[80] Carden, P. Private communication between P Carden (Ricardo consulting engineers) and O Taylor. 19-07-2008.

[81] Kataoka, T., Suzuki, Y., Kato, N., Kikuchi, T. et al., "Measurement of Oil Film Pressure in the Main Bearings of an Operating Engine Using Thin-Film Sensors," SAE Int. J. Engines 1(1):352-358, 2009, doi:10.4271/2008-01-0438.

[82] Dursunkaya, Z. and Keribar, R., "Simulation of Secondary Dynamics of Articulated and Conventional Piston Assemblies," SAE Technical Paper 920484, 1992, doi:10.4271/9

[83] Ricardo Software, "PISDYN 5.0 user manual," Section C-18.

[84] Jeng, Y., 1992, "Theoretical Analysis of Piston-Ring Lubrication Part 1-Fully Flooded Lubrication," STLE Tribology Transactions, 35, pp. 696-706.

[85] Jocsak, J., Wong, V, W., Tian, T., "The effects of cylinder liner finish on piston ring-pack friction," Proceedings of ICEF04 2004 Fall Technical Conference of the ASME Internal Combustion Engine Division October 24-27, 2004, Long Beach, California USA. ICEF2004-952

[86] Ito, A., Chubachi, Y., Yamamoto, T., Tanaka, N. et al., "A Study on Effects of Low Viscosity Engine Oil and MoDTC on Piston Friction Losses in a DI Diesel Engine," SAE Technical Paper 2015-01-2044, 2015, doi:10.4271/2015-01-2044.

[87] Taylor, R.I., Morgan, N.M., "Friction, oil film thickness and wear of piston rings: Impact of lubricant," Presentation to 5th World Tribology Congress, Turin, Italy, September 2013.

[88] Bolander, N, W., Steenwyk, B, D., Kumar, A., and Sadeghi, F. "Film Thickness and Friction Measurement of Piston Ring Cylinder Liner Contact With Corresponding Modeling Including Mixed Lubrication," Proceedings of ICEF04 2004 Fall Technical Conference of the ASME Internal Combustion Engine Division October 24-27, 2004, Long Beach, California USA. ICEF2004-903

[89] Kimura, Y. and Murakami, M., "Analysis of Piston Friction - Effects of Cylinder Bore Temperature Distribution and Oil Temperature," SAE Int. J. Fuels Lubr. 5(1):1-6, 2012, doi:10.4271/2011-01-1746.

[90] Carden, P., Bell, D., Priest, M., and Barrell, D., "Piston Assembly Friction Losses: Comparison of Measured and Predicted Data," SAE Technical Paper 2006-01-0426, 2006, doi:10.4271/2006-01-0426.

[91] Plail, J., "Prediction of piston skirt and ring pack hydrodynamic and boundary lubrication forces in a motored 1.5L gasoline engine," BP confidential report. 2008.

[92] Tomanik, E., "Modelling of the Asperity Contact Area on Actual 3D Surfaces," SAE Technical Paper 2005-01-1864, 2005, doi:10.4271/2005-01-1864.

[93] Taylor, O., Pearson, R., and Stone, R., "Reduction of CO_2 Emissions through Lubricant Thermal Management During the Warm Up of Passenger Car Engines," SAE Technical Paper 2016-01-0892, 2016, doi:10.4271/2016-01-0892.

[94] Nattrass, S. and Davenport, A., "Application of a Split Lubrication Gasoline Engine to the Screening and Understanding of Friction Modifier Behaviour," SAE Int. J. Fuels Lubr. 5(1):511-522, 2012, doi:10.4271/2011-01-2134.

[95] Hanke, W., Buschbeck, R., Letourneau, S., Sinclair, D. et al., "Power Cylinder System Friction and Weight Optimization in High Performance Gasoline Engines," SAE Technical Paper 2009-01-1958, 2009, doi:10.4271/2009-01-1958.

[96] Ricardo Software "RINGPAK 5.0 user manual".

[97] Patir, N. and Cheng, H. S. 1978. "An average flow model for determining effects of three-dimensional roughness on partial hydrodynamic lubrication," ASME J. Lubrication Technol., 100 , pp. 12–17.

[98] Meira, J., Filho, A., Melo, W. and Ribeiro, E., "Strategies for Energy Savings with Use of Constant and Variable Oil Pump Systems," SAE Technical Paper 2011-36-0150, 2011, doi:10.4271/2011-36-0150.

[99] Taylor, R.I., Nagatomi, E., Doki, S., Dixon, R.T., "Tribology and Energy Efficiency," Presentation to World Tribology Congress, Kyoto, 2009.

[100] Calabretta, M., Cacciatore, D., and Carden, P., "Valvetrain Friction - Modeling, Analysis and Measurement of a High Performance Engine Valvetrain System," SAE Int. J. Engines 3(2):72-84, 2010, doi:10.4271/2010-01-1492.

[101] Goetze. "Piston Ring Handbook". http://korihandbook.federalmogul.com/en. Accessed 02/May/2016

[102] Private communication between Taylor, O and Plint, G 24 November 2008.

[103] Plint. A. G., "Friction Force Measurement in Reciprocating Tribometers," STLE 2011

[104] Staley, D., Pryor, B., and Gilgenbach, K., "Adaptation of a Variable Displacement Vane Pump to Engine Lube Oil Applications," SAE Technical Paper 2007-01-1567, 2007, doi:10.4271/2007-01-1567.

[105] Cehreli, Z. and Durgun, Z., "Lubrication System Development on 5-Cylinder Engine," SAE Technical Paper 2007-01-2577, 2007, doi:10.4271/2007-01-2577.

[106] Tao, W., Yuan, Y., Liu, E., Hill, J. et al., "Robust Optimization of Engine Lubrication System," SAE Technical Paper 2007-01-1568, 2007, doi:10.4271/2007-01-1568.

[107] Taylor, O., "Lubricant circuit analysis by mathematical modelling", Report 002. BP Internal report. 2008.

[108] Corbishley, R., OudeNijeweme. D., "NBPT Ford Fox 1.0L Correlated Flowmaster Model," Mahle technical report NBPT0102063RD. March-2014. Commissioned and managed by Taylor, O for BP.

[109] Rundo, M. and Squarcini, R., "Experimental Procedure For Measuring The Energy Consumption Of Ic Engine Lubricating Pumps During A Nedc Driving Cycle," SAE paper number 2009-01-1919, 2009.

[110] Arata, T., Novi, N., Ariga, K., Yamashita, A. et al., "Development of a Two-Stage Variable Displacement Vane Oil Pump," SAE Technical Paper 2012-01-0408, 2012, doi:10.4271/2012-01-0408.

[111] Voigt, D., "Reduction of fuel consumption using regulated oil pumps," MTZ worldwide December 2003, Volume 64.

[112] Schulz-Andres, H. Kamarys, D., “Temperature-controlled Lubricating Oil Pumps Save Fuel,” 7th LuK Symposium April 2002.

[113] Turner, J., Popplewell, A., Patel, R., Johnson, T. et al., "Ultra Boost for Economy: Extending the Limits of Extreme Engine Downsizing," SAE Int. J. Engines 7(1):2014, doi:10.4271/2014-01-1185.

[114] Reyes Belmonte, M., Copeland, C., Hislop, D., Hopkins, G. et al., "Improving Heat Transfer and Reducing Mass in a Gasoline Piston Using Additive Manufacturing," SAE Technical Paper 2015-01-0505, 2015, doi:10.4271/2015-01-0505.

[115] Rooney, D. “Performance testing of 3 different oil pump technologies using 3 different oil viscosities,” commissioned report for BP, report number RD14/60201.1. Ricardo Plc.

[116] Toyoda, F., Kobayashi, Y., Miura, Y., and Koga, Y., "Development of Variable Discharge Oil Pump," SAE Technical Paper 2008-01-0087, 2008, doi:10.4271/2008-01-0087.

[117] Loganathan, S., Sivanantham, R., and kumar, J., "Investigations on Reduction of Power Consumption of Oil Pump for New Advanced Multijet Diesel Engine," SAE Technical Paper 2009-01-1463, 2009, doi:10.4271/2009-01-1463.

[118] Weber, C., Brumley, A., Whiston, F, D., Schamel, A., and Wirth, M., “1.6 SCTI: The New EcoBoost DI-Turbo Engine with Central Direct Injection for Ford’s Volume Carlines,” 19th Aachener Kolloquium Fahrzeug- und Motorentechnik 2010

[119] Jung, M., Muller, H., Frohlich, G., Bohme, J. and Eiser, A.,”The New 1.8l TFSI from Audi, Longitudinally Installed for the Audi A4 and A5,” 16th Aachener Kolloquium Fahrzeug- und Motorentechnik 2007.

[120] Burke, R. D., Brace, C. J., Stark, R. and Pegg, I., “Investigation into the Benefits of Reduced Oil Flows in Internal Combustion Engines,” International Journal of Engine Research. May 28, 2014.

[121] Ardey, N., Wichtl, R., Steinmayr, T., Kaufmann, M., Hiemesch, D., Stütz, W., “The new BMW 3-cylinder and 4-cylinder diesel engines with TwinPower Turbo technology,” 35. Internationales Wiener Motorensymposium 2014.

[122] Mancò, S., Nervegna, N., Rundo, M., and Armenio, G., "Modelling and Simulation of Variable Displacement Vane Pumps for IC Engine Lubrication," SAE Technical Paper 2004-01-1601, 2004, doi:10.4271/2004-01-1601.

[123] Ernst, R., Friedfeldt, R., Lamb, S., Lloyd-Thomas, D., Philips, P., Russel, R., Zenner, T., “The New 3 Cylinder 1.0L Gasoline Direct Injection Turbo Engine from Ford,” 20th Aachen Colloquium Automobile and Engine Technology 2011.

[124] Maccherini, R., “A complete loop of numerical analyses about variable oil pump,” Presentation to the Automotive Simulation Congress in Munich. October 2013.

[125] Fabiani, M., Mancò, S., Nervegna, N., Rundo, M. et al., "Modelling and Simulation of Gerotor Gearing in Lubricating Oil Pumps," SAE Technical Paper 1999-01-0626, 1999, doi:10.4271/1999-01-0626.

[126] Mancò, S., Nervegna, N., Rundo, M., Armenio, G. et al., "Gerotor Lubricating Oil Pump for IC Engines," SAE Technical Paper 982689, 1998, doi:10.4271/982689.

[127] Ribeiro, E., Melo, W., and Filho, A., "Application of electric oil pumps on automotive systems," SAE Technical Paper 2005-01-4086, 2005, doi:10.4271/2005-01-4086.

[128] EPA (2016). "Dynamometer Drive Schedules," accessed 6/Mar/2016. https://www3.epa.gov/otaq/emisslab/testing/dynamometer.htm

[129] E/ECE/324/Rev.1/Add.82/Rev.5-E/ECE/TRANS/505/Rev.1/Add.82/Rev.5. Annex 4a, Type I test, 6.3.2. http://www.unece.org/trans/main/wp29/wp29regs81-100.html, Regulation No.83 Rev 5. Accessed 1/May/2015

[130] Andrews, G., Ounzain, A., Li, H., Bell, M. et al., "The Use of a Water/Lube Oil Heat Exchanger and Enhanced Cooling Water Heating to Increase Water and Lube Oil Heating Rates in Passenger Cars for Reduced Fuel Consumption and CO2 Emissions During Cold Start.," SAE Technical Paper 2007-01-2067, 2007, doi:10.4271/2007-01-2067.

[131] Shayler, P., Allen, A., Leong, D., Pegg, I., Brown, A.J., and Dumenil, J.C., "Characterising Lubricating Oil Viscosity to Describe Effects on Engine Friction," SAE Technical Paper 2007-01-1984, 2007, doi:10.4271/2007-01-1984.

[132] Kunze, K., Wolff, S., Lade, I., and Tonhauser, J., "A Systematic Analysis of CO2-Reduction by an Optimized Heat Supply during Vehicle Warm-up," SAE Technical Paper 2006-01-1450, 2006, doi:10.4271/2006-01-1450.

[133] Revereault, P., Rouaud, C., and MarchI, A., "Fuel Economy and Cabin Heating Improvements Thanks to Thermal Management Solutions Installed in a Diesel Hybrid Electric Vehicle," SAE Technical Paper 2010-01-0800, 2010, doi:10.4271/2010-01-0800.

[134] Hess,U. Mitterer, A. Neugebauer, S. Riegert, P. Seider, G. "Heat Management of the New BMW In-Line 6-Cylinder Engine," MTZ 11/2005 Volume 66

[135] Zammit, J., Shayler, P., Gardiner, R. and Pegg, I., "Investigating the Potential to Reduce Crankshaft Main Bearing Friction During Engine Warm-up by Raising Oil Feed Temperature," SAE Int. J. Engines 5(3):2012, doi: 10.4271/2012-01-1216.

[136] Carden, P. Preston, M. "V-Sim report: BP Vehicle simulation support," BP Internal report. October 2013.

[137] Chisaki, J., Yoshijima, K., Kikuchi, T., Morinaka, S. et al., "Development of a New 2.0-Liter Fuel-Efficient Diesel Engine," SAE Technical Paper 2013-01-0310, 2013, doi:10.4271/2013-01-0310.

[138] Law, T., Shayler, P.J. and Pegg, I., "Investigations of sump design to improve the thermal management of oil temperature during engine warm up" Institution of Mechanical Engineers. (2007) VTMS8: Vehicle thermal management systems conference & exhibition, 8th, Nottingham, 20-24 May 2007, p299-309

[139] Roberts, A., Brooks, R., Shipway, P., Gilchrist, R. et al., "Reducing Energy Losses from Automotive Engine Lubricants by Thermal Isolation of the Engine Mass," SAE Technical Paper 2014-01-0672, 2014, doi:10.4271/2014-01-0672.

[140] Brace, C. J., Burke, R. D. and Moffa, J. (2009), "Increasing accuracy and repeatability of fuel consumption measurement in chassis dynamometer testing," Proceedings of the Institution of Mechanical Engineers, Part D: Journal of Automobile Engineering, 223 (9). pp. 1163-1177. ISSN 0954-4070

[141] Singh, T., Nolte, R., Calamiello, A., Cedric Rouaud, C., "Holistic Thermal Management for Future CO_2 Challenges," ATZ worldwide July 2015, Volume 117, Issue 7-8, pp 20-25

[142] Mock, P. German, J. "The future of vehicle emissions testing and compliance," ICCT Nov 2015.

[143] ECE/TRANS/180/Add.15. http://www.unece.org/fileadmin/DAM/trans/main/wp29/wp29r-1998agr-rules/ECE-TRANS-180a15e.pdf Accessed 3/Mar/2016

[144] United States Application Number or PCT International application number 29/529,959 filed on June 11, 2014. First inventor: Taylor, O. Reading, UK.

[145] Schatz, O., "Cold Start Improvements With a Heat Store," SAE Technical Paper 910305, 1991, doi:10.4271/910305.

[146] Heath, R. and Mo, C., "A Modular Approach to Powertrain Modelling for the Prediction of Vehicle Performance, Economy and Emissions," SAE Technical Paper 960427, 1996, doi:10.4271/960427.

[147] http://media.caranddriver.com/files/2014-ford-focus-st2014-ford-focus-st-full-specs.pdf Accessed 08-2016.

[148] Taylor, O., Deighan, T., Carden, P., "Calculation of friction and wear of Ford ZETEC valvetrain for BP," RD.13/50701.2. March 2013.

[149] Zhu, G., and Taylor, C.M., "Tribological Analysis and Design of a Modern Automobile Cam and Follower," Professional Engineering Publishing Limited. 2001.

[150] Evans, C.R., and Johnson, K.L., "The rheological properties of elastohydrodynamic lubricants," Proc IMechE, Volume 200 Chapter 5, pgs. 303-312. 1986.

[151] Mufti, R.A., and Jefferies, A., 2008, "Novel method of measuring tappet rotation and the effect of lubricant rheology," Tribology International, 41, 1039-1048. 2008.

[152] Taylor, O., Preston, M., Carden, P., "V-SIM report: BP vehicle simulation support," RD.13/354201.2 October 2013.

[153] Private communication between Taylor, O. and Revereault, P. (Ricardo Consulting Engineers). June, 2016.

[154] Goodfellow, C., Revéreault, P., Gaedt, L., Kok, D. et al., "Simulation Based Concept Analysis for a Micro Hybrid Delivery Van," SAE Technical Paper 2005-01-1161, 2005, doi:10.4271/2005-01-1161.

[155] Lyu, M. and Rogers, B., "Study for Better Vehicle Fuel Economy in a Commercial Vehicle Using Vehicle Simulation," SAE Technical Paper 2006-01-1237, 2006, doi:10.4271/2006-01-1237.

¥ = Permission to reproduce this image has been granted by Ricardo Plc:

Figure 13. Big-end bearing cross section showing the mesh used in the finite element analysis.¥

Figure 17. Comparison of wear between predicted locations and those seen in a used engine.¥

Figure 25 Location and magnitude of maximum shear rates predicted for Runs 1 and 14 to 17 at 22 Bar BMEP engine load and 2000 rev/min.¥

Figure 26. Hydrodynamic pressure area plots for simulation Runs 13 and 19.¥

Figure 32. Measurement of the bore deviation from cylindrical for Cylinder 1.¥

Figure 54. SHW VDOP oil pump fitted to the 1.0 Ford EcoBoost engine. The image shows the pump with the front cover removed.¥

Figure 58. Oil pump testing rig.¥

Figure 100. Block model of the V-SIM control structure.¥

-END-